universität wien

DISSERTATION

Characterisation of tourmalines from different environments and correlations between structural and chemical data

Verfasser

Mag. Bakk. rer. nat. Andreas Ertl

angestrebter akademischer Grad

Doktor der Naturwissenschaften (Dr. rer. nat.)

Wien, am 2. März 2009

Studienkennzahl lt. Studienblatt: A 091 426

Dissertationsgebiet lt. Studienblatt: 426 – Erdwissenschaften

Betreuer: O. Prof. Dr. E. Tillmanns

Table of contents

PART 1……6

1 Introduction……6

1.1 General introduction……6

1.2 Previous work on the crystal chemistry of tourmaline……7

1.3 Aim of the present work……9

2 Tourmaline from the elbaite-schorl series from the Himalaya Mine, Mesa Grande, California, U.S.A.: A detailed investigation……11

2.1 Abstract……11

2.2 Introduction……12

2.3 Experimental details……13

2.3.1 Sample selection……13

2.3.2 Crystal-structure refinement……14

2.3.3 Chemical analysis……15

2.3.4 Spectroscopic investigations……17

2.3.5 OH determinations……18

2.3.6 Li NMR spectroscopy……18

2.4 Results and discussion……19

2.5 Conditions of formation for tourmaline-bearing cavities in the Himalaya dike……23

2.6 Acknowledgements……27

2.7 References……28

3 Substitution mechanism in tourmalines of the "fluor-elbaite"-rossmanite series from Wolkenburg, Saxony, Germany……61

3.1 Abstract……61

3.2 Introduction……61

3.3 Methods……63

3.3.1 Sample selection……63

3.3.2 Crystal structures……63

3.3.3 Chemical analysis……...64

3.4 Results and discussion……66

3.5 Acknowledgements……69

3.6 References……..69

4 Investigations on Fe^{2+}- and Mn^{2+}-rich tourmaline……85

4.1 Abstract……..85

4.2 Introduction and previous work……86

4.3 Experimental details……...87

4.3.1 Crystal-structure refinement……..87

4.3.2 Chemical analyses……87

4.3.3 Mössbauer analysis…….…….....89

4.3.4 Optical sprectra…….…….....89

4.4 Results and discussion…….……...89

4.4.1 Mössbauer Results…….……89

4.4.2 Optical spectra……...91

4.4.3 Crystal chemistry and structural analysis……..92

4.4.3.1 Fe-rich tourmaline……....92

4.4.3.2 Mn-rich tourmaline……..93

4.4.3.3 Oxidation experiments……97

4.5 Acknowledgements……...…….98

4.6 References……...……...98

5 Li-bearing, disordered Mg-rich tourmalines from the pegmatite-marble contact from the Austroalpine basement units (Styria, Austria)……120

5.1 Summary……..120

5.2 Introduction……120

5.3 Geology……...121

5.4 Experimental……...123

5.4.1 Sample selection……123

5.4.2 Chemical composition……123

5.4.3 Crystal Structure……123

5.5 Results……124

5.5.1 Discussion of the tourmaline structure……...124

5.5.2 REEs and trace elements in the tourmalines…….....126

5.5.3 Discussion of the Eu and Yb anomaly in the tourmalines……126

5.5.4 Discussion of the origin of the tourmalines and their pegmatitic host rocks…….126

5.5.5 Discussion of formation temperatures……...128

5.5.6 Geochemistry of the micaschists……....128

5.6 Acknowledgements……..…129

5.7 References……...130

6 Metamorphic ultra-high-pressure tourmalines: Structure, chemistry, and correlations to *PT* conditions……..150

6.1 Abstract……..150

6.2 Introduction and previous work……150

6.3 Tourmaline stability and regional geology of the ultra-high-pressure massifs…….....151

6.4 Experimental details……...153

6.4.1 Sample selection……153

6.4.2 Crystal structure refinements……..153

6.4.3 Chemical analysis……...154

6.5 Results……....154

6.6 Discussion……..156

6.7 Acknowledgements……..157

6.8 References……158

7 Summary…….177

Zusammenfassung……..180

References……184

Acknowledgements…….....189

Curriculum Vitae…….....190

PART 2 – Publications…….202

PART 1

1 Introduction

1.1 General introduction

Tourmaline is an extremely important mineral because of its relevance in the geosciences, for its technical applications and its use as gemstone. The tourmaline group consists of more than a dozen end members, which occur in many different geological environments (e.g., Hawthorne and Henry, 1999).

Tourmaline composition gives information on the thermal and fluid history of rocks in which it develops, is intimately associated with some of the world's premier metallic ore deposits, retains chemical signatures of the sources of tourmaline detritus in clastic rocks, yields isotopic evidence for the environmental sources of the boron that makes up tourmaline, is an extremely critical link in the boron cycle on the Earth and has many other useful petrogenetic features (e.g., Dutrow and Henry, 2000; Gaweda et al., 2002; Goerne, 1998; Henry, 2003). Varying chemical compositions of tourmaline reflect the chemical conditions of rocks where tourmaline forms and have been used as an important petrologic indicator of different geologic environments in previous investigations (e.g., Henry and Guidotti, 1985; Jolliff et al., 1986; Dyar et al., 1999; Novák et al., 1999; Selway, 1999; Roda-Robles et al., 2004).

Tourmaline belongs to the most common piezo- and pyroelectric materials that are technically used (e.g., Prasad et al., 2005). Natural tourmaline is used for piezoelectric pressure transducers for dynamic pressure measurements (e.g., Wilson, 2003). Tourmaline has a high mechanical stability and is resistant to many acids and alkaline solutions. Tourmalines can be used up to 900 °C, the actual technical limit is 750-780 °C. Additionally, tourmaline displays significant pyroelectricity (e.g., Hawkins et al., 1995; Lally and Cummiskey, 2003). Tourmaline is also used as electronic components, e.g., as transducers, mainly because of the anisotropy of its properties (Adeoye and Adewoye, 2004). More recent applications of tourmaline are in functional fibers (Zhenggang et al., 2005). Tourmaline is also very well known as gemstone which occurs in more colors and combinations of colors than any other gemstone variety; it also shows a remarkable dichroism (e.g., Dietrich, 1985; Dirlam et al., 2002). Tourmaline compositions can also be used as indicator of emerald mineralization (Galbraith, 2007).

Tourmalines are complex aluminium-borosilicates with strongly varying compositions because of isomorphous replacements (solid solutions). The tourmaline mineral group is chemically one of the most complicated groups of silicate minerals, with the general formula $X\ Y_3\ Z_6\ [T_6O_{18}]\ (BO_3)_3\ V_3\ W$. The structure of tourmaline is characterized by six-membered tetrahedral rings (*T* sites), whose apical oxygens point toward the (-) c-pole, producing the acentric nature of the structure.

In this section the possible occupants of the different sites in the tourmaline structure and the relation between these sites will be discussed. The tetrahedral sites in tourmaline are primarily occupied by Si, and sometimes also (usually) by small amounts of Al and B (e.g., Hawthorne et al., 1993; Ertl et al., 1997, 2003b, 2005, 2006a, 2006c; Hughes et al., 2000, 2004). Above the tetrahedra are triangular BO_3 groups that lie parallel to the (0001) plane. Planar rings of tetrahedra are linked by two types of octahedra, *Z* and *Y***,** which share edges to form brucite-like fragments. The *Z* octahedron is relatively small, somewhat distorted, and occupied predominantly by trivalent cations such as Al^{3+}, Fe^{3+}, Cr^{3+} and V^{3+}, but can contain significant amounts of the divalent cations Mg^{2+} (e.g., Ertl et al., 2002, 2003a). Z-site cations serve as linkages among structural fragments along a three-fold screw axis. The *Y* site is a relatively regular octahedron occupied by a wide array of multivalent cations, most commonly Li^{1+}, Mg^{2+}, Fe^{2+}, Mn^{2+}, Cu^{2+}, Al^{3+}, Cr^{3+}, V^{3+}, Fe^{3+}, Mn^{3+} and Ti^{4+}. Most structural refinements indicate that there is minor *Y*-site vacancy (e.g., Hawthorne et al., 1993; Taylor et al., 1995; Ertl et al., 1997, 2006a). When Fe^{2+} occurs at the Y site, Mg could not occupy both neighbouring Z sites (Bloodaxe et al., 1999). At the same time, even if certain cations occur only at the Y sites, they could have various coordination environments. This was related to the degree of cationic ordering in the structure by Oliveira et al. (2002). They explained that a high degree of cationic ordering is corresponding to a small number of non-equivalent sites and attributed various degrees of cationic ordering to different geologic geneses (Oliveira et al., 2002). The *X* site is a nine-coordinated trigonal antiprism, located along the three-fold axis of symmetry. It is most commonly occupied by Na and Ca, or vacant, and in rare cases occupied by K and Ag (London et al., 2006). It is not clear whether small amounts of Pb and H_2O occupy this site (Ertl et al., 2006a, 2007). There are 31 anions in the structural formula which are located in 8 distinct sites, O(1) through O(8) (Donnay and Buerger, 1950; Donnay and Barton, 1972). The O(2) and O(4)-O(8) sites are occupied exclusively by O^{2-}. The single O(1) site, termed the *W* site in the structural formula, is located along the three-fold axis central to the pseudo-hexagonal ring of tetrahedra and can contain OH^{1-}, O^{2-} or F^{1-}. The three O(3) sites, termed the *V* site**,** typically contain OH^{1-}, but can also contain significant amounts of O^{2-}. The *W* site is unique because F^{1-} partitions completely into this site, and O^{2-} also tend to partition into this site relative to OH^{1-} (Grice and Ercit, 1993; MacDonald and Hawthorne, 1995; Ertl et al., 2006a, 2006b).

Although substantial research efforts have been devoted to analytical work (except to the light elements B, Li and H), the relationship between structural features and site-occupancies is poorly understood.

1.2 Previous work on the crystal chemistry of tourmaline

In this chapter the present status of research about the correlations between structural and chemical data is given. The substitution of Al for Mg at the *Z* site was already described by different authors (Grice and

Ercit, 1993; Hawthorne et al., 1993; MacDonald and Hawthorne, 1995; Taylor et al., 1995; Bloodaxe et al., 1999; Bosi and Lucchesi, 2004). Hawthorne et al. (1993) asserted that the Mg content at the *Z* site cannot be determined on the basis of scattering power alone because of the similarity of Mg and Al with respect to X-ray scattering. Because of considerable differences in ionic radius between Al and Mg, their quantity can be determined from mean bond lengths. Hawthorne et al. (1993) and Grice and Ercit (1993) obtained linear relations between mean bond-lengths and the radii of constituent cations. Bloodaxe et al. (1999) used the method of Hawthorne et al. (1993) to determine the extent of order of Mg and Al between the two octahedral sites by minimizing the differences between grand mean octahedral bond-length and bond lengths calculated from the radii of constituent cations. However, because of significant amounts of Fe^{3+} (and maybe Ti^{4+}) at the *Z* site of many tourmalines and the influence of the *Y*-site occupation to the <*Z*-O> distance, an accurate determination of the Mg content at this site is still problematic. Pieczka (2000) published an interesting paper about modelling of some structural parameters of tourmalines on the basis of their chemical composition. Pieczka (2000) found in some (Fe^{3+},Al)-rich tourmalines (buergerites and schorls) and Al-rich dravites differences between the observed and predicted values of <*Z*-O> and <*Y*-O> mean sizes, as well as the *a* and *c* unit-cell parameters; these differences suggest some kind of disordering of Fe^{3+} and Al or Mg and Al between *Y* and *Z* sites. Also the correlation between an O^{2-} occupation at the *W* site and the Al-Mg disordering between the *Y* and the *Z* site is not clear at all. There is no explanation for some strongly disordered tourmalines which are occupied by an OH at the W site (e.g., Marschall et al., 2004). The precise determination of the Al-Mg disordering in tourmalines is important for the petrology because it reflects also the *PT* conditions during the crystallisation.

Li was usually determined only in colourless, light green and pink tourmalines (Fe- and Mn-bearing elbaites) in the past, and only in rare cases in black and brownish tourmalines. However, since it was shown by Novák et al. (1999) that there is no crystal chemical gap between the elbaite-schorl and the dravite-schorl series as was thought before, it is clear that many tourmalines were not chemically characterised accurately enough in the past.

Within the last 12 years in some tourmalines a significant substitution of Si by B was found (Ertl et al., 1997; Ertl & Brandstätter, 1998; Hughes et al., 2000; Kalt et al., 2001; Marler and Ertl, 2002; Schreyer et al., 2002a, 2002b; Hughes et al., 2004; Ertl et al., 2005, 2006a, 2006c, 2007). Because of the analytical challenge many questions are still open. There is yet no adequate explanation for the mechanism of the incorporation of tetrahedrally coordinated boron into the tourmaline structure. It is still not easy to verify the presence of B at the *T* site. Especially just by using only microprobe data, as it is usually done, tetrahedrally coordinated B can be overlooked. The incorporation of B at the *T* site in tourmaline can be important for the petrology because it indicates higher pressures during crystallisation (e.g., Schreyer et al., 2000).

Ertl et al. (2002) have shown that the bond-angle distortion of the *Z* octahedron in a tourmaline is largely a function of the <Y-O> distance of that tourmaline [for all tourmalines where the V site is occupied by 3 (OH) apfu], although the occupant of the V site also affects that distortion. In principle does this observation lead to an estimation of the OH content at the *V* site. Because of poorly characterised OH contents of tourmalines in the past (no water estimation or too high errors) it is yet not possible to use this above mentioned correlation for a quantitative OH estimation. No structural correlation has been found up to date to estimate the OH content at the *W* site. Here is also the same problem evident: Because of the lack of high quality water measurements in tourmalines it is problematic to find such a possible correlation.

1.3 Aim of the present work

The present work aims at strategic research into the crystallography and crystal chemistry, including the analysis of light elements, of novel tourmalines, also involving unusual tourmaline solid solutions. Most of the tourmalines published in the past were not completely characterized, especially with respect for light elements and structural studies. Hence, correlations between structural features like bond lengths, bond angles, occupancies, and the chemistry could often not be characterised. More recent investigations indicate that such relationships are relatively complex.

The aim of this work was the structural characterisation and classification of novel tourmalines (including unusual tourmaline solid solutions), in order to find correlations between crystal chemistry and structural features. A better understanding of structural features in correlation with the crystal chemistry could also be important for technical applications.

The major aims of this work are as follows:

- to characterise in detail the crystallography of different tourmaline samples by using a CCD diffractometer.
- to characterise the chemical compositions in detail, including also light elements and the valence states of Fe by using EMPA, SIMS, ICP-MS, and spectroscopic methods (e.g., Mössbauer spectroscopy, IR spectroscopy).
- to compare structural and chemical data to work out correlations between structural features, like bond lengths, bond angles, refined occupancies, and site occupants.

This strategic research will, firstly, provide a very important knowledge and data base for future studies in the innovative fields of applied petrology and mineralogy by characterising novel tourmalines.

A systematic study of different tourmalines in different geologic environments, which are petrologically well characterised, can lead to important correlations especially between Al-Mg disorder at the *Y* site and the *Z* site and temperature but also between *PT* conditions and the *T*-site occupancy. The estimated OH and F contents are also of interest, because tourmaline is an important petrogenetic indicator for fluid-rock interactions. Such findings and correlations can be useful by petrologists as well as by geologists.

2 Tourmaline from the elbaite-schorl series from the Himalaya Mine, Mesa Grande, California, U.S.A.: A detailed investigation

2.1 ABSTRACT

Detailed chemical, Mössbauer, infrared, optical and structural data were obtained on 12 tourmaline samples from gem pockets in the Himalaya mine, San Diego County, California, U.S.A. One of these tourmalines shows strong color zonation from core to rim and shows correspondingly strong compositional zonation. Some elemental abundances increase from core to rim (Ca, Li), others increase, peak, and decrease (Mn^{2+}, F) in the zoned crystal. The elements Li and F that are normally coupled in abundance are decoupled in this zoned tourmaline. When lepidolite starts crystallizing the F content in tourmaline decreases. The black core of this crystal is an Al-rich, Mn-bearing "oxy-schorl". A yellowish green, intermediate Mn-rich "fluor-elbaite" zone contains a relatively high Mn content with ~6 wt% MnO. The nearly colorless "fluor-elbaite" rim has the highest Li content of all zones. There is an inverse correlation between the lattice parameter *a* (for ≥15.84 Å) and the Li content (r^2 = 0.96). Mössbauer studies from the different zones within this crystal show that the relative fraction of Fe^{3+} increases continuously from the Fe-rich core to the Fe-poor rim-near zone, reflecting the increasing fugacity of oxygen in the pegmatite pocket. In the very outside Fe-poor rim the relative fraction of Fe^{3+} decreases again. There is an excellent positive correlation between the lattice parameter *a* (for ≥15.84 Å) and the (Fe^{2+} + Mn^{2+}) content in tourmalines from the elbaite-schorl series (r^2 = 0.99). Lower values than 15.84 Å for lattice parameter *a* can be derived by an increasing $^{[4]}$B content in samples which usually have a (Fe^{2+} + Mn^{2+}) content of <0.1 apfu. There is an inverse correlation between <Y-O> and the Al and Fe^{3+} content at the Y site in tourmalines from the elbaite-schorl series (r^2 = 0.98). Within the core of the crystal, the T site contains ~0.3 apfu $^{[4]}$Al whereas in the Al- and Li-rich tourmalines it contains ~0.2 apfu $^{[4]}$B. The intermediate zones contain mixed occupations of Si, Al and B. Similar to $^{[4]}$B-bearing tourmalines from other localities, a positive correlation between Al at the Y site and $^{[4]}$B was found (r^2 = 0.93) in tourmalines from the Himalaya Mine. Another positive correlation was found between (Mn^{2+} + Fe^{2+}) and $^{[4]}$Al in tourmalines from this locality (r^2 = 0.99). These correlations indicate that, in the short-range order configurations, ^{Y}Al is coupled from $^{[4]}$B, whereas Mn^{2+} and Fe^{2+} are coupled with $^{[4]}$Al. Beryllium is very low in the Fe-rich core (BeO =7 ppm) and increases concomitantly with the Al content (r^2 = 0.97). The zone with the highest Al content also has the highest Be content (BeO = 76 ppm).

To get the most accurate OH data for the investigated tourmaline samples the OH determinations in this study were undertaken by different methods (SIMS, hydrogen manometry, continuous-flow mass spectrometry). These analyses indicate that some elbaites contain a mixed occupation of F, OH and O at

the W site. It can be concluded that the approximate assumption OH = 4 - F is only valid for elbaitic tourmalines with FeO + MnO < 8 wt%.

2.2 INTRODUCTION

The Himalaya Mine was the most productive tourmaline mine for gem and specimen-grade elbaite in North America. The mine, famous for multi-colored elbaite, is found in a miarolitic boron-enriched LCT-type granitic pegmatite in norite (Fisher et al. 1998). K/Ar and $^{40}Ar/^{39}Ar$ ages, which were determined on muscovite, lepidolite, and biotite, are the range ~98-93 Ma (Foord 1976; Snee and Foord 1991; Fisher et al. 1998). Mining operations on the Himalaya dike system began on the Himalaya claim in 1898. In 1899 tourmaline was discovered on the San Diego property, and in 1904 the San Diego Tourmaline Mining Company was organized to work the deposits (Foord 1977). In addition to tourmaline, quartz, feldspar (oligoclase-albite, microcline, and orthoclase), lepidolite, muscovite, schorl, and spessartine are also common. Foord (1977) and Fisher et al. (1998) further described beryl, fluorapatite, manganocolumbite-manganotantalite, stibiocolumbite-stibiotantalite, microlite (sometimes uranium-bearing), and gahnite as (common to uncommon) primary minerals. Sterrett (1904) gives the detailed forms of different well-crystallized elbaite crystals from the deposit.

The central portion of each dike (pocket zone) is characterized by large crystal size, as well as chemical and color zonation in tourmaline, garnet, micas, and other minerals (Foord 1977). Within this zone are cavities (sometimes filled with clay), several cm to more than a meter in maximum dimension, which contain free-standing euhedral crystals.

This investigation focuses on the changes in chemical composition and structural data during the crystallization of tourmaline in the pockets. In addition, efforts were made to determine the OH content in the different tourmaline zones as accurately as possible. Hence, different methods for the water estimation were used.

For the first time accurate occupancy at the T site is assigned for Li-bearing tourmaline from this locality. Different substitutions for Si were described for the T site in the past. A substitution of Al^{3+} for Si^{4+} was first proposed by Buerger et al. (1962). The relationship between <*T*-O> distances and Al occupancy in the ring was first described by Foit and Rosenberg (1979) and Foit (1989). Foit (1989) described a positive correlation between $^{[4]}$Al and the <T-O> distance (r = 0.70). MacDonald and Hawthorne (1995) have shown by crystal structure analyses in combination with chemical analyses that Mg-rich tourmaline samples can contain significant amounts of $^{[4]}$Al (up to ~0.5 apfu) and that there is a good linear positive correlation between <T-O> and $^{[4]}$Al (<T-O> = 1.620 + 0.0162 $^{[4]}$Al, with r = 0.961).

Tourmaline compositions containing excess boron (above the putative $B_{3.00}$ *apfu*) have been reported by Dyar et al. (1994) and Dyar et al. (1998). Structure studies of Al-rich and Li-bearing tourmalines (elbaite, liddicoatite, olenite, "oxy-rossmanite") showed that B substitutes for Si in significant amounts (up to ~0.8 apfu) at the tetrahedral site in natural tourmaline (Ertl et al. 1997, 2005, 2006, 2007; Hughes et al. 2000, 2001; Schreyer et al. 2002). Structure studies by Hughes et al. (2004) and Ertl and Hughes (2002) on Fe-bearing olenite and on Al-rich schorl (all tourmaline samples from the same locality as the B-rich olenite from Ertl et al. 1997) also show substantial amounts of $^{[4]}B$. ^{11}B magic angle spinning nuclear magnetic resonance (MAS NMR) spectroscopic studies on Al-rich and Li-rich natural tourmaline samples (from different localities) by Tagg et al. (1999) and Marler and Ertl (2002) confirmed the existence of $^{[4]}B$ in these samples (0.1-0.8 *apfu* $^{[4]}B$). Synthetic Al-rich tourmaline can also contain significant $^{[4]}B \Leftrightarrow {}^{[4]}Si$ substitutions as shown with ^{11}B MAS NMR, EELS (electron energy loss spectroscopy), and structure studies (Wodara and Schreyer 1997; Wodara and Schreyer 1998; Schreyer et al. 2000; Wodara and Schreyer 2001; Marler et al. 2000; 2002). "Oxy-rossmanite", with the formula $^{X}(\square_{0.53}Na_{0.46}Ca_{0.01})\ ^{Y}(Al_{2.35}Li_{0.32}Mn^{2+}_{0.28}Fe^{2+}_{0.04}Ti^{4+}_{0.01})\ ^{Z}Al_6\ ^{T}(Si_{5.51}Al_{0.25}B_{0.24})O_{18}\ (BO_3)_3\ ^{V}[(OH)_{2.80}O_{0.20}]\ ^{W}[O_{0.86}(OH)_{0.10}F_{0.04}]$ (sample REDT4; Ertl et al. 2005), gave for the first time a clear indication that it is possible to have significant amounts of both $^{[4]}B$ and $^{[4]}Al$ in an Al-rich tourmaline. Although the structure refinements showed significant amounts of $^{[4]}B$, the <*T*-O> bond-lengths (~1.620 Å) masked the incorporation of $^{[4]}B$ because of the concomitant incorporation of $^{[4]}Al$ (Ertl et al. 2005).

2.3 EXPERIMENTAL DETAILS

2.3.1 Sample selection

The first sample selected for this study is a light pink elbaite (SS4). It is a euhedral crystal, from a pocket (mined in the 1980s), about 1 cm in length and ~5 mm in diameter. The rim portion was used in this work.

Sample GRR 916 is an approximately 2 cm long portion of a nearly uniform color pale purplish pink tourmaline crystal about 8 mm in diameter, obtained from a gem pocket in the Himalaya Mine in February, 1982. The rim portion was used in this work.

Sample GRR1365a is a portion of an approximately 8 mm diameter light pink crystal obtained from a gem pocket in the Himalaya Mine in November, 1981.

Sample GRR 565a is a 1.2 cm long, 1.3 cm wide portion of a uniformly colored, light-pink crystal tourmaline obtained from pre-1966 production. The core of this sample was used for optical spectroscopy and for microprobe analysis.

A color-zoned sample was chosen (sample HIM, also called GRR 2254; Fig. 1) for extensive studies. This idiomorphic 36 mm diameter crystal (the crystal which was used is a fragment ~4 cm in length from a crystal believed to be ~7 cm in total length) associated with albite, lepidolite, and quartz, was obtained from a pocket that was mined ~1985. Different color zones within the sample are designated. HIM1 (black; inner core), HIM2 (black; outer core), HIM3 (yellowish-greenish intermediate zone), HIM4 (pale pink intermediate zone), HIM5 (near-colorless rim). By observing this sample (HIM) and of other tourmaline crystals from this locality that show a very similar zonation and size, it is clear that the albite crystallization (on the tourmaline pyramidal faces) started during the crystallization of the outer core (position of HIM2), because albite crystals (up to ~15 mm), as inclusion of the tourmaline, were only found at the positions of the zones HIM2-HIM5. Lepidolite crystallization (on the tourmaline pyramidal faces) started during the crystallization of the pink zone HIM4 (inclusions of lepidolite were only found in zones HIM4 and HIM5). These strongly-zoned tourmaline crystals show the prismatic forms [120], [-100] (usually not clearly differentiated because of a strong striation parallel to the *c*-axis), and the pyramidal forms [101] and, very rarely, [021].

Sample HMGC1 (also called GRR 2597) is a euhedral, colorless, pale-green needle about 1 mm in length and ~150 μm in diameter obtained from the Green Cap Room (extracted in 1998). This generation of tourmaline coats nearby pink tourmaline to make watermelon tourmaline. Because of the small diameter of this crystal, a piece of the entire needle was used for crystal structure determination and for the subsequent chemical analysis. Hence no differentiation could be made between rim and core. However, the microprobe data show only little variation (Tab. 4) hence, a strong zonation in this crystal is not expected.

2.3.2 Crystal-structure refinement

Samples of the elbaite-schorl series were mounted on a Bruker Apex CCD diffractometer equipped with graphite-monochromated Mo *K*α radiation. Refined cell-parameters and other crystal data are listed in Table 1. Redundant data were collected for a sphere of reciprocal space, and absorption was corrected using semi-empirical methods as implemented in the program SADABS (Bruker AXS, Inc. 2003). A total of 4500 frames were collected for each sample, at 0.20^{o} frame width, and a scan time of 15s, and a detector distance of 5 cm; data from $0\text{-}30^{0}$ θ were used in the refinement.

The structure was refined using a tourmaline starting model and the Bruker SHELXTL V. 6.10 package of programs, with neutral-atom scattering factors and terms for anomalous dispersion. For H1, the hydrogen atom associated with O1, the O1-H1 bond distance was restrained to be within one σ of 0.86, the expected bond distance as measured by X-ray diffractometry. Neutral-atom scattering factors and terms for anomalous dispersion were employed throughout the refinement. Refinement was performed with

anisotropic displacement parameters for all non-hydrogen atoms, and the structure was refined on F^2. In Table 1 crystal data and details of the refinement are listed, in Table 2 the atomic parameters; in Table 3 selected interatomic distances are presented.

B, *Z* (=Al), O1-O8, and H3 were constrained to fully occupy their respective sites, and the tourmaline Y site was modeled with Al and Fe (for the Fe-rich samples) respectively with Li (for the Li-rich samples) scattering factors. Hawthorne (2002) showed by application of bond-valence theory that Li cannot occur at the Z site. However, because the simultaneous refinement of too large a portion of the total scattering can lead to significant negative correlations between site occupancy and scale factor and the persuasive arguments of Hawthorne (2002), Al_Z was fixed at $Al_{1.00}$ (Table 2; Z site fully occupied with Al). Occupancy of the T site was modeled with Si and B scattering factors, with the assumption that (Si + B) = 1. The H atom associated with O3 (H3) was easily located in the difference map, and subsequently refined. In the samples HIM1, HIM2, HIM3, SS4 and HMGC1 the H atom near O1 was found and subsequently refined. In the F-rich samples HIM4 and HIM5 the occupancy of the W site (O1 site) was modeled with O and F with the assumption that (O + F) = 1. Table 2 contains the atom coordinates and equivalent-isotropic displacement parameters, and Table 3 lists selected bond-lengths.

Also of other (pale pink) tourmaline crystals from this locality were crystal structure analyses undertaken (GRR 1365, GRR916, HMC1). These samples have higher lattice parameters (GRR1365: a = 15.835 Å, c = 7.099 Å, R = 0.015; GRR916: a = 15.844 Å, c = 7.102 Å, R = 0.018; HMC1: a = 15.835 Å, c = 7.102 Å, R = 0.016), and lower refined $^{[4]}B$ values than sample HIM4 and SS4. These properties suggest that these samples have lower contents of $^{[4]}B$ than the samples HIM4 and SS4.

2.3.3 Chemical analysis

After completion of the structure refinement, the crystals selected for crystal structure determination were mounted in plugs and polished for chemical analysis. All elements except B, Li, Be, and H were determined with a Cameca SX51 electron microprobe (EMP) equipped with five wavelength-dispersive spectrometers (Universität Heidelberg). Operating conditions: 15 kV accelerating voltage, 20 nA beam current and beam diameter 5 μm. Peaks for all elements were measured for 10 s, except for Mg (20 s), Cr (20 s), Ti (20 s), Zn (30 s), and F (40 s). Natural and synthetic silicate and oxide standards were used for calibration (Ertl et al. 2003). The analytical data were reduced and corrected using the PAP routine. A modified matrix correction was applied assuming stoichiometric O atoms and all non-measured components as B_2O_3. Accuracy of the electron-microprobe analyses and correction procedure were checked by measuring three reference tourmalines (98114: elbaite, 108796: dravite, 112566: schorl). Compositions of these tourmaline samples are presented in the context of an interlaboratory comparison study (Dyar et al. 1998, 2001). Under the described conditions, analytical errors on all analyses are ±1% relative for major elements and ±5% relative for minor elements.

The elbaite sample SS4 was analyzed for Si, Al, Ti, Mg, Mn, Ca, Na, K and F by EMPA (electron microprobe analysis) at several institutions participating in a related project on the interlaboratory reproducibility of tourmaline analyses. Analytical instrumentation, experimental conditions, and standards are described by Dyar et al. (2001). EMPA scans at the University of Houston were used to screen for zoning in tourmaline; this elbaite sample showed no zoning. An average of 22 analyses from four different laboratories was obtained for this sample, and analytical errors are estimated to be ±0.5-2% for major elements and ±10-20% for minor elements.

Concentrations of H, Be, Li, and B were determined by secondary-ion mass spectrometry (SIMS) with a CAMECA ims 3f ion microprobe (Universität Heidelberg). Primary O-ions were accelerated to 10 keV. The mass spectrometer's energy window was set to 40 eV. An offset of 75 V was applied to the secondary accelerating voltage of 4.5 kV so that secondary ions with an initial energy of 75 ±20 eV were analyzed (energy filtering). This adjustment suppresses effects of light elements related to the matrix (Ottolini et al. 1993). For B, Be, and Li the primary current was 20 nA, resulting in a sputtering surface ~30 μm in diameter. The spectrometer's mass resolution, M/ΔM, for B, Be and Li was set to ~1100 (10%) to suppress interferences ($^{6}LiH^{+}$, $^{10}BH^{+}$, Al^{3+}). Secondary ions ^{7}Li, ^{9}Be and ^{11}B were collected under an ion-imaged field of 150 μm diameter.

For H, the primary beam current was 25 nA and M/ΔM was set to ~400 (10%). To reduce the rate of contamination with water, a smaller field aperture was chosen (Marschall and Ludwig 2004); thus, the analyzed area was restricted to 10 μm in diameter in the center of the scanned area. This method reduces the effect of contamination due to water, which was found to be higher on the edge of the primary beam spot than in the center. Contamination by water was further reduced using a cold trap cooled with liquid nitrogen attached to the sample chamber of the ims 3f instrument. The count rates of the isotopes monitored (^{1}H, ^{7}Li, ^{9}Be, and ^{11}B) were normalized to the count rate of ^{30}Si.

The relative ion-yield (RIY) for B and H was determined using three different samples of tourmaline as reference material: elbaite (98144), dravite (108796) and schorl (112566), all described and analyzed by Dyar et al. (1998, 2001). For reference material for Li and Be, the standard glass SRM610 (NIST) with concentrations for Li and Be published by Pearce et al. (1997) was used. The relative reproducibility (1σ) for the RIY of B, Li, and Be was <1%. Matrix effects and the uncertainty of the element concentrations in the reference material limit the accuracy of the analysis. The relative uncertainty is estimated to be <20% for Li and Be, and <10% for B and H (Ertl et al. 2006).

In absence of chemical analyses, Tagg et al. (1999) and Hughes et al. (2001) used an average value for H_2O (2.86 wt%; mean value of all tourmaline samples in Dyar et al. 1998) in their studies on Li-rich tourmalines (elbaites). The value of H_2O determined by SIMS analysis (3.67 wt%) is significantly higher than that average value, but is similar to determined H_2O values for Al-rich, Li-rich, Fe- and Mn-poor tourmalines by Dyar et al. (1998) and Selway et al. (1998). However, the H_2O value determined by

SIMS for the pink Himalaya Mine elbaite may be slightly high, as F + OH = 4.20 *apfu* (Table 4).

Mössbauer analysis. Tourmaline separates were crushed to fine powders under acetone before mounting in a sample holder confined by cellophane tape; 20 mg of the Fe-richer HIM1 and HIM2 samples were used, ~40 mg of HIM3 and HIM4, and ~280 mg of HIM5 and SS4 were mounted. For the latter samples, the necessity of packing the most possible sample in the holder (needed to optimize signal to noise for this low Fe composition) outweighed concerns relating to preferred sample orientation, so no binder was used. The resultant sample thicknesses ranged from ~0.5 mg Fe/cm^2 for the Fe-rich samples to ~0.004 mg Fe/cm^2 for HIM5 and SS4, all well below the thin absorber thickness approximation of Long et al. (1983) (Figure 1). Room temperature Mössbauer spectra were acquired to determine Fe^{2+} and Fe^{3+} contents in the Mineral Spectroscopy Laboratory at Mount Holyoke College. A source of 20-80 mCi ^{57}Co in Rh was used on a WEB Research Co. spectrometer. Run times were 1-10 days. Results were calibrated against an α-Fe foil of 6 μm thickness and 99% purity.

The spectra were fit using an in-house program generously made available to us by Eddy De Grave and Toon Van Alboom at the University of Ghent, in Belgium. The Dist3e program models spectra using quadrupole splitting (or hyperfine field, for magnetic materials) distributions for which the subspectra are constituted by Lorentzian shaped lines; it uses velocity approximations rather than solving the full Hamiltonian. This program does not presume any particular shape of the distribution. Results of these fits are given in Table 5 and Figure 2, with site assignments based on the conventions of Dyar et al. (1998).

In the absence of *any* data on recoil-free fractions for Fe in different sites and valences in the tourmaline structure, peak areas were assumed to correspond directly to the abundance of the species in the sample; it is recognized that this assumption (and the use of a potentially preferentially oriented absorber) may unavoidably contribute to the overall large errors on the Fe^{3+} and Fe^{2+} distributions in this sample. Thus, that errors on site assignments (i.e. peak areas) can be estimated in these spectra to be roughly ± 5-15% (especially in the low-Fr samples). Errors on isomer shift and quadrupole splitting of isolated peaks are usually ±0.02 mm/s, but because these spectra contain heavily overlapped peaks, the errors may be as high as ±0.05 mm/s.

2.3.4 Spectroscopic Investigations

Samples for optical absorption spectroscopy were prepared as polished slabs oriented with the c-axis in the plane of the slab. Optical absorption spectra were taken with a Cary 17I spectrometer and previously reported, in part, in Reinitz and Rossman (1988). Samples for infrared absorption spectroscopy were prepared from a wedge of the master sample, GRR 2254, by preparing a slice that went from the rim to the core oriented such that the c-axis was in the plane of the slice. Infrared spectra were obtained with a Nicolet Magna 860 infrared spectrometer

Irradiations of GRR 565 were performed with a 137-Cs source at a rate of 1.4 Mrad per day and heating experiments were performed in air.

2.3.5 OH Determinations

To get the most accurate OH data for the investigated tourmaline samples the OH determinations in this study were performed by different methods. All samples were analyzed by SIMS as described above. The zones HIM1-HIM5 were additionally analyzed by thermal extraction followed by uranium reduction followed, in turn, by hydrogen manometry. Therefore ~7-47 mg powder (Table 4) of each zone, which was carefully separated, was used. Further, a recently developed method for hydrogen analysis involving micro-extraction and continuous-flow mass spectrometry was used (O'Leary et al., 2007), which is briefly described below.

Micro H-extraction analysis. In this method a thermal extraction followed by uranium reduction was used, followed, in turn, by continuous-flow mass spectrometry. A small aliquot of the tourmaline section was separated by microsawing from the master piece and then was coarsely ground such that many of the grains were in the 212 to 425 micrometer size range. These grindings were examined under a microscope and 40 to 380 micrograms of grains free of visible inclusions were separated. The grains were preheated at ~500 ºC for 45 minutes to remove surface water. The grains were then dehydrated at 1120 ºC for 30 minutes following the procedures in O'Leary et al. (2007). After dehydration, representative grains were checked by Raman spectroscopy to verify that they were completely decomposed with no OH remaining. Zoisite was used as a calibration standard as described in O'Leary et al. (2007) and two or three analyses were obtained on each zone of the sample.

OH by IR overtones. An experimental method, which is now under development was also tried, using the integrated intensity of the OH bands in the 7000 cm^{-1} region of the infrared spectrum. Spectra are obtained on an oriented single crystal in the E\\c and E⊥c directions. The total integrated area (E\\c + 2×E⊥c) was then determined (Fig. 15). A series of tourmalines (mostly elbaites) analyzed the micro-extraction continuous-flow mass spectrometry method were used to define the relationship between integrated area and OH band intensity.

2.3.6 Li NMR spectroscopy

Material of the pale pink elbaite sample SS4 was also used for Li NMR spectroscopy. This sample contains relatively little Mn, and only traces of Fe and Ti (higher concentrations of Fe and Ti would result in a green color). Low concentrations of transition elements are desirable for optimal NMR resolution. ^{6}Li and ^{7}Li MAS NMR spectra were recorded with a Bruker ASX 400 spectrometer operating at a frequency of 155.51 MHz. Single-pulse excitation with a pulse width of 2 μs was used for the solid-state

experiments. The spectrum is an average of 8000 scans, with 4 s delay time between acquisitions. The sample was spun at a frequency of 8.25 kHz. The ^{7}Li chemical shift was referenced to the resonance of LiCl.

2.4 RESULTS AND DISCUSSION

Formula of the analyzed tourmaline samples. On the basis of chemical data (EMPA, SIMS, U-extraction, continuous-flow mass spectrometry), as well as structural data, the following optimized formulae (for procedure see notes in Table 4) for the different samples are given:

HIM1: $^{X}(Na_{0.58}Ca_{0.03}K_{0.01}\square_{0.38})\ ^{Y}(Al_{1.07}Fe^{2+}_{1.06}Mn^{2+}_{0.33}Fe^{3+}_{0.20}Li_{0.15}Zn_{0.09}Mg_{0.01}Ti^{4+}_{0.01}\square_{0.08})$
$^{Z}(Al_{5.95}Fe^{3+}_{0.05})\ B_3\ ^{T}(Si_{5.74}Al_{0.26})\ O_{27}\ ^{V}(OH)_3\ ^{W}[O_{0.36}F_{0.35}(OH)_{0.29}]$

HIM2: $^{X}(Na_{0.76}Ca_{0.07}K_{0.01}\square_{0.16})\ ^{Y}(Al_{1.14}Mn^{2+}_{0.50}Li_{0.49}Fe^{2+}_{0.45}Fe^{3+}_{0.11}Zn_{0.09}Ti^{4+}_{0.01}\square_{0.21})\ ^{Z}Al_6\ B_3$
$^{T}(Si_{5.77}Al_{0.20}B_{0.03})\ O_{27}\ ^{V}(OH)_3\ ^{W}[F_{0.69}(OH)_{0.26}O_{0.05}]$

HIM3: $^{X}(Na_{0.74}Ca_{0.12}\square_{0.14})\ ^{Y}(Al_{1.30}Mn^{2+}_{0.80}Li_{0.67}Fe^{3+}_{0.02}Fe^{2+}_{0.01}Ti^{4+}_{0.01}\square_{0.19})\ ^{Z}Al_6\ B_3\ ^{T}(Si_{5.78}Al_{0.17}B_{0.05})$
$O_{27}\ ^{V}(OH)_3\ ^{W}[F_{0.77}(OH)_{0.19}O_{0.04}]$

HIM4: $^{X}(Na_{0.51}Ca_{0.16}\square_{0.33})\ ^{Y}(Al_{1.80}Li_{1.08}Mn^{2+}_{0.01}\square_{0.11})\ ^{Z}Al_6\ B_3\ ^{T}(Si_{5.77}B_{0.23})\ O_{27}\ ^{V}(OH)_3$
$^{W}[F_{0.58}(OH)_{0.32}O_{0.10}]$

HIM5: $^{X}(Na_{0.51}Ca_{0.19}\square_{0.30})\ ^{Y}(Al_{1.62}Li_{1.13}Mn^{2+}_{0.09}Fe^{2+}_{0.01}\square_{0.15})\ ^{Z}Al_6\ B_3\ ^{T}(Si_{5.89}B_{0.11})\ O_{27}\ ^{V}(OH)_3$
$^{W}[F_{0.66}(OH)_{0.34}]$

HMGC1: $^{X}(Na_{0.59}Ca_{0.28}\square_{0.13})\ ^{Y}(Al_{1.38}Li_{0.91}Mn^{2+}_{0.27}Fe^{2+}_{0.21}Ti^{4+}_{0.02}\square_{0.21})\ ^{Z}(Al_{5.92}Mg_{0.08})\ B_3$
$^{T}(Si_{5.85}Al_{0.08}B_{0.07})\ O_{27}\ ^{V}(OH)_3\ ^{W}[F_{0.79}(OH)_{0.21}]$

SS4: $^{X}(Na_{0.53}Ca_{0.10}\square_{0.37})\ ^{Y}(Al_{1.80}Li_{1.05}Mn^{2+}_{0.02}\square_{0.13})\ ^{Z}Al_6\ B_3\ ^{T}(Si_{5.78}B_{0.23})\ O_{27}\ ^{V}(OH)_3\ ^{W}[(OH)_{0.54}F_{0.46}]$

For a more clear comparison the occupants of each site for every investigated sample together with the tourmaline species are listed in Table 6.

T-site occupancy. A spectroscopic investigation by MAS NMR of ^{11}B by Tagg et al. (1999) showed the presence of small amounts of $^{[4]}$B in the pale pink elbaite sample SS4 from the Himalaya mine. The results of site-scattering refinement and the reduced <*T*-O> distance in combination with the chemical data provide a confirmation of the existence of $^{[4]}$B (~0.2 apfu) in this sample (Table 2, 3, 4). Many of these investigated tourmaline samples contain a mixed occupation, with Si, Al and B at the T site. The core sample HIM1 (schorl) contains some $^{[4]}$Al (0.26 apfu) at the T site (Table 4). Towards the near-rim zone of HIM4 the amount of $^{[4]}$Al decreases while $^{[4]}$B increases (Table 4). The zone HIM4 and sample SS4 contain the highest amount of $^{[4]}$B (0.23 apfu; Table 4) of all investigated tourmaline samples from the Himalaya Mine. This value is consistent with the values that have been estimated by refinement (Table 2). In the rim (HIM5) the amount of $^{[4]}$B decreases further. In the late-stage crystallized elbaite sample HMGC1 from the Green Cap pocket a mixed occupation was found ($Si_{5.85}Al_{0.08}B_{0.07}$; Table 4). Similar to

investigated $^{[4]}$B-bearing tourmalines from other localities (Ertl et al. 2006, 2007) a positive correlation between Al at the Y site and $^{[4]}$B in tourmalines from the Himalaya Mine was found (r^2 = 0.93; Fig. 3). Another positive correlation was found between (Mn^{2+} + Fe^{2+}) and $^{[4]}$Al in tourmalines from the Himalaya Mine (r^2 = 0.99; Fig. 4). These correlations indicate that in the short-range order configurations ^{Y}Al is coupled with $^{[4]}$B (Ertl et al. 2006), whereas Mn^{2+} and Fe^{2+} are coupled with $^{[4]}$Al, as was already assumed by Ertl et al. (2003). It can be proposed that beryllium, which will also occupy the *T* site, is very low in the Fe-rich core (HIM1: BeO =7 ppm), but increases simultaneously with the Al content. HIM4, the zone with highest Al content also has the highest Be content (BeO = 76 ppm) (Table 4). A positive correlation between Al at the Y site and BeO for the zones HIM1(core) to HIM4 is shown in Fig. 5 (r^2 = 0.97). In the rim zone HIM5 ^{Y}Al and BeO is decreasing again.

Y-site and Z-site occupancy. The core sample of the strongly zoned crystal, an Al-rich "oxy-schorl", also contains a significant amount of Fe^{3+} (20%; Table 5). Mössbauer studies from the different zones within this crystal show that the relative fraction of Fe^{3+} increases continuously from the Fe-rich core towards to the Fe-poor rim (up to 85% Fe^{3+} in HIM4; Table 5), reflecting the increasing fugacity of oxygen in the pegmatite pocket. The highest amount of ^{Y}Al within these zones has the intermediate zone HIM4, a "fluor-elbaite" (Table 4, 6). This zone has also the highest amount of $^{[4]}$B within this crystal. There is already a significant Mn^{2+} content in the core (0.33 apfu), which is increasing in zone HIM2, and reaches the maximum content in zone HIM3 (0.80 apfu; ~6 wt% MnO; Table 4). In the next zone HIM4 it is very low (0.01 apfu), and in the rim HIM5 it is again increasing slightly (0.09 apfu). The Mg content in most samples is below detection limit. The Fe-rich core (HIM1) contains a small amount of Mg (0.01 apfu; Table 4). Interestingly the late-stage "fluor-elbaite" from the Green Cap pocket contains 0.34 wt% MgO (0.08 apfu; Table 4), which seems to be unusual for elbaite. It is not clear from what source this Mg content derived.

All investigated tourmaline samples contain vacancies at the Y site in the range of ~0.1-0.2 pfu (Table 4, 6). It is possible that small vacancies in Al-rich and Li-bearing, Fe-, Mn-, and Mg-poor tourmalines (elbaite, liddicoatite, olenite) could be real and not a result of systematic errors in chemical analyses, because many analyses (including the light elements) of such tourmalines by different authors show vacancies of ~0.1-0.2 pfu at the *Y* site (Ertl et al. 1997, 2003, 2004, 2006, 2007; Hughes et al. 2000, 2004; Kalt et al. 2001; Novák et al. 1999; Prowatke et al. 2003; Schreyer et al. 2002; Selway et al. 1998). Ertl et al. (2006) proposed short-range order configurations with $^{Y}(Al_2\square)$, which may be responsible for these vacancies. The chemical data of samples HIM2 and HMGC1 show total sums which are close to 100% (Table 4). Sample HIM2 is especially well-characterized because of three consistent water values. Both samples, HIM2 and HMGC1, show 0.21 pfu vacancies at the Y site (Table 4, 6).

A ^{7}Li MAS NMR spectrum of the light pink elbaite (sample SS4) shows one relatively sharp signal at *ca*. 0.1 ppm that gives further evidence that a significant amount of Li is present in this tourmaline sample. Actually, it is not possible to obtain information about the coordination number(s) of

Li from this spectrum, nor was it possible to distinguish between sites with the same coordination but of different size (Park et al. 2000a, 2000b). The Li content continuously increases from the core (HIM1) to the rim (HIM5). The nearly colorless "fluor-elbaite" rim (HIM5) has the highest Li content of all zones (Table 4). The F content increases, has its peak in the Mn^{2+}- and Al-rich "fluor-elbaite" zone (HIM3), decreases in zone HIM4 ($^{[4]}$B-bearing, Al-rich "fluor-elbaite"), and increases again in the rim zone HIM5 (Table 4). The elements Li and F that are normally coupled in abundance are decoupled in this zoned tourmaline crystal. The highest F content with 0.79 apfu shows the late-stage "fluor-elbaite" from the Green Cap pocket. There is an inverse correlation between the lattice parameter *a* and the Li content (r^2 = 0.96; Fig. 6) for all tourmalines with lattice parameters ≥15.84 Å. Lattice parameters below this value can be derived by an increasing $^{[4]}$B content and by a decreasing Li content (e.g., data from Ertl et al. 2006, 2007).

Ertl et al. (2003) proposed that the lattice parameter *a* of Mn-rich (Li-bearing) tourmalines is largely a function of the cation occupancy of the Y site (r^2 = 0.97). Bosi et al. (2005) showed that along the elbaite-schorl series in samples from the Cruzeiro pegmatite, Minas Gerais, Brazil, <Y-O> is inversely correlated with ^{Y}Al (r^2 = 0.96). A similar correlation was observed in tourmalines of the elbaite-schorl series from the Himalaya Mine (r^2 = 0.94). However, an inverse correlation between <Y-O> and the Al and Fe^{3+} content (Al + 0.4Fe^{3+}) at the Y site in these tourmalines gave a better residual value (r^2 = 0.96; Fig. 7). Similar to Al, Fe^{3+} also has a relatively low effective ionic radius compared to Fe^{2+}, Mn^{2+}, and Li (Shannon 1976). To prove if a general trend is present, I also included in this correlation other recent data from ^{Y}Al-, Li- and Fe-bearing tourmalines (Bosi et al. 2005; Burns et al. 1994; Cámara et al. 2002; Ertl et al. 2005, 2006; Hughes et al. 2002, 2004; Schreyer et al. 2002). Although more samples were included, the r^2 value was higher (r^2 = 0.98; Fig. 8). Because Fe-rich tourmalines from Li-pegmatites can contain a significant Fe^{3+}-component (Table 5) it is important also to include this component into that correlation (Fig. 7, 8). There is a very good positive correlation between the lattice parameter *a* and the (Fe^{2+} + Mn^{2+}) content (r^2 = 0.99; Fig. 9) for tourmaline samples with lattice parameters ≥15.84 Å. Lattice parameters below this value can be derived by an increasing $^{[4]}$B content (as pointed out before) and usually by a (Fe^{2+} + Mn^{2+}) content of <0.1 apfu (Ertl et al. 2006, 2007; Bosi et al. 2005; Schreyer et al. 2002). There exists a positive correlation between the <Y-O> distance and the <T-O> distance (r^2 = 1.00; Fig. 10), which is valid for all samples from the Himalaya Mine with <1.8 apfu Al at the Y site.

A positive correlation was found between <Y-O> and <Z-O> in all samples from the Himalaya Mine, which contain only Al at the Z site (r^2 = 0.89; Fig. 11). This correlation can be explained by inductive effects of <Y-O> by <Z-O> because two oxygen atoms (O2 and O3) are shared by the YO_6 and the ZO_6 octahedra.

X-site occupancy. The Ca content increases continuously from core (HIM1) to rim (HIM5). The sample HMGC1 has the highest content of Ca. A nearly colorless, late-stage "fluor-elbaite" from the Green Cap pocket has the highest Ca content of all tourmalines from this study. There is an inverse correlation between Ca and <X-O> in Li-rich tourmalines (>0.60 apfu Li) from the Himalaya Mine (r^2 = 0.96; Fig. 12). The Na content increases from Fe-rich inner core (HIM1) to the outer core (HIM2), and decreases then in the zones HIM3 and HIM4. Only the Fe-rich inner and outer core samples (HIM1, HIM2) show a significant K content (0.01 apfu; Table 4). The highest vacancies at the X site ($\square_{0.38}$) of all investigated samples shows the inner core sample (HIM1). There is a very good positive correlation between the F content and the X-site charge in tourmalines from the Himalaya Mine (r^2 = 1.00; Fig. 13). This correlation is not valid for Mg-bearing (>0.01 apfu Mg) and Ca-rich samples (>0.20 apfu Ca) as sample HMGC1. The X-site vacancy and the F content are inversely correlated in tourmalines from the Himalaya Mine (r^2 = 0.89; Fig. 14).

V- and W-site occupancy. The elements Li and F that are normally coupled in abundance are decoupled in this zoned tourmaline. Whereas F increases simultaneously with the Li content in the zones HIM1 to HIM3, there is a lower F value in the zones HIM4 and HIM5 (compared to zone HIM3), while the Li content is still increasing. In the HIM sample I could observe lepidolite inclusions only in the zones HIM4 and HIM5. Hence, it seems that the F content in tourmaline decreases when lepidolite begins to crystallize because a significant F content is partitioned into lepidolite.

Accurate OH contents of tourmalines have proven difficult to obtain (e.g., Ertl et al., 2005). This study provided the opportunity to compare several independent methods of OH determination.

Ottolini and Hawthorne (1999) demonstrated that, in the case of elbaitic tourmalines, it is a reasonable assumption to calculate the OH content as OH = 4 - F *apfu,* as the bond-valence requirements of O^{2-} at the O1 and O3 sites cannot be satisfied with Li at the Y site. Chemical analyses (including the light elements) of the samples HIM5, HMGC1 and SS4, of elbaites from other localities (Dyar et al. 1998; Federico et al. 1998; Novák et al. 1999; Cámara et al. 2002), of the elbaitic olenite from the type locality in Russia (Schreyer et al. 2002), and also of rossmanite from the type locality (Selway et al. 1998) are supportive of this assumption.

For tourmalines of the series schorl-elbaite where FeO + MnO > 8 wt%, the sum of OH + F is about 3.5-3.7 *apfu* (this study; Dyar et al. 1998; Federico et al. 1998; Novák et al. 1999, Table 2, sample 8-1-1). For tourmalines from this study with (FeO + MnO) < 8 wt% the sum of OH + F ≈ 4 (3.9-4.2 pfu; Table 4). Hence, I conclude that the approximate assumption OH = 4 - F is only valid for elbaitic tourmalines that are relatively low in Fe and Mn (FeO + MnO < 8 wt%).

The sum of OH + F of the boron-rich olenite from Styria, Austria, with an occupation of ~($Al_{2.4}Li_{0.4}\square_{0.2}$) at the Y site, is ~3.4 pfu (Ertl et al. 1997; Hughes et al. 2000). For "oxy-rossmanite", another Al-rich tourmaline, from Eibenstein an der Thaya, Lower Austria, with an occupation of

~($Al_{2.4}Li_{0.3}Mn^{2+}_{0.3}$) at the Y site, the sum of OH + F is ~3.0 pfu (Ertl et al. 2005). These relatively low values for OH + F are mainly a consequence of the relatively high Al^{3+}-content at the Y site.

Analysis of water in elbaites is problematic because the crystals often contain fluid inclusions. Thus, conventional methods that extract water from a bulk sample may give erroneous values. Methods that allow the distinction between structural OH and fluid inclusions, like IR spectroscopy, offer advantages for future tourmaline analyses. Finally, these analyses indicate that some elbaites contain a mixed occupation of F, OH and O at the W site, as pointed out before.

Direct determination of the OH. A variety of methods discussed above were used to determine the absolute hydrogen concentration in tourmalines HIM1-5 and HMGC1. The results are tabulated below.

	Micro-extraction	U-extraction	SIMS	IR overtones
Sample	Wt% H_2O (Std. Dev.)	Wt% H_2O	Wt% H_2O	Wt% H_2O
HIM1	3.20(7)	2.90	2.75	2.97
HIM2	2.99(2)	2.95	3.03	3.14
HIM3	-	2.75	3.16	3.22
HIM4	3.30(4)	3.01	3.28	3.28
HIM5	3.52(8)	3.70	3.30	3.36

2.5 CONDITIONS OF FORMATION FOR TOURMALINE-BEARING CAVITIES IN THE HIMALAYA DIKE

Overview. Chemical petrologists tend to regard tourmaline as a "garbage-can" mineral, a phase with exceedingly variable compositions record in some simple, direct way the chemical variations of the medium from which the tourmaline crystals grew (e.g., Jolliff et al. 1986). Crystallographers recognize that the complex compositions of tourmaline arise from highly coupled substitutions among multiple crystallographic sites (e.g., this study), such that the structure of tourmaline dictates the composition to a large degree. Both perspectives are correct to an extent. The chemical variations from dark core to light rim in sample HIM (GRR 2254) record some very commonly observed changes from aluminous Fe-rich schorl to Mn, Li, and F-rich elbaite, but not in such a way that it can be deduced with confidence the composition of the medium from which the tourmaline grew (e.g., Na and F are highly correlated, but Li and F are not, even though it can be expected that the Li content of the tourmaline-forming medium in the pockets was high, and at the maximum for the dike).

Tourmaline of the common solid solutions among schorl-dravite, foitite, and olenite is stable over a wide range of conditions (e.g., Rosenberg and Foit 1979; London et al. 1996; Wolf and London 1997), such that the presence of tourmaline normally offers little insight into the pressures and temperatures attending the formation of pockets. Elbaite, however, has not been reliably synthesized. Two studies that cite elbaite growths are incomplete and methodologically flawed (Tomisaka 1968; Vorbach 1989). Efforts by one of us (DL) using synthetic mixes with and without elbaite starting materials have failed to find a stability field for elbaite at 200 MPa and temperatures from 450°-700°C.

Chemical Conditions. In addition to fluorine-rich elbaite, minerals including hambergite, $Be_2BO_3(OH)$, and stibiotantantalite, $Sb(Ta,Nb)O_4$, attest to a high degree of chemical fractionation attained at the pocket stage of the Himalaya dike. The border zone along portions of the Himalaya dike is biotite granite lacking even "black" tourmaline or garnet. Though not unusual, the chemical fractionation from margins to pocket was extremely efficient in this dike.

Arredondo et al. (2001) deduced that the activity of H_2O increased from pegmatite margins to pocket zone during crystallization of the Himalaya dike based on the low but increasing hydroxyl content of garnet. This is an important observation, because if correct, it implies that the magma filling the dike was not H_2O-saturated until the end. Had the magma been saturated from the start, then the activity of H_2O would not have varied except slightly for the effects of cooling (Burnham, 1979). An abundance of Fe^{2+} and Fe^{3+} in tourmaline, but no Mn^{3+} in tourmaline or garnet, loosely brackets the oxidation state of the system between FMQ and manganosite (Mn^{2+}) -hausmanite (mixed Mn^{2+}-Mn^{3+}) (Huebner and Sato 1970). Reinitz and Rossman (1988) concluded that the pink color of elbaite results from oxidation of Mn^{2+} to Mn^{3+} *via* natural ionizing radiation, i.e., after the formation of Mn^{2+}-bearing tourmaline. The fO_2 with the pockets, however, was probably closer to the equilibrium between manganosite-hausmanite because mixed Mn^{2+}-Mn^{3+} phosphates and oxides are common products of subsolidus reactions in similarly evolved pegmatites (e.g., London and Burt 1981).

The abundance of elbaite and lepidolite reflect high concentrations of B and F in the pocket-forming medium. That medium would have become alkaline and sodic, as speciation reactions increasingly favor the formation of alkali fluoride and borate components. With the formation of alkali borates and fluorides in melt or vapor, the cognate crystalline assemblage becomes increasingly silicic, potassic, and peraluminous (London 1989, 2004). Consequently, potassic minerals (micas, K-feldspar), peraluminous minerals (mica, tourmaline, topaz), and abundant quartz dominate the pocket-zone assemblage. In the Himalaya tourmaline (sample HIM), increasing Na and F from core to margin result from increasing sodium fluoride component of the growth medium.

At the pocket stage in the Himalaya dike, iron and manganese were probably limiting components on the amount of tourmaline that could form. Iron contents are near or at detection level in the colorless or light-colored specimens analyzed for this study. In addition, the presence of hambergite signifies an excess of boron over that needed to form tourmaline. Wolf and London (1997) observed that when iron is a

limiting component of tourmaline-forming reactions (i.e., boron in excess), then the total Fe content of coexisting melt drops to near-detection levels (by EMPA). Saturation in spessartine buffers the Mn content of pegmatitic melts at ~ 1 wt% MnO (London et al., 2001). As the activities of Li and F components rise through crystal fractionation, however, then these components plus Mn become compatible in micas and in tourmaline. Once Mn becomes compatible in Li-tourmaline and micas, then spessartine becomes unstable (London et al. 2001), and the ~1 wt% MnO in the residual melt is subsequently distributed among competing phases (mostly micas and tourmaline, but also tantalates, phosphates, etc.).

Zeolites including laumontite, stilbite, and heulandite, clays including kaolinite, palygorskite, cookeite, and Ca-Mg-montmorillonite, calcite, and an abundance of iron oxide staining constitute the last association of pocket-forming minerals in the Himalaya dike (Foord et al., 1986). From a chemical standpoint, the abundance of zeolites, palygorskite, montmorillonite, and calcite represents a "late-stage mini-flood of Ca" (Jahns 1981), which Jahns (1981) ascribed to back reaction and leaching of early-formed pegmatitic plagioclase, but which Foord et al. (1986) and London (2005) attribute mostly to bi-metasomatic exchange between pegmatite pockets and mafic host rocks. The principal question is where kaolinite fits in the paragenetic sequence. Foord et al. (1986) believed it to be the last product of pocket consolidation. Considering the low levels of Mg (Fe, and Ca) in the late-stage elbaite, and the correspondingly low levels of these constituents in the coexisting melt, London (2008) proposed that the kaolinite should be the first-formed clay in the pocket, with other CaMg-products forming from kaolinite as the pockets become open to an influx of components from the host rocks. The pervasive, deep-red staining from iron oxides, however, is almost certainly a result of influx to the pocket zones from surrounding rocks. That Fe could not have been present at the time when the elbaite crystallized.

Pressure-Temperature Conditions. The pressure and temperature during pocket formation in the Himalaya dike have been estimated, but the conditions remain uncertain. The dike lacks lithium aluminosilicates, which have proven useful for deducing the relative P-T conditions of Li-rich pegmatites (London 1984). Feldspar thermometry has been applied successfully to other miarolitic pegmatites in San Diego County (Morgan and London 1999), where temperatures indicated inward crystallization of the Little Three dike, Ramona, along an isotherm of ~ 400°-450°C, dropping perhaps to 375°-400°C at the pocket stage. Though feldspar thermometry has not been conducted on the Himalaya dike, temperatures in the range of 375°-400°C would be consistent with the deposition of zeolites and clays immediately following the crystallization of tourmaline (e.g., Thompson 1970; Abdel-Samad et al. 1989).

An oxygen and hydrogen isotopic study by Taylor et al. (1979) constitutes the most thorough source of information about the temperatures of crystallization in the Himalaya dike. That work, however, contains a peculiar contradiction. Based on oxygen isotope fractionations between coexisting quartz-K-feldspar and quartz-muscovite, Taylor et al. (1979) state that the crystallization of the dike began at ~ 730°C upon emplacement, and that the temperature fell to 565°-525°C at the stage of pocket formation.

Fig. 16 shows their actual data plotted on their Figure 7 as derived from their Table 1 (Taylor et al. 1979). Despite a large spread, the temperatures of the main pegmatitic stage cluster around the ***low-temperature*** end of their calibration, between 550° and 650°C, and the pocket zone actually falls at the ***high-temperature*** end, close to 700°C. This is not a typographic or drafting error: the values of $\delta^{18}O$ for quartz, K-feldspar, and muscovite are lower, and fractionation factors between them smaller, in minerals from the pocket zone than in the massive pegmatite (see Table 1 in Taylor et al. 1979).

Taylor et al. (1979) used isochores derived from fluid inclusions in quartz from the miarolitic cavities to correct homogenization temperatures to entrapment temperatures at 570°C, the temperature of pocket formation as represented by their oxygen isotopic data, with the resultant pressure estimate of 200 to 210 MPa. Thus, Taylor et al. (1979) put the Himalaya dike at 725°C, 210 MPa, upon emplacement. London (1986) recalculated the fluid inclusion isochores from the complete data set in Foord (1976) and found that the isochores possessed steeper P-T slopes. London (1986) observed that spodumene is more common than petalite in most tourmaline-rich miarolitic pegmatites, and so London (1986) extrapolated Foord's (1976) isochores to the reaction boundary between spodumene, petalite, and quartz (London 1984). That process yielded an estimate of 425°-475°C and 240-280 MPa for pocket formation, similar to a larger inclusion data set from spodumene- and elbaite-rich pegmatites in Afghanistan (London, 1986). Though the temperature appears to be reasonable based on the associated zeolites and clays, the pressure is higher than anticipated for the miarolitic class of pegmatites. This led Černý and Ercit (2005) to catalogue the spodumene- and elbaite-rich miarolitic pegmatites more in line with the massive rare-element pegmatites than with the other types of miarolitic bodies. London (2008) has perhaps reconciled the disparity by suggesting that small, thin dikes like the Himalaya crystallize ~150°-250°C below their liquidus temperatures all the way to the end of their consolidation, and pocket temperatures of 350°-400°C would bring the Himalaya pegmatite in line with lower pressures (200 MPa) and the isochoric extrapolations (but still in the field of petalite, not spodumene).

Physical state of the pocket-forming medium. Hydrothermal aqueous fluid containing small quantities of CO_2 and low to very low total salinities typify the compositions of fluid inclusions trapped by quartz and some other minerals in miarolitic cavities from Li- and B-rich pegmatites (Foord 1976; London 1986; Foord et al. 1991). Though this may represent a fluid phase that was last in contact with the miarolitic crystalline materials, it does not represent the bulk composition of the medium from which those crystals grew. That bulk medium would have been alkaline, flux-rich, silicate-rich, and H_2O-rich. It might have consisted of multiple coexisting fluid phases, or a single fluid phase, because high alkalinity, flux content, and H_2O content all serve to enhance miscibility among silicate and aqueous components (reviewed in London 2005, 2008). In the very few experimental simulations or measurements on these types of hydrous, flux-rich fluids, their viscosities at 500°-550°C and elevated fluid pressures are exceedingly low: < 10 Pa, which is the viscosity of vegetable or mineral oil at 25°C (see summaries in

London 2005, 2008). Fluids of such low viscosity could not suspend crystals, and hence all crystallization from such a fluid must be anchored to the sidewalls of the cavity. This is in fact how most crystallization appears in miarolitic cavities of pegmatites: inward from and initially anchored to the sidewalls of the pockets. However, miarolitic cavities in pegmatites, including the Himalaya dike, are commonly packed with dense clay, and large, perfect crystals and crystal fragments are suspended in that clay. London (2005) noted that an experimental fluid phase of composition (sodic, 18.3 wt% B_2O_3, 13.5 wt% H_2O) similar to those inferred for the alkaline, flux-rich late-stage liquids in miarolitic cavities could be quenched to a durable, water-insoluble glass. London (2005) suggested, therefore, that such fluids must undergo very large and rapid changes in viscosity upon cooling, from the low-viscosity fluid described above at 500°-550°C to glass at low temperatures. Whether the pocket-forming fluid solidifies directly to glass, or goes through a gellation step prior to reaching a glass transition, is not known. However, the pocket clays themselves resemble the products of gel crystallization (very fine-grained and massive) more than devitrified glass (which tends to develop radial spherules). Whether gel or glass, the transition from low- to high-viscosity of the pocket-forming medium occurs before the primary crystallization within the pockets has ceased. If the glass (or gel) transition temperatures for such flux-rich liquids can be measured, then the actual temperatures of pocket formation would be better constrained.

2.6 ACKNOWLEDGMENTS

Samples from the Himalaya Mine and collecting permissions at the mine were provided by William F. Larson, Fallbrook, California. William B. Simmons Jr., University of New Orleans, loaned pink elbaite sample SS4. Special thanks are due to K. Ferguson for the H_2O determination by U-extraction. I am grateful to Bernd Marler and Sandra Grabowski, Bochum, Germany, who assisted for the NMR measurements. Special thanks to A. Wagner, Vienna, Austria, for sample preparation work. This work was supported in part by Österreichischer Fonds zur Förderung der wissenschaftlichen Forschung (FWF) project no. P20509.

2.7 REFERENCES CITED

Abdel-Samad, F.A., Hassanein, S.A., and Rabie, F.H. (1989) Stability diagram of palygorskite-smectite system and its application in Calcareous soils. Egyptian Journal of Soil Science, 29, 237-249.

Arredondo, E.H., Rossman, G.R., and Lumpkin, G.R. (2001) Hydrogen in spessartine-almandine garnets as a tracer of granitic pegmatite evolution. American Mineralogist, 86, 485-490.

Bancroft, P. (1984) Gem and crystal treasures. Fallbrook, California. Western Enterprises/Mineralogical Record, Inc., 98-110.

Blattner, P. and Bird, G.W. (1974) Oxygen isotope fractionation between quartz and K-feldspar at 600□C. Earth and Planetary Science Letters, 23, 21-27.

Bosi, F., Andreozzi, G.B., Federico, M., Graziani, G., and Lucchesi, S. (2005) Crystal chemistry of the elbaite-schorl series. American Mineralogist, 90, 1784-1792.

Bruker AXS Inc. (2003) Sadabs. Bruker AXS Inc., Madison, Wisconsin, USA.

Buerger, M.J., Burnham, C.W., and Peacor, D.R. (1962) Assessment of the several structures proposed for tourmaline. Acta Crystallographica, 15, 583-590.

Burnham, C.W (1979) Magmas and hydrothermal fluids. In Geochemistry of hydrothermal ore deposits, 2nd ed. (Barnes, H.L, ed.). John Wiley and Sons, New York, 71-136.

Burns, P.C., MacDonald, D.J., and Hawthorne, F.C. (1994) The crystal chemistry of manganese-bearing elbaite. Canadian Mineralogist, 32, 31-41.

Cámara, F., Ottolini, L., and Hawthorne, F. (2002) Crystal chemistry of three tourmalines by SREF, EMPA, and SIMS. American Mineralogist, 87, 1437-1442.

Černý, P. and Ercit, T.S. (2005) The classification of granitic pegmatites revisited. Canadian Mineralogist, 43, 2005-2026.

Dyar, M.D., Francis, C.A., Wise, M.A., Guidotti, C.V., McGuire, A.V., and Robertson, J.D. (1994) Complete chemical characterization of tourmaline. Eos, Transactions of the American Geophysical Union, 75, Spring Meeting Supplement no. 16, 187.

Dyar, M.D., Taylor, M.E., Lutz, T.M., Francis, C.A., Guidotti, C.V., and Wise, M. (1998) Inclusive chemical characterization of tourmaline: Mössbauer study of Fe valence and site occupancy. American Mineralogist, 83, 848-864.

Dyar, M.D., Wiedenbeck, M., Robertson, D., Cross, L.R., Delaney, J.S., Ferguson, K., Francis, C.A., Grew, E.S., Guidotti, C.V., Hervig, R.L., Hughes, J.M., Husler, J., Leeman, W., McGuire, A.V., Rhede, D., Rothe, H., Paul, R.L., Richards, I., and Yates, M. (2001) Reference Minerals for the Microanalysis of Light Elements. Geostandards Newsletter, 25, 441-463.

Ertl, A. and Hughes, J.M. (2002) Crystal structure of aluminum-rich schorl overgrown by boron-rich olenite from Stoffhütte, Koralpe, Austria. Mineralogy and Petrology, 75, 69-78.

Ertl, A., Pertlik, F., and Bernhardt, H.-J. (1997) Investigations on olenite with excess boron from the Koralpe, Styria, Austria. Österreichische Akademie der Wissenschaften, Mathematisch-Naturwissenschaftliche Klasse, Abteilung I, Anzeiger, 134, 3-10.

Ertl, A., Hughes, J.M., Prowatke, S., Rossman, G.R., London, D., and Fritz, E.A. (2003) Mn-rich tourmaline from Austria: structure, chemistry, optical spectra, and relations to synthetic solid solutions. American Mineralogist, 88, 1369-1376.

Ertl, A., Schuster, R., Prowatke, S., Brandstätter, F., Ludwig, T., Bernhardt, H.-J., Koller, F., and Hughes J.M. (2004) Mn-rich tourmaline and fluorapatite in a Variscan pegmatite from Eibenstein an der Thaya, Bohemian massif, Lower Austria. European Journal of Mineralogy, 16, 551-560.

Ertl, A., Rossman, G.R., Hughes, J.M., Prowatke, S., and Ludwig, T. (2005) Mn-bearing "oxy-rossmanite" with tetrahedrally-coordinated Al and B from Austria: structure, chemistry, and infrared and optical spectroscopic study. American Mineralogist, 90, 481-487.

Ertl, A., Hughes, J.M., Prowatke, S., Ludwig, T., Prasad, P.S.R., Brandstätter, F., Körner, W., Schuster, R., Pertlik, F., and Marschall, H. (2006) Tetrahedrally-coordinated boron in tourmalines from the liddicoatite-elbaite series from Madagascar: Structure, chemistry, and infrared spectroscopic studies. American Mineralogist, 91, 1847-1856.

Ertl, A., Hughes, J.M., Prowatke, S., Ludwig, T., Brandstätter, F., Körner, W., and Dyar, M.D. (2007) Tetrahedrally-coordinated boron in Li-bearing olenite from "mushroom" tourmaline from Momeik, Myanmar. Canadian Mineralogist, 45, 891-899.

Federico, M., Andreozzi, G.B., Lucchesi, S., Graziani, G., and Cesarmendes, J. (1998) Compositional variation of tourmaline in the granitic pegmatite dykes of the Cruzeiro Mine, Minas Gerais, Brazil. Canadian Mineralogist, 36, 415-431.

Fischer, R.X. and Tillmanns, E. (1988) The equivalent isotropic displacement factor. Acta Crystallographica, C44, 775-776.

Foit, F.F., Jr. (1989) Crystal chemistry of alkali-deficient schorl and tourmaline structural relationships. American Mineralogist, 74, 422-431.

Foit, F.F., Jr. and Rosenberg, P.E. (1979) The structure of vanadium-bearing tourmaline and its implications regarding tourmaline solid solutions. American Mineralogist, 64, 788-798.

Foord, E.E. (1976) Mineralogy and petrogenesis of layered pegmatite-aplite dikes in the Mesa Grande district, San Diego County, California. Ph. D. thesis, 326 p., Stanford University, Stanford, California, U.S.A.

Foord, E.E. (1977) Famous Mineral Localities: The Himalaya Dike System, Mesa Grande District, San Diego County, California. Mineralogical Record, 8, Number 6, 461-474.

Foord, E.E., Starkey, H.C., and Taggart, J.E., Jr. (1986) Mineralogy and paragenesis of "pocket" clays and associated minerals in complex granitic pegmatites, San Diego County, California. American Mineralogist, 71,.428-439.

Foord, E.E., London, D., Kampf, A.R., Shigley, J.E., and Snee, L.W. (1991) Gem-bearing pegmatites of San Diego County, California. In Geological excursions in southern California and Mexico (Walawender, M.J. and Hanan, B.B., eds.). Department of Geological Sciences, San Diego State University, San Diego, California, 128-146.

Fisher, J., Foord, E. E., and Bricker, G. A. (1998) The geology, mineralogy, and history of the Himalaya mine, Mesa Grande, San Diego County, California. Rocks & Minerals, Volume 73, May/June.

Frenz, B.A. (1997) SDP for Windows Reference Manual. B.A. Frenz & Associates, Inc., College Station, Texas, 201 pps.

Gonzalez-Carreno, T., Fernandez, M., and Sanz, J. (1988) Infrared and Electron Microprobe Analysis of Tourmalines. Physics and Chemistry of Minerals, 15, 452-460.

Hawthorne, F.C. and Henry, D.J. (1999) Classification of the minerals of the tourmaline group. European Journal of Mineralogy, 11, 201-215.

Hawthorne, F.C. (2002) Bond-valence constraints on the chemical composition of tourmaline. Canadian Mineralogist, 40, 789-797.

Huebner, J.S. and Sato, M. (1970) The oxygen fugacity-temperature relationships of manganese oxide and nickel oxide buffers. American Mineralogist, l.55, 934-952.

Hughes, J.M., Ertl, A., Dyar, M.D., Grew, E.S., Shearer, C.K., Yates, M.G., and Guidotti, C.V. (2000) Tetrahedrally coordinated boron in a tourmaline: Boron-rich olenite from Stoffhütte, Koralpe, Austria. Canadian Mineralogist, 38, 861-868.

Hughes, J.M., Ertl, A., Dyar, M.D., Grew, E., Wiedenbeck, M., and Brandstätter, F. (2004) Structural and chemical response to varying $^{[4]}$B content in zoned Fe-bearing olenite from Koralpe, Austria. American Mineralogist, 89, 447-454.

Hughes, K.-A., Hughes, J.M., and Dyar, M.D. (2001) Chemical and structural evidence for $^{[4]}B \Leftrightarrow {}^{[4]}Si$ substitution in natural tourmalines. European Journal of Mineralogy, 13, 743-747.

Jolliff, B.L., Papike, J.J., and Shearer, C.K. (1986) Tourmaline as a recorder of pegmatite evolution: Bob Ingersoll pegmatites, Black Hills, South Dakota. American Mineralogist, 71, 472-500.

Kalt, A., Schreyer, W., Ludwig, T., Prowatke, S., Bernhardt, H.-J., and Ertl, A. (2001): Complete solid solution between magnesian schorl and lithian excess-boron olenite in a pegmatite from Koralpe (eastern Alps, Austria). European Journal of Mineralogy, 13, 1191-1205.

London, D. (1984) Experimental phase equilibria in the system $LiAlSiO_4$-SiO_2-H_2O: a petrogenetic grid for lithium-rich pegmatites. American Mineralogist, 69, 995-1004.

London, D. (1986) Formation of tourmaline-rich gem pockets in miarolitic pegmatites. American Mineralogist, 71, 396-405.

London, D. (1989) Lithophile rare element concentration in silicic rocks: the alkaline trend in granitic systems. (abstr) Geological and Mineralogical Associations of Canada, Program with Abstracts, 14, A21.

London, D. (2004) Vertical zonation of alkalis in mineralized granites and pegmatites. (abstr). Geological and Mineralogical Associations of Canada, Abstracts Volume, 29, 197.

London, D. (2005) Granitic pegmatites: an assessment of current concepts and directions for the future. Lithos, 80, 281-303.

London, D. (2008) Pegmatites. Canadian Mineralogist Special Publication, in press.

London, D. and Burt, D.M. (1982) Alteration of spodumene, montebrasite, and lithiophilite in pegmatites of the White Picacho district, Arizona. American Mineralogist, 67, 97-113.

London, D., Morgan, G.B. VI, and Wolf, M.B. (1996) Boron in granitic rocks and their contact aureoles. In Boron: Mineralogy, Petrology, and Geochemistry of Boron in the Earth's Crust (Grew, E.S. and Anovitz, L., eds.), Mineralogical Society of America Reviews in Mineralogy, 33, 299-330.

London, D., Evensen, J.M., Fritz, E., Icenhower, J.P., Morgan, G.B. VI, and Wolf, M.B. (2001) Enrichment and accommodation of manganese in granite-pegmatite systems. (abstr) 11th Annual Goldschmidt Conference Abstract 3369, Lunar Planetary Institute Contribution 1088, Lunar Planetary Institute, Houston (CD-ROM).

Long, G.J., Cranshaw, T.E., and Longworth, G. (1983) The ideal Mössbauer effect absorber thickness. Mössbauer Effect Ref. Data J., 6, 42-49.

Marler, B. and Ertl, A. (2002) Nuclear magnetic resonance and infrared spectroscopic study of excess-boron olenite from Koralpe, Styria, Austria. American Mineralogist, 87, 364-367.

Marler, B., Borowski, M., Wodara, U., and Schreyer, W. (2000) The structure of synthetic excess-boron-tourmaline. Berichte der Deutschen Mineralogischen Gesellschaft, Beihefte zum European Journal of Mineralogy, 12, No. 1, 120 (abstract).

Marler, B., Borowski, M., Wodara, U., and Schreyer, W. (2002) Synthetic tourmaline (olenite) with excess boron replacing silicon in the tetrahedral site: II. Structure analysis. European Journal of Mineralogy, 14, 763-771.

Marschall, H.R. and Ludwig, T. (2004) The low-boron contest: minimising surface contamination and analysing boron concentrations at the ng/g-level by secondary ion mass spectrometry. Mineralogy and Petrology, 81, 265-278.

MacDonald, D.J. and Hawthorne, F.C. (1995) The crystal chemistry of Si ⇔ Al substitution in tourmaline. Canadian Mineralogist, 33, 849-858.

Morgan, G.B. VI and London, D. (1999) Crystallization of the Little Three layered pegmatite-aplite dike, Ramona District, California. Contributions to Mineralogy and Petrology, 136, 310-330.

Novák, M., Selway, J.B., Černý, P., Hawthorne, F.C., and Ottolini, L. (1999) Tourmaline of the elbaite-dravite series from an elbaite-subtype pegmatite at Bližná, southern Bohemia, Czech Republik. European Journal of Mineralogy, 11, 557-568.

O'Leary, J.A., Rossman, G.R., and Eiler, J.M. (2007) Hydrogen analysis in minerals by continuous-flow mass spectrometry. American Mineralogist, 92, 1990-1997.

O'Neil, J.R. and Taylor, H.P. (1967) The oxygen isotope and cation exchange chemistry of feldspars. American Mineralogist, 52, 1414-1437.

O'Neil, J.R. and Taylor, H.P. (1969) Oxygen isotope equilibrium between muscovite and water. Journal of Geophysical Research, 74, 6012-6022.

Ottolini, L., and Hawthorne, F.C. (1999) An investigation of SIMS matrix effects on H, Li and B ionization in tourmaline. European Journal of Mineralogy, 11, 679-690.

Park, S.H., Daniels, P., and Gies, H. (2000a) RUB-23, a new microporous lithosilicate containing spiro-5 building units. Microporous and Mesoporous Materials 37, no. 2, 129-143.

Park, S.-H., Parise, J.B., Gies, H., Liu, H., Grey, C.P., and Toby, B.H. (2000b) A new porous lithosilicate with a high ionic conductivity and ionexchange capacity. Journal of the American Chemical Society, 122(44), 11023-11024.

Perkins, W.T., Pearce, N.J.G., and Westgate, J.A. (1997) The development of laserablation ICP-Ms and calibration strategies; examples from the analyses of trace elements in volcanic glass shards and sulfide minerals. Geostandards Newsletter, 21, 115-144.

Pieczka, A., Kraczka, J., and Zabinski, W. (1997) Mössbauer spectra of Fe^{3+}-poor schorls: reinterpretation of the spectra on a basis of an ordered structure model. Abstract to Tourmaline 1997 International Symposium on Tourmaline, Nové Mesto na Morave, Czech Republic, 74-75.

Prince, E., Donnay, G., and Martin, R.F. (1973) Neutron diffraction refinement of an ordered orthoclase structure. American Mineralogist, 58, 500-507.

Prowatke, S., Ertl, A., and Hughes, J.M. (2003) Tetrahedrally-coordinated Al in Mn-rich, Li- and Fe-bearing olenite from Eibenstein an der Thaya, Lower Austria: A chemical and structural investigation. Neues Jahrbuch Mineralogie Monatshefte, 2003, 385-395.

Reinitz, I.M. and Rossman, G.R. (1988) The role of natural radiation in tourmaline coloration. American Mineralogist 73, 822-825.

Rosenberg, P.E and Foit, F.F., Jr. (1979) Synthesis and characterization of alkali-free tourmaline. American Mineralogist, 64, 180-186.

Schreyer, W., Wodara, U., Marler, B., van Aken, P.A., Seifert, F., and Robert, J.L. (2000) Synthetic tourmaline (olenite) with excess boron replacing silicon in the tetrahedral site: I. Synthesis conditions, chemical and spectroscopic evidence. European Journal of Mineralogy, 12, 529-541.

Schreyer, W., Hughes, J., Bernhardt, H.-J., Kalt, A., Prowatke, S., and Ertl, A. (2002) Tetrahedral boron in olenite from the type locality: A chemical and structural investigation. European Journal of Mineralogy, 14, 935-942.

Selway, J.B., Novák, M., Hawthorne, F.C., Černý, P., Ottolini, L., and Kyser, T.K. (1998) Rossmanite, □$(LiAl_2)Al_6(Si_6O_{18})(BO_3)_3(OH)_4$, a new alkali-deficient tourmaline: Description and crystal structure. American Mineralogist, 83, 896-900.

Shannon, R.D. (1976) Revised effective ionic radii and systematic studies of interatomic distances in halides and chalcogenides. Acta Crystallographica, A32, 751-767.

Snee, L.W. and Foord, E.E. (1991) $^{40}Ar/^{39}Ar$ thermochronology of granitic pegmatites and host rocks, San Diego County, California. Geological Society of America Annual Meeting abstracts with programs, San Diego, California, Oct. 21-24, 1991, 23(5), 189.

Sokolov, P.B., Gorskaya, M.G., Gordienko, V.V., Petrova, M.G., Kretser, Yu.L., and Frank-Kamentskii, V.A. (1986) Olenite, $Na_{1-x}\ Al_3\ Al_6\ B_3\ Si_6\ O_{27}\ (O,OH)_4$ – novyy vysokoglinozemistyy mineral iz gruppy turmalinov. Translated title: Olenite $Na_{1-x}\ Al_3\ Al_6\ B_3\ Si_6\ O_{27}\ (O,OH)_4$ – a new high-alumina mineral of the tourmaline group. (in Russian) Zapiski Vsesoyuznogo Mineralogicheskogo Obshchestva. 115(1), 119-123 (in American Mineralogist, 73, 441).

Sterrett, D.B. (1904) Tourmaline from San Diego County, California. American Journal of Science, 17, 459-465.

Tagg, S.L., Cho, H., Dyar, M.D., and Grew, E.S. (1999) Tetrahedral boron in naturally occurring tourmaline. American Mineralogist, 84, 1451-1455.

Taylor, B.E., Foord, E.E., and Friedrichsen, H. (1979) Stable isotope and fluid inclusion studies of gem-bearing granitic pegmatite-aplite dikes, San Diego County, California. Contributions to Mineralogy and Petrology, 68, 187-205.

Thompson, A.B. (1970) Laumontite equilibria and the zeolite facies. American Journal of Science, 269, 267-275.

Tomisaka, T. (1968) Syntheses of some end-members of the tourmaline group. Mineralogical Journal (Japan), 5, 355-364.

Vorbach, A. (1989) Experimental examinations on the stability of synthetic tourmalines in temperatures from 250° C to 750° C and pressures up to 4 kb. Neues Jahrbuch für Mineralogie. Abhandlungen, 161, 69-83.

Wodara, U. and Schreyer, W. (1997) Turmaline mit Borüberschuß im System Na_2O-Al_2O_3-B_2O_3-SiO_2-H_2O (NABSH). Berichte der Deutschen Mineralogischen Gesellschaft, Beihefte zum European Journal of Mineralogy, 9, No. 1, 394 (abstract).

Wodara, U. and Schreyer, W. (1998) Tetrahedral boron in tourmalines of the system Na_2O-Al_2O_3-B_2O_3-SiO_2-H_2O. Terra Abstracts, Abstract supplement No. 1 to Terra Nova, 10, 68-69 (abstract).

Wodara, U. and Schreyer, W. (2001) X-site vacant Al-tourmaline: a new synthetic end-member. European Journal of Mineralogy, 13, 521-532.

Wolf, M.B. and London, D. (1997) Boron in granitic magmas: stability of tourmaline in equilibrium with biotite and cordierite. Contributions to Mineralogy and Petrology, 130, 12-30.

Wright, S.E., Foley, J.A., and Hughes, J.M. (2000) Optimization of site occupancies in minerals using quadratic programming. American Mineralogist, 85, 524-531.

TABLE 1. Crystal data and results of tourmalines from the elbaite-schorl series from the Himalaya Mine, Mesa Grande, California, U.S.A.

Unit cell

Least squares (space group: *R*3m), # reflections in cell refinement, total measured reflections:

HIM1:	*a* (Å) = 15.9530(4),	*c* = 7.1328(4),	5,618,	11,651
HIM2:	*a* (Å) = 15.9224(3),	*c* = 7.1250(3),	5,651,	11,476
HIM3:	*a* (Å) = 15.9096(3),	*c* = 7.1235(2),	5,704,	11,479
HIM4:	*a* (Å) = 15.8304(3),	*c* = 7.0968(3),	5,654,	11,306
HIM5:	*a* (Å) = 15.8405(3),	*c* = 7.1016(2),	5,665,	11,290
HMGC1:	*a* (Å) = 15.8775(3),	*c* = 7.1169(3),	5,430,	11,185
SS4:	*a* (Å) = 15.8111(4),	*c* = 7.0892(4),	5,834,	11,892

R_{int}‡ (before – after absorption correction), unique reflections, refined parameters:

HIM1:	0.0357 – 0.0224,	1,120,	97
HIM2:	0.0309 – 0.0163,	1,115,	96
HIM3:	0.0304 – 0.0151,	1,109,	96
HIM4:	0.0230 – 0.0147,	1,106,	95
HIM5:	0.0225 – 0.0165,	1,103,	95
HMGC1:	0.0374 – 0.0198,	1,109,	94
SS4:	0.0284 – 0.0183,	1,346,	97

*R*1*****, $F_o > 4\sigma_{(Fo)}$, largest difference peaks, (+,-, $e^{-}\cdot Å^{-3}$), goodness-of-fit§:

HIM1:	0.0148,	0.55,	0.35,	1.135
HIM2:	0.0154,	0.41,	0.42,	1.092
HIM3:	0.0169,	0.58,	0.38,	1.132
HIM4:	0.0148,	0.36,	0.31,	1.220
HIM5:	0.0130,	0.43,	0.35,	1.166
HMGC1:	0.0180,	0.97,	0.38,	1.122
SS4:	0.0129,	0.52,	0.20,	1.213

---

* $R1 = \Sigma| |F_o| - |F_c| | / \Sigma|F_o|$.

‡ $R_{int} = \Sigma|F_o^2 - F_o^2(\text{mean})| / \Sigma[F_o^2]$.

§ GooF = $S = \{\Sigma[w(F_o^2 - F_c^2)^2] / (n-p)\}^{1/2}$.

TABLE 2. Table of positional parameters and their estimated standard deviations of tourmalines from the elbaite-schorl series from the Himalaya Mine.

Atom	*Sample*	*x*	*y*	*z*	U_{eq}	*Occ*
Na	HIM1	0	0	¾	0.027(1)	$Na_{0.62(1)}$
	HIM2	0	0	¾	0.0227(7)	$Na_{0.854(9)}$
	HIM3	0	0	¼	0.0210(6)	$Na_{0.956(9)}$
	HIM4	0	0	¼	0.0160(5)	$Na_{0.768(7)}$
	HIM5	0	0	¾	0.0153(5)	$Na_{0.823(7)}$
	HMGC1	0	0	¾	0.0161(5)	$Na_{1.069(9)}$
	SS4	0	0	¼	0.0176(5)	$Na_{0.697(6)}$
AlY	HIM1	0.87575(3)	1/2x	0.3497(4)	0.0109(1)	$Al_{0.524(5)}Fe_{0.476}$
	HIM2	0.87600(4)	1/2x	0.3540(3)	0.0114(2)	$Al_{0.797(4)}Fe_{0.203}$
	HIM3	0.12395(5)	1/2x	-0.3551(3)	0.0118(2)	$Al_{0.972(4)}Mn_{0.028}$
	HIM4	0.12302(6)	1/2x	-0.3491(3)	0.0091(3)	$Al_{0.565(5)}Li_{0.435}$
	HIM5	0.87663(6)	1/2x	0.3511(2)	0.0093(3)	$Al_{0.561(4)}Li_{0.439}$
	HMGC1	0.87624(6)	1/2x	0.3553(3)	0.0108(3)	$Al_{0.814(6)}Li_{0.186}$
	SS4	0.12247(5)	1/2x	-0.3489(3)	0.0083(2)	$Al_{0.584(4)}Li_{0.416}$
AlZ	HIM1	0.70185(3)	0.73869(3)	0.3659(4)	0.0071(1)	$Al_{0.991(3)}Fe_{0.009}$
	HIM2	0.70219(3)	0.73896(3)	0.3701(3)	0.0078(1)	$Al_{1.00}$
	HIM3	0.29766(3)	0.26091(3)	-0.3706(3)	0.0080(1)	$Al_{1.00}$
	HIM4	0.29670(2)	0.25991(3)	-0.3745(2)	0.0084(1)	$Al_{1.00}$
	HIM5	0.70318(2)	0.74007(2)	0.3744(2)	0.00812(9)	$Al_{1.00}$
	HMGC1	0.70276(3)	0.73963(3)	0.3739(2)	0.0078(1)	$Al_{1.00}$
	SS4	0.29658(2)	0.25982(2)	-0.3751(2)	0.00742(7)	$Al_{1.00}$
B	HIM1	0.88991(8)	2x	0.5224(5)	0.0089(4)	$B_{1.00}$
	HIM2	0.89022(8)	2x	0.5269(4)	0.0086(4)	$B_{1.00}$
	HIM3	0.10964(9)	2x	0.4720(4)	0.0086(4)	$B_{1.00}$
	HIM4	0.10910(7)	2x	0.4703(3)	0.0089(3)	$B_{1.00}$
	HIM5	0.89086(6)	2x	0.5299(3)	0.0086(3)	$B_{1.00}$
	HMGC1	0.89071(9)	2x	0.5310(4)	0.0083(4)	$B_{1.00}$
	SS4	0.10919(6)	2x	0.4700(3)	0.0075(2)	$B_{1.00}$
T	HIM1	0.80807(2)	0.81008(3)	0.9762(4)	0.0067(1)	$Si_{1.00}$
	HIM2	0.80799(3)	0.80996(3)	0.9812(3)	0.00691(9)	$Si_{1.00}$
	HIM3	0.19204(3)	0.19008(3)	0.0179(3)	0.0069(1)	$Si_{1.00}$
	HIM4	0.19192(2)	0.18988(2)	0.0159(2)	0.0063(1)	$Si_{0.961(4)}B_{0.039}$
	HIM5	0.80804(2)	0.81007(2)	0.9847(2)	0.0059(1)	$Si_{0.964(4)}B_{0.036}$
	HMGC1	0.80799(3)	0.80994(3)	0.9853(2)	0.0067(1)	$Si_{1.00}$
	SS4	0.19185(2)	0.18980(2)	0.0157(2)	0.00576(8)	$Si_{0.971(3)}B_{0.029}$

H3	HIM1	0.735(3)	1/2x	0.590(6)	0.05(1)	$H_{1.00}$
	HIM2	0.736(3)	1/2x	0.611(7)	0.05(1)	$H_{1.00}$
	HIM3	0.265(3)	1/2x	0.400(6)	0.05(1)	$H_{1.00}$
	HIM4	0.262(3)	1/2x	0.398(7)	0.06(1)	$H_{1.00}$
	HIM5	0.738(2)	1/2x	0.591(5)	0.042(9)	$H_{1.00}$
	HMGC1	0.736(3)	1/2x	0.584(6)	0.014(8)	$H_{1.00}$
	SS4	0.259(3)	1/2x	0.414(5)	0.05(1)	$H_{1.00}$
O1	HIM1	0	0	0.1967(8)	0.037(1)	$O_{1.00}$
	HIM2	0	0	0.2008(8)	0.045(1)	$O_{1.00}$
	HIM3	0	0	-0.2013(8)	0.047(2)	$O_{1.00}$
	HIM4	0	0	-0.2040(4)	0.0367(9)	$O_{0.35(6)}F_{0.65}$
	HIM5	0	0	0.2019(4)	0.043(1)	$O_{0.18(6)}F_{0.82}$
	HMGC1	0	0	0.2037(6)	0.039(1)	$O_{1.00}$
	SS4	0	0	-0.2073(5)	0.0276(6)	$O_{1.00}$
O2	HIM1	0.93837(6)	2x	0.4905(5)	0.0188(4)	$O_{1.00}$
	HIM2	0.93887(6)	2x	0.4974(4)	0.0199(4)	$O_{1.00}$
	HIM3	0.06086(6)	2x	0.4999(4)	0.0214(4)	$O_{1.00}$
	HIM4	0.06022(5)	2x	0.5042(3)	0.0172(3)	$O_{1.00}$
	HIM5	0.93975(5)	2x	0.4978(3)	0.0180(3)	$O_{1.00}$
	HMGC1	0.93949(6)	2x	0.5029(3)	0.0187(4)	$O_{1.00}$
	SS4	0.06030(4)	2x	0.5046(3)	0.0154(2)	$O_{1.00}$
O3	HIM1	0.7323(1)	1/2x	0.4672(5)	0.0131(3)	$O_{1.00}$
	HIM2	0.7316(1)	1/2x	0.4719(4)	0.0127(3)	$O_{1.00}$
	HIM3	0.2685(1)	1/2x	-0.4726(3)	0.0129(3)	$O_{1.00}$
	HIM4	0.2649(1)	1/2x	-0.4764(3)	0.0151(2)	$O_{1.00}$
	HIM5	0.7337(1)	1/2x	0.4761(3)	0.0144(2)	$O_{1.00}$
	HMGC1	0.7317(1)	1/2x	0.4756(3)	0.0122(3)	$O_{1.00}$
	SS4	0.2644(1)	1/2x	-0.4765(3)	0.0143(2)	$O_{1.00}$
O4	HIM1	0.90647(6)	2x	0.9071(5)	0.0115(3)	$O_{1.00}$
	HIM2	0.90672(6)	2x	0.9105(3)	0.0111(3)	$O_{1.00}$
	HIM3	0.09312(6)	2x	0.0894(3)	0.0110(3)	$O_{1.00}$
	HIM4	0.09360(5)	2x	0.0894(3)	0.0115(2)	$O_{1.00}$
	HIM5	0.90668(5)	2x	0.9113(2)	0.0109(2)	$O_{1.00}$
	HMGC1	0.90711(6)	2x	0.9127(3)	0.0108(3)	$O_{1.00}$
	SS4	0.09376(4)	2x	0.0892(3)	0.0105(2)	$O_{1.00}$

O5	HIM1	0.8123(1)	1/2x	0.8842(5)	0.0115(3)	$O_{1.00}$
	HIM2	0.8132(1)	1/2x	0.8881(3)	0.0114(3)	$O_{1.00}$
	HIM3	0.1863(1)	1/2x	0.1117(3)	0.0114(3)	$O_{1.00}$
	HIM4	0.1867(1)	1/2x	0.1119(3)	0.0121(2)	$O_{1.00}$
	HIM5	0.81342(9)	1/2x	0.8892(3)	0.0113(2)	$O_{1.00}$
	HMGC1	0.8143(1)	1/2x	0.8907(3)	0.0109(3)	$O_{1.00}$
	SS4	0.18713(8)	1/2x	0.1116(3)	0.0106(2)	$O_{1.00}$
O6	HIM1	0.80240(7)	0.81278(8)	0.2013(5)	0.0100(2)	$O_{1.00}$
	HIM2	0.80276(7)	0.81295(8)	0.2060(3)	0.0010(2)	$O_{1.00}$
	HIM3	0.19699(8)	0.18694(8)	-0.2068(3)	0.0099(2)	$O_{1.00}$
	HIM4	0.19519(6)	0.18467(6)	-0.2095(3)	0.0101(2)	$O_{1.00}$
	HIM5	0.80444(6)	0.81470(6)	0.2095(2)	0.0098(2)	$O_{1.00}$
	HMGC1	0.80354(8)	0.81349(8)	0.2101(3)	0.0096(2)	$O_{1.00}$
	SS4	0.19506(5)	0.18459(5)	-0.2097(3)	0.0091(1)	$O_{1.00}$
O7	HIM1	0.71440(7)	0.71384(7)	0.8973(5)	0.0091(2)	$O_{1.00}$
	HIM2	0.71423(7)	0.71398(7)	0.9014(3)	0.0090(2)	$O_{1.00}$
	HIM3	0.28582(8)	0.28592(7)	0.0982(3)	0.0088(2)	$O_{1.00}$
	HIM4	0.28648(6)	0.28607(6)	0.0944(3)	0.0091(1)	$O_{1.00}$
	HIM5	0.71380(6)	0.71414(5)	0.9054(2)	0.0086(1)	$O_{1.00}$
	HMGC1	0.71407(8)	0.71426(7)	0.9049(3)	0.0085(2)	$O_{1.00}$
	SS4	0.28645(5)	0.28607(5)	0.0939(3)	0.0082(1)	$O_{1.00}$
O8	HIM1	0.79008(8)	0.72921(8)	0.5360(5)	0.0106(2)	$O_{1.00}$
	HIM2	0.79016(8)	0.72928(8)	0.5406(3)	0.0104(2)	$O_{1.00}$
	HIM3	0.20981(8)	0.27067(9)	0.4589(3)	0.0103(2)	$O_{1.00}$
	HIM4	0.20947(6)	0.26999(6)	0.4549(3)	0.0101(2)	$O_{1.00}$
	HIM5	0.79046(6)	0.72992(6)	0.5448(2)	0.0098(2)	$O_{1.00}$
	HMGC1	0.79025(8)	0.72949(9)	0.5443(3)	0.0099(2)	$O_{1.00}$
	SS4	0.20954(5)	0.27018(5)	0.4545(3)	0.0092(1)	$O_{1.00}$

Note: Definition for U_{eq} see Fischer and Tillmanns (1988).

TABLE 3. Selected interatomic distances (Å) in tourmalines from the elbaite-schorl series from the Himalaya Mine.

X-	**HIM1**	**HIM2**	**HIM3**	**HIM4**	**HIM5**	**HMGC1**	**SS4**
O2 (x3)	2.515(3)	2.466(2)	2.446(2)	2.446(2)	2.437(2)	2.421(2)	2.447(2)
O5 (x3)	2.764(2)	2.757(2)	2.750(2)	2.741(1)	2.744(1)	2.743(2)	2.744(1)
O4 (x3)	2.817(2)	2.815(2)	2.809(2)	2.808(1)	2.805(1)	2.805(2)	2.809(1)
Mean	**2.699**	**2.679**	**2.668**	**2.665**	**2.662**	**2.656**	**2.667**
Y-							
O2 (x2)	1.983(3)	1.982(1)	1.983(1)	1.967(1)	1.971(1)	1.984(1)	1.9616(9)
O6 (x2)	2.034(1)	2.028(1)	2.027(1)	1.965(1)	1.979(1)	2.008(1)	1.9639(9)
O1	2.034(3)	2.029(3)	2.029(3)	1.976(2)	1.997(2)	2.015(2)	1.955(2)
O3	2.152(2)	2.161(2)	2.161(2)	2.144(2)	2.152(2)	2.164(2)	2.144(1)
Mean	**2.037**	**2.035**	**2.035**	**1.997**	**2.008**	**2.027**	**1.992**
Z-							
O6	1.858(1)	1.853(1)	1.851(1)	1.8597(9)	1.8561(9)	1.849(1)	1.8592(8)
O8	1.882(1)	1.880(1)	1.882(1)	1.8860(9)	1.8857(9)	1.883(1)	1.8835(8)
O7	1.878(1)	1.880(1)	1.880(1)	1.8837(9)	1.8846(8)	1.884(1)	1.8821(7)
O8’	1.920(1)	1.918(1)	1.915(1)	1.9022(9)	1.9037(9)	1.910(1)	1.8992(8)
O7’	1.953(1)	1.952(1)	1.952(1)	1.9461(9)	1.9510(8)	1.955(1)	1.9452(7)
O3	1.9760(8)	1.9696(8)	1.9671(8)	1.9575(7)	1.9539(6)	1.957(2)	1.9548(6)
Mean	**1.911**	**1.909**	**1.908**	**1.9059**	**1.9058**	**1.906**	**1.9040**
T-							
O6	1.6098(11)	1.6060(11)	1.6047(12)	1.6041(10)	1.6006(9)	1.6036(12)	1.6022(8)
O7	1.6162(10)	1.6143(10)	1.6136(11)	1.6093(8)	1.6082(8)	1.6106(11)	1.6076(7)
O4	1.6240(6)	1.6252(6)	1.6261(6)	1.6217(5)	1.6229(5)	1.6255(7)	1.6193(4)
O5	1.6373(7)	1.6391(7)	1.6406(8)	1.6369(6)	1.6371(6)	1.6405(8)	1.6337(5)
Mean	**1.6218**	**1.6212**	**1.6213**	**1.6180**	**1.6172**	**1.6201**	**1.6157**
B-							
O2	1.358(3)	1.358(3)	1.359(3)	1.362(2)	1.360(2)	1.356(3)	1.361(2)
O8(x2)	1.383(2)	1.383(2)	1.383(2)	1.381(1)	1.382(2)	1.385(2)	1.379(1)
Mean	**1.375**	**1.375**	**1.375**	**1.375**	**1.375**	**1.375**	**1.373**

TABLE 4. Compositions of tourmalines from the elbaite-schorl series from the Himalaya Mine, California, U.S.A (standard deviation in brackets).

	HIM1[1]	HIM1[2]	HIM2[1]	HIM2[2]	HIM3[1]	HIM3[2]	HIM4[1]	HIM4[2]	HIM5[1]	HIM5[2]	HMGC1[1]	HMGC1[2]	SS4[1]	SS4[2]
SiO_2	34.34(20)	34.34	35.28(23)	35.28	35.77(22)	35.77	37.08(28)	37.08	37.68(13)	37.68	36.67(15)	36.67	37.15(17)	37.15
TiO_2	0.06(6)	0.06	0.09(1)	0.09	0.06(3)	0.06	0.01(1)	0.01	0.01(1)	0.01	0.17(2)	0.17	b. d.	-
B_2O_3	10.20	10.40	10.74(1)	10.74	10.92(2)	10.92	12.93(37)	12.03	12.68(5)	11.53	11.60(1)	11.15	12.91(8)	12.04
Al_2O_3	36.66(14)	37.00	37.93(20)	38.06	38.76(16)	39.21	42.61(19)	42.53	40.90(21)	41.37	38.77(14)	39.22	42.45(15)	42.59
FeO_{total}	9.43(25)	-	4.04(10)	-	0.20(6)	-	0.01(1)	-	0.09(4)	-	1.58(8)	-	0.01(1)	-
FeO*	7.64	7.64	3.27	3.27	0.06	0.06	-	-	0.06	0.06	-	1.58[7]	-	-
Fe_2O_3*	1.99	1.99	0.86	0.86	0.15	0.15	0.01	0.01	0.04	0.04	-	-	0.01	0.01
MnO	2.31(9)	2.31	3.61(18)	3.61	5.87(17)	5.87	0.08(2)	0.08	0.69(4)	0.69	1.97(7)	1.97	0.17(3)	0.17
MgO	0.04(1)	0.04	b. d.	-	b. d.	-	b. d.	-	b. d.	-	0.34(1)	0.34	b. d.	-
CaO	0.10(1)	0.10	0.38(3)	0.38	0.71(3)	0.71	0.95(13)	0.95	1.13(9)	1.13	1.63(4)	1.63	0.62(3)	0.62
Li_2O	0.23	0.23	0.74(1)	0.74	1.03(1)	1.03	1.73(2)	1.73	1.80(3)	1.80	1.41(1)	1.41	1.68(2)	1.68
ZnO	0.72(6)	0.72	0.77(3)	0.77	0.02(1)	0.02	0.01(1)	0.01	0.02(1)	0.02	0.02(1)	0.02	0.01(1)	0.01
Na_2O	1.80(5)	1.80	2.39(12)	2.39	2.35(7)	2.35	1.68(4)	1.68	1.69(4)	1.69	1.91(4)	1.91	1.76(5)	1.76
K_2O	0.03(1)	0.03	0.03(7)	0.03	0.02(1)	0.02	0.01(1)	0.01	0.01(1)	0.01	0.01(1)	0.01	0.02(1)	0.02
F	0.67(3)	0.67	1.33(11)	1.33	1.51(5)	1.51	1.17(11)	1.17	1.33(11)	1.33	1.56(5)	1.56	0.94(9)	0.94
H_2O[3]	2.75	-	3.03(7)	-	3.16(4)	-	3.28(1)	-	3.30(2)	-	3.20(2)	-	3.67(1)	-
H_2O[4]	2.90	-	2.95	-	2.75	-	3.01	-	3.70	-	-	-	-	-
H_2O[5]	3.20(7)	-	2.99(2)	-	-	-	3.30(4)	-	3.52(8)	-	-	-	-	-
H_2O[6]	2.95	2.95	2.99	2.99	2.96	2.96	3.20	3.20	3.51	3.20	-	3.02	-	3.41
O≡F	-0.28	-0.28	-0.56	-0.56	-0.64	-0.64	-0.49	-0.49	-0.56	-0.56	-0.66	-0.66	-0.40	-0.40
Sum	99.46	100.00	99.85	100.00	99.55	100.00	100.99	100.00	100.99	100.00	100.18	100.00	100.99	100.00
N	31	31	31	31	31	31	31	31	31	31	31	31	31	31
Si (apfu)	5.77	5.74	5.78	5.77	5.81	5.78	5.70	5.77	5.85	5.89	5.82	5.85	5.69	5.77
$^{[4]}B$	0.00	0.00	0.04	0.03	0.06	0.05	0.43	0.23	0.22	0.11	0.18	0.07	0.41	0.23
$^{[4]}Al$	0.23	0.26	0.18	0.20	0.13	0.17	0.00	0.00	0.00	0.00	0.00	0.08	0.00	0.00
Sum T site	6.00	6.00	6.00	6.00	6.00	6.00	6.13	6.00	6.07	6.00	6.00	6.00	6.10	6.00
$^{[3]}B$	2.96	3.00	3.00	3.00	3.00	3.00	3.00	3.00	3.00	3.00	3.00	3.00	3.00	3.00
Al	7.03	7.02	7.14	7.14	7.28	7.30	7.72	7.80	7.48	7.62	7.26	7.30	7.66	7.80
Fe^{2+}	1.08	1.06	0.45	0.45	0.01	0.01	0.00	0.00	0.01	0.01	0.21	0.21	0.00	0.00
Fe^{3+}	0.25	0.25	0.11	0.11	0.02	0.02	0.00	0.00	0.00	0.00	-	-	0.00	0.00
Mn^{2+}	0.33	0.33	0.50	0.50	0.81	0.80	0.01	0.01	0.09	0.09	0.27	0.27	0.02	0.02

Mg	0.01	0.01	0.00	0.00	0.00	0.00	0.00	0.00	0.00	0.00	0.08	0.08	0.00	0.00
Li	0.16	0.15	0.49	0.49	0.67	0.67	1.07	1.08	1.12	1.13	0.90	0.91	1.03	1.05
Zn	0.09	0.09	0.09	0.09	0.00	0.00	0.00	0.00	0.00	0.00	0.00	0.00	0.00	0.00
Ti^{4+}	0.01	0.01	0.01	0.01	0.01	0.01	0.00	0.00	0.00	0.00	0.02	0.02	0.00	0.00
Sum Y, Z sites	8.96	8.92	8.79	8.79	8.80	8.81	8.80	8.89	8.70	8.85	8.74	8.79	8.72	8.87
Ca	0.03	0.03	0.07	0.07	0.12	0.12	0.16	0.16	0.19	0.19	0.28	0.28	0.10	0.10
Na	0.59	0.58	0.76	0.76	0.74	0.74	0.50	0.51	0.51	0.51	0.59	0.59	0.52	0.53
K	0.01	0.01	0.01	0.01	0.00	0.00	0.00	0.00	0.00	0.00	0.00	0.00	0.00	0.00
□	0.37	0.38	0.16	0.16	0.14	0.14	0.34	0.33	0.30	0.30	0.13	0.13	0.38	0.37
Sum X site	1.00	1.00	1.00	1.00	1.00	1.00	1.00	1.00	1.00	1.00	1.00	1.00	1.00	1.00
Sum cations	18.55	18.54	18.66	18.63	18.66	18.67	18.59	18.56	18.47	18.55	18.61	18.66	18.45	18.48
OH	3.31	3.29	3.27	3.26	3.20	3.19	3.28	3.32	3.62	3.34	3.39	3.21	3.75	3.54
F	0.36	0.35	0.69	0.69	0.78	0.77	0.57	0.58	0.65	0.66	0.78	0.79	0.45	0.46
Sum OH + F	3.67	3.64	3.96	3.95	3.98	3.96	3.85	3.90	4.27	4.00	4.17	4.00	4.20	4.00

Note: [1]HIM1: Average of 8 EMP analyses; H_2O: 1 SIMS analysis; B_2O_3, Li_2O and BeO (7 ppm): 1 SIMS analysis; HIM2: Average of 12 EMP analyses; H_2O: Average of 3 SIMS analyses; B_2O_3, Li_2O and BeO (22 ppm): Average of 2 SIMS analyses; HIM3: Average of 10 EMP analyses; H_2O: Average of 2 SIMS analyses; B_2O_3, Li_2O and BeO (39 ppm): Average of 2 SIMS analyses; HIM4: Average of 12 EMP analyses; H_2O: Average of 3 SIMS analyses; B_2O_3, Li_2O and BeO (76 ppm): Average of 3 SIMS analyses; HIM5: Average of 12 EMP analyses; H_2O: Average of 2 SIMS analyses; B_2O_3, Li_2O and BeO (31 ppm): Average of 3 SIMS analyses; HMGC1: Average of 12 EMP analyses; H_2O: Average of 3 SIMS analyses; B_2O_3, Li_2O and BeO (50 ppm): Average of 3 SIMS analyses; SS4: Average of 22 EMP analyses; B_2O_3, Li_2O and BeO (28 ppm): Average of 8 SIMS analyses; H_2O: Average of 4 SIMS analyses. [2]Weight percent of B_2O_3 and Al_2O_3 calculated for an optimized formula by considering the <T-O> distances (Table 3), by fixing the SiO_2 content, and by taking care that the formulae are charge-balanced. The optimized Al_2O_3 content only slightly differs (≤1%) to the measured Al_2O_3 content. Al_2O_3 is the component with the highest amounts in all samples, hence the absolute error is believed to be here more significant than for other oxides. * FeO and Fe_2O_3 were recalculated by using Mössbauer spectroscopic data (Table 5). [3]Water analyses by SIMS. [4]Water analyses by U-extraction. Weight of the analyzed samples: HIM1: ~32 mg, HIM2: ~19 mg, HIM3: ~47 mg, HIM4: ~30 mg, HIM5: ~7 mg. [5]Water analyses by a new method of micro-extraction H-analysis (described in the text under OH determinations), [6]Optimized water content: The average value of the available water contents derived from different methods was calculated. In case OH + F > 4.00 pfu, the value was reduced till OH + F = 4.00. [7]Because of insufficient material for a Mössbauer investigation (see sample selection) the optical absorption spectrum (which did not give an indication for a significant amount of Fe^{3+}) of this crystal was used for the estimation of the valence state of the Fe content. B. d.: below detection limit.

TABLE 5. Mössbauer parameters of tourmaline samples from the Himalaya Mine, Mesa Grande, California, U.S.A.

		HIM1	HIM2	HIM3	HIM4	HIM5	SS4
Sample Thickness		35	35	100	100	35	280
$^{[Y1]}Fe^{2+}$	δ, mm/s	1.08	1.09	1.01	1.02	1.03	1.03
	Δ, mm/s	2.52	2.50	2.47	2.44	2.44	2.44
	Γ, mm/s	0.25	0.25	0.28	0.25	0.25	0.25
	% Area	29	35	28	9	49	29
$^{[Y2]}Fe^{2+}$	δ, mm/s	1.08	1.06		1.16	1.17	1.02
	Δ, mm/s	2.31	2.31		2.70	2.57	2.73
	Γ, mm/s	0.3	0.30		0.24	0.25	0.25
	% Area	32	31		5	15	15
$^{[Y3]}Fe^{2+}$	δ, mm/s	1.03	1.05	1.05			
	Δ, mm/s	1.80	1.55	1.76			
	Γ, mm/s	0.55	0.59	0.25			
	% Area	20	15	3			
$^{[Y\ or\ T]}Fe^{3+}$	δ, mm/s	0.14	0.21	0.15	0.11	0.21	0.22
	Δ, mm/s	0.50	0.37	0.54	0.58	0.42	0.42
	Γ, mm/s	0.30	0.34	0.26	0.30	0.30	0.30
	% Area	16	19	50	65	30	40
$^{[Y\ or\ Z]}Fe^{3+}$	δ, mm/s	0.35		0.23	0.45	0.40	0.52
	Δ, mm/s	0.99		0.87	0.92	0.83	0.83
	Γ, mm/s	0.30		0.25	0.40	0.40	0.40
	% Area	3		12	21	6	16
$^{[Y\ or\ Z]}Fe^{3+}$	δ, mm/s			0.60			
	Δ, mm/s			0.94			
	Γ, mm/s			0.25			
	% Area			7			
	χ^2	2.95	0.74	1.55	5.91	1.09	0.49
	Total Fe^{3+}	19	19	69	86	36	56

TABLE 6. Occupants of the different sites in each investigated tourmaline sample from the Himalaya Mine, Mesa Grande, California, U.S.A.

sample	X site	Y site	Z site	T site	W site	tourmaline
HIM1	$Na_{0.58}Ca_{0.03}K_{0.01}\square_{0.38}$	$Al_{1.07}Fe^{2+}_{1.06}Mn^{2+}_{0.33}Fe^{3+}_{0.20}Li_{0.15}Zn_{0.09}Mg_{0.01}Ti^{4+}_{0.01}\square_{0.08}$	$Al_{5.95}Fe^{3+}_{0.05}$	$Si_{5.74}Al_{0.26}$	$O_{0.36}F_{0.35}(OH)_{0.29}$	Al-rich "oxy-schorl"
HIM2	$Na_{0.76}Ca_{0.07}K_{0.01}\square_{0.16}$	$Al_{1.14}Mn^{2+}_{0.50}Li_{0.49}Fe^{2+}_{0.45}Fe^{3+}_{0.11}Zn_{0.09}Ti^{4+}_{0.01}\square_{0.21}$	$Al_{6.00}$	$Si_{5.77}Al_{0.20}B_{0.03}$	$F_{0.69}(OH)_{0.26}O_{0.05}$	Al- and Mn^{2+}-rich "fluor-elbaite"
HIM3	$Na_{0.74}Ca_{0.12}\square_{0.14}$	$Al_{1.30}Mn^{2+}_{0.80}Li_{0.67}Fe^{3+}_{0.02}Fe^{2+}_{0.01}Ti^{4+}_{0.01}\square_{0.19}$	$Al_{6.00}$	$Si_{5.78}Al_{0.17}B_{0.05}$	$F_{0.77}(OH)_{0.19}O_{0.04}$	Mn^{2+}- and Al-rich "fluor-elbaite"
HIM4	$Na_{0.51}Ca_{0.16}\square_{0.33}$	$Al_{1.80}Li_{1.08}Mn^{2+}_{0.01}\square_{0.11}$	$Al_{6.00}$	$Si_{5.77}B_{0.23}$	$F_{0.58}(OH)_{0.32}O_{0.10}$	Al-rich "fluor-elbaite"
HIM5	$Na_{0.51}Ca_{0.19}\square_{0.30}$	$Al_{1.62}Li_{1.13}Mn^{2+}_{0.09}Fe^{2+}_{0.01}\square_{0.15}$	$Al_{6.00}$	$Si_{5.89}B_{0.11}$	$F_{0.66}(OH)_{0.34}$	"fluor-elbaite"
HMGC1	$Na_{0.59}Ca_{0.28}\square_{0.13}$	$Al_{1.38}Li_{0.91}Mn^{2+}_{0.27}Fe^{2+}_{0.21}Ti^{4+}_{0.02}\square_{0.21}$	$Al_{5.92}Mg_{0.08}$	$Si_{5.85}Al_{0.08}B_{0.07}$	$F_{0.79}(OH)_{0.21}$	"fluor-elbaite"
SS4	$Na_{0.53}Ca_{0.10}\square_{0.37}$	$Al_{1.80}Li_{1.05}Mn^{2+}_{0.02}\square_{0.13}$	$Al_{6.00}$	$Si_{5.77}B_{0.23}$	$(OH)_{0.54}F_{0.46}$	Al-rich elbaite

Note: The V site is in all samples occupied by $(OH)_3$ and the B site by $B_{3.00}$.

TABLE 7. Possible short-range order configurations in tourmalines from the elbaite-schorl series from the Himalaya Mine, Mesa Grande, California, U.S.A.

	X site	Y site	T site	W site	Reference
[1.1]	□	Al_3	Si_4B_2	OH	-
[1.2]	□	Al_2Li	Si_6	OH	Selway et al. (1998), Hughes et al. (2000)
[1.3]	□	Al_2Fe^{2+}	Si_6	O	-
[1.4]	□	Al_2Mn^{2+}	Si_6	O	-
[2.1]	Na	$Mn^{2+}{}_2Al$	Si_6	O	Ertl et al. (2003)
[2.2]	Na	$Mn^{2+}{}_2Fe^{3+}$	Si_6	O	-
[2.3]	Na	$Mn^{2+}{}_2Al$	Si_5Al	OH/F	Ertl et al. (2003)
[2.4]	Na	$Mn^{2+}{}_2Al$	Si_5Al	OH/F	modified after Ertl et al. (2003)
[2.5]	Na	$Mn^{2+}{}_2Fe^{3+}$	Si_5Al	OH/F	-
[2.6]	Na	$Fe^{2+}{}_2Al$	Si_6	O	modified after Ertl et al. (2003)
[2.7]	Na	$Fe^{2+}{}_2Fe^{3+}$	Si_6	O	-
[2.8]	Na	$Fe^{2+}{}_2Al$	Si_5Al	OH/F	modified after Ertl et al. (2003)
[2.9]	Na	$Fe^{2+}Mn^{2+}Al$	Si_5Al	OH/F	-
[2.10]	Na	$Fe^{2+}{}_2Fe^{3+}$	Si_5Al	OH/F	-
[2.11]	Na	Al_2Fe^{2+}	Si_5Al	O	Ertl et al. (2003)
[2.12]	Na	$AlFe^{2+}Fe^{3+}$	Si_5Al	O	-
[2.13]	Na	Al_2Mn^{2+}	Si_5Al	O	modified after Ertl et al. (2003)
[2.14]	Na	$AlMn^{2+}Fe^{3+}$	Si_5Al	O	-
[2.15]	Na	$AlFe^{2+}Li$	Si_6	OH/F	Ertl et al. (2006)
[2.16]	Na	$AlMn^{2+}Li$	Si_6	OH/F	Ertl et al. (2003)
[2.17]	Na	Al_2Li	Si_5Al	OH/F	-
[2.18]	Na	Al_2Li	Si_6	O	-
[2.19]	Na	Al_2□	Si_6	OH/F	-
[2.20]	Na	Al_3	Si_4B_2	O	-
[3.1]	Ca	Al_2□	Si_5B	OH/F	Ertl et al. (2006)
[3.2]	Ca	Li_2Al	Si_6	OH/F	Ertl et al. (2006)

Note: The Z site of all listed short-range order configurations is occupied by Al_6. The V site (O3 sites) is occupied by $(OH)_3$. For short-range orders [1.1] and [1.2] the W site was occupied with (OH) because of the inverse correlation between the F content and the X-site vacancy ($r^2 = 0.89$; Fig. 12). Also Henry (2005) showed that a summary and evaluation of >560 tourmaline analyses from many different tourmaline varieties illustrates that in tourmalines with more than 0.5 X-site vacancies there is little or no F present in the tourmaline. All other short-range orders with Li at the Y site are assumed to have F at the W site.

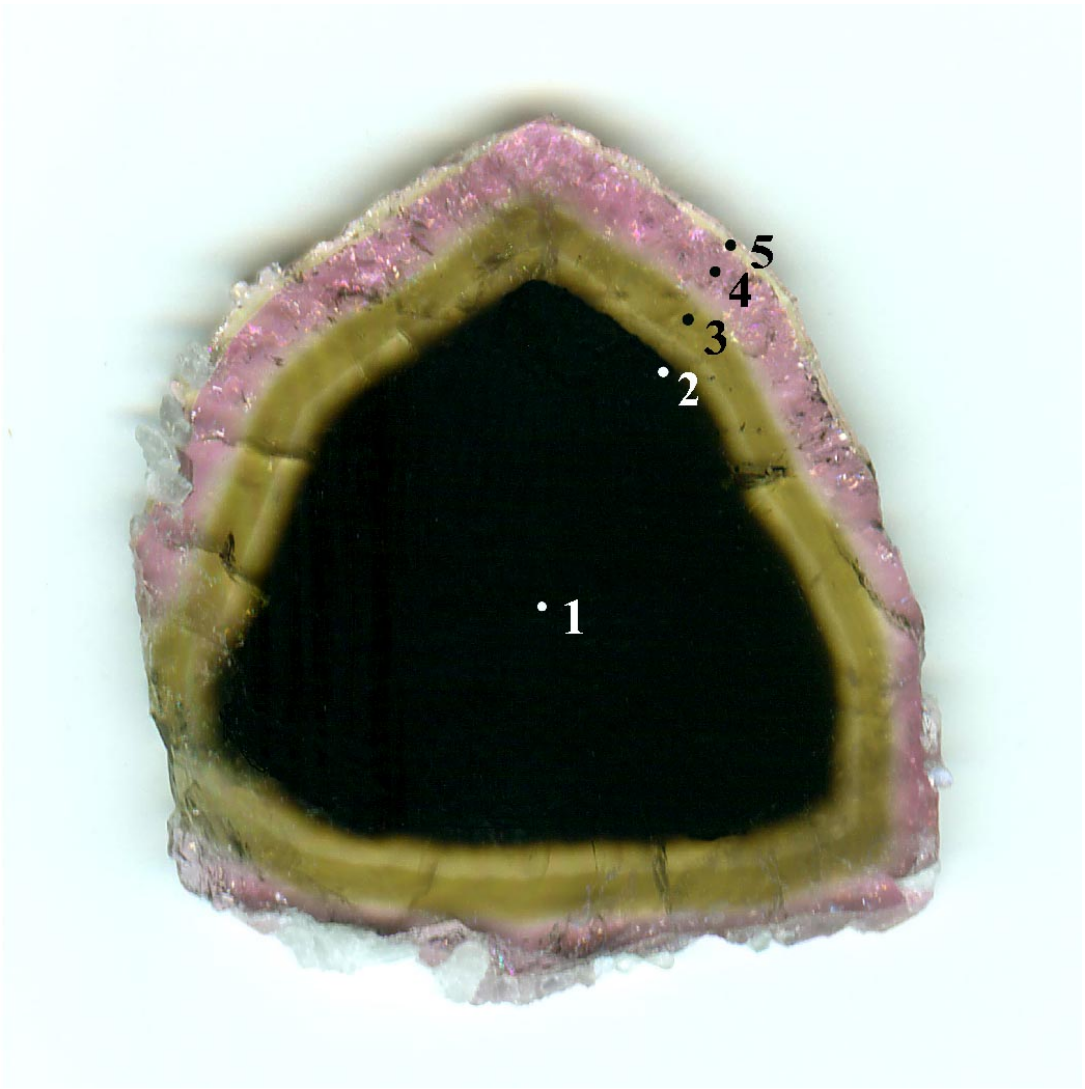

FIGURE 1. A color zoned tourmaline crystal (sample HIM, also called GRR 2254), obtained from a pocket, Himalaya Mine, Mesa Grande, San Diego County, California. Slice with 36 mm in diameter, cut perpendicular to the *c*-axis.

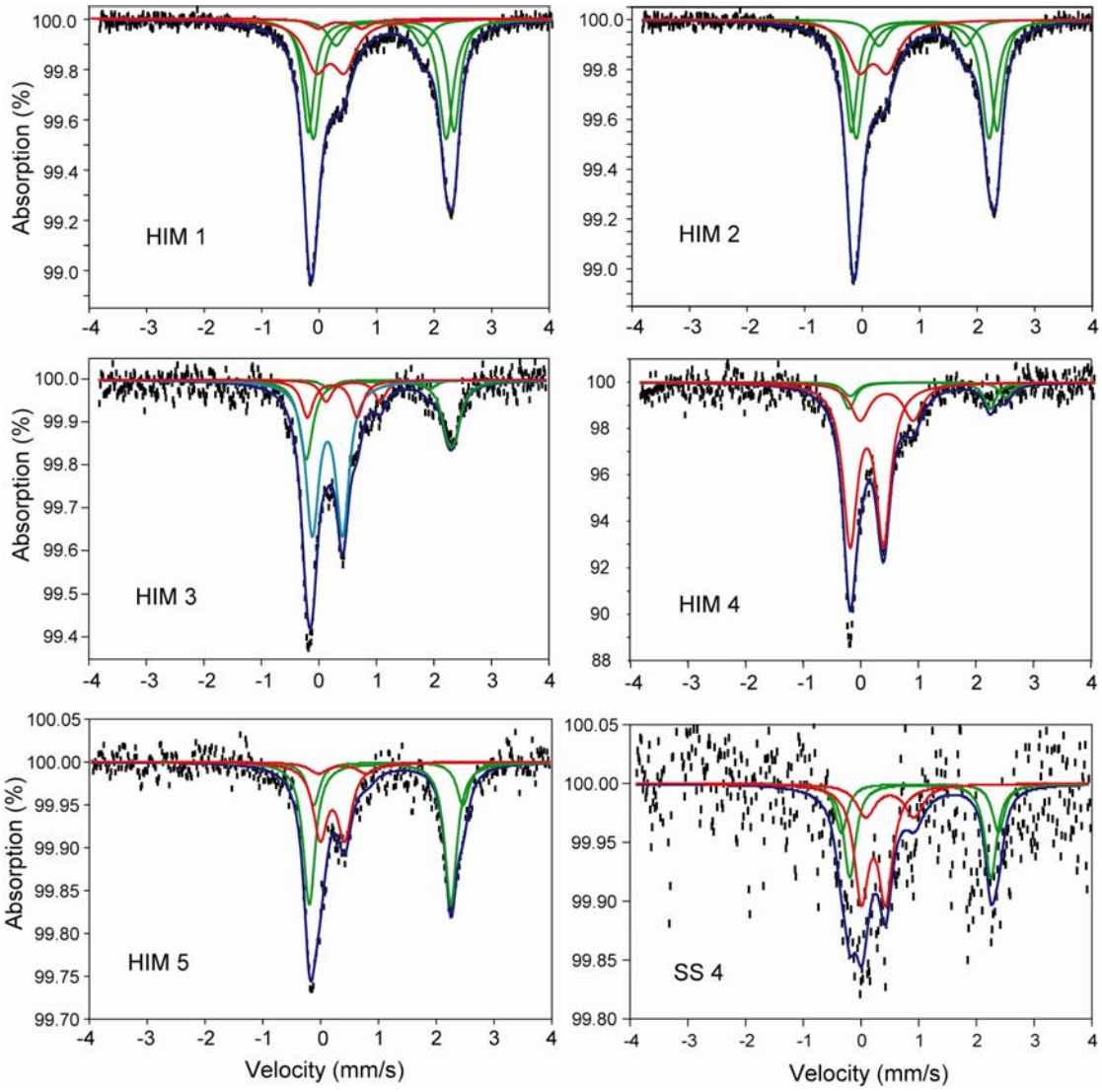

FIGURE 2. 295K Mössbauer spectra of Himalaya Mine tourmalines. Sample SS4 is extremely low in Fe, and although its spectrum was acquired for 10 days, its data show considerable scatter.

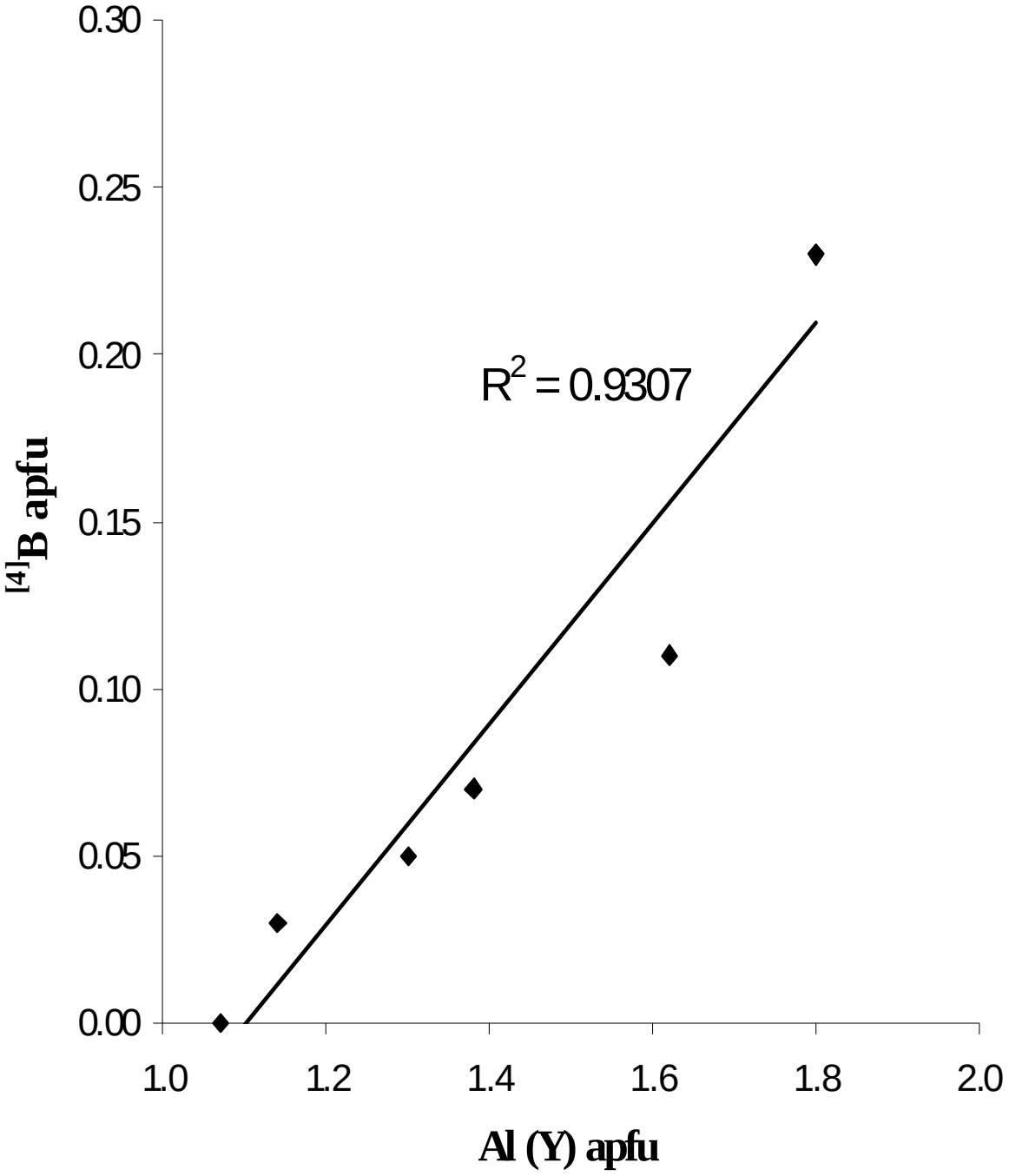

FIGURE 3. Correlation between Al at the Y site and tetrahedrally coordinated B in tourmalines from the Himalaya Mine, Mesa Grande, San Diego County, California.

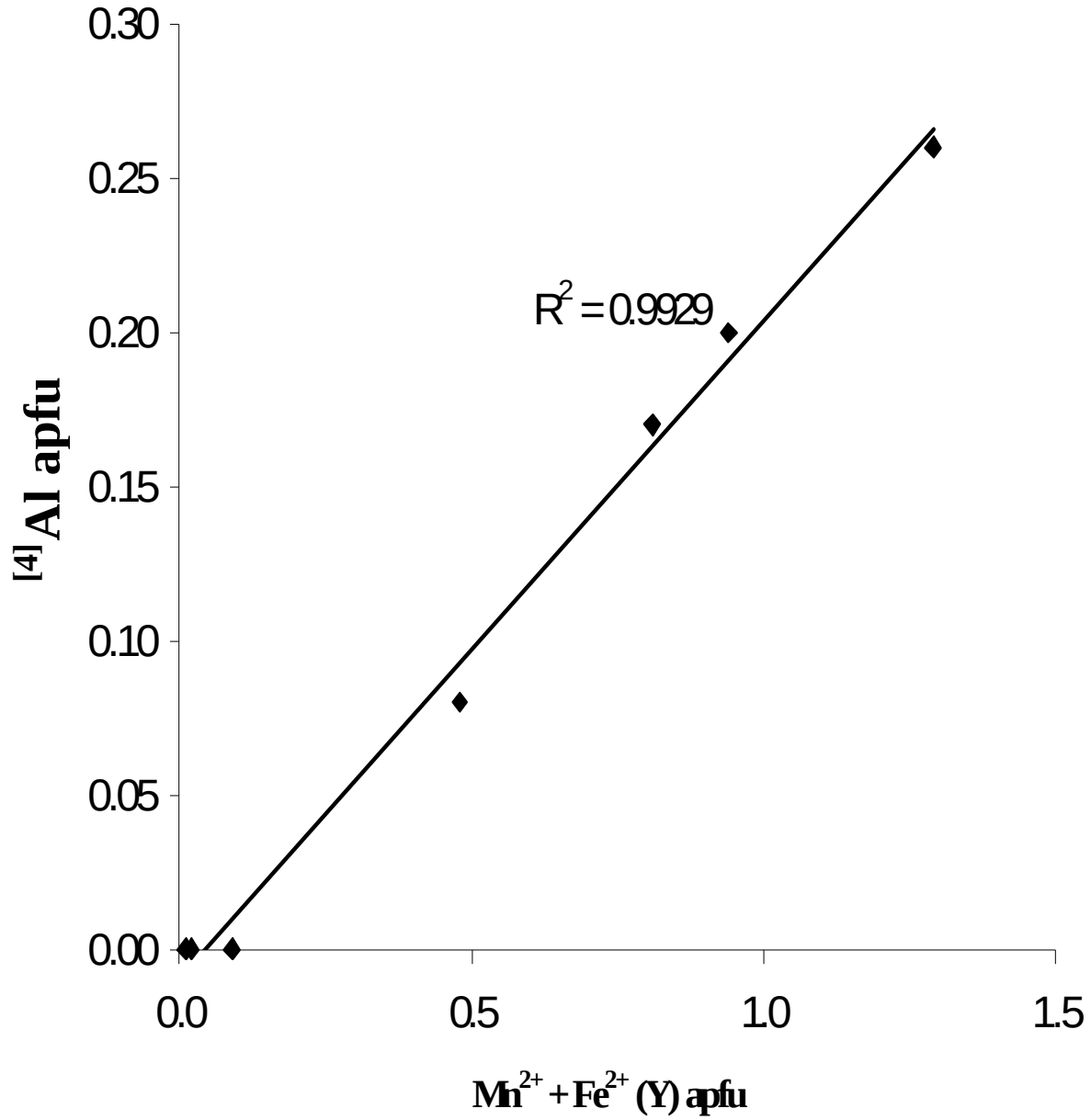

FIGURE 4. Correlation between Mn^{2+} + Fe^{2+} at the Y site and tetrahedrally coordinated Al in tourmalines from the Himalaya Mine, Mesa Grande, San Diego County, California, U.S.A.

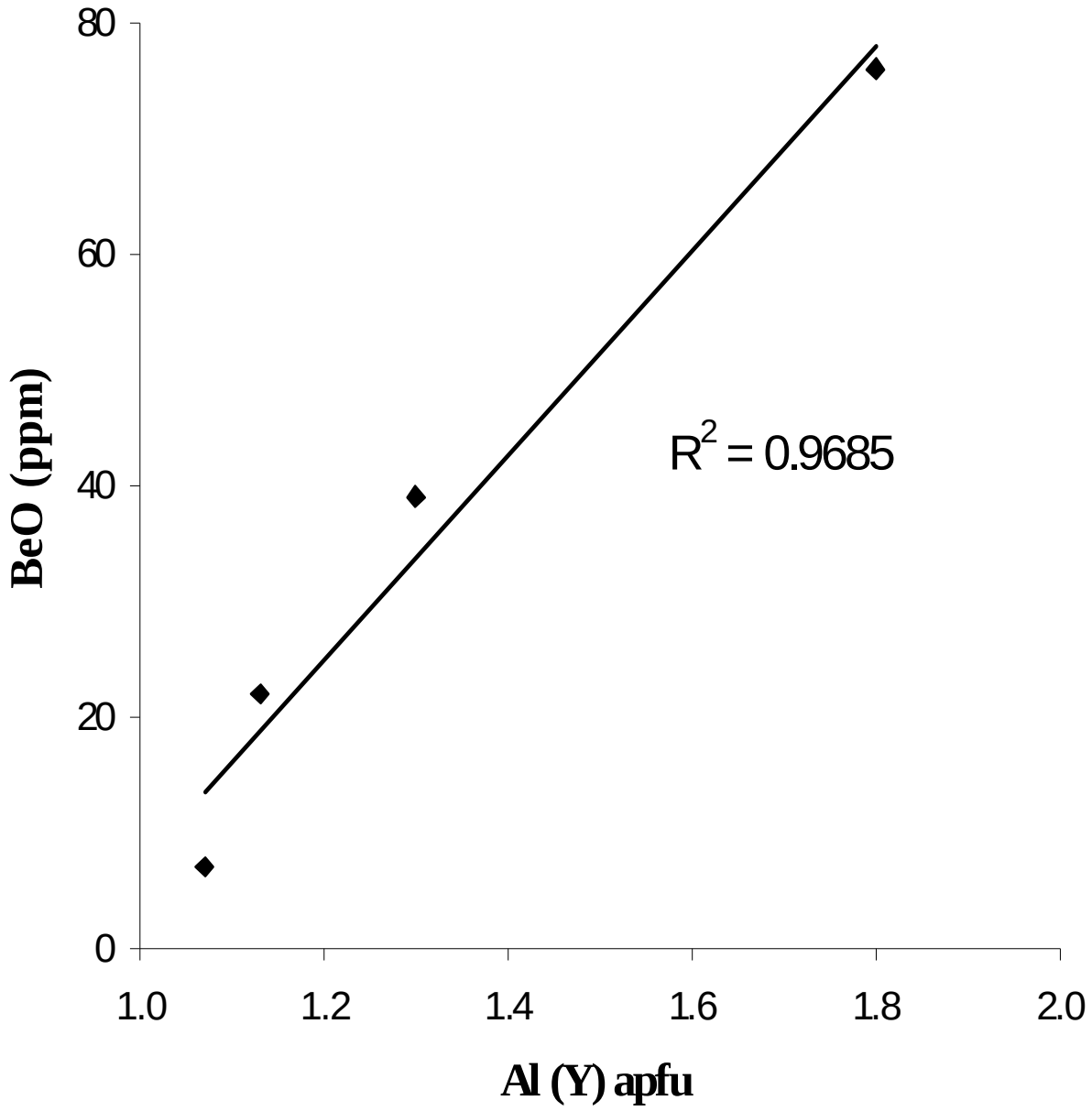

FIGURE 5. Correlation between Al at the Y site and BeO for the zones HIM1 (core; very left square) to HIM4 (rim near zone; very right square) for tourmalines from the elbaite-schorl series from the Himalaya Mine. In the rim zone HIM5 ^{Y}Al and BeO is decreasing again.

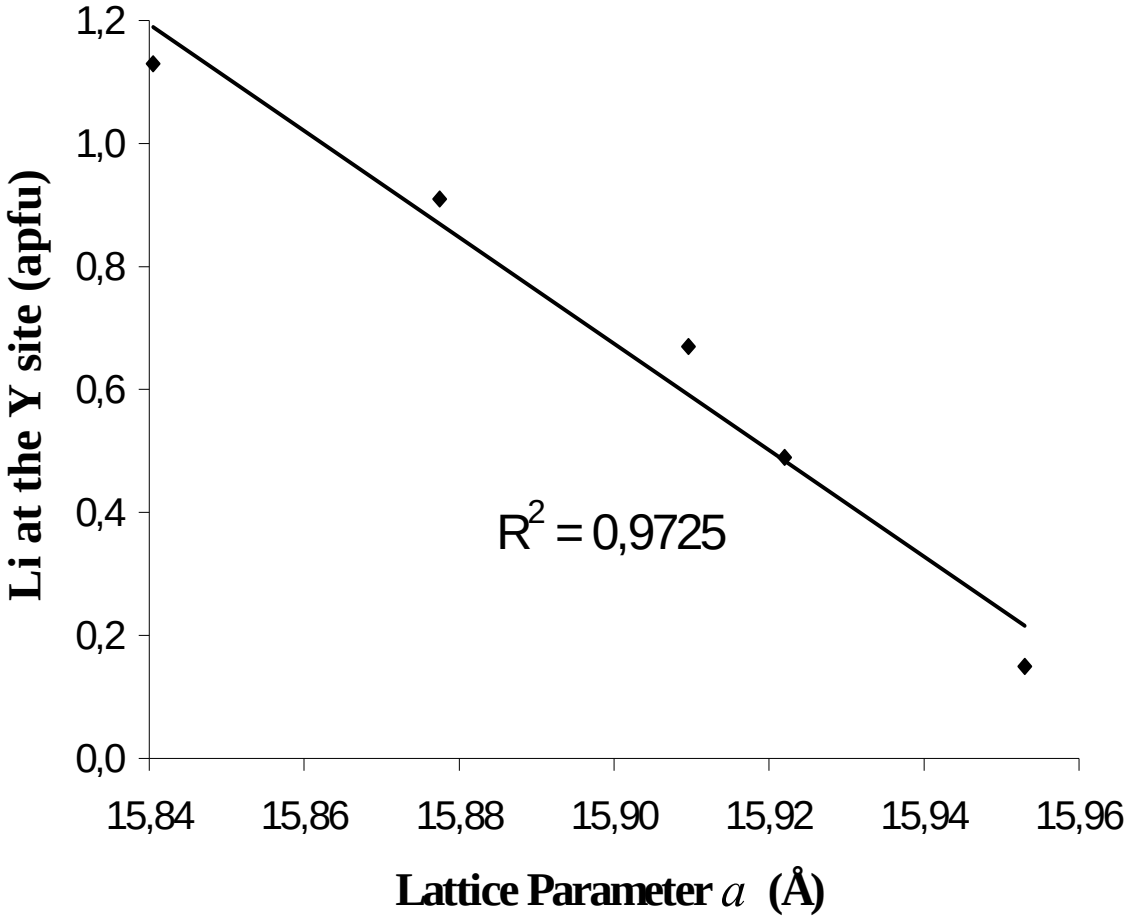

FIGURE 6. Correlation between the lattice parameter *a* and the Li content in tourmalines from the elbaite-schorl series (from the pocket zone) from the Himalaya Mine. All these tourmalines contain MgO contents <0.4 wt%. Valid for lattice parameters ≥15.84 Å. Lattice parameters below this value can be derived by an increasing $^{[4]}$B content ($B_{total} \geq 3.2$ apfu).

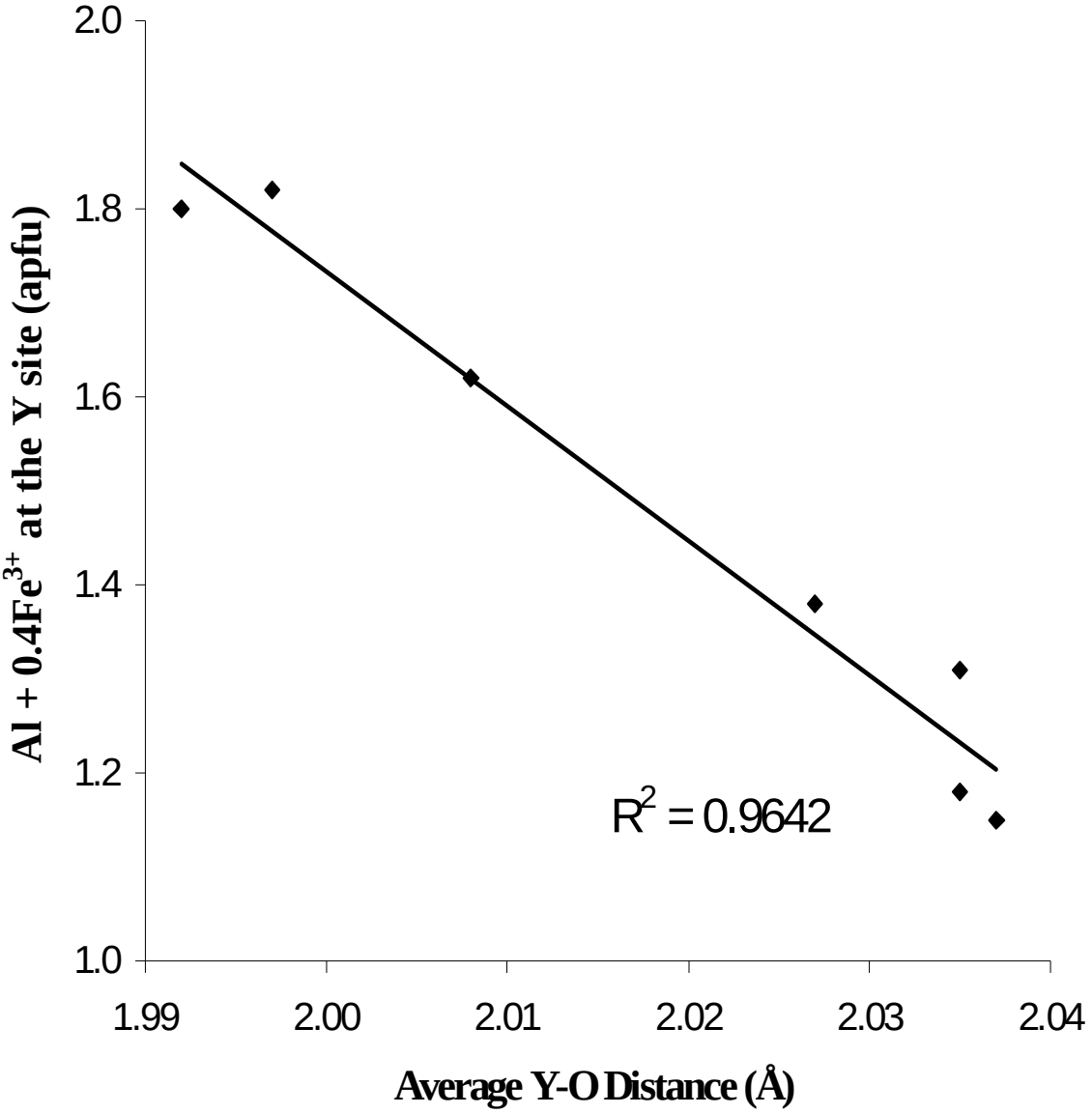

FIGURE 7. Correlation between the <Y-O> distance and the Al and Fe^{3+} content at the Y site in tourmalines from the elbaite-schorl series (from the pocket zone) from the Himalaya Mine, Mesa Grande, San Diego County, California, U.S.A. In all samples FeO + MnO <12 wt% and $^{Z}(Mg+Fe^{3+})$ <0.1 apfu.

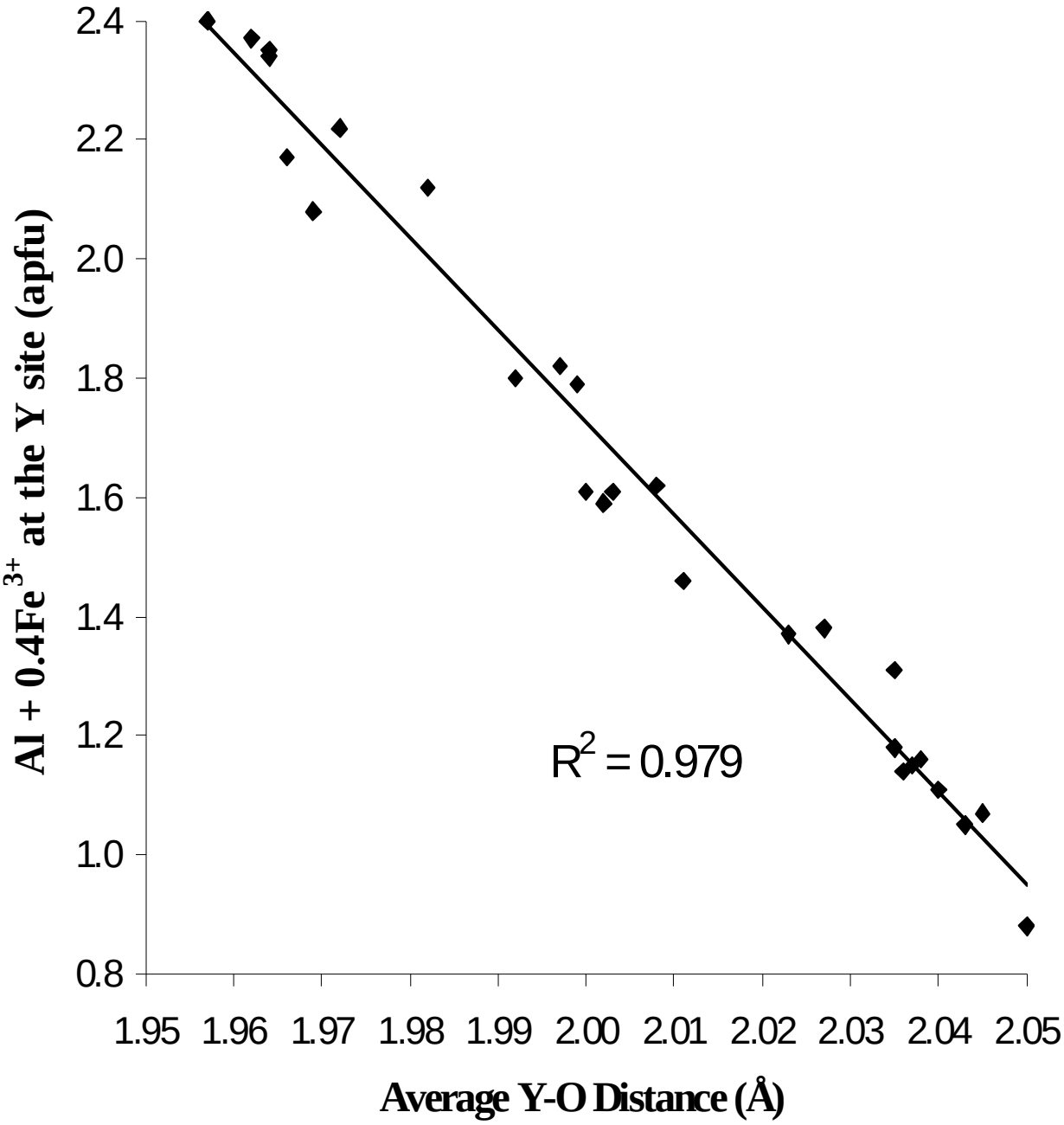

FIGURE 8. Correlation between the <Y-O> distance and Al and Fe^{3+} content at the Y site. Data from ^{Y}Al-, Li- and Fe-bearing tourmalines from this study and from Bosi et al. (2005), Burns et al. (1994), Cámara et al. (2002), Ertl et al. (2005, 2006), Hughes et al. (2002, 2004), Schreyer et al. (2002), Selway et al. (1998). Data of samples with a significant Fe content (>0.5 wt% FeO) were only included when spectroscopic data on the valence state of Fe (e.g., Mössbauer data) was available. All these samples are poor in Mg (≤0.15 apfu Mg).

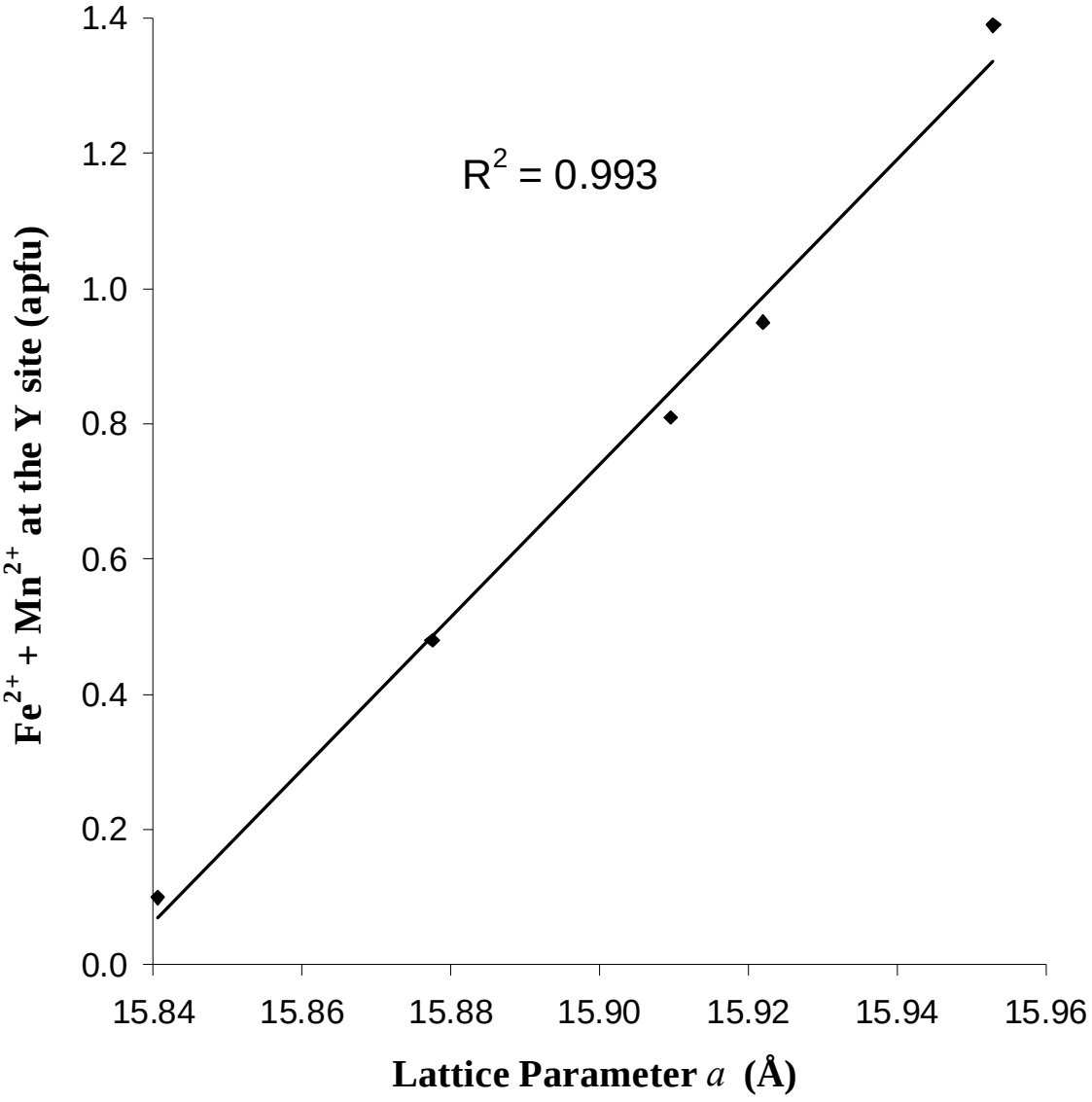

FIGURE 9. Correlation between the lattice parameter *a* and the (Fe^{2+} + Mn^{2+}) content in tourmalines from the Himalaya Mine. All these tourmalines contain MgO contents <0.4 wt%. Valid for samples with lattice parameter *a* ≥15.84 Å. Lattice parameters below this value can be derived by an increasing $^{[4]}B$ content (B_{total} ≥ 3.2 apfu).

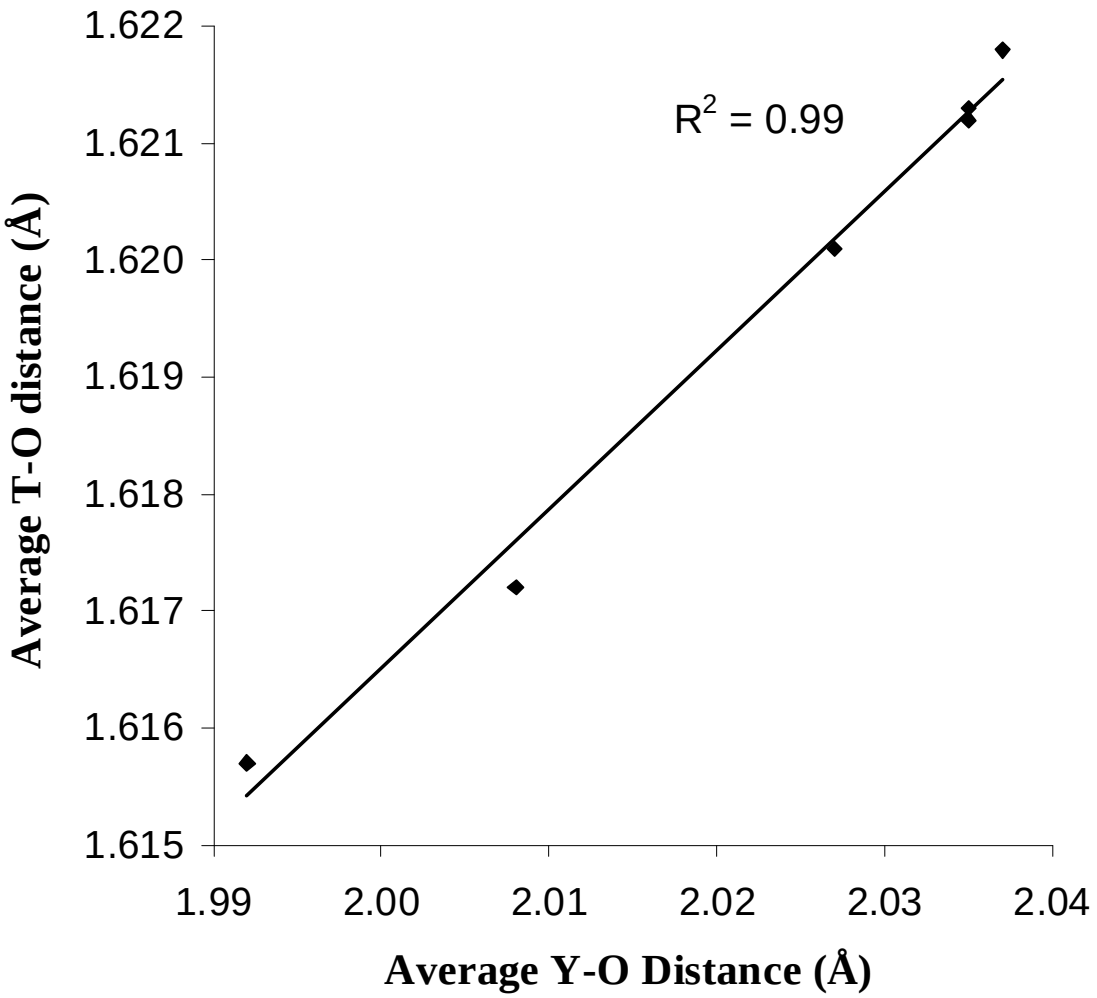

FIGURE 10. Correlation between the <Y-O> distance and the <T-O> distance in tourmalines from the Himalaya Mine (sample HIM4 was excluded because it is an outlier and it is not clear, if there is maybe a higher error on this value; for all investigated samples $r^2 = 0.92$).

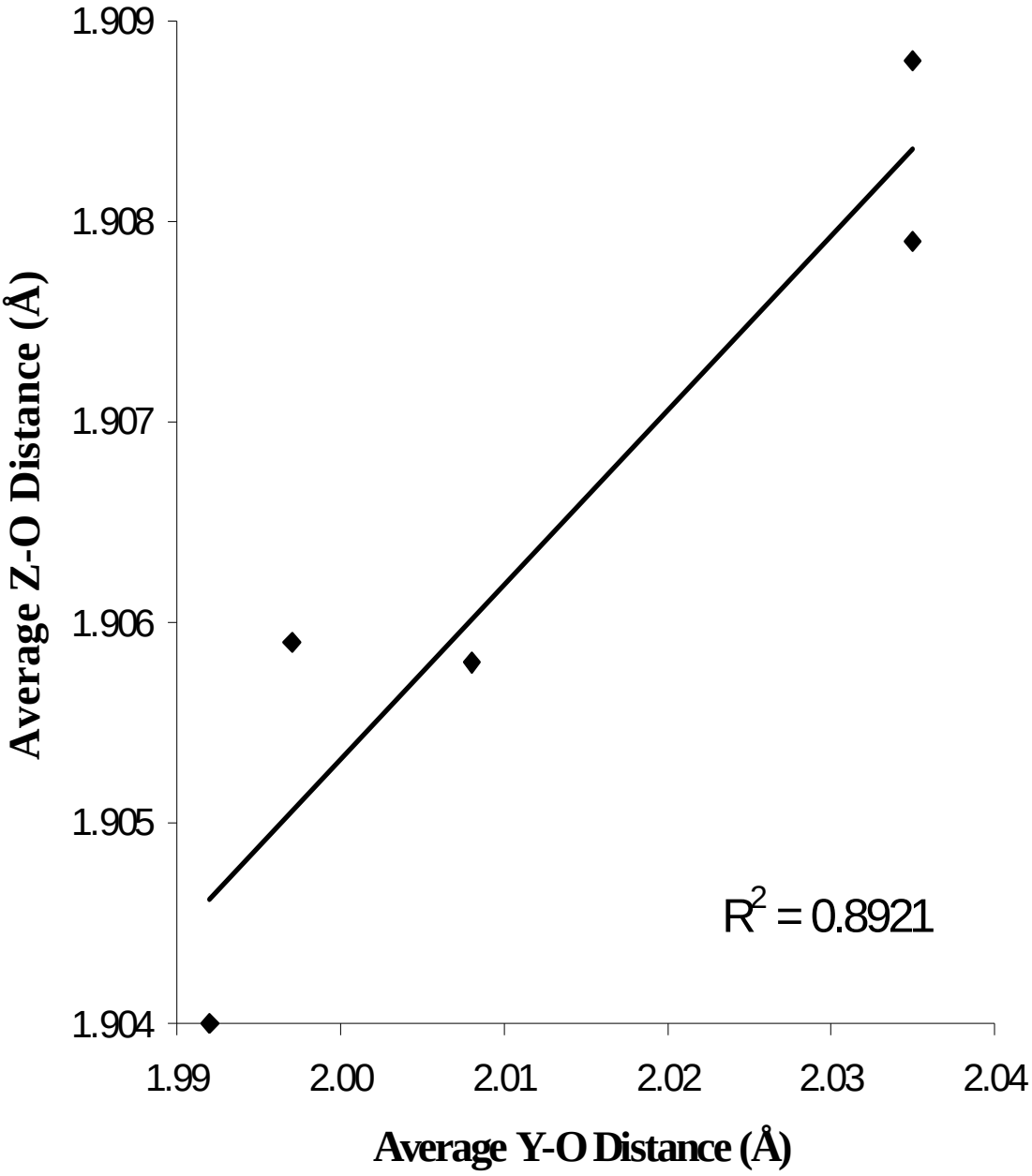

FIGURE 11. Correlation between <Y-O> and <Z-O> in tourmalines from the Himalaya Mine, which contain only Al at the Z site (HIM2, HIM3, HIM4, HIM5, SS4).

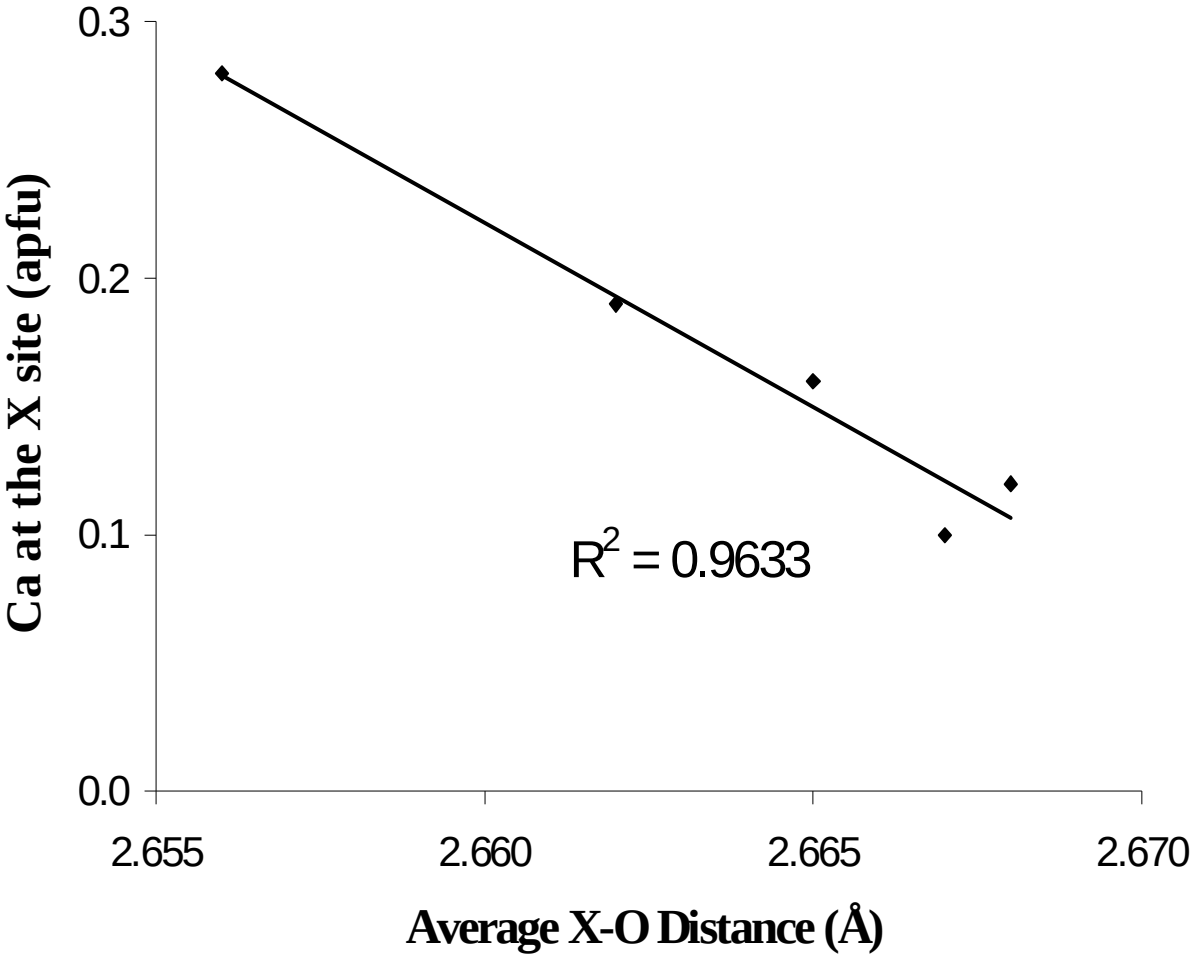

FIGURE 12. Correlation between Ca and <X-O> in Li-rich (>0.60 apfu) tourmalines from the Himalaya Mine, Mesa Grande, San Diego County, California, U.S.A.

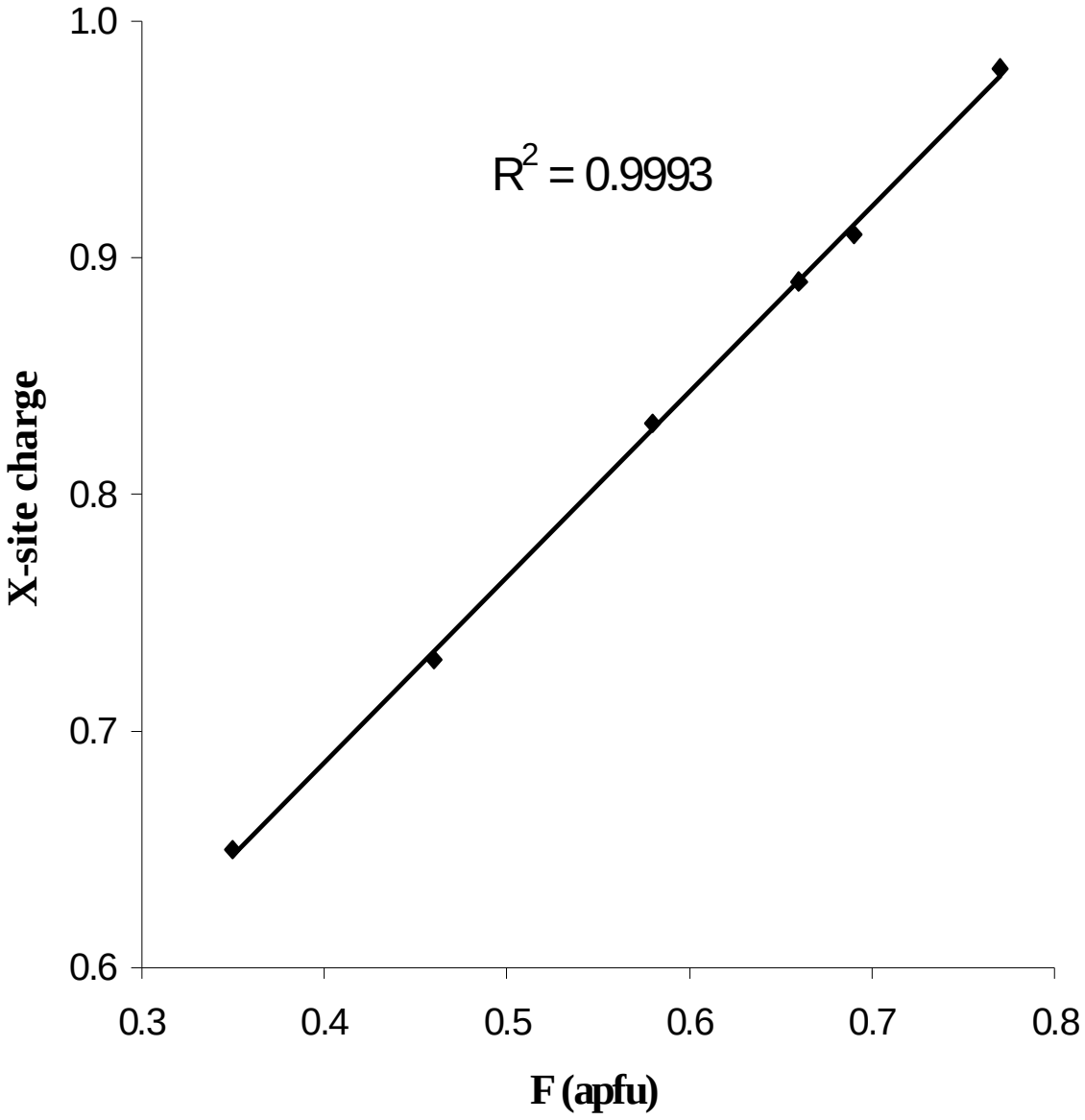

FIGURE 13. Correlation between the F content and the X-site charge in tourmalines from the elbaite-schorl series (with a liddicoatite component of maximum ~19 mol.%) from the Himalaya Mine.

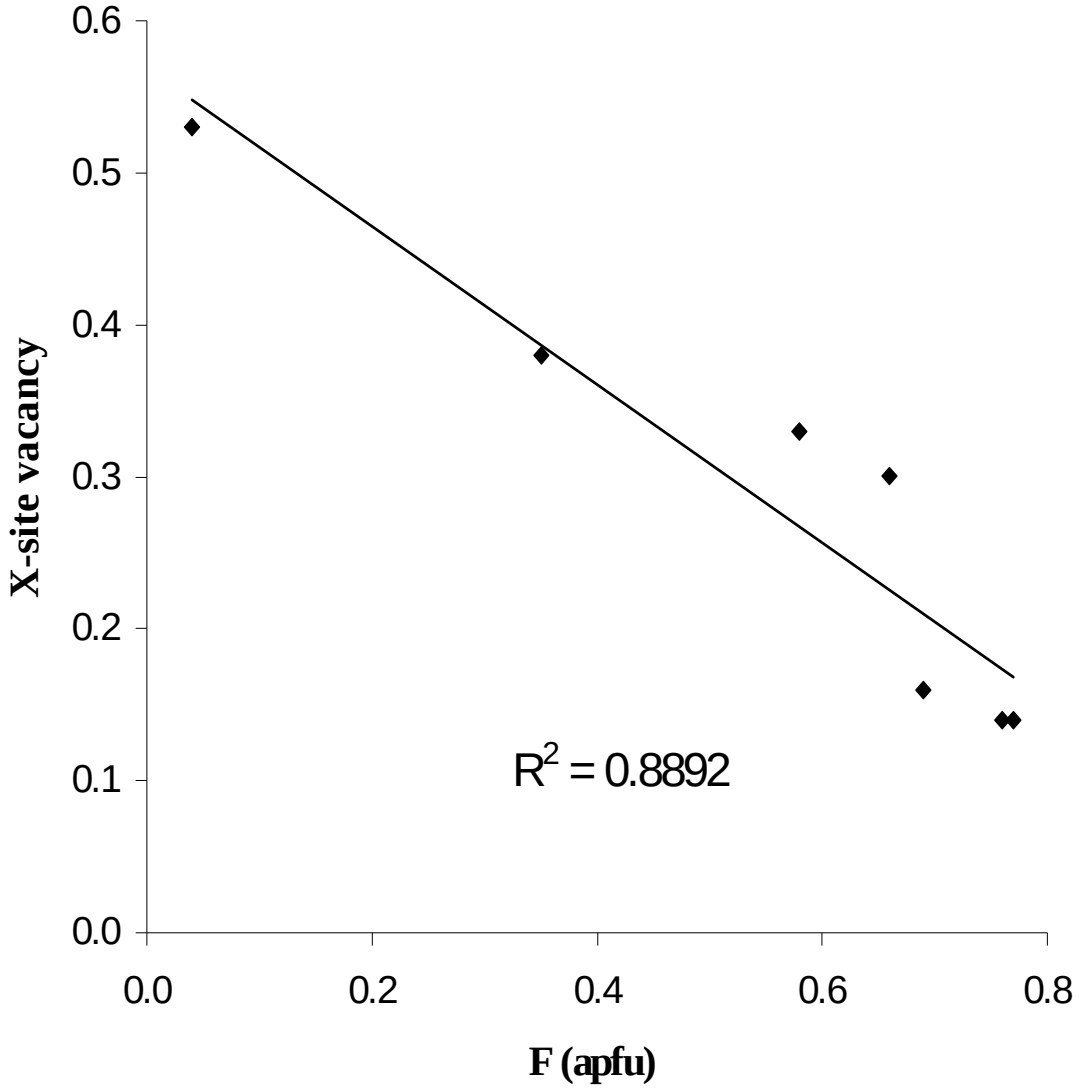

FIGURE 14. Correlation between the F content and the X-site vacancy in tourmalines from the Himalaya Mine.

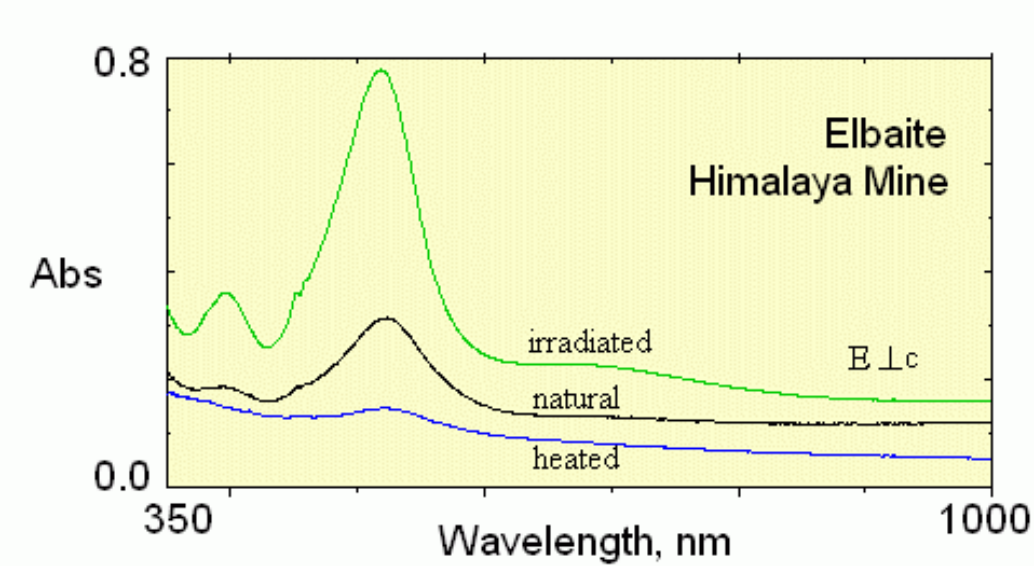

FIGURE 15. Optical absorption spectra of GRR 565a from Reinitz and Rossman (1988) as mined in the Himalaya Mine (natural), after heating at 600 ºC (for 1 h) to decolorize it (heated); and after irradiation with 32 Mrad of Cs-137 gamma rays to turn it darker pink. All spectra are normalized to 1.0 mm thickness and are offset vertically for clarity. The chemical analysis of this sample gave MnO: 1.19 wt%, FeO: 0.02 wt% (Rossman and Mattson, 1986).

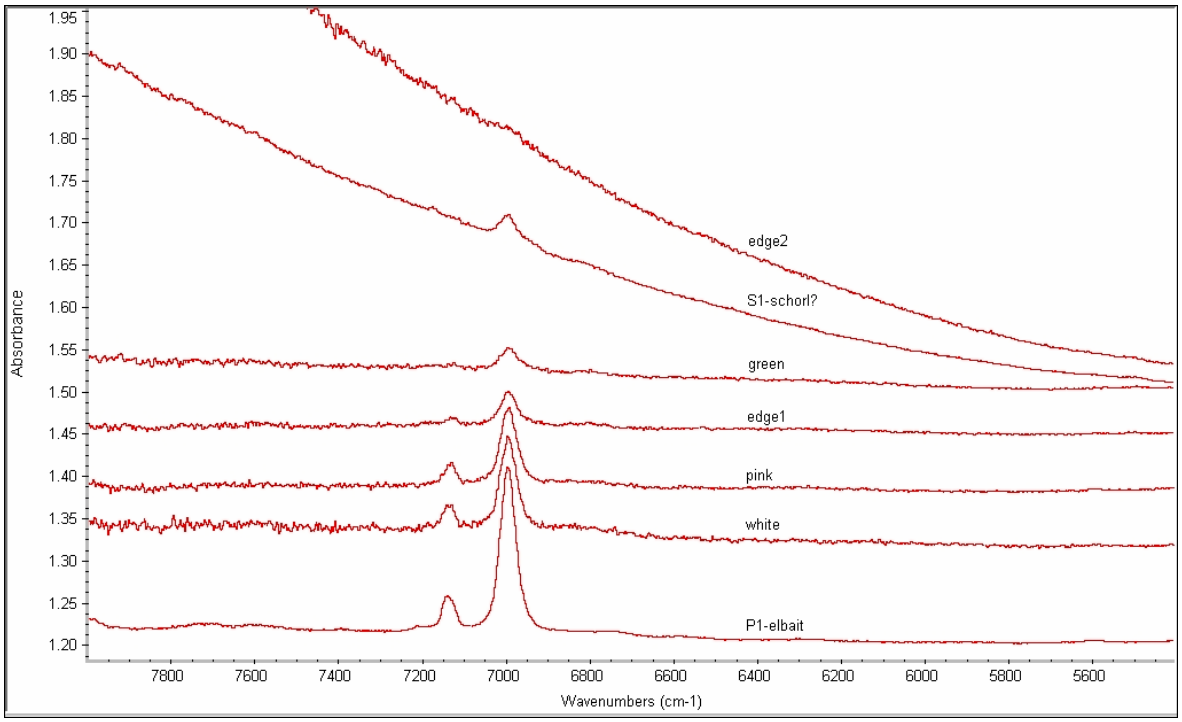

FIGURE 16. Near infrared spectra of the samples HIM1-HIM5 (including intermediate zones) from the Himalaya Mine in the OH overtone region. Thickness: ~1.4 mm.

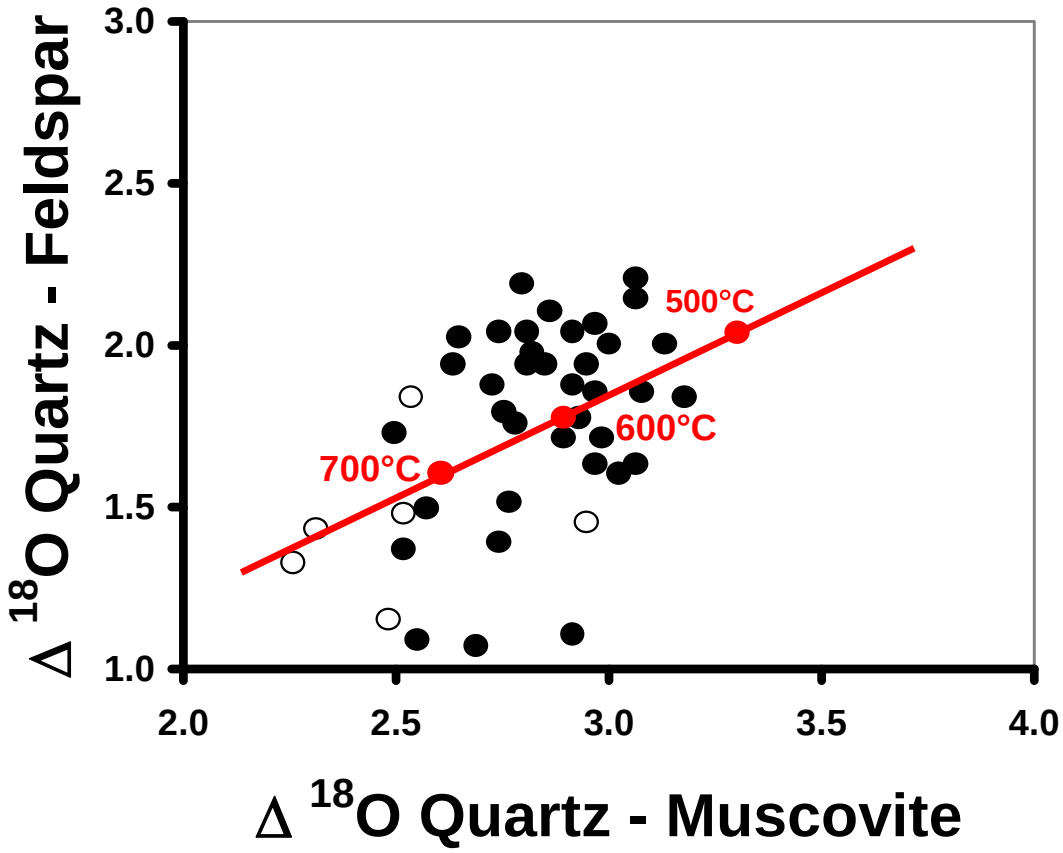

FIGURE 17. Plots of oxygen isotope fractionation between coexisting mineral pairs, redrafted from Taylor et al. (1979). Temperature scale is based on calibrations for (a) quartz-muscovite and (b) quartz-alkali feldspar and quartz-muscovite from Blattner and Bird (1976) and O'Neil and Taylor (1967, 1969). Solid circles are from massive graphic granite pegmatite and aplite, open circles are samples from miarolitic cavities.

3 Substitution mechanism in tourmalines of the “fluor-elbaite”-rossmanite series from Wolkenburg, Saxony, Germany

3.1 Abstract

Single-crystal structure and chemical (EMPA, SIMS, TGA) data were obtained from three pale coloured to colourless Al- and Li-rich tourmalines from a pegmatite from Wolkenburg near Limbach-Oberfrohna, Saxony, Germany. Tourmaline samples of the “fluor-elbaite”-rossmanite solid solution series were chemically (including the light elements) and structurally characterized for the first time. The crystal chemical formulae of these three investigated samples range from a “fluor-elbaite” dominant composition with $^{X}(Na_{0.65}\square_{0.29}Ca_{0.06})$ $^{Y}(Al_{1.64}Li_{1.12}Mn^{2+}_{0.10}Fe^{2+}_{0.02}\square_{0.12})$ $^{Z}Al_6$ $(BO_3)_3$ $^{T}(Si_{5.90}B_{0.10})$ O_{18} $(OH)_3$ $[F_{0.72}(OH)_{0.18}O_{0.10}]$, over $^{X}(Na_{0.54}\square_{0.45}Ca_{0.01})$ $^{Y}(Al_{1.90}Li_{0.97}Mn^{2+}_{0.03}Fe^{2+}_{0.01}\square_{0.09})$ $^{Z}Al_6$ $(BO_3)_3$ $^{T}(Si_{5.82}B_{0.18})$ O_{18} $^{V}(OH)_3$ $^{W}[(OH)_{0.51}F_{0.37}O_{0.12}]$ to Na-rich rossmanite with the composition $^{X}(\square_{0.51}Na_{0.48}Ca_{0.01})$ $^{Y}(Al_{2.02}Li_{0.71}Mn^{2+}_{0.03}\square_{0.24})$ $^{Z}Al_6$ $(BO_3)_3$ $^{T}(Si_{5.69}Al_{0.17}B_{0.14})$ O_{18} $^{V}(OH)_3$ $^{W}[(OH)_{0.70}F_{0.26}O_{0.04}]$. When the rossmanite component increases, while the “fluor-elbaite” component decreases, the olenite component also increases. In a pegmatitic system where essentially no Fe, Mn, Ti and Mg are available, the Li content is an important factor, which seems to control the amount of Si in tourmaline (r^2 = 1.00 for samples from the “fluor-elbaite”-rossmanite-“oxy-rossmanite” series). Once the Li^{1+} content is lower, Al^{3+} cations (with a higher oxidation state) must occupy the *Y* site. For a charge-balanced formula, other cation sites must therefore have lower bulk charges. This can be achieved by increasing vacancies at the *X* site and increasing amounts of trivalent cations at the *T* site. In the Wolkenburg tourmalines of the “fluor-elbaite”-rossmanite series both substitutions are observed. For the investigated tourmalines a modified (coupled) Tschermaks’ substitution with $^{X}\square + {}^{Y}Al^{3+} + {}^{T}(Al, B)^{3+} \leftrightarrow {}^{X}Na^{+} + {}^{Y}Li^{+} + {}^{T}Si^{4+}$ can be proposed. The F content is dependent on the charge of the *X*-site occupants (r^2 = 1.00). There is also a good negative correlation between the charge of the *X*-site occupants and the *X*-O2 distance (r^2 = 1.00), which can be used in the future to draw some conclusions about the *X*-site occupancy when only single-crystal structure data are available.

3.2 Introduction

Only a few localities with pale pink or pale green coloured elbaites are known in Germany. All localities of tourmalines which are believed to be Na- and Li-rich tourmalines are located in Saxony: in the Saxonian granulite massif, as for instance the Amerika quarry near Penig (VOLLSTÄDT & BAUMGÄRTEL 1977, WITTERN 2001) and a pegmatite vein near Wolkenburg (HAAKE et al. 1994), different localities near the village of Ehrenfriedersdorf, Erzgebirge (WITTERN 2001), and at the village of

Wolkenstein, Marienberg district, Erzgebirge (VOLLSTÄDT & BAUMGÄRTEL 1977). These pale coloured tourmalines from Saxony were not characterized chemically and structurally to date. Hence, it was of interest to determine to which mineral species these tourmalines belong. For this purpose, pale coloured tourmalines from Wolkenburg, collected by one of the authors (L. N.) in 1984, were used for this study.

HAWTHORNE & HENRY (1999) gave the general chemical formula of the tourmaline-group minerals as $X\,Y_3\,Z_6\,[T_6O_{18}]\,(BO_3)_3\,V_3\,W$ [V site = O3 site, W site = O1 site]. The X site is usually occupied by Na, Ca, and by small amounts of K. Sometimes this site is vacant (e.g., by foitite, FOIT 1989). The Y site in tourmaline can be occupied by Al, Li, Mg, Fe^{2+}, Fe^{3+}, Mn^{2+}, Mn^{3+}, Ti^{4+}, Cu, V^{3+} and Cr^{3+}, while the Z site is mostly occupied by Al, in Mg-bearing tourmalines substituted partly by Mg and Ti^{4+}, occasionally by Fe^{3+}, and rarely by V^{3+} and Cr^{3+} (GRICE & ERCIT 1993, FOIT & ROSENBERG 1979, HAWTHORNE et al. 1993, MACDONALD & HAWTHORNE 1995, TAYLOR et al. 1995, BLOODAXE et al. 1999, ERTL et al. 2003a, b, BOSI & LUCCHESI 2004, and BOSI et al. 2004). The T site is usually occupied by Si but sometimes also by Al (*e.g.,* FOIT & ROSENBERG 1979; MACDONALD & HAWTHORNE 1995) and B (ERTL et al. 1997, 2008, and references therein). The endmember formula of elbaite, $Na(Li_{1.5}Al_{1.5})Al_6(BO_3)_3[Si_6O_{18}](OH)_3(OH)$, was published by WINCHELL (1933) for the first time (ERTL 2008). The endmember formula of "fluor-elbaite", $Na(Li_{1.5}Al_{1.5})Al_6(BO_3)_3[Si_6O_{18}](OH)_3F$, the F-analogue of elbaite, was proposed by HAWTHORNE & HENRY (1999) for the first time. Liddicoatite, with the endmember formula $Ca(Li_2Al)Al_6(BO_3)_3[Si_6O_{18}](OH)_3F$, which represents the Ca-analogue of "fluor-elbaite", was described by DUNN et al. (1977). The chemistry and crystal structures of tourmalines of the liddicoatite-elbaite series were studied by ERTL et al. (2006). Rossmanite, with the simplified formula $\square(LiAl_2)Al_6(BO_3)_3(Si_6O_{18})(OH)_4$, was described by SELWAY et al. (1998). "Oxy-rossmanite", with the endmember formula $\square(Li_{0.5}Al_{2.5})Al_6(BO_3)_3(Si_6O_{18})(OH)_3O$ (HAWTHORNE & HENRY 1999), the O-analogue of rossmanite, was also found to occur in nature (ERTL et al., 2005). The chemistry (without light elements data) of rossmanite from lepidolite-subtype pegmatites was described by SELWAY et al. (1999) and from a petalite-subtype pegmatite by SELWAY et al. (2000).

The Saxonian Granulite Massif, which forms part of the Saxothuringian zone of the European Variscides, was intruded in Variscan times (~333 Ma) during the final stage of exhumation (2-3 kbar) by granitic (monzogranite) and pegmatitic bodies (VON QUADT 1993, GOTTESMANN et al. 1994, TISCHENDORF et al. 1995, NASDALA et al. 1996, KRÖNER et al. 1998). The granulites are mainly composed of quartz, mesoperthitic orthoclase and almandine, associated with minor amounts of kyanite, sillimanite, oligoclase, corundum and hercynitic spinel (ANDERSON et al. 1998). Oxygen, deuterium and nitrogen isotopes and also REE's indicate that the granulite was the source rock of the granitic melt, which was generated due to the influx of H_2O (MÜLLER et al. 1987, REINHARDT & KLEEMANN 1994). The more evolved rare-element pegmatites (which contain elbaite and lepidolite) may be related to the Mittweida monzogranite (ANDERSON et al. 1998). A microbeam XAFS study of saline fluid inclusions in quartz from

a granitic pegmatite (near Knaumühle in the Saxonian Granulite Massif) yielded temperature estimations up to 430°C (ANDERSON et al. 1998). Samples described in this present study originate from a small (2 metres wide) pegmatite vein, embedded in granulite, that is exposed in close proximity to a railway track at the right (i.e., Eastern) slope of the Zwickauer Mulde valley, about 350 metres South-East of the Wolkenburg castle. In this pegmatite, dravite, schorl, colourless, pale pink, pale blue and green tourmalines, as well as lepidolite, muscovite, biotite, amblygonite, apatite, orthoclase, quartz, and cordierite (partially as "pinite") were found (HAAKE et al. 1994). In this investigation the results of a structural and chemical investigation of three hydrothermal grown Li-bearing tourmalines from miarolitic pockets from one pegmatitic vein are reported, which for the first time were found to represent a solid solution between "fluor-elbaite" and rossmanite.

3.3 Methods

3.3.1 Sample selection

From a suite of small single crystals (ranging from ~1 mm up to ~1 cm in length), three crystal fragments were selected for structural characterization (Table 1) and subsequent chemical analyses. The first fragment, WOLO, is from the pale orange-pink half of a bicoloured crystal (~2 mm in length); the other half shows a pale green colour. The second, WOLC, is from a colourless to very pale pink crystal ~3 mm in length). The third, WOLP, is from a fragment of a pink crystal ~3 mm in size. The investigated fragments were generally clear and free of inclusions. Although sample WOLO taken from a zoned crystal (as described above), the small investigated tourmaline fragments, which are in the range ~120-250 μm (Table 1), are relatively homogeneous as is indicated by the standard deviations in Table 4. Just samples WOLC and WOLP show zonations in MnO which are in the range ~0.2 wt% and ~0.4 wt%, respectively. However, the Mn content is relatively low in the investigated samples and is not considered an essential component, except for the colour (e.g., ERTL et al. 2003b, 2005). As the samples were found ~25 years ago as single crystals in the dump of broken pegmatitic materal (during the construction of a railway), no more specific details about the pockets can be given. Although pink coloured Li-tourmaline was quite common in the past, to our knowledge no Li-tourmaline crystals were found in recent years in this pegmatitic outcrop, which is still visible.

3.3.2 Crystal structures

The three fragments were mounted on a Nonius KappaCCD diffractometer equipped with graphite-monochromated Mo *K*α radiation. Highly redundant data were collected at room temperature for an approximate sphere of reciprocal space, and were integrated and corrected for Lorentz, polarization,

absorption and background factors using Nonius software (see Table 1 for details).

The structures were refined using SHELXL97 (SHELDRICK, 1997) and a tourmaline starting model from FORTIER & DONNAY (1975). Initial refinement cycles led to preliminary $R1(F)$ values of ~2.0 %, and the H atom bonded to the O3 atom was located from a difference-Fourier map and freely refined. Subsequent refinement was performed with anisotropic thermal parameters for all non-hydrogen atoms. Site occupancies were refined according to well-known characteristics of the tourmaline structure (Na was refined at the *X* site, Al and Li were refined at the *Y* site, Si and B were refined at the *T* site; for other details see Table 2). The *Z*-site occupation was fixed with Al in all samples, after the released occupancy did not verify the occurrence of Fe and/or Mn at this position. The refinements converged at $R1(F)$ values of 1.5 % (WOLO, WOLC) and 1.6 % (WOLP). Table 1 provides crystal data and details of the structure refinement of these samples. In Table 2, the atomic parameters are listed, and in Table 3 selected interatomic distances are listed.

3.3.3 Chemical analysis

The three crystal fragments used for the structure refinement were prepared as a polished section for chemical analysis. Concentrations of all elements except B, Li, Be, and H were determined with a Cameca SX51 electron microprobe (EPMA) equipped with five wavelength-dispersive spectrometers (University of Heidelberg). The operating conditions were 15 kV accelerating voltage, 20 nA beam current, with a beam diameter of 5 μm. Peaks for all elements were measured for 10 s, except for Mg Kα (20 s), Cr Kα (20 s), Ti Kα (20 s), Zn Kα (30 s), and F Kα (40 s). Because the F Kα line interferes with the Fe and Mn Lα lines, the measured F values require a correction. Kalt et al. (2001) gave a formula for correcting this interference. Because of a typographical error in the original published formula of KALT et al. (2001), the following corrected version of the formula: $F = F_{meas} - (-0.000055\ FeO^2 + 0.00889\ FeO - 0.0044) + 0.015\ MnO$ was used. Natural and synthetic silicate and oxide standards were used for calibration (ERTL et al. 2003b). The analytical data were reduced and corrected using the PAP routine. A modified matrix-correction was applied assuming a stoichiometric proportion of O atoms and all non-measured components were assumed to be B_2O_3. The accuracy of the electron-microprobe analyses and the correction procedure were checked by measuring three samples of reference tourmalines (98114: elbaite, 108796: dravite, 112566: schorl). Compositions of these tourmaline samples were presented in the context of an interlaboratory comparison (DYAR et al. 1998, 2001). Under the described conditions, analytical errors on all analytical results are ±1% relative for major elements and ±5% relative for minor elements.

Concentrations of H, Li, Be and B were determined by secondary ion mass spectrometry (SIMS) with a CAMECA ims 3f ion microprobe (Universität Heidelberg). Primary O^{2-} ions were accelerated to 14.5 keV and secondary ions were accelerated to a nominal 4.5 keV. An offset of 75 V was applied to the

secondary accelerating voltage so that secondary ions with an initial energy of 75 ± 20 eV were analyzed (energy-filtering). The offset is chosen in order to minimise possible matrix effects for Li, Be, B (OTTOLINI et al. 1993) and H.

For Li, Be and B the primary beam current was 10 nA, resulting in a beam diameter of ~ 20 μm. The spectrometer's mass resolution M/ΔM was set to ~1100 (±10%) to suppress interferences and the imaged field was 150 μm in diameter.

For determination of H the primary beam current was 20 nA, M/ΔM was set to ~400 (±10%) and the imaged field was set to 25 μm (nominal value). To reduce the influence of *in situ* contamination with water, a small field-aperture (d = 400 μm) was chosen, which limited the analysed area to ~ 5 μm in diameter. The partial pressure of H_2O in the sample chamber was reduced using the LN_2 cold trap and magnetic field coils were used to compensate magnetic fields near the sample. Due to the high H concentration in tourmaline it was not necessary to analyse with multiple values for the primary beam current as described in Ludwig & Stalder (2007), where the method applied for this work is documented.

The relative ion yield (RIY) for B and H was determined using three different tourmalines as reference material: elbaite (98144), dravite (108796) and schorl (112566), all described and analyzed by DYAR et al. (1998, 2001). For Li and Be the standard glass SRM610 (NIST) was used as reference material; concentrations (prefered averages) for Li and Be were taken from Pearce *et al*. (1997). The RIYs of Li and B were corrected for the Fe + Mn concentration in the samples and in the reference materials, respectively (OTTOLINI & HAWTHORNE, 1999). While the matrix of SRM610 is very different from tourmalines, for Li the SRM610 has two distinct advantages: it is homogeneous and its Li concentration is very well determined. This is in contrast to the elbaite 98144, whose Li concentration is inhomogeneous (DYAR et al. 2001, Table 11) which makes it problematic to use this sample as a standard. Using the three tourmalines as reference material, a correlation of RIY(H) with the concentration of monovalent cations (Li, Na, K) in the tourmaline can be found. The RIYs were corrected for that correlation.

The relative precision (1σ) of single H, Li, Be and B SIMS analyses on all samples and reference materials was better than 1%. Matrix effects and the uncertainty of the element concentrations in the reference materials limit the accuracy and thus dominate the uncertainty of the SIMS analyses. Based on OTTOLINI et al. (1993), OTTOLINI & HAWTHORNE (1999) and our own observations the worst case deviation in the accuracy is estimated to be better than 20% for H and Li and better than 10% for Be and B. Table 4 contains complete chemical-analytical data for the tourmalines from Wolkenburg, Saxony.

For another determination of the OH content of the tourmaline sample WOLP, ~15 mg of the remaining tourmaline crystal were used for thermogravimetric analysis (TGA), which was performed on the Mettler-Toledo TGA/SDTA 851 (Universität Wien). The powder was heated from 25°C to 1100°C (5°C/min) under a stream of N_2 gas (gas flow: 25 ml/min).

3.4 Results and discussion

Compositional and structural trends. Because the *T*-site occupancy in two samples (WOLO, WOLC) exceeds slightly 6 apfu (Table 4), B_2O_3 was calculated in the optimized formulae as 9 – Si (apfu) = B (apfu) (iterated until the calculated SiO_2 value was identical with the measured value; see also ERTL et al. 2006) (Table 4). B_2O_3 for the optimized formula for sample WOLP was corrected with the same factor which resulted from the correction procedure for WOLC (as described above), because of the very similar (MnO + FeO) and the relative similar Li_2O content. For all samples the formulae were calculated by using the SIMS data of Li and H, based on 31 (O,OH,F). Using this method, the structural formulae of these tourmaline samples are:

WOLO: $^{X}(Na_{0.65}\square_{0.29}Ca_{0.06})\ ^{Y}(Al_{1.64}Li_{1.12}Mn^{2+}_{0.10}Fe^{2+}_{0.02}\square_{0.12})\ ^{Z}Al_6\ (BO_3)_3\ ^{T}(Si_{5.90}B_{0.10})\ O_{18}\ ^{V}(OH)_3\ ^{W}[F_{0.72}(OH)_{0.18}O_{0.10}]$

WOLC: $^{X}(Na_{0.54}\square_{0.45}Ca_{0.01})\ ^{Y}(Al_{1.90}Li_{0.97}Mn^{2+}_{0.03}Fe^{2+}_{0.01}\square_{0.09})\ ^{Z}Al_6\ (BO_3)_3\ ^{T}(Si_{5.82}B_{0.18})\ O_{18}\ ^{V}(OH)_3\ ^{W}[(OH)_{0.51}F_{0.37}O_{0.12}]$

WOLP: $^{X}(\square_{0.51}Na_{0.48}Ca_{0.01})\ ^{Y}(Al_{2.02}Li_{0.71}Mn^{2+}_{0.03}\square_{0.24})\ ^{Z}Al_6\ (BO_3)_3\ ^{T}(Si_{5.69}Al_{0.17}B_{0.14})\ O_{18}\ ^{V}(OH)_3\ ^{W}[(OH)_{0.70}F_{0.26}O_{0.04}]$

These formulae are in good agreement with the formulae derived from the crystal-structure refinements (Table 2); it is noteworthy that the good agreement also applies to the refined O:F ratios on the O1 site.

Using valid and proposed current tourmaline endmember species (HAWTHORNE & HENRY 1999), the tourmaline samples from Wolkenburg can essentially be described as a solid solution of "fluor-elbaite" and rossmanite components. Sample WOLO consists of 47 mol% "fluor-elbaite", 29 mol% rossmanite, 10 mol% olenite and 6 mol% liddicoatite. Sample WOLC consists of 45 mol% rossmanite, 33 mol% "fluor-elbaite" and 16 mol% olenite. Sample WOLP consists of 51 mol% rossmanite, 27 mol% olenite and 12 mol% "fluor-elbaite". When the rossmanite component increases, the olenite component (Na at the *X* site, Al_3 at the *Y* site; HAWTHORNE & HENRY 1999) also increases. All three analysed samples have only relatively small Fe, Mn and Ti contents (sum of FeO, MnO and TiO_2 < 1 wt.%; Table 4). Hence, the component of other tourmaline endmembers (*e.g.,* schorl), which are in the range of a few percent, can be neglected.

X-site occupation. In the Wolkenburg tourmaline samples the charge of all *X*-site occupants correlates positively with the F content (Fig. 1; r^2 = 1.00). There is also a good negative correlation between the number of vacancies at the *X* site and the F content (Fig. 2; r^2 = 1.00). Already HENRY (2005) showed in an evaluation of ~600 chemical analyses of different tourmaline varieties that with more than 0.5 *X*-site vacancies there is little or no F present in the tourmaline. ERTL et al. (2002) stated that the *Y*-site occupants and the F content mainly explain the distortion of the XO_9 polyhedron. The presence of F enlarges the bond-length distortion of the XO_9 polyhedron. Furthermore, ERTL et al. (2001) found a

reliable relationship between the *X*-O2 distance and the mean ionic radius of the *X*-site occupants in Mg- and/or Fe-rich tourmalines. In the Li-rich Wolkenburg tourmalines there is a good negative correlation between the charge of the *X*-site occupants and the *X*-O2 distance (Fig. 3; r^2 = 1.00). Hence, the *X*-O2 distance gives more useful information than the <*X*-O> distance, which is not varying very much (Table 3). There is another good negative correlation between the Na content and Al at the *Y* site (Fig. 4; r^2 = 1.00). This correlation might be explained because of the requirement of a charge-balanced formula. The Na-^{Y}Al correlation in Fig. 4 (r^2 = 1.00) is a charge balance substitution, which can be extended to a modified (coupled) Tschermaks' substitution with $^{X}\square + {}^{Y}Al^{3+} + {}^{T}(Al, B)^{3+} \leftrightarrow {}^{X}Na^{+} + {}^{Y}Li^{+} + {}^{T}Si^{4+}$.

Y-site occupation. The *Y* site in the Wolkenburg samples is mainly occupied by Al, Li, and minor amounts of Mn and Fe (Table 4). There is a good correlation between Al at the *Y* site and the <*Y*-O> distance (Fig. 5; r^2 = 1.00). This correlation allows a good estimation of the Al content of the *Y* site in tourmalines which contain essentially only Al and Li at the *Y* site. Both *a* and *c* unit-cell parameters (Table 1) increase with increasing Li content (this neglects the influence of the number of vacancies on the *X* site as well as the other sites, which show only very small variations of their average bond-length distances; Table 3).

Z-site occupation. The *Z* site in all our investigated samples is completely occupied by Al. The <*Z*-O> distance maintains a nearly constant and relatively low value for all samples (1.907 Å; Table 3). Similar distances were observed in other elbaite and rossmanite samples (*e.g.,* BURNS et al. 1994, SELWAY et al. 1998). Small amounts of Fe (≤0.02 apfu) in the investigated samples might theoretically occupy the *Z* site if they are present as Fe^{3+} (no Mössbauer data is available from these samples). However, such small amounts are not detectable by structure refinement.

T-site occupation. The *T* site shows in our samples a mixed occupation of Si, B and also Al. Tetrahedrally coordinated B is indicated by both chemical data (including light element analysis as B_2O_3; Table 4) and structural data (Tables 2 & 3). The refinement of the Si:B ratio on the *T* site gives values for $^{[4]}$B in the range ~0.1-0.2 apfu (Table 2), in good agreement with the chemical data (Table 4). Also the slightly reduced <*T*-O> distances (contrary to the ideal Si-O distance of ~1.620 Å in tourmaline; MACDONALD & HAWTHORNE 1995), which are in the range 1.617-1.618 Å (Table 3), clearly indicate the presence of small amounts of $^{[4]}$B. Only sample WOLP was assigned with a mixed occupation including also $^{[4]}$Al. This sample shows the lowest amount of Si and the chemical analysis indicates an occupation of $^{T}(Si_{5.69}Al_{0.17}B_{0.14})$e (Table 4). This seems to be realistic, because in the event that the difference from 6 apfu would be completely filled either by B or Al, the <*T*-O> distance would show a significantly lower or higher value (~1.615 Å and ~1.623 Å, respectively) than the measured value of 1.618 Å (Table 3, ERTL et al. 2001, 2006). Also the refined Si:B ratio on the *T* site is in good agreement with the optimized formula (Tables 3 & 4). Similarly mixed *T*-site occupations were already observed in "oxy-rossmanite" (ERTL et al. 2005). Thus, it seems not surprising that rossmanite samples show a mixed occupation at the *T* site.

Even for rossmanite from the type locality, the relatively low <*T*-O> distance of 1.614 Å (SELWAY et al. 1998) might give an indication for some $^{[4]}$B. The investigated samples from Wolkenburg show a clear positive correlation between Al at the *Y* site and the refined $^{[4]}$B content (Fig. 6; r^2 = 0.98). Such a correlation is not surprising because this seems to be a general trend in Al-rich and Li-bearing tourmalines as already observed for tourmalines from the olenite-elbaite-liddicoatite series (HUGHES et al. 2004; ERTL et al. 2006, 2007). Interestingly, I found a good positive correlation between Li and Si contents for the Wolkenburg samples (Fig. 7; r^2 = 1.00). By adding the "oxy-rossmanite" samples from Eibenstein, Lower Austria (ERTL et al. 2005), which show also a significant deficiency in Si, the correlation still stays very good (Fig. 7; r^2 = 1.00). An explanation for this relation is probably the need for a charge-balanced formula in the absence of Fe, Mn and Mg. Once the Li^{1+} content is decreasing during crystal growth, higher-charged Al^{3+} cations must occupy the *Y* site. For a charge-balanced formula, other cation sites must therefore have lower bulk charges. This can be achieved by increasing vacancies at the *X* site and increasing amounts of trivalent cations at the *T* site. In fact, both possibilities can be observed in the Wolkenburg samples.

V- and W-site occupations. ERTL et al. (2002) showed that the bond-angle distortion (σ_{oct}^2) of the ZO_6 octahedron in a tourmaline is largely a function of the <*Y*-O> distance of that tourmaline, although the occupant of the O3 site (*V* site) also affects that distortion. The covariance, *r*, of <*Y*-O> and the σ_{oct}^2 of the ZO_6 octahedron is -0.991 for all investigated tourmalines that are occupied by 3 (OH) groups, including the samples from HUGHES et al. (2004). The tourmaline samples from Wolkenburg fall on the *V* site = 3 (OH) line in figure 3 from ERTL et al. (2002). It is, however, only possible to do a semi-quantitative estimation of the OH content of the O3 site by using this relationship. Hence, I assume that the *V* site in all investigated samples is filled by ~3.0 (OH). The optimized formula for the sample WOLO gives the *W*-site occupation with $[F_{0.72}(OH)_{0.18}O_{0.10}]$, whereas the *W* site for the samples WOLC and WOLP are occupied by $[(OH)_{0.51}F_{0.37}O_{0.12}]$ and $[(OH)_{0.70}F_{0.26}O_{0.04}]$, respectively. Although the SIMS H_2O content of sample WOLP is consistent with the content determined by TGA, it is not clear, if the small amounts of O content at the *W* site are real, or if they are just a result of the error in the H_2O estimation. An OH content just ~3% higher than the measured value would be required to completely fill the difference to the measured F content of a fully occupied *W* site in all samples with OH. As pointed out before, the F content, as estimated from refinements of the O:F ratio on the O1 site, is in good agreement with the chemical data (Tables 2 & 4).

3.5 Acknowledgements

I am grateful to Andreas Wagner, Vienna, Austria, for sample preparation. Special thanks to George R. Rossman for a preliminary review. This work was supported by Österreichischer Fonds zur Förderung der wissenschaftlichen Forschung (FWF) project no. P20509.

3.6 References

ANDERSON, A.J., MAYANOVIC, R.A. & BAJT, S. (1998): A microbeam XAFS study of aqueous chlorozinc complexing up to 430°C in fluid inclusions from the Knaumühle granitic pegmatite, Saxonian Granulite Massif, Germany. – Can. Mineral. **36:** 511-524.

BLOODAXE, E. S., HUGHES, J. M., DYAR, M. D., GREW, E. S. & GUIDOTTI, C. V. (1999): Linking structure and chemistry in the schorl-dravite series. – Amer. Mineral. **84:** 922-928.

BOSI, F. & LUCCHESI, S. (2004): Crystal chemistry of the schorl-dravite series. – Eur. J. Mineral. **16:** 335-344.

BOSI, F., LUCCHESI, S. & REZNITSKII, L. (2004): Crystal chemistry of the dravite–chromdravite series. – Eur. J. Mineral. **16:** 345-352.

BURNS, P. C., MACDONALD, D. J. & HAWTHORNE, F. C. (1994): The crystal chemistry of manganese-bearing elbaite. – Amer. Mineral. **32:** 31-41.

DUNN, P. J., APPLEMAN, D. E. & NELEN, J. E. (1977): Liddicoatite, a new calcium end-member of the tourmaline group. – Amer. Mineral. **62:** 1121-1124.

DYAR, M. D., TAYLOR, M. E., LUTZ, T. M., FRANCIS, C. A., GUIDOTTI, C. V. & WISE, M. (1998): Inclusive chemical characterization of tourmaline: Mössbauer study of Fe valence and site occupancy. – Amer. Mineral. **83:** 848-864.

DYAR, M. D., WIEDENBECK, M., ROBERTSON, D., CROSS, L. R., DELANEY, J. S., FERGUSON, K., FRANCIS, C. A., GREW, E. S., GUIDOTTI, C. V., HERVIG, R. L., HUGHES, J. M., HUSLER, J., LEEMAN, W., MCGUIRE, A. V., RHEDE, D., ROTHE, H., PAUL, R. L., RICHARDS, I. & YATES, M. (2001): Reference minerals for the microanalysis of light elements. – Geostand. Newsl. **25:** 441-463.

ERTL, A. (2008): About the nomenclature and the type locality of elbaite: A historical review. – Mitt. Österr. Mineral. Ges. **154:** 35-44.

ERTL, A., PERTLIK, F. & BERNHARDT, H.-J. (1997): Investigations on olenite with excess boron from the Koralpe, Styria, Austria. – Österr. Akad. Wiss., Math.-Naturw. Kl., Abt. I, Anz. **134:** 3-10.

ERTL, A., HUGHES, J. M. & MARLER, B. (2001): Empirical formulae for the calculation of <*T*-O> and *X*-O2 bond lengths in tourmaline and relations to tetrahedrally-coordinated boron. – N. Jb. Mineral. Mh. **12:** 548-557.

ERTL, A., HUGHES, J. M., PERTLIK, F., FOIT F. F. JR., WRIGHT, S. E., BRANDSTÄTTER, F. & MARLER, B. (2002): Polyhedron distortions in tourmaline. – Can. Mineral. **40:** 153-162.

ERTL, A., HUGHES, J.M., BRANDSTÄTTER, F., DYAR, M.D. & PRASAD, P.S.R. (2003a): Disordered Mg-bearing olenite from a granitic pegmatite from Goslarn, Austria: A chemical, structural, and infrared spectroscopic study. – Can. Mineral. **41:** 1363-1370.

Ertl, A., Hughes, J.M., Prowatke, S., Rossman, G.R., London, D. & Fritz, E.A. (2003b): Mn-rich tourmaline from Austria: structure, chemistry, optical spectra, and relations to synthetic solid solutions. – Am. Mineral. **88:** 1369-1376.

ERTL, A., ROSSMAN, G. R., HUGHES, J. M., PROWATKE, S. & LUDWIG, T. (2005): Mn-bearing "oxy-rossmanite" with tetrahedrally-coordinated Al and B from Austria: structure, chemistry, and infrared and optical spectroscopic study. – Amer. Mineral. **90:** 481-487.

ERTL, A., HUGHES, J. M., PROWATKE, S., LUDWIG, T., PRASAD, P. S. R., BRANDSTÄTTER, F., KÖRNER, W., SCHUSTER, R., PERTLIK, F. & MARSCHALL, H. (2006): Tetrahedrally coordinated boron in tourmalines from the liddicoatite-elbaite series from Madagascar: Structure, chemistry, and infrared spectroscopic studies. – Amer. Mineral. **91:** 1847-1856.

ERTL, A., HUGHES, J. M., PROWATKE, S., LUDWIG, T., BRANDSTÄTTER, F., KÖRNER, W. & DYAR, M. D. (2007): Tetrahedrally coordinated boron in Li-bearing olenite from "mushroom" tourmaline from Momeik, Myanmar. – Can. Mineral. **45:** 891-899.

ERTL, A., TILLMANNS, E., NTAFLOS, T., FRANCIS, C., GIESTER, G., KÖRNER, W., HUGHES, J.M., LENGAUER, C. & PREM, M. (2008): Tetrahedrally coordinated boron in Al-rich tourmaline and its relationship to the pressure–temperature conditions of formation. – Eur. J. Mineral. **20:** 881-888.

FISCHER, R. X. & TILLMANNS, E. (1988): The equivalent isotropic displacement factor. Acta Crystallogr. **C44:** 775-776.

FOIT, F. F., Jr. (1989): Crystal chemistry of alkali-deficient schorl and tourmaline structural relationships. – Amer. Mineral. **74:** 422-431.

FOIT, F. F. & ROSENBERG, P. E. (1979): The structure of vanadium-bearing tourmaline and its implications regarding tourmaline solid solutions. – Amer. Mineral. **64:** 788-798.

FORTIER, S. & DONNAY, G. (1975): Schorl refinement showing composition dependence of the tourmaline structure. – Can. Mineral. **13:** 173-177.

GOTTESMANN B., WASTERNACK J. & MÄRTENS S. (1994): The Gottesberg tin deposit (Saxony): geological and metallogenic characteristic. In: SELTMANN, R., KÄMPF, H. & MÖLLER, P. (Eds.): Metallogeny of collisional orogens. – Czech Geol. Survey, 110-115, Prague.

GRICE, J. D. & ERCIT, T. S. (1993): Ordering of Fe and Mg in the tourmaline crystal structure: The correct formula. – N. Jb. Mineral. Abh. **165:** 245-266.

HAAKE, R., FLACH, S. & BODE, R. (1994): Mineralien und Fundstellen, Bundesrepublik Deutschland, Teil II. 1st ed., 244 pp., Bode Verlag GmbH, Haltern, Germany.

HAWTHORNE, F. C., MACDONALD, D. J. & BURNS, P. C. (1993): Reassignment of cation site-occupancies in tourmaline: Al-Mg disorder in the crystal structure of dravite. - Amer. Mineral. **78:** 265-270.

HAWTHORNE, F. C. & HENRY, D. J. (1999): Classification of the minerals of the tourmaline group. - Eur. J. Mineral. **11:** 201-215.

HENRY, D. J. (2005) Fluorine – X-site vacancy avoidance in natural tourmaline: internal vs. external control. 2005 Goldschmidt Conference, May 20-25, Moscow, Idaho, USA, Abstracts Volume, abstract no. 1318.

HUGHES, J. M., ERTL, A., DYAR, M .D., GREW, E. S., WIEDENBECK, M. & BRANDSTÄTTER, F. (2004): Structural and chemical response to varying $^{[4]}$B content in zoned Fe-bearing olenite from Koralpe, Austria. – Amer. Mineral. **89:** 447-454.

KALT, A., SCHREYER, W., LUDWIG, T., PROWATKE, S., BERNHARDT, H.-J. & ERTL, A. (2001): Complete solid solution between magnesian schorl and lithian excess-boron olenite in a pegmatite from Koralpe (eastern Alps, Austria). – Eur. J. Mineral., **13:** 1191-1205.

KRÖNER, A., JAECKEL, P., REISCHMANNN, T. & KRONER, U. (1998): Further evidence for an early Carboniferous (~340 Ma) age of highgrade metamorphism in the Saxonian Granulite Complex. – Geol. Rundschau **86:** 751-766.

LUDWIG, T. & STALDER, R. (2007): A new method to eliminate the influence of in-situ contamination in SIMS analysis of hydrogen. – J. Anal. Atom. Spec. **22:** 1415-1419.

MACDONALD, D. J. & HAWTHORNE, F. C. (1995): The crystal chemistry of Si ⇔ Al substitution in tourmaline. – Can. Mineral. **33:** 849-858.

MÜLLER, A., STIEHL, G., BÖTTGER, T., BOTHE, H.K., GEBHARDT, O., GEISLER, M., HANDEL, D., NITZSCHE, H.M., SCHMÄDICKE, E. & GERSTENBERGER, H. (1987): Geochemical, stable isotope and petrographic investigations of granulites, pyriclasites and metagranulitic rocks of the Sächsisches Granulitgebirge. – ZFI-Mitt. **133:** 145-205.

NASDALA, L., GRUNER, T., NEMCHIN, A.A., PIDGEON, R.T. & TICHOMIROWA, M. (1996): New SHRIMP ion microprobe measurement on zircons from Saxonian magmatic and metamorphic rocks. – Proceedings of the Freiberg Isotope Colloquium, Freiberg, University of Mining and Technology, 205-214.

OTTOLINI, L. & HAWTHORNE, F. C. (1999): An investigation of SIMS matrix effects on H, Li and B ionization in tourmaline. – Eur. J. Mineral. **11:** 679-690.

OTTOLINI, L., BOTTAZZI, P. & VANNUCCI, R. (1993): Quantification of lithium, beryllium, and boron in silicates by secondary Ion Mass Spectrometry using conventional energy filtering. Anal. Chem. **65:** 1960-1968.

OTWINOWSKI, Z., BOREK, D., MAJEWSKI, W. & MINOR, W. (2003): Multiparametric scaling of diffraction intensities. – Acta Crystallogr. **A59:** 228-234.

PEARCE N., PERKINS W. T., WESTGATE J. A., GORTON M. P., JACKSON S. E., NEAL C. R. & CHENERY S. P. (1997): A compilation of new and published major and trace element data for NIST SRM 610 and NIST SRM 612 glass reference materials. – Geostand. Newsl., **21:** 115–144.

REINHARDT, J. & KLEEMANN, U. (1994): Extensional unroofing of granulitic lower crust and related low-pressure, high-temperature metamorphism in the Saxonian Granulite Massif, Germany. – Tectonophys. **238:** 71-94.

SELWAY, J.B., NOVÁK, M., HAWTHORNE, F.C., ČERNÝ, P., OTTOLINI, L. & KYSER, T.K. (1998): Rossmanite, □ [$LiAl_2$] $Al_6Si_6O_{18}$ $(BO_3)_3$ $(OH)_4$, a new alkali-deficient tourmaline: description and crystal structure. Amer. Mineral. **83:** 896-900.

SHELDRICK, G.M. (1997): SHELXL-97, a program for crystal structure refinement. University of Göttingen, Germany.

TAYLOR, M. C., COOPER, M. A. & HAWTHORNE, F. C. (1995): Local charge-compensation in hydroxyl-deficient uvite. – Can. Mineral. **33:** 1215-1221.

TISCHENDORF, G., DILL, H.G. & FÖRSTER, H.-J. (1995) Metallogenesis of the Saxothuringian Basins. In: DALLMEYER, R.D., FRANKE, W. & WEBER, K. (eds.): Tectono-Stratigraphic Evolution of the Central and East European Orogens. 266-273, Springer, Heidelberg.

VOLLSTÄDT, H. & BAUMGÄRTEL, R. (1977): Einheimische Edelsteine, 2nd ed., 232 pp., Steinkopff Verlag, Dresden, Germany.

VON QUADT, A. (1993): The Saxonian Granulitmassif: New aspects from geochronological studies. – Geol. Rundschau **82:** 516-530.

WINCHELL, A. N. (1933): Elements of optical mineralogy: an introduction to microscopic petrography. Part 2, Description of minerals with special reference to their optic and microscopic characters. 459 pp. (3rd ed.), John Wiley & Sons, New York, U.S.A.; Chapman & Hall, London, Great Britain.

WITTERN, A. (2001): Mineralfundorte und ihre Minerale in Deutschland. 1st ed., 286 pp., E. Schweizerbart'sche Verlagsbuchhandlung, Stuttgart, Germany.

TABLE 1. Crystal data, data collection information and refinement details for tourmalines of the "fluor-elbaite"-rossmanite series from Wolkenburg, Glauchau, Saxony, Germany.

Sample	WOLO	WOLC	WOLP
a, *c* (Å)	15.844(2), 7.105(1)	15.824(2), 7.096(1)	15.819(2), 7.094(1)
V (Å^3)	1544.6(4)	1538.8(4)	1537.4(4)
Crystal dimensions (mm)	0.12 x 0.12 x 0.13	0.17 x 0.22 x 0.25	0.15 x 0.18 x 0.23
Collection mode, $2\theta_{max}$ (°)	full sphere, 69.94	full sphere, 69.88	full sphere, 69.90
h, k, l ranges	-25/25, -21/21, -11/11	-25/25, -21/21, -11/11	-25/25, -21/21, -11/11
Total reflections measured	3026	3018	3017
Unique reflections	1647 (R_{int} 0.79%)	1640 (R_{int} 0.84%)	1642 (R_{int} 1.04%)
$R1(F)$, $wR2_{all}(F^2)$	1.45%, 3.91%	1.50%, 3.91%	1.63 %, 4.17%
Flack *x* parameter	0.034(64)	0.005(69)	-0.005(75)
'Observed' refls. [$F_o > 4\sigma(F_o)$]	1637	1621	1627
Extinct. coefficient	0.00413(16)	0.00263(13)	0.00195(12)
No. of refined parameters	96	96	96
GooF	1.109	1.153	1.145
$(\Delta/\sigma)_{max}$	0.001	0.001	0.001
$\Delta\sigma_{min}$, $\Delta\sigma_{max}$ (e/Å^3)	-0.48, 0.62	-0.32, 0.48	-0.35, 0.51

Note: Diffractometer: Nonius KappaCCD system; space group *R*3*m*; multi-scan absorption correction (OTWINOWSKY et al. 2003); refinement on F^2. Unit-cell parameters have been refined from roughly 1500 reflections in each case.

TABLE 2. Table of positional parameters and their estimated standard deviations for tourmalines of the "fluor-elbaite"-rossmanite series from Wolkenburg, Glauchau, Saxony, Germany.

Site	*Sample*	*x*	*y*	*z*	U_{eq}	*Occ.*
X	WOLO	0	0	0.7650(2)	0.0189(4)	$Na_{0.74(1)}$
	WOLC	0	0	0.7662(3)	0.0219(7)	$Na_{0.55(1)}$
	WOLP	0	0	0.7672(3)	0.0221(7)	$Na_{0.59(1)}$
Y	WOLO	0.87626(4)	1/2x	0.36638(8)	0.0071(2)	$Al_{0.579(3)}Li_{0.421}$
	WOLC	0.87770(4)	1/2x	0.36341(8)	0.0075(2)	$Al_{0.636(4)}Li_{0.364}$
	WOLP	0.87745(4)	1/2x	0.36346(8)	0.0076(2)	$Al_{0.693(4)}Li_{0.307}$
Z	WOLO	0.70314(2)	0.73994(2)	0.38882(3)	0.00548(6)	$Al_{1.00}$
	WOLC	0.70341(2)	0.74014(2)	0.38963(4)	0.00572(6)	$Al_{1.00}$
	WOLP	0.70340(2)	0.74006(2)	0.38990(4)	0.00590(7)	$Al_{1.00}$
B	WOLO	0.89093(4)	2x	0.5441(2)	0.0057(2)	$B_{1.00}$
	WOLC	0.89093(5)	2x	0.5443(2)	0.0061(2)	$B_{1.00}$
	WOLP	0.89091(5)	2x	0.5447(2)	0.0059(2)	$B_{1.00}$
T	WOLO	0.80810(1)	0.81012(1)	0.99889(3)	0.00413(7)	$Si_{0.986(3)}B_{0.014}$
	WOLC	0.80822(2)	0.81025(2)	0.99828(3)	0.00427(7)	$Si_{0.976(3)}B_{0.024}$
	WOLP	0.80824(2)	0.81028(2)	0.99800(4)	0.00457(7)	$Si_{0.974(3)}B_{0.026}$
H3	WOLO	0.739(2)	1/2x	0.599(4)	0.026(6)	$H_{1.00}$
	WOLC	0.742(2)	1/2x	0.619(5)	0.05(1)	$H_{1.00}$
	WOLP	0.743(2)	1/2x	0.614(5)	0.042(9)	$H_{1.00}$
O1	WOLO	0	0	0.2174(3)	0.0395(8)	$O_{0.22(5)}F_{0.78}$
	WOLC	0	0	0.2212(3)	0.0260(6)	$O_{0.71(5)}F_{0.29}$
	WOLP	0	0	0.2235(3)	0.0242(6)	$O_{0.72(5)}F_{0.28}$
O2	WOLO	0.93973(3)	2x	0.5108(1)	0.0147(2)	$O_{1.00}$
	WOLC	0.93963(4)	2x	0.5077(1)	0.0129(2)	$O_{1.00}$
	WOLP	0.93964(4)	2x	0.5073(2)	0.0126(2)	$O_{1.00}$
O3	WOLO	0.73415(8)	1/2x	0.4909(1)	0.0119(2)	$O_{1.00}$
	WOLC	0.73686(9)	1/2x	0.4913(1)	0.0123(2)	$O_{1.00}$
	WOLP	0.73777(9)	1/2x	0.4912(2)	0.0124(2)	$O_{1.00}$
O4	WOLO	0.90658(3)	2x	0.9258(1)	0.0081(1)	$O_{1.00}$
	WOLC	0.90600(4)	2x	0.9250(1)	0.0082(2)	$O_{1.00}$
	WOLP	0.90588(4)	2x	0.9246(1)	0.0090(2)	$O_{1.00}$
O5	WOLO	0.81301(7)	1/2x	0.9036(1)	0.0084(1)	$O_{1.00}$
	WOLC	0.81231(7)	1/2x	0.9030(1)	0.0082(2)	$O_{1.00}$
	WOLP	0.81247(8)	1/2x	0.9026(1)	0.0094(2)	$O_{1.00}$

O6	WOLO	0.80448(4)	0.81480(4)	0.22390(9)	0.0071(1)	$O_{1.00}$
	WOLC	0.80513(4)	0.81568(5)	0.22401(9)	0.0073(1)	$O_{1.00}$
	WOLP	0.80542(5)	0.81597(5)	0.2242(1)	0.0073(1)	$O_{1.00}$
O7	WOLO	0.71373(4)	0.71395(4)	0.91986(7)	0.0061(1)	$O_{1.00}$
	WOLC	0.71354(4)	0.71381(4)	0.92076(8)	0.0064(1)	$O_{1.00}$
	WOLP	0.71332(5)	0.71369(5)	0.92116(9)	0.0066(1)	$O_{1.00}$
O8	WOLO	0.79047(4)	0.73003(4)	0.55908(8)	0.0073(1)	$O_{1.00}$
	WOLC	0.79048(5)	0.72991(5)	0.56010(9)	0.0074(1)	$O_{1.00}$
	WOLP	0.79056(5)	0.72995(6)	0.56039(9)	0.0073(1)	$O_{1.00}$

Note: Definition for U_{eq} see Fischer and Tillmanns (1988).

TABLE 3. Selected interatomic distances (Å) in tourmalines of the "fluor-elbaite"-rossmanite series from Wolkenburg, Glauchau, Saxony, Germany.

X-	**WOLO**	**WOLC**	**WOLP**
O2 (x3)	2.449(2)	2.470(2)	2.477(2)
O5 (x3)	2.748(1)	2.749(1)	2.743(1)
O4 (x3)	2.807(1)	2.812(1)	2.810(2)
Mean	**2.668(1)**	**2.677(1)**	**2.677(2)**
Y-			
O2 (x2)	1.9654(8)	1.9549(8)	1.9542(8)
O6 (x2)	1.9784(8)	1.9642(8)	1.9576(8)
O1	2.001(1)	1.9564(8)	1.951(1)
O3	2.141(1)	2.133(1)	2.118(1)
Mean	**2.005(1)**	**1.988(1)**	**1.982(1)**
Z-			
O6	1.8583(6)	1.8647(7)	1.8683(8)
O7	1.8828(6)	1.8826(7)	1.8821(7)
O8	1.8879(6)	1.8861(7)	1.8864(7)
O8'	1.9025(6)	1.9002(7)	1.9000(7)
O7'	1.9490(6)	1.9456(7)	1.9410(7)
O3	1.9585(5)	1.9614(6)	1.9639(6)
Mean	**1.907(1)**	**1.907(1)**	**1.907(1)**
T-			
O6	1.6028(7)	1.6061(7)	1.6091(8)
O7	1.6106(6)	1.6093(7)	1.6100(7)
O4	1.6223(4)	1.6194(4)	1.6190(5)
O5	1.6363(4)	1.6329(5)	1.6324(5)
Mean	**1.618(1)**	**1.617(1)**	**1.618(1)**
B-			
O2	1.360(2)	1.360(2)	1.361(2)
O8 (x2)	1.3828(9)	1.381(1)	1.380(1)
Mean	**1.375(1)**	**1.374(1)**	**1.374(1)**

TABLE 4. Composition of tourmalines of "fluor-elbaite"-rossmanite series from Wolkenburg, Saxony, Germany (wt.%, standard deviation in brackets).

	WOLO[1]	WOLO[2]	WOLC[1]	WOLC[2]	WOLP[1]	WOLP[3]
SiO_2 wt.%	37.87(19)	37.87	37.58(18)	37.58	36.61(58)	36.61
TiO_2	0.01(1)	0.01	0.01(1)	0.01	0.00(1)	-
B_2O_3	12.17(21)	11.53	12.26(30)	11.88	12.07(23)	11.70
Al_2O_3	41.61(13)	41.61	43.27(41)	43.27	44.72(49)	44.72
Cr_2O_3	0.01(1)	0.01	0.01(1)	0.01	0.01(1)	0.01
FeO	0.13(3)	0.13	0.05(3)	0.05	0.01(2)	0.01
MnO	0.78(6)	0.78	0.21(7)	0.21	0.20(9)	0.20
MgO	0.01(1)	0.01	0.00(0)	-	0.00(1)	0.00
ZnO	0.01(1)	0.01	0.01(1)	0.01	0.01(1)	0.01
CaO	0.38(2)	0.38	0.05(4)	0.05	0.08(4)	0.08
Na_2O	2.16(5)	2.16	1.80(4)	1.80	1.59(8)	1.59
K_2O	0.01(1)	0.01	0.01(1)	0.01	0.01(1)	0.01
Li_2O	1.79(1)	1.79	1.55(8)	1.55	1.14(10)	1.14
H_2O	3.04(1)	3.04	3.40(15)	3.40	3.57(25)	3.57
F	1.47(5)	1.47	0.75(12)	0.75	0.52(19)	0.52
O≡F	-0.62	-0.62	-0.32	-0.32	-0.22	-0.22
Sum	100.83	100.19	100.64	100.26	100.32	99.95
Si *apfu*	5.85	5.90	5.79	5.82	5.66	5.69
$^{[4]}$B	0.25	0.10	0.26	0.18	0.22	0.14
$^{[4]}$Al	-	-	-	-	0.12	0.17
Sum *T* site	6.10	6.00	6.05	6.00	6.00	6.00
$^{[3]}$B	3.00	3.00	3.00	3.00	3.00	3.00
Al	6.00	6.00	6.00	6.00	6.00	6.00
Sum *Z* site	6.00	6.00	6.00	6.00	6.00	6.00
Al	1.58	1.64	1.86	1.90	2.03	2.02
Fe^{2+}	0.02	0.02	0.01	0.01	-	-
Mn^{2+}	0.10	0.10	0.03	0.03	0.03	0.03
Li	1.11	1.12	0.96	0.97	0.71	0.71
Sum *Y* sites	2.81	2.88	2.86	2.91	2.77	2.76
Ca	0.06	0.06	0.01	0.01	0.01	0.01
Na	0.65	0.65	0.54	0.54	0.48	0.48
□	0.29	0.29	0.45	0.45	0.51	0.51
Sum *X* site	1.00	1.00	1.00	1.00	1.00	1.00
Sum cations	18.62	18.59	18.46	18.46	18.26	18.25
OH	3.16	3.18	3.50	3.51	3.68	3.70
F	0.72	0.72	0.37	0.37	0.26	0.26
Sum OH + F	3.88	3.90	3.87	3.88	3.94	3.96

Note: [1] Chemical data by EMPA and SIMS. Average of 25 EMP analyses for WOLO, 17 EMP analyses for WOLC and 10 EMP analyses for WOLP. H_2O: Average of 3 SIMS analyses for WOLO and WOLP, average of 4 SIMS analyses for WOLC. B_2O_3, Li_2O, Be: Average of 3 SIMS analyses for WOLO, average of 5 SIMS analyses for WOLC, average of 4 SIMS analyses for WOLP. [2] Wt. percent for an optimized formula, where B_2O_3 is calculated for Si + B = 9.00 apfu. [3] B_2O_3 for the optimized formula was calculated by using the same correction factor as for sample WOLC (more details in text). For sample WOLO Be = 29 ppm, for sample WOLC Be = 19 ppm, and for sample WOLP Be = 12 ppm. Total Mn and Fe calculated as MnO and FeO. Cl is below the detection limit in all samples. A component is not considered significant unless its value exceeds the uncertainty. The H_2O content of sample WOLP was determined by TGA with 3.6±1 wt.%.

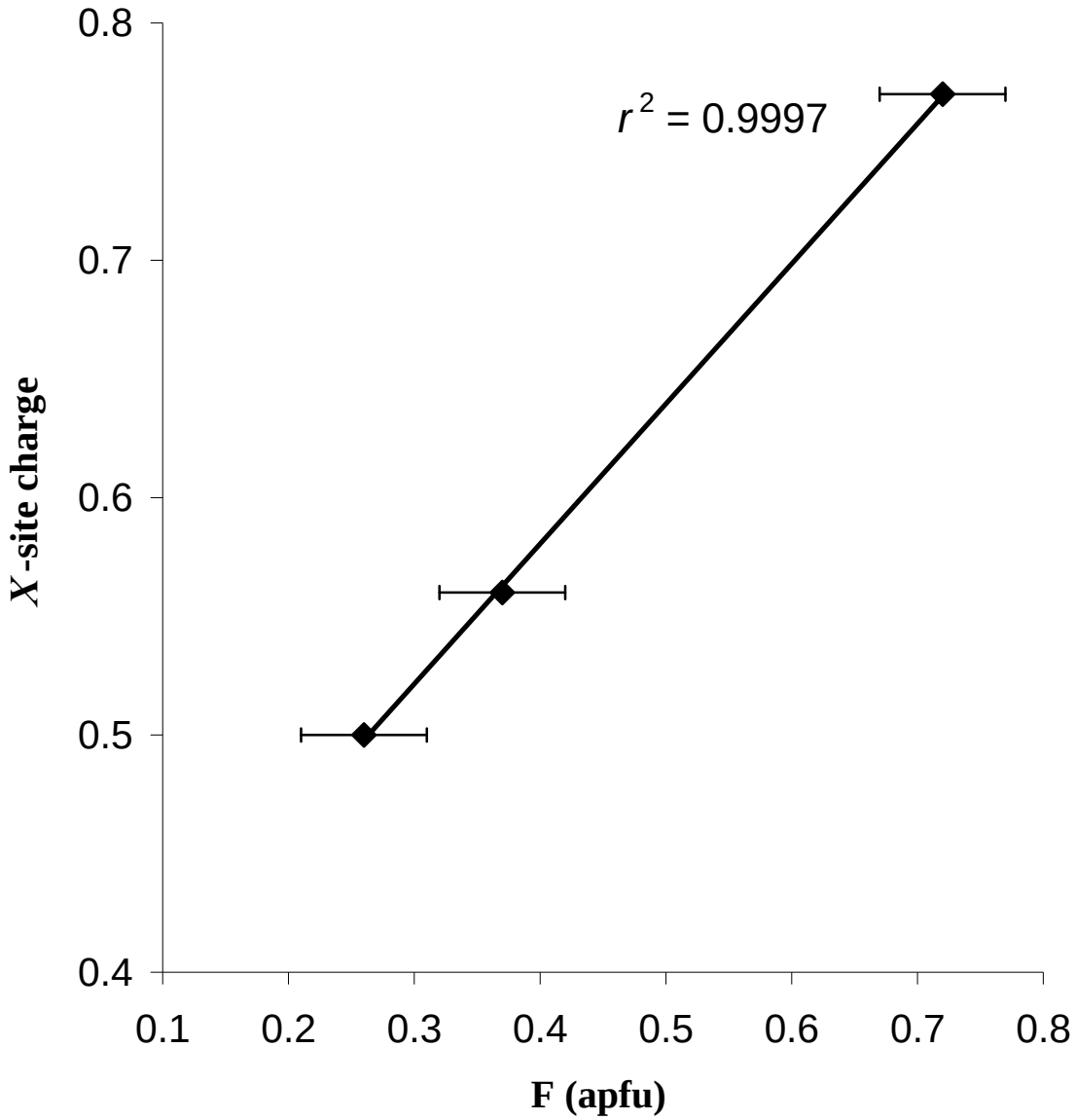

FIGURE 1. Relationship between the charge of the *X*-site occupants and the F content in tourmalines of the "fluor-elbaite"-rossmanite series from Wolkenburg, Saxony, Germany. Horizontal bars: average estimated standard deviation (±1σ).

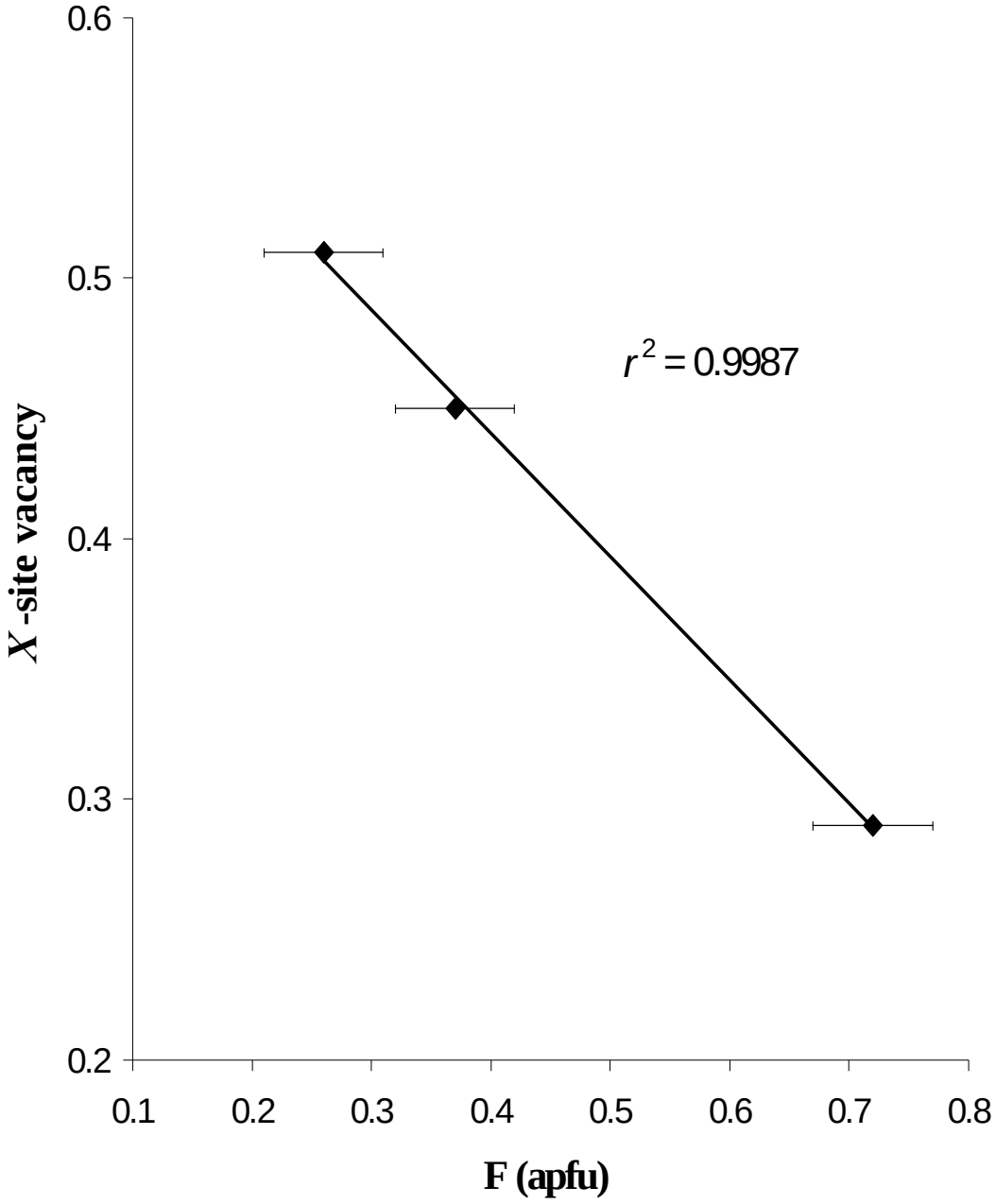

FIGURE 2. Relationship between the number of the vacancies at the *X* site and the F content in tourmalines of the "fluor-elbaite"-rossmanite series from Wolkenburg, Saxony, Germany. Horizontal bars: average estimated standard deviation (±1σ).

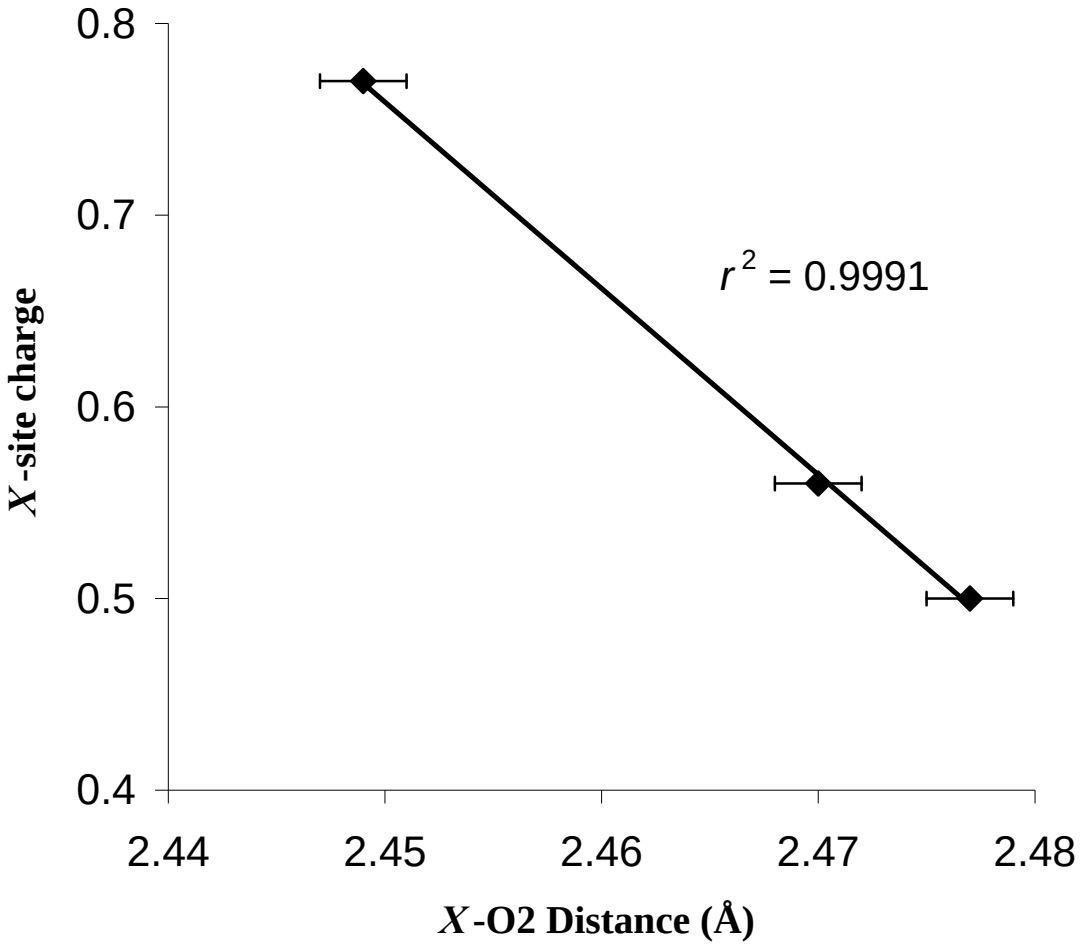

FIGURE 3. Relationship between the average charge of the *X*-site occupants and the *X*-O2 distance in tourmalines of the "fluor-elbaite"-rossmanite series from Wolkenburg, Saxony, Germany. Horizontal bars: average estimated standard deviation (±1σ).

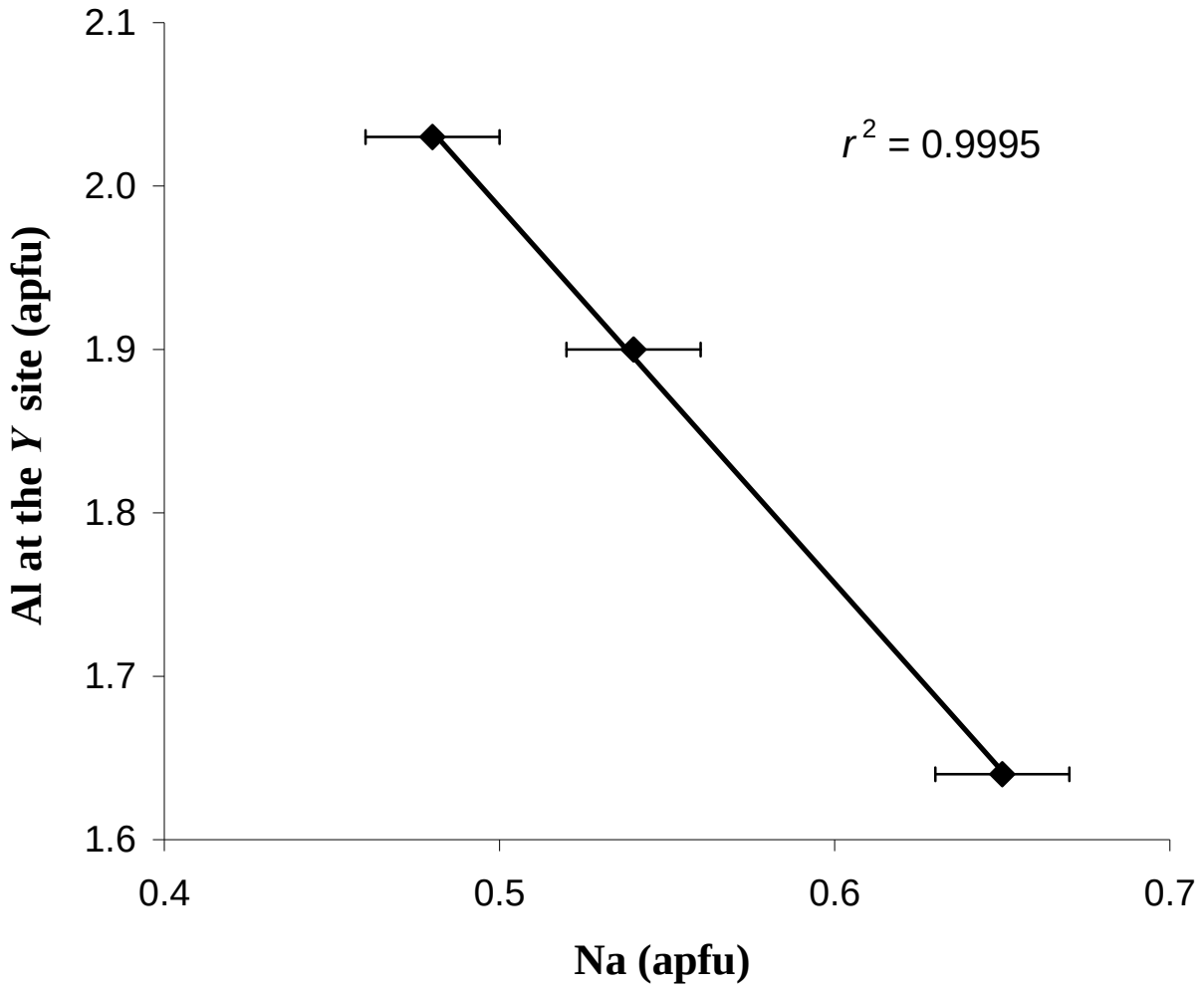

FIGURE 4. Relationship between Al at the *Y* site and the Na content in tourmalines of the "fluor-elbaite"-rossmanite series from Wolkenburg, Saxony, Germany. Horizontal bars: average estimated standard deviation (±1σ).

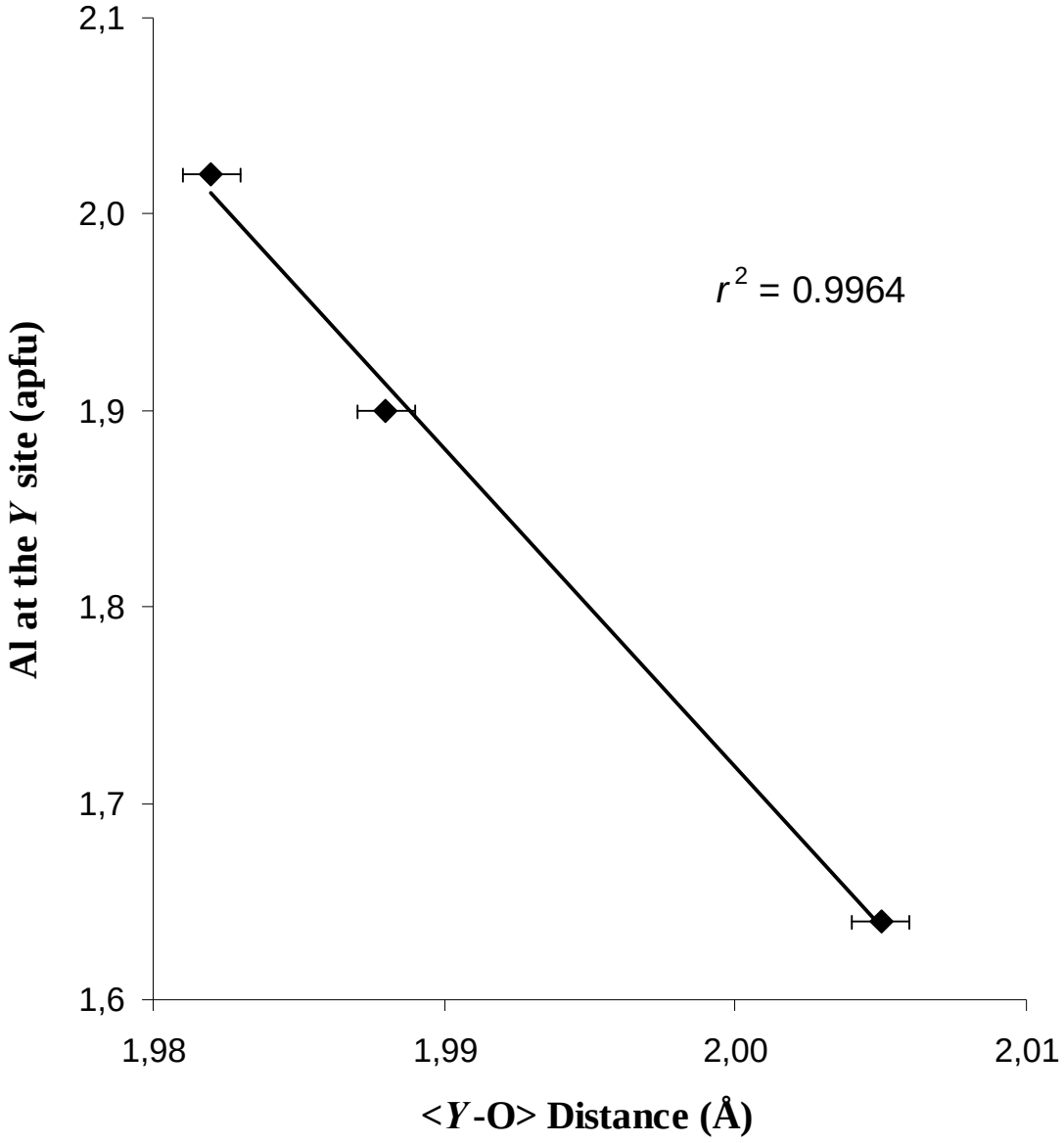

FIGURE 5. Relationship between Al at the *Y* site and the <*Y*-O> distance in tourmalines of the "fluor-elbaite"-rossmanite series from Wolkenburg, Saxony, Germany. Horizontal bars: average estimated standard deviation (±1σ).

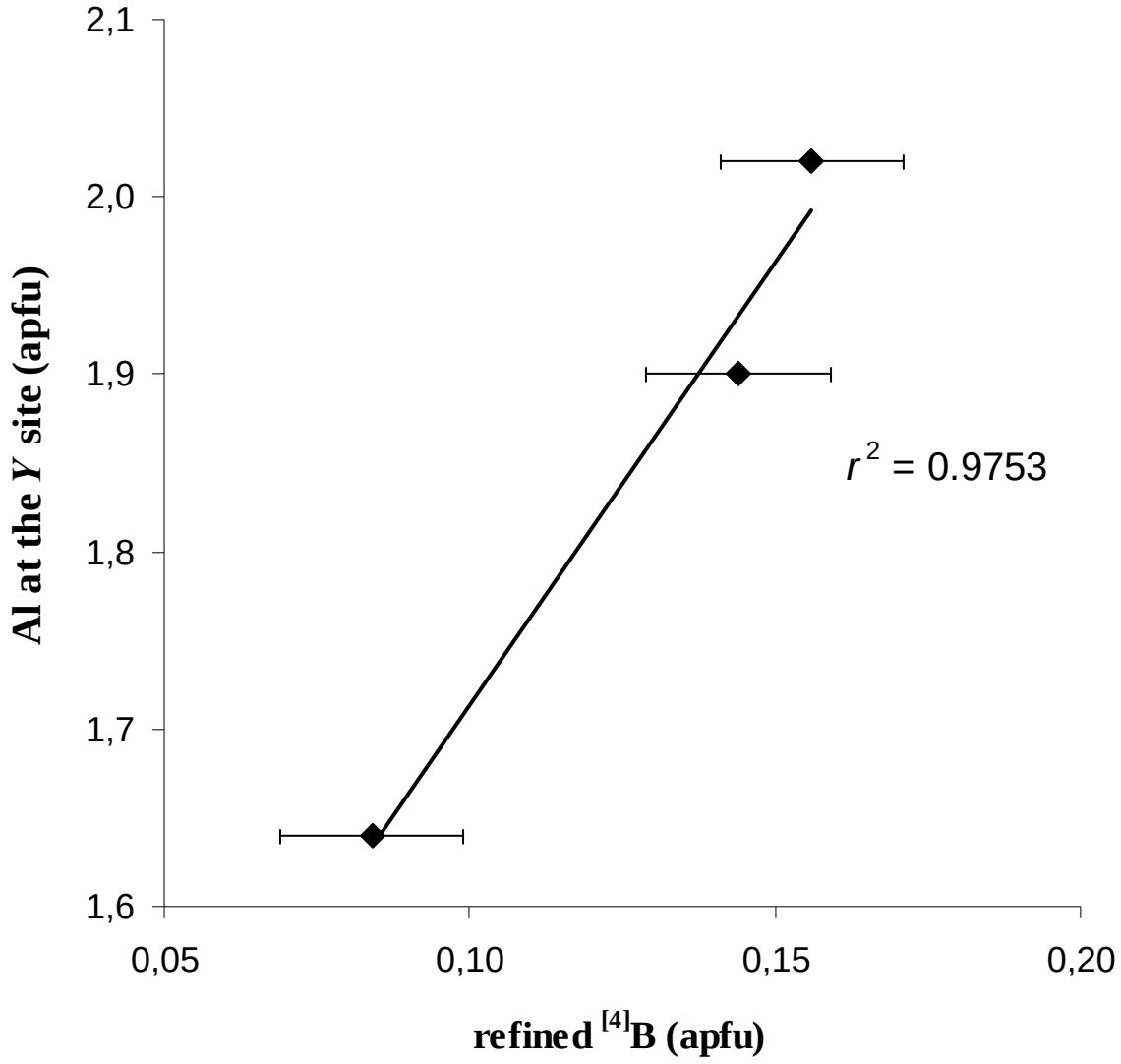

FIGURE 6. Relationship between Al at the *Y* site and the refined $^{[4]}$B content in tourmalines of the "fluor-elbaite"-rossmanite series from Wolkenburg, Saxony, Germany. We plotted the refined $^{[4]}$B content because measuring of B_2O_3 by SIMS it is still problematic and therefore we decided to use the refined $^{[4]}$B values of our high-quality structure refinements (Table 1). Horizontal bars: average estimated standard deviation (±1σ).

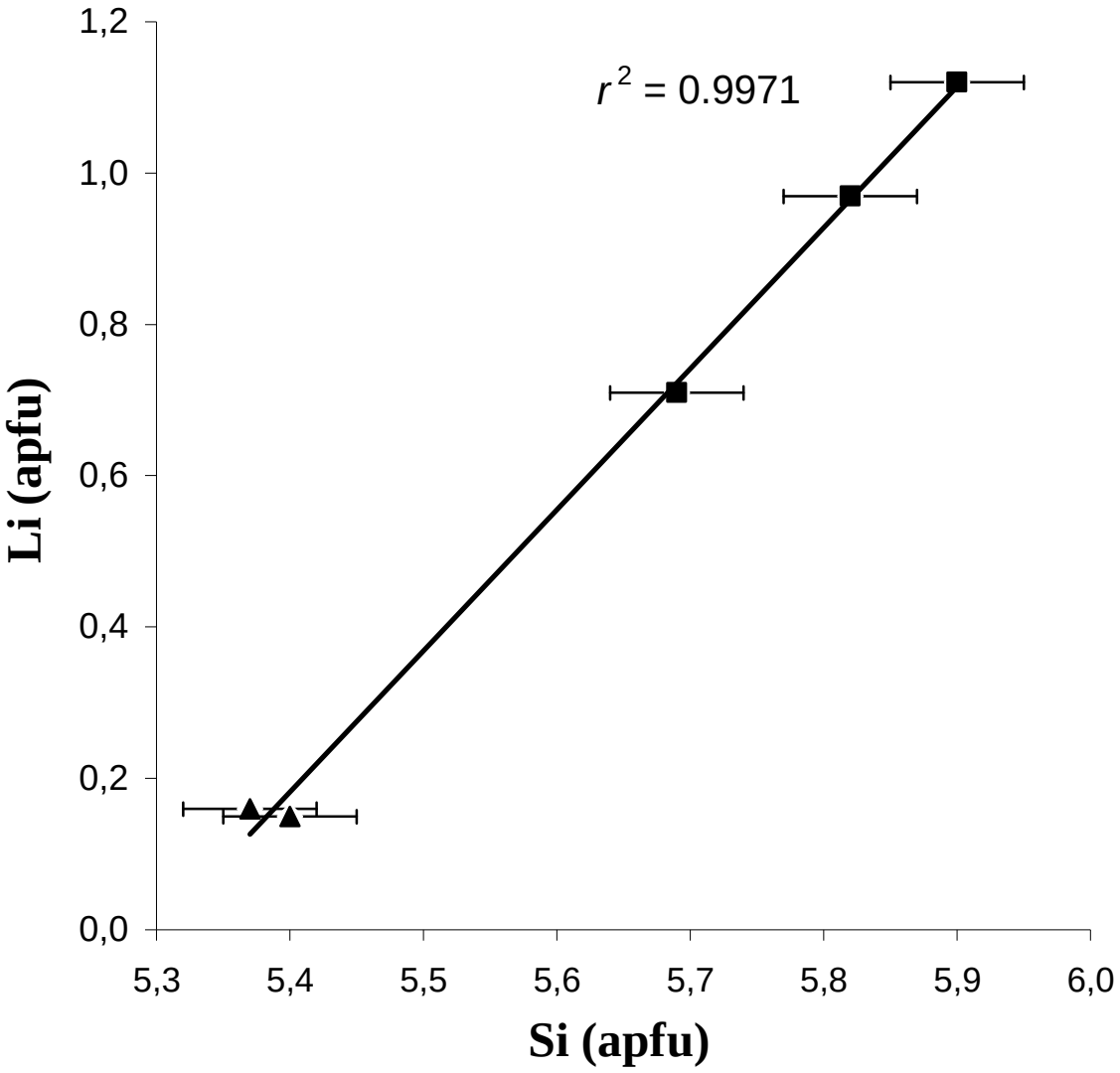

FIGURE 7. Relationship between Li (SIMS data) and Si (EMPA data) in tourmalines of the "fluor-elbaite"-rossmanite series from Wolkenburg, Saxony, Germany (squares), and two samples of "oxy-rossmanite" (triangles) from Eibenstein, Lower Austria (EMPA and SIMS data of REDT1 and REDT2 from ERTL et al. 2005). Horizontal bars: average estimated standard deviation (±1σ).

4 Investigations on Fe^{2+} and Mn^{2+}-rich tourmaline

4.1 ABSTRACT

A very Fe^{2+}-rich and a very Mn^{2+}-rich tourmaline was used to test whether Fe^{2+} and Mn^{2+} substitute on the Z site of tourmaline to a detectable degree. A Fe-rich schorl from a pegmatite near Blocherleitengraben, Lower Austria, was characterized by crystal-structure determination, chemical analyses (EMPA, ICP-MS, TGA), and Mössbauer and optical spectroscopy. The sample has very large amounts of Fe^{2+} (~2.3 apfu), and substantial amounts of Fe^{3+} (~1.0 apfu) and Mn^{2+} (~0.3 apfu). On basis of the chemical data, the structural refinement and the spectroscopic data, the first proposed formula was determined by assigning the entire amount of Fe^{3+} and Ti^{4+} to the Z site and the amount of Fe^{2+} and Fe^{3+} from delocalized electrons to the Y-Z ED doublet: $^{X}(Na_{0.88}Ca_{0.07}K_{0.02}\square_{0.03})$ $^{Y}(Fe^{2+}_{2.02}Al_{0.41}Mn^{2+}_{0.32}Fe^{3+}_{0.23}Zn_{0.02})$ $^{Z}(Al_{4.82}Fe^{3+}_{0.78}Fe^{2+}_{0.23}Ti^{4+}_{0.14}Mg_{0.03})$ $^{T}(Si_{5.92}Al_{0.08})O_{18}$ $(BO_3)_3$ $^{V}(OH)_3$ $^{W}[O_{0.49}F_{0.28}(OH)_{0.23}]$ with a = 16.039(1), c = 7.254(1) Å. This first formula would proof the lack of Fe^{2+} at the Z site, apart from that connected with delocalization of a hopping electron.

For the second proposed formula two ED doublets (delocalized electrons between Y-Z and Y-Y) were considered: $^{X}(Na_{0.88}Ca_{0.07}K_{0.02}\square_{0.03})$ $^{Y}(Fe^{2+}_{1.84}Al_{0.48}Mn^{2+}_{0.32}Fe^{3+}_{0.34}Zn_{0.02})$ $^{Z}(Al_{4.75}Fe^{3+}_{0.67}Fe^{2+}_{0.41}Ti^{4+}_{0.14}Mg_{0.03})$ $^{T}(Si_{5.92}Al_{0.08})O_{18}$ $(BO_3)_3$ $^{V}(OH)_3$ $^{W}[O_{0.49}F_{0.28}(OH)_{0.23}]$. This second formula requires some Fe^{2+} (~0.3 apfu) at the Z site, apart from that connected with delocalization of a hopping electron.

A Mn-rich tourmaline from a pegmatite at Elba Island, Italy, was characterized by crystal-structure determination, chemical analyses (EMPA, AAS, TGA) and optical spectroscopy. The optimized structural formula is $^{X}(Na_{0.63}Ca_{0.01}\square_{0.36})$ $^{Y}(Mn^{2+}_{1.29}Al_{1.12}Li_{0.46}Ti^{4+}_{0.03}Fe^{2+}_{0.01}\square_{0.09})$ $^{Z}Al_6$ $^{T}(Si_{5.96}Al_{0.04})O_{18}$ $(BO_3)_3$ $^{V}(OH)_3$ $^{W}[F_{0.51}(OH)_{0.35}O_{0.14}]$, with a = 15.951(2), c = 7.138(1) Å. Within an 3σ error there is no clear evidence for Mn at the Z site by a tentative refinement of Al↔Mn. The problems of inaccuracies in determination of site occupancy and enlarged <Z-O> distances (up to ~1.91 Å) in tourmaline because of the presence of large cations at the Y site are discussed. A positive correlation ($R^2 \approx 0.87$) was found between <Y-O> and <Z-O> distances in tourmalines (olenite, elbaite) where the Z site is only occupied by Al.

During heating of these Fe^{2+}- and Mn^{2+}-rich tourmalines at 750°C, some Fe and, respectively, Mn of the Y site was exchanged with some Al of the Z site, while simultaneously oxidizing to Fe^{3+}/Mn^{3+}. The refined ^{Z}Fe content was larger after heating (increase by ~37%) than before oxidizing. The refined ^{Y}Fe content was smaller and the <Y-O> distance was significantly reduced than before heating (2.064 → 2.001 Å). A similar effect was observed for the oxidized Mn^{2+}-rich tourmaline (<Y-O>: 2.038 → 1.982 Å). Simultaneously OH and F were expelled from both samples as indicated by structural refinements and

optical absorption spectra. The final product after heating the schorl was a buergerite with approximately all Fe^{2+} oxidized to Fe^{3+} as demonstrated by structural and spectroscopic data; its colour had changed from blackish to brown-red. After heating the Mn^{2+}-rich tourmaline at 750°C for 30 hours, the previously dark yellow sample was very dark brown-red, as expected for the oxidation of Mn^{2+} to Mn^{3+}. The unit-cell parameter *a* decreased during heating whereas the *c* parameter showed a slight increase.

4.2 INTRODUCTION AND PREVIOUS WORK

The general chemical formula of the tourmaline-group minerals can be written as $X\ Y_3\ Z_6\ [T_6O_{18}]\ (BO_3)_3\ V_3\ W$, as proposed in the definitive work of Hawthorne and Henry (1999). These authors and Hawthorne (1996, 2002) suggest occupancies at these sites as follows:

X = Ca, Na, K, □ (vacancy)

Y = Li, Mg, Fe^{2+}, Mn^{2+}, Al, Cr^{3+}, V^{3+}, Fe^{3+}

Z = Mg, Al, Fe^{3+}, V^{3+}, Cr^{3+}

T = Si, Al, B

V = OH, O

W = OH, F, O

Structural and chemical studies of Fe^{2+}-rich tourmalines by Grice and Ercit (1993), Bloodaxe et al. (1999), Francis et al. (1999), and Cámara et al. (2002) found no evidence for significant amounts of Fe^{2+} on the Z site, consistent with the site assignments of Hawthorne and Henry (1999). Further, based on the thermal changes in mean sizes of the Y and Z octahedra of Mössbauer spectra of thermally oxidized Fe-rich tourmalines, Pieczka and Kraczka (2001, 2004) and Kraczka and Pieczka (2000) concluded that Fe^{2+} (and Mn^{2+}) occupies only the Y octahedral sites.

Similarly, Mn-rich tourmalines, structurally and chemically characterized by Nuber and Schmetzer (1984), Burns et al. (1994), and Ertl et al. (2003, 2004), did not show any evidence of Mn^{2+} at the Z site. However, Bosi and Lucchesi (2004) and Bosi et al. (2005a, 2005b) interpreted their structural and chemical studies on tourmaline as having up to ~0.23 apfu Fe^{2+} and up to ~0.10 apfu Mn^{2+} on the Z site. Their Mössbauer studies indicated that all Fe is in octahedral coordination (Bosi and Lucchesi 2004). Ertl and Hughes (2002) also assigned 0.08 apfu Fe^{2+} to the Z site of a B-rich schorl. However, it is not clear if this amount of Fe occurs as Fe^{3+} at the Z site because no Mössbauer spectroscopic investigation was performed. To resolve this incongruity over the presence of minor Fe^{2+} and Mn^{2+} on the Z site in tourmaline, this possibility was tested by chemically and structurally characterizing a notably Fe^{2+}-rich (and Mn^{2+}-bearing) schorl associated with magnetite, spessartine, biotite, feldspar, and quartz from a

pegmatite from Blocherleitengraben, Lower Austria (Ertl 1995). The characterization was done through a combination of crystal-structure determination, chemical analyses (EMPA, ICP-MS), and Mössbauer data on both untreated samples (BLS1 and BLS2) and subsequently heat-treated (oxidized) BLS2 sample (BLS2H1, BLS2H2). This investigation also includes new data from structure refinements of a very Mn-rich tourmaline from Elba Island, Italy (sample MNELB3 – untreated, and MNELB3H – subsequently heat-treated) and literature structural data for Mn-rich tourmalines from Lower Austria, and discusses the problem of uncertainties and inaccuracies in determination of site occupancies.

4.3 EXPERIMENTAL DETAILS

4.3.1 Crystal-structure refinement

The tourmaline crystal structures were determined at ambient temperature with either a Bruker Apex CCD or a Nonius KappaCCD single-crystal diffractometer using graphite-monochromated Mo K_α radiation. Crystal data, data collection information and refinement details are given in Table 1. Redundant data were collected for an approximate sphere of reciprocal space, and were integrated and corrected for Lorentz and polarization factors, and absorption correction**,** using the Bruker program SAINTPLUS for BLS1 (Bruker AXS Inc. 2001) or the Nonius programs COLLECT and DENZO-SMN (Nonius 2007); multi-scan absorption correction (Otwinowski et al. 2003) for the remaining samples. The structures were refined with SHELXL-97 (Sheldrick 2007) except BLS1 (SHELXTL 6.12; Bruker AXS Inc. 2001) using scattering factors for neutral atoms**.** During all refinements, the X site was modeled with Na scattering factors and unconstrained multiplicity, and the Y site and Z site were similarly modeled using Al and Fe scattering factors in Fe-rich tourmaline as well as Al and Mn in Mn-rich tourmaline. The T site was modeled using Si scattering factors, but with fixed occupancy of $Si_{1.00}$, because refinement with unconstrained multiplicity showed this site to be essentially fully occupied by Si within error limits. The B site was modeled with fixed occupancy of $B_{1.00}$. The H site was freely refined. Refinement was performed with anisotropic thermal parameters for all non-hydrogen atoms. Table 2 lists the atom parameters, and Table 3 presents selected interatomic distances.

4.3.2 Chemical analyses

One Fe-rich and Mn-bearing sample (BLS1, from Blocherleitengraben, Lower Austria) used for structural determination was a small fragment extracted from the core of a black tourmaline crystal (~1 cm in diameter) obtained from a metamorphic pegmatite near Blocherleitengraben, Lower Austria. Sample BLS2 (small fragment extracted from an area near the core of the same tourmaline crystal), which has refined structural formula very close to that of BLS1 (see below), was not chemically analyzed. The

second sample (MNELB3) was a dark yellow fragment taken from the most Mn-rich zone of a yellowish tourmaline crystal that was ~7 mm long and ~5 mm in diameter, which grew in a pocket in a granitic pegmatite at Elba, Italy. Both tourmaline crystals are in the collection of the first author.

Electron microprobe analyses (EMPA) were obtained with a Cameca SX51 electron microprobe equipped with five wavelength-dispersive spectrometers. Operating conditions were 15 kV accelerating voltage, 20 nA beam current and a 5 μm beam diameter. Peaks for all elements were measured for 10 s, except for Mg (20 s), Cr (20 s), Ti (20 s), Zn (30 s), and F (40 s). Because the F Kα line interferes with the Fe and Mn Lα lines, the measured F values require a correction. Kalt et al. (2001) gave a formula for correcting this interference. Because of a typographical error in the original published formula of Kalt et al. (2001), the following corrected version of the formula was used: $F = F_{meas} - (-0.000055\ FeO^2 + 0.00889\ FeO - 0.0044) + 0.015\ MnO$. Natural and synthetic silicate and oxide standards were used for standards (Ertl et al. 2003). The analytical data were reduced and corrected using the PAP routine. A modified matrix correction was applied assuming stoichiometric O atoms and all non-measured components as B_2O_3. B_2O_3 was calculated assuming B = 3.00 apfu and because there was no clear evidence for $^{[4]}B$ in either investigated tourmaline sample. The accuracy of the electron-microprobe analyses and the correction procedure was checked by analyzing three reference tourmalines (98114: elbaite, 108796: dravite, 112566: schorl). Compositions of these tourmaline samples are presented in the context of an interlaboratory comparison study (Dyar et al. 1998, 2001). Under the described conditions, analytical errors on all analyses are ± 1% relative for major elements and ± 5% relative for minor elements (Table 4).

The sample preparation for ICP-MS analysis was performed in a clean-laboratory using ultrapure acids. To remove surface contamination the tourmaline grains were leached in 2.5 n HCl for 15 minutes at about 80 °C. Chemical sample digestion was performed in tightly sealed Teflon beakers using a 3:1 HF/HNO_3 mixture. After about 2 weeks at ~150 °C the samples were evaporated and transformed into nitrates by HNO_3. ICP-MS analyses were performed on an ELAN 6100 (Perkin Elmer/SCIEX; University of Vienna).

To determine the OH content of the tourmaline samples, ~32 mg of the core material of the schorl crystal and ~20 mg of the Mn-rich elbaite were used for thermogravimetric analysis (TGA), performed on the Mettler-Toledo TGA/SDTA 851 (University of Vienna). The powder was heated up from 25 °C to 1100 °C (5 °C/min) by using an N_2 gas (gas flow: 25 ml/min). To determine also the stability under the (O_2-bearing) atmosphere ~32 mg powder of the schorl sample were heated up to 1100 °C under air.

4.3.3 Mössbauer Analysis

Approximately 10 mg of each sample (natural and oxidized schorl) were gently crushed under acetone, then mixed with a sugar-acetone solution designed to form sugar coatings around each grain and prevent preferred orientation. Grains were gently heaped in a sample holder confined by Kapton tape. Mössbauer spectra were acquired at 295 K using a source of 40 mCi ^{57}Co in Rh on a WEB Research Co. model WT302 spectrometer (Mount Holyoke College) and corrected to remove the fraction of the baseline due to the Compton scattering of 122 keV gamma rays by electrons inside the detector. Run times were 24 hours with baseline counts of 9 and 32 million. Spectra were collected in 2048 channels and corrected for nonlinearity. Data were modeled using an in-house program from the University of Ghent, in Belgium called DIST_3E (an implementation of software described in Wivel and Mørup, 1981), which uses model-independent quadrupole splitting distributions for which the subspectra are constituted by Lorentzian shaped lines. Peak areas were not corrected for differential recoil-free fractions for Fe^{2+} and Fe^{3+} because the appropriate correction factors do not exist.

4.3.4 Optical spectra

Approximately 5 × 10 mm crystal fragments of both the unheated and heated Fe-rich tourmaline were prepared as doubly polished 0.030 mm thick thin-sections. Approximately 3 × 8 mm crystal fragments of both the unheated and heated Mn-rich tourmaline were prepared as ~0.6 mm thick doubly polished plates. Polarized optical absorption spectra in the 390-1100 nm range were obtained at about one nm resolution with a locally-built microspectrometer system (California Institute of Technology, Pasadena) consisting of a 1024-element Si diode-array detector coupled to a grating spectrometer system *via* fiber optics to a highly-modified NicPlan® infrared microscope containing a calcite polarizer. A pair of conventional 10x objectives was used as an objective and a condenser. Spectra were obtained through the Fe-rich and Mn-rich zones of the samples with the clearest areas.

4.4 RESULTS AND DISCUSSION

4.4.1 Mössbauer Results

The Mössbauer spectra of the natural and oxidized Fe-rich tourmaline (sample BLS) at 295 K are shown in Figure 1. Before oxidation, the spectrum resembles a typical tourmaline spectrum as described by Dyar et al. (1998), with ~55% of the total Fe as Fe^{2+}, ~28% in an electron-delocalized site (shared between Fe^{2+} and Fe^{3+}), and ~17% as Fe^{3+}. The Mössbauer spectrum of the natural tourmaline sample was fit to a total of four distributions. Mössbauer parameters (Table 5) are in general agreement with those

reported by Dyar et al. (1998), in the following manner. The first two doublets have parameters corresponding to octahedral Fe^{2+}, although the Mössbauer results alone cannot distinguish which of the sites is occupied. The third doublet, which has an isomer shift of 0.93 mm/s, lies in the range for electron delocalized peaks, sharing an electron between Fe^{2+} and Fe^{3+}. Thus, the doublet's area must be split between the two valence states. Finally, the last distribution, with an isomer shift of 0.44 mm/s, represents Fe^{3+} in octahedral coordination; again, a specific site assignment to the Y or Z site cannot be made on the basis of these Mössbauer data alone. There is no evidence for the presence of Fe in tetrahedral coordination. After oxidation 100% of the Fe is oxidized to Fe^{3+} (Table 5).

To determine the total % Fe^{3+} in the natural schorl sample, it is necessary to assign half of the electron delocalized Fe to Fe^{3+}, and half to Fe^{2+}. On the basis of these data, it can be concluded that this sample contains ~31% of the total Fe as Fe^{3+}, with an absolute error of ± 5% due to the significant overlap of the peaks in the spectrum.

Determination of site assignments for the various Fe cations is difficult because the Mössbauer effect determines only the coordination number of the site and the valence state of the Fe atoms. The correspondence between specific sets of isomer shift and quadrupole splitting and a site assignment must always be based on analogous Mössbauer measurements of minerals with known Mössbauer parameters for similar sites, or, fundamentally, on corroborating single crystal structure refinements on the same samples. Assignment of the Fe^{2+} doublets to Y sites in the Dyar et al. (1998) paper was mainly based on the compelling theoretical models of Pieczka (1997), Pieczka and Kraczka (1997) and Pieczka et al. (1998), who used structural analyses and chemical composition as the basis for their models. They concluded that Fe^{2+} occupies *only* the Y site in the structure, and argued that previous assignment of Fe^{2+} to the Z site simply does not make crystallochemical sense. They assigned the multiple doublets, previously attributed to Fe^{2+} in Y and Z, to combinations of nearest and next nearest neighbors exclusively around the Y site. They further proposed that the gradual decrease in quadrupole splitting in successive subcomponents of the $^{[Y]}Fe^{2+}$ distribution (which is also accompanied by line broadening) is due to the decreasing contributions of ionic bonding in the Y octahedron when cations with higher charge are present as next nearest neighbors. Subsequent single-crystal XRD analysis of a subset of nine samples studied by Dyar et al. (1998) and Bloodaxe et al. (1999) confirmed that this model was consistent for those samples. They found no evidence for Fe^{2+} occupancy in the Z site, thus validating the assignment of Fe^{2+} Mössbauer doublets to the Y site, at least in their samples.

In the current work, doublets assigned to octahedral Fe^{2+} could, in theory, represent either the three subcomponents of the $^{Y}Fe^{2+}$ distribution or two $^{Y}Fe^{2+}$ distributions and a $^{Z}Fe^{2+}$ distribution, as suggested by Burns (1972) and Saegusa et al. (1979). Distinguishing between these two models in this case depends on the XRD results. Likewise, the interpretation of Fe in electron delocalization requires that the Fe atoms that are sharing electrons be in adjacent sites. Ferrow (1994) assigned the ED (electron delocalized) doublets in tourmaline to have IS values of 0.86, 0.84, and 0.71 mm/s for Y-Y, Y-Z, and Z-Z

electrons, respectively. The doublet, which has an area of 13%, in the present study has IS = 0.93 mm/s, within the error consistent with both Y-Y and Y-Z delocalization, because Z-Z delocalization is less probable in the tourmaline structure (as figured out below). If the delocalization occurs between both Y-Y and Y-Z, in approximately equal proportions, the following configurations should be considered:

Y-Y = $^{Y}Fe^{3+}$ - $^{Y}Fe^{2+}$ ↔ $^{Y}Fe^{2+}$ - $^{Y}Fe^{3+}$ ($^{Y}Fe^{2+}$ at any time is ~7% of Fe_{tot}).

Y-Z = $^{Y}Fe^{2+}$ - $^{Z}Fe^{3+}$ ↔ $^{Y}Fe^{3+}$ - $^{Z}Fe^{2+}$ ($^{Z}Fe^{2+}$ at any time is in the range ~0-7% of Fe_{tot}).

Accepting this interpretation, the area of the ED doublet would give support for the existence of a very small amount (ca. 0-0.23 apfu at any time) of Fe^{2+} at the Z site.

An additional Mössbauer interpretation to the interpretation above (on the basis of Ferrow, 1994) is also discussed here. In the investigated schorl sample (BLS) most probably $^{Y}Fe^{2+}$ is shared with $^{Z}Fe^{3+}$ present at one of the two adjacent Z sites, equal to $2.02/3 \cdot 0.78/6 \cdot 2 \approx 0.18$, while for $^{Z}Fe^{2+}$ – $^{Z}Fe^{3+}$ delocalization only $0.78/6 \cdot 0.23/6 \cdot 2 << 0.01$. These values indicate that ED $^{Y}Fe^{2+}$ – $^{Z}Fe^{3+}$ seems to be more probable than $^{Z}Fe^{2+}$ – $^{Z}Fe^{3+}$ and, in addition, the latter must be only connected with the less likely $^{Z}Fe^{2+}$ – $^{Z}Fe^{3+}$ clusters within the spiral chains of the Z-centered octahedra. Fe^{2+} and Fe^{3+} as well as the remaining octahedrally coordinated ions should be distributed on the Y and Z sites "statistically", so ascribing the ED doublet only to the Fe^{2+} and Fe^{3+} pair is not very likely, because other ED-cationic-pairs are also probable, *e.g.* Fe^{2+} – Ti^{4+} or Mn^{2+} – Fe^{3+}.

4.4.2 Optical Spectra

The optical spectra of the Blocherleitengraben schorl are characteristic of a high Fe-content tourmaline containing both Fe^{2+} and Fe^{3+}. The spectrum contains Fe^{2+} bands near 720 and 1120 nm that are much more intense in the E⊥direction. Such an intensity difference between the E\\c and E⊥c directions indicates that an Fe^{2+}-Fe^{3+} interaction is occurring (Mattson and Rossman 1987). There are also weak indications of a Fe^{2+}-Ti^{4+} intervalence charge transfer band near 420 nm and a Mn^{3+} band near 530 nm. The heated schorl (BLS2H2, see below for details) shows a nearly complete loss of Fe^{2+} bands.

The optical spectra of the Mn-rich tourmaline reflect the variation in color from yellow at one end of the whole crystal to a darker yellow-brown at the other. The yellow regions show a weak, sharp, spin-forbidden Mn^{2+} feature near 415 nm, weak Fe^{2+} features near 720 nm and 1120 nm, and OH overtone bands near 1430 nm. In the darker portion of the crystal, the Fe^{2+} features are more intense. Also, a significant difference is seen in the E\\c and E⊥c intensity of the two Fe^{2+} bands indicating that some Fe^{2+}-Fe^{3+} interaction is occurring in the darker region. There also is a broad band near 420 nm typical of Fe^{2+}-Ti^{4+} intervalence charge transfer (Mattson and Rossman 1988).

4.4.3 Crystal Chemistry and Structural Analysis

4.4.3.1 Fe-rich tourmaline

The pegmatitic schorl from Blocherleitengraben, Lower Austria (BLS1) has very high amounts of Fe^{2+} (~2.18 apfu) and significant amounts of the larger Mn^{2+} (~0.32 apfu). This is reflected in the <Y-O> distance of 2.063 Å (Table 3), which is the highest observed in tourmaline to date. The high-quality structural refinement (R = 1.27%) is in very good agreement with the chemical data. The measured X-site occupancy (11.4 e) is within the given error in good agreement with the refined occupancy (11.5 e). The sum of Y- and Z-site occupancy (Σ: 164.8 e) shows very good agreement (difference: ~0.2%) with the sum of the refined occupancies (Σ: 165.2 e). Because of this excellent agreement between chemical and structural data the site occupations can be addressed very accurately. The calculated water content of 2.70 wt% is consistent with the water content of 2.6(1) wt% as determined by TGA. The O-dominance at the W site indicates that this tourmaline is an O-dominant analogue of schorl. The crystal structure of this sample breaks down at ~950 °C in air (onset: 920 °C, endset: 970 °C), and in N_2 at ~860 °C (onset: 840 °C, endset: 910 °C). The final products after heating to 1100 °C were hematite and mullite (identified by X-ray powder diffraction analyses).

Based strictly on the structural refinements (and considering the associated error) the Z site occupancy in BLS1 is determined to be in the range $^{Z}(Al_{4.80}Fe_{1.20})$ - $^{Z}(Al_{4.76}Fe_{1.24})$, reflecting ~37-38% of the total Fe at the Z site. By including the uncertainty in the Fe^{3+} determination by Mössbauer spectroscopy, the range of Fe^{3+} in this sample is ~26-36% (~31±5%) of the total Fe. The amount of Fe^{3+} is resulting from ~17% $^{[6]}Fe^{3+}$ and ~14% $^{[6]}Fe^{3+}$ from the ED doublet (Fe^{2+}-Fe^{3+} ED; Table 6). Further, by taking into account the error of the chemical analysis and the Mössbauer study, the sum of the estimated amount of Fe^{3+} is approximately consistent with the amount of Fe at the Z site resulting from the refinement within uncertainty. However, by taking into consideration the errors of the structure refinement (3σ) and the Mössbauer data and accepting that Ti^{4+} could occupy the Z site and that there are delocalized electrons which are hopping between the Y site and the Z site, and/or the Y site, the Z site can contain no additional Fe (considering only a $^{Y}Fe^{2+} – {}^{Z}Fe^{3+}$ delocalization) and ~6% Fe (considering a $^{Y}Fe^{2+} – {}^{Y}Fe^{3+}$ and a $^{Y}Fe^{2+} – {}^{Z}Fe^{3+}$ delocalization) of the total Fe.

Thus, on basis of the chemical data, the structural refinement and the Mössbauer data, the first proposed formula was determined by assigning the entire amount of Fe^{3+} (the amount of Fe^{2+} and Fe^{3+} from the Y-Z ED doublet were assigned to the Y and Z site) and Ti^{4+} to the Z site: $^{X}(Na_{0.88}Ca_{0.07}K_{0.02}\square_{0.03})$ $^{Y}(Fe^{2+}_{2.02}Al_{0.41}Mn^{2+}_{0.32}Fe^{3+}_{0.23}Zn_{0.02})$ $^{Z}(Al_{4.82}Fe^{3+}_{0.78}Fe^{2+}_{0.23}Ti^{4+}_{0.14}Mg_{0.03})$ $^{T}(Si_{5.92}Al_{0.08})O_{18}$ $(BO_3)_3$ $^{V}(OH)_3$ $^{W}[O_{0.49}F_{0.28}(OH)_{0.23}]$. The assigned Y-site occupants give 24.1 e/site which is in good agreement with the refined occupancy of 23.8(1) e. The assigned Z-site occupants give 15.4 e/site, again in good agreement

with the refined occupancy of 15.6(1) e. This first formula would prove the lack of Fe^{2+} at the Z site, apart from that connected with delocalization of a hopping electron.

For a second proposed formula both ED doublets (Y-Z and Y-Y) were considered: $^{X}(Na_{0.88}Ca_{0.07}K_{0.02}\square_{0.03})$ $^{Y}(Fe^{2+}_{1.84}Al_{0.48}Mn^{2+}_{0.32}Fe^{3+}_{0.34}Zn_{0.02})$ $^{Z}(Al_{4.75}Fe^{3+}_{0.67}Fe^{2+}_{0.41}Ti^{4+}_{0.14}Mg_{0.03})$ $^{T}(Si_{5.92}Al_{0.08})O_{18}$ $(BO_3)_3$ $^{V}(OH)_3$ $^{W}[O_{0.49}F_{0.28}(OH)_{0.23}]$. The assigned Y-site occupants give 23.8 e/site, in good agreement with the refined occupancy. The assigned Z-site occupants give 15.5 e/site which agrees well with the refined occupancy. This second formula requires some Fe^{2+} (~0.3 apfu) at the Z site, apart from that connected with delocalization of a hopping electron.

Bosi and Lucchesi (2004) and Bosi et al. (2005a, 2005b) recently assigned up to ~0.23 apfu Fe^{2+} to the Z site in tourmaline of the schorl-dravite series (their samples 60e, l3l, L3h) by a new minimization procedure that simultaneously accounts for both structural and chemical data. The total Fe content of these samples is in the range ~0.8-1.7 apfu which is, however, distinctly lower than the Fe content of the sample which was investigated (~3.3 apfu Fe). However, it is unnecessary to assign some Fe^{2+} to the Z site if there is enough Fe^{3+}, which they assigned to the Y site, to occupy the Z site in the same amount. Kahlenberg and Veličkov (2000) described the refinement (R = 2.3%) of the site occupancies of a synthetic, almost Fe^{3+}-free foitite ($Fe^{2+}_{1.53(2)}$ and $Fe^{3+}_{0.05(2)}$ by EMPA and Mössbauer spectroscopy) and revealed that the Z site is filled exclusively with Al within one standard deviation. They conclude that this result is in accord with an observed <Z-O> distance of 1.915 Å, if the determinative relation between the ionic radius of the cation at the Z site and <Z-O> given by Grice and Ercit (1993) is employed. Kahlenberg and Veličkov (2000) give a bond-valence sum of 2.961 valence units (*v.u.*) for the Z site, which is very close to the ideal value of 3 *v.u.* for trivalent Al.

4.4.3.2 Mn-rich tourmaline

A refinement in Bosi et al. (2005a) suggests 0.08 ± 0.02 apfu Mn occupies (for 6 atoms) the Z site in their most Mn-rich tourmaline sample from Elba Island, Italy (Tsl2g; 9.6 wt% MnO). The Mn-content of several different Mn-bearing elbaite crystals from pegmatite pockets from Elba Island, Italy, was checked. The most Mn-rich sample, with a similar Mn content as the Mn-rich samples from Elba published by Bosi et al. (2005a), was subsequently characterized by microprobe analysis. The portion of this crystal richest in Mn (and with dark yellow colour) was separated and structurally and chemically characterized (sample MNELB3; Tables 1-4). The unit-cell parameters of MNELB3 are very similar or even higher then those from the Mn-richest samples from Bosi et al. (2005a) (a = 15.9398(6)-15.9461(5) Å, c = 7.1363(3)-7.1380(3) Å). Using the chemical data and the structure refinement, the final structural formula is $^{X}(Na_{0.63}Ca_{0.01}\square_{0.36})$ $^{Y}(Mn^{2+}_{1.29}Al_{1.12}Li_{0.46}Ti^{4+}_{0.03}Fe^{2+}_{0.01}\square_{0.09})$ $^{Z}Al_6$ $^{T}(Si_{5.96}Al_{0.04})O_{18}$ $(BO_3)_3$ $^{V}(OH)_3$ $^{W}[F_{0.51}(OH)_{0.35}O_{0.14}]$. The crystal structure of this tourmaline breaks down at ~920 °C in N_2 (onset: 910 °C,

endset: 935 °C). The final (crystallized) product after heating to 1100 °C was mullite (identified by X-ray powder diffraction analyses). A tentative refinement of the Al:Mn ratio on the Z site gave 5.95:0.05(2). Within a 3σ error there is no clear evidence for Mn at the Z site. However, before assigning the relatively large Mn^{2+} to the Z site it seems to be more realistic that the significantly smaller Ti^{4+} will occupy this site. $^{[6]}Ti^{4+}$ has an effective ionic radius which is ~25% smaller than $^{[6]}Mn^{2+}$ (Shannon 1976).

It is also possible that there are very small amounts of Mn^{3+} present in this sample, which could theoretically also occupy the Z site. However, the optical spectra indicate that there is very little Mn^{3+} in the yellow regions of the unheated sample making it unlikely that a significant amount (>1% of the total Mn) of Mn^{3+} will contribute to the structural formula.

To determine if the refinement procedures of Mn^{2+}-rich tourmalines from Austria (Ertl et al. 2003) can be modified to indicate possible Mn^{2+} at the Z site, the restrictions of the occupancy of the Z site, while maintaining the T site and the B site at full occupancy ($Si_{1.00}$, $B_{1.00}$), were removed. However, even in the most Mn-rich tourmaline sample (sample BT; MnO: ~9 wt %), the unconstrained occupancy decreased slightly to $Al_{0.996}$. Thus, the Z site is, within error, solely occupied by Al. Hence, there is no clear evidence in the Austrian Mn-rich tourmaline samples that significant amounts of Mn^{2+} occupy the Z site.

An assessment of inaccuracies in the determination of site occupancy can be examined to establish the magnitude of their contributions. Because the simultaneous refinement of too large a portion of the total scattering can lead to significant correlations between site occupancy and scale factor, subsequent to the successful refinement detailed above in the new refinements of the Mn-rich tourmalines from Ertl et al. (2003) the T and B sites were fixed at full occupancy. Releasing the multiplicity of all cation sites (X, Y, Z, T, B) at the same time, as was done by Bosi et al. (2005a) in the refinements of the Mn-rich tourmalines from Elba, Italy, could be problematic because of the uncertainties mentioned above. Thus, larger errors in their structural refinements as were given can be considered. The possibility can not be ruled out, but, however, there is no compelling evidence for Mn^{2+} at the Z site in tourmaline, even in the sample with a very high Mn-content. In addition, the argument of <Z-O> distances up to ~1.911 Å as evidence for $^{Z}Mn^{2+}$ (Bosi et al. 2005a) is not convincing because tourmalines with significantly lower Mn contents show similar <Z-O> distances. Burns et al. (1994) determined a <Z-O> distance of 1.910 Å for a tourmaline with ~6 wt% MnO (no Mg and only 0.02 apfu Fe; sample NP1). Nuber and Schmetzer (1981) described a liddicoatite (with no significant amounts of Fe, Mn and Mg) with a <Z-O> distance of 1.909 Å. "Oxy-rossmanite" from Austria, the Al-richest tourmaline known to date, with only ~2 wt% MnO (and 0.04 apfu Fe^{2+}, no Mg; Ertl et al. 2005), shows also <Z-O> distances up to 1.910 Å. Also, Mn-rich tourmalines studied by Ertl et al. (2003), which showed no indication of Mn^{2+} on the Z site (as noted above), have slightly enlarged <Z-O> distances, up to 1.910 Å. Burns et al. (1994) noted that the scatter in the <Z-O> values in the Mn-bearing elbaites is presumably due to inductive effects rather than compositional variants. This is in agreement with the curve for the Z site produced by Hawthorne et al.

(1993). Two oxygen atoms (O6 and O3) are shared by the YO_6 and the ZO_6 octahedra. Figure 5 shows that there is indeed a positive correlation ($R^2 \approx 0.87$) between the <Y-O> and the <Z-O> distances of tourmalines that are only occupied with Al at the Z site, supporting the argument that a slightly enlarged <Z-O> value is induced by changes in the occupancy of the YO_6 octahedron. Such a supposition was already presented by Burns et al. (1994), MacDonald & Hawthorne (1995) and Hawthorne (1996). In conclusion, there is no doubt that the Y-site occupation has also an influence on the <Z-O> distance.

Structural data of 54 Al- and Li-bearing tourmaline crystals with refined structure were selected from the literature (Table 7, 8). In this set of data the <Z–O> mean bond length varies from 1.902 do 1.913 Å. For the set of the Li- and Al-bearing tourmalines most of the authors accept that the Z site is occupied only by Al (Donnay and Barton 1972; Donnay 1977; Nuber and Schmetzer 1981, 1984; Gorskaya et al. 1982, Grice and Ercit 1993; Burns et al. 1994; MacDonald and Hawthorne 1995; Ertl et al. 1997, 2003, 2004a, b, 2005, 2006; Selway et al. 1998; Hughes et al. 2000, 2004; Schreyer et al. 2002; Cámara et al. 2002; Marler et al. 2002; Prowatke et al. 2003). However, Bosi et al. (2005a, b) who refined the structure of Mn-bearing to Mn-rich elbaite and of tourmalines of the elbaite-schorl series, assumed that increase of the <Z–O> distance up to ~1.911 Å can be a result of Mn^{2+}–Al or Fe^{2+}–Al disorders. Ertl et al. (2004) and Cempírek et al. (2006) studied structures of two Fe-bearing olenite crystals from Austria and Czech, with <Z–O> distances elongated to 1.913 Å and 1.910 Å, respectively, and explained this as results of Mg–Al disorder. But in the case of both crystals the observed increase of the <Z–O> distance could also be an effect of influence of larger Y-cations, as explained below.

Bosi et al. (2005a) show in their paper on Mn-bearing tourmalines from the Elba Island a good correlation between $^{Y}Mn^{2+}$ and $^{Z}Mn^{2+}$ inferred from their SREF (structure refinement) data. However, a correlation with a similar quality can be obtained for the observed $<Z\text{-}O>_{SREF}$ and the total Mn^{2+} content in their Mn-rich tourmaline samples (Fig. 6). This correlation indicates a value of about 1.902 Å for Mn-free tourmaline, as typical value for <Z-O> for crystals with similar ratios among Al, Li and Mn. Thus, the observed difference between this value and the <Z-O> in their elbaite sample (no. Elb2rim) should be treated as an effect of different Y site populations (higher amounts of the relatively large Li in contrast to the smaller Li-content in the Mn-rich tourmaline samples from that study). Similarly, its Y-site population is quite different from that in the remaining crystals investigated, in which high amounts of Mn^{2+} mainly result from a deficiency of Li. Moreover, Mn-Al disorder should not be a linear function of composition, as it was shown by Bosi *et al.* (2005) in Figs 2 and 3 ("Manganese disorder is positively correlated to total Mn content"), because a disorder in these Mn-tourmalines should be random. Concluding, it seems that small differences in the <Z-O> distances rather result from differences in Y-site populations and differences in ionic radii of Y cations bonded to the O(3) and O(6) oxygens, which are also bonded to the Z cation. On that score, my opinion fully contradicts that of the cited authors.

Therefore is an unequivocal explanation about the reasons of the elongation of <Z–O> is very important for a correct assumption of the cation populations at the Y and Z sites, and for the evaluation of a possible Fe^{2+}–Al and Mn^{2+}–Al disorder in the tourmaline structure.

Above presented remarks on the Bosi et al. (2005) results, and a <Z–O> *vs* <Y–O> covariation for some Li- and Al-bearing tourmalines (Fig. 5) clearly show a relation between both parameters, but for the complete set of data it is less obvious because of <Y–O> being commonly a complex function of amounts of Y-site cations. However, this relation suggests that the population of the Y-site cations with ionic radii varying from 0.535 Å ($^{[6]}Al^{3+}$) to 0.83 Å ($^{[6]}Mn^{2+}$) can affect the $<^{Z}Al–O>$ observed in SREF. To check the effect of the different Y cations (Fe^{2+}, Mn^{2+}, Mg, Zn, Fe^{3+}, Al, Li, Ti^{4+}) and the Y-site vacancies on the $<^{Z}Al–O>$ distances, a multiple regression of $<^{Z}Al_{Z}–O>_{SREF}$ *vs* numbers of the typical Y-site occupants ($N_{Fe2+(Y)}$, $N_{Mn2+(Y)}$, $N_{Mg(Y)}$, $N_{Zn(Y)}$, $N_{Fe3+(Y)}$, $N_{Al(Y)}$, $N_{Li(Y)}$ and $N_{Ti4+(Y)}$) has been tested according to the following equation:

$<^{Z}Al–O>_{SREF} = <^{Z}Al–O>_{Y=vac.} + \Sigma N_i C_i$, where $C_i = <^{Z}Al–O>_{Y=vac.} - <^{Z}Al–O>_{Y=i}$ where *i* denotes changing Y-site occupants mentioned above, and C_i - a change in $<^{Z}Al–O>$ induced by i^{th}–Y-cation, measured versus mean bond length of ZO_6 octahedron shared with empty (vacant) Y-site.

Already for the initial set of data, good statistical parameters of fitting have been achieved ($R > 0.69$; SE < 0.002 Å, MAE ≈ 0.001 Å, Fig. 7a). Except for a few crystals, the remaining ones scatter regularly around the line $<^{Z}Al–O>_{SREF} = <^{Z}Al–O>_{pred.}$. Talking similar values of the estimated parameters C_i for bivalent cations (Fe, Mn, Mg and Zn) into consideration, the amounts of these respective ions have been added, and in the final solution the regression of $<^{Z}Al–O>_{SREF}$ *vs* ($N_{Fe2+(Y)+Mn2+(Y)+Mg(Y)+Zn(Y)}$, $N_{Fe3+(Y)}$, $N_{Al(Y)}$, $N_{Li(Y)}$, and $N_{Ti(Y)}$) was checked. After removing the outliers, two almost equivalent solutions have been achieved, both with the quality of the fit distinctly improved:

1) $<^{Z}Al–O>_{SREF} = 1.8884(71) + 0.0089(24)N_{Fe2+(Y)+Mn2+(Y)+Mg(Y)+Zn(Y)} + 0.0097(391)\ N_{Fe3+(Y)} + 0.0067(25)N_{Al(Y)} + 0.0039(23)N_{Li(Y)} + 0.0136(136)N_{Ti(Y)}$ with *R ≈ 0.83, SE = 0.0013 Å, MAE = 0.0010 Å* for *n = 47* crystals,

and

2) $<^{Z}Al–O>_{SREF} = 1.8865(67) + 0.0097(23)N_{Fe2+(Y)+Mn2+(Y)+Mg(Y)+Zn(Y)} + 0.0107(367)\ N_{Fe3+(Y)} + 0.0073(24)N_{Al(Y)} + 0.0045(22)N_{Li(Y)} + 0.0088(128)N_{Ti(Y)}$, with *R ≈ 0.85, SE = 0.0013 Å, MAE = 0.0010 Å* for *n = 45* crystals.

Fig. 7b presents the $<Z–O>_{pred.}$ *vs.* $<Z–O>_{obs.}$ covariation in the second model solution.

In both solutions C_0 (equal 1.8884 or 1.8864 Å) corresponds to a hypothetical <Al–O> distance in the ZO_6 octahedron shared with an empty Y site. The location of a *i*-cation at the triade of YO_6 octahedra increases the $<^{Z}Al–O>$ distance for about the value C_iN_i, *e.g.* for elbaite with $Al_{1.5}Li_{1.5}$ the predicted $<^{Z}Al–O>$ bond length should be equal to ~1.904 Å, for liddicoatite ($AlLi_2$) ~1.903 Å, for dravite and schorl ~1.915-1.916 Å, and for olenite (Al_3) ~1.908 Å. For buergerite this parameter may achieve 1.918-1.919 Å, but this value is associated with a low significance level because Fe^{3+} is present only in two crystals in

very small amounts (0.02-0.03 apfu). These results also indicate that in (Al,Li)-tourmaline with a deficiency of Y cations the observed $<^{Z}Al–O>$ distance may be slightly lower than 1.904 Å. Concluding, the results clearly show that possible Fe^{2+}–Al and Mn^{2+}–Al, or even Mg–Al disorders in (Al,Li)-bearing tourmalines are overestimated, due to not considering the effects of large Y cations on mean dimensions of the smaller ZO_6 octahedron (cations from both sites form bonds with the same oxygen atoms on O(3) and O(6) sites). If it is assumed that the standard deviation (*sd*) in the bond length estimation by SREF were equal to *ca* 0.002 Å, the calculated residuals between the SREF values and predicted ones from the presented model range typical within ±1*sd*.

4.4.3.3 Oxidation experiments

Sample BLS2 (extracted from the area near the core of the schorl crystal from Blocherleitengraben) was heated in air at 700°C for 10 hours (BLS2H1). The <Y-O> distance was smaller (2.006 Å) than before heating (2.064 Å), which is consistent with the oxidation of a large amount of Fe^{2+} (Table 3). While the <Z-O> distance did not change significantly, the refined ^{Z}Fe content was larger than before oxidizing (Table 2). Simultaneously the refined ^{Y}Fe content was smaller than before heating (decrease by about 11.6%). The same observation was done after heating BLS2H1 a second time at 750°C for 72 hours (BLS2H2; Table 2). After the second heat-treatment, in this sample were found ~2.03 apfu ^{Y}Fe and ~1.49 apfu ^{Z}Fe by refinement (Table 2). The untreated single crystal had, before any heating, ~2.46 apfu ^{Y}Fe and ~1.09 apfu ^{Z}Fe (Table 2). These observations can be explained by a distinct Fe ↔ Al exchange between the Y and Z sites during oxidation. During this process OH was fully expelled, probably as H_2O, and the minor amount of F (on O1 site) was also lost completely (within error limits). No H near O3 was found by refinement in the heated samples BLS2H1 and BLS2H2. The unit-cell parameter *a* decreased during the first heating step, but had not changed any further after the second heating step (Table 1). In constrast, the *c* parameter showed a slight increase after both heating steps, resulting in a slight net volume increase during the second heating. The final product was a buergerite with approximately all Fe^{2+} oxidized to Fe^{3+} (Table 5, Figs. 2-3). The structural data of this "synthetic" buergerite is very similar to data of natural buergerite except that there is three times as much Fe^{3+} at the Z site (for comparison with structural data of buergerite from Mexico see Barton 1969; Grice and Ercit 1992; updated chemical data in Dyar et al. 1998). The Fe^{2+} absorption bands at 710 nm and 1130 nm region in the E\\c direction of the optical spectrum disappeared as a result of the heating process as did the overtones of the OH stretching bands near 1430 nm. Likewise, the very intense Fe^{2+} bands enhanced by interaction with Fe^{3+} in the E ⊥ c direction also vanished after heating. Upon heating, the previously blackish crystal fragment became brown-red; the transparency was unchanged.

Similar effects were observed during heating of the Mn-rich tourmaline. After heating of MNELB3 at 750°C for 30 hours (sample MNELB3H) the <Y-O> distance was strongly decreasing from 2.038 to 1.982 Å (Table 2). During oxidation some Mn of the Y site was exchanged with some Al of the Z site. Before heating ~1.23 apfu ^{Y}Mn (no clear evidence for Mn at the Z site) was found by refinement. After heating ~0.88 apfu ^{Y}Mn and ~0.39 apfu ^{Z}Mn were found by refinement (Table 2). A significant portion of the OH (at the O3 site) was released during oxidation as was indicated by an increased U_{eq} of the H atom (~0.03 → ~0.08 Å^2) in sample MNELB3H (Table 2). Moreover, the F content (0.57(7) F apfu according to refinement) decreased considerably (0.14(4) apfu after heating). The unit-cell parameter *a* decreased during heating whereas the *c* parameter showed a slight increase (Table 1). After heating at 750°C for 30 hours, the dark yellow sample was very dark brown-red, with unchanged transparency (Fig. 8), as expected for the oxidation of Mn^{2+} to Mn^{3+}. The visible-NIR absorption spectrum (Fig. 4) showed broad bands near 532 nm and ~1040 nm, which are due to Mn^{3+}. The remaining brown component of the red color arises from residual Mn^{2+} as evidenced by the sharp, spin-forbidden band at 421 nm. Interestingly, the sharp band in the unheated sample that corresponds to the spin-forbidden transition of Mn^{2+} occurs at 415 nm, as previously observed in Mn-rich tourmalines from the Lundazi District of Zambia by Mattson and Rossman (1986). The shift in band position is not fully understood but may originate from the exchange of Mn from the Y to the Z site. The OH overtone bands can be seen near 1430 nm of both spectra of the unheated sample but decreases significantly in the spectrum of the heated sample (Fig. 4).

4.5 ACKNOWLEDGMENTS

Special thanks to G. Knobloch, Aggsbach-Dorf, Austria, for providing the schorl sample and A. Wagner, Vienna, Austria, for preparing the samples. This work was supported by Österreichischer Fonds zur Förderung der wissenschaftlichen Forschung (FWF) project no. P20509.

4.6 REFERENCES

Barton, R., Jr. (1969) Refinement of the crystal structure of buergerite and the absolute orientation of tourmalines. Acta Crystallographica, B25, 1524-1533.

Bloodaxe, E.S., Hughes, J.M., Dyar, M.D., Grew, E.S., and Guidotti, C.V. (1999) Linking structure and chemistry in the schorl-dravite series. American Mineralogist, 84, 922-928.

Bosi, F. and Lucchesi, S. (2004) Crystal chemistry of the schorl-dravite series. European Journal of Mineralogy, 16, 335-344.

Bosi, F., Agrosì, G., Lucchesi, S., Melchiorre, G., and Scandale, E. (2005a) Mn-tourmaline from island of Elba (Italy): Crystal chemistry. American Mineralogist, 90, 1661-1668.

Bosi, F., Andreozzi, G.B., Federico, M., Graziani, G., and Lucchesi, S. (2005b) Crystal chemistry of the elbaite-schorl series. American Mineralogist, 90, 1784-1792.

Bruker AXS Inc. (2001) SaintPlus, Version 6.45. Bruker AXS Inc., Madison, Wisconsin, USA.

Burns, R.G. (1972) Mixed valencies and site occupancies of iron in silicate minerals from Mössbauer spectroscopy. Canadian Journal of Spectroscopy, 17, 51-59.

Burns, P.C., MacDonald, D.J., and Hawthorne, F.C. (1994) The crystal chemistry of manganese-bearing elbaite. Canadian Mineralogist, 32, 31-41.

Cámara, F., Ottolini, L., and Hawthorne, F.C. (2002) Chemistry of three tourmalines by SREF, EMPA, and SIMS. American Mineralogist, 87, 1437-1442.

Cempírek, J., Novák, M., Ertl, A., Hughes, J.M., Rossman, G.R., and Dyar, M.D. (2006): Fe-bearing olenite with tetrahedrally coordinated Al from an abyssal pegmatite of the Bohemian massif at Kutná Hora: Structure, crystal chemistry, and optical spectra. Canadian Mineralogist, 44, 23-30.

Donnay, G. (1977) Structural mechanism of pyroelectricity in tourmaline. Acta Crystallographica, A33, 927-932.

Donnay, G. and Barton, R., Jr. (1972) Refinement of the crystal structure of elbaite and the mechanism of tourmaline solid solution. Tschermaks Mineralogische und Petrographische Mitteilungen, 18, 273-286.

Dyar, M.D., Taylor, M.E., Lutz, T.M., Francis, C.A., Guidotti, C.V., and Wise, M. (1998) Inclusive chemical characterization of tourmaline: Mössbauer study of Fe valence and site occupancy. American Mineralogist, 83, 848-864.

Dyar, M.D., Wiedenbeck, M., Robertson, D., Cross, LR., Delaney, J.S., Ferguson, K., Francis, C.A., Grew, E.S., Guidotti, C.V., Hervig, R.L., Hughes, J.M., Husler, J., Leeman, W., McGuire, A.V., Rhede, D., Rothe, H., Paul, R.L., Richards, I., and Yates, M. (2001) Reference Minerals for the Microanalysis of Light Elements. Geostandards Newsletter, 25, 441-463.

Ertl, A. (1995) Elbait, Olenit, Dravit-Buergerit-Mischkristalle, Dravit, Uvit und ein neuer Al-Turmalin (?) von österreichischen Fundstellen. Mitteilungen der Österreichischen Mineralogischen Gesellschaft, 140, 55-72.

Ertl, A. and Hughes, J.M. (2002) The crystal structure of an Al-rich schorl overgrown by boron-rich olenite from Koralpe, Styria, Austria. Mineralogy and Petrology, 75, 69-78.

Ertl, A., Pertlik, F., and Bernhardt, H.-J. (1997) Investigations on olenite with excess boron from the Koralpe, Styria, Austria. Österreichische Akademie der Wissenschaften, Mathematisch-Naturwissenschaftliche Klasse, Abt. I, Anzeiger, 134, 3-10.

Ertl, A., Hughes, J.M., Pertlik, F., Foit F.F. Jr., Wright, S.E., Brandstätter, F., and Marler, B. (2002) Polyhedron distortions in tourmaline. Canadian Mineralogist, 40, 153-162.

Ertl, A., Hughes, J.M., Prowatke, S., Rossman, G.R., London, D., and Fritz, E.A. (2003): Mn-rich tourmaline from Austria: structure, chemistry, optical spectra, and relations to synthetic solid solutions. American Mineralogist, 88, 1369-1376.

Ertl, A., Pertlik, F., Dyar, M.D., Prowatke, S., Hughes, J.M., Ludwig, T., and Bernhardt, H.-J. (2004a) Olenite with tetrahedrally coordinated Fe^{3+} from Eibenstein, Austria: structural, chemical, and Mössbauer data. Canadian Mineralogist, 42, 1057-1063.

Ertl, A., Schuster, R., Prowatke, S., Brandstätter, F., Ludwig, T., Bernhardt, H.-J., Koller, F., and Hughes, J.M. (2004b): Mn-rich tourmaline and fluorapatite in a Variscan pegmatite from Eibenstein an der Thaya, Bohemian massif, Lower Austria. European Journal of Mineralogy, 16, 551-560.

Ertl, A., Rossman, G.R., Hughes, J.M., Prowatke, S., and Ludwig, T. (2005) Mn-bearing "oxy-rossmanite" with tetrahedrally-coordinated Al and B from Austria: structure, chemistry, and infrared and optical spectroscopic study. American Mineralogist, 90, 481-487.

Ertl, A., Hughes, J.M., Prowatke, S., Ludwig, T., Prasad, P.S.R., Brandstätter, F., Körner, W., Schuster, R., Pertlik, F., and Marschall, H. (2006) Tetrahedrally-coordinated boron in tourmalines from the liddicoatite-elbaite series from Madagascar: Structure, chemistry, and infrared spectroscopic studies. American Mineralogist, 91, 1847-1856.

Ferrow, E.A. (1994) Mössbauer effect study of the crystal chemistry of tourmaline. Hyperfine Interactions, 91, 689-695.

Fischer, R.X. and Tillmanns, E. (1988) The equivalent isotropic displacement factor. Acta Crystallographica, C44, 775-776.

Francis, C.A., Dyar, M.D., Williams, M.L., and Hughes, J.M. (1999) The occurrence and crystal structure of foitite from a tungsten-bearing vein at Copper Mountain, Taos County, New Mexico. Canadian Mineralogist, 37, 1431-1438.

Gorskaya, M.G., Frank-Kamenetskaya, O.V., Rozhdestvenskaya, I.V., and Frank-Kamenetskii, V.A. (1982) Refinement of the crystal structure of Al-rich elbaite, and some aspects of the crystal chemistry of tourmalines. Soviet Physics Crystallography, 27, 63-66.

Grice, J.D. and Ercit, T.S. (1993) Ordering of Fe and Mg in the tourmaline crystal structure: The correct formula. Neues Jahrbuch für Mineralogie Abhandlungen, 165, 245-266.

Hawthorne, F.C. (1996) Structural mechanisms for light-element variations in tourmaline. Canadian Mineralogist, 34, 123-132.

Hawthorne, F.C. (2002) Bond-valence constraints on the chemical composition of tourmaline. Canadian Mineralogist, 40, 789-797.

Hawthorne, F.C. and Henry, D.J. (1999) Classification of the minerals of the tourmaline group. European Journal of Mineralogy, 11, 201-215.

Hawthorne, F.C., MacDonald, D.J., and Burns, P.C. (1993) Reassignment of cation site-occupancies in tourmaline: Al-Mg disorder in the crystal structure of dravite. American Mineralogist, 78, 265-270.

Hughes, J.M., Ertl, A., Dyar, M.D., Grew, E., Shearer, C.K., Yates, M.G., and Giudotti, C.V. (2000) Tetrahedrally coordinated boron in a tourmaline: Boron-rich olenite from Stoffhütte, Koralpe, Austria. Canadian Mineralogist, 38, 861-868.

Hughes, K.-A., Hughes, J.M., and Dyar, M.D. (2001) Chemical and structural evidence for $^{[4]}B \Leftrightarrow {}^{[4]}Si$ substitution in natural tourmalines. European Journal of Mineralogy, 13, 743-747.

Hughes, J.M., Ertl, A., Dyar, M.D., Grew, E., Wiedenbeck, M., and Brandstätter, F. (2004) Structural and chemical response to varying $^{[4]}B$ content in zoned Fe-bearing olenite from Koralpe, Austria. American Mineralogist, 89, 447-454.

Kahlenberg, V. and Veličkov, B. (2000) Structural investigations on a synthetic alkali-free hydrogen-deficient Fe-tourmaline (foitite). European Journal of Mineralogy, 12, 947-953.

Kalt, A., Schreyer, W., Ludwig, T., Prowatke, S., Bernhardt, H.-J., and Ertl, A. (2001) Complete solid solution between magnesian schorl and lithian excess-boron olenite in a pegmatite from Koralpe (eastern Alps, Austria). European Journal of Mineralogy, 13, 1191-1205.

Kraczka, J. and Pieczka, A. (2000) Mössbauer study of thermal oxidation of Fe^{2+} in tourmaline. Molecular Physics Reports, 30, 80-85.

MacDonald, D.J. and Hawthorne, F.C. (1995) The crystal chemistry of Si $\Leftrightarrow$ Al substitution in tourmaline. Canadian Mineralogist, 33, 849-858.

Marler, B., Borowski, M., Wodara, U., and Schreyer, W. (2002) Synthetic tourmaline (olenite) with excess boron replacing silicon in the tetrahedral site: II. Structure analysis. European Journal of Mineralogy, 14, 763-771.

Mattson, S.M and Rossman, G.R. (1986) Yellow, Mn-rich elbaite with Mn-Ti intervalence charge transfer. American Mineralogist, 71, 599-602.

Mattson, S.M and Rossman, G.R. (1987) Fe^{2+}-Fe^{3+} interactions in tourmaline. Physics and Chemistry of Minerals, 14, 163-171.

Mattson, S.M and Rossman, G.R. (1988) Fe^{2+}-Ti^{4+} charge transfer in stoichiometric Fe^{2+}, Ti^{4+} -minerals. Physics and Chemistry of Minerals, 16, 78-82.

Nonius (2007) COLLECT; DENZO-SMN. Nonius BV, Delft, The Netherlands.

Nuber, B. and Schmetzer, K. (1981) Strukturverfeinerung von Liddicoatit. Neues Jahrbuch für Mineralogie Monatshefte, 1981, 215-219.

Otwinowski, Z., Borek, D., Majewski, W., and Minor, W. (2003) Multiparametric scaling of diffraction intensities. Acta Crystallographica, A59, 228-234.

Pieczka, A. (1997) Statistical interpretation of structural parameters of tourmaline iron ordering in octahedral sites. Tourmaline 1997 International Symposium on Tourmaline, Nové Mesto na Morave, Czech Republic, 70-71.

Pieczka, A. and Kraczka, J. (1997) Thermal oxidation of Fe^{2+} ions in the schorl-dravite series and its significance in the analysis of distribution of Fe^{2+} octahedral ions. Tourmaline 1997 International Symposium on Tourmaline, Nové Mesto na Morave, Czech Republic, 72-73.

Pieczka, A. and Kraczka, J. (2001) X-ray and Mössbauer study of Fe^{2+} thermal oxidation in Fe-Mg-Al-tourmaline. Bulletin Liaison S.F.M.C., 13, 42-43.

Pieczka, A. and Kraczka, J. (2004) Oxidized tourmalines – a combined chemical, XRD and Mössbauer study. European Journal of Mineralogy, 16, 309-321.

Pieczka A., Kraczka J., and Żabiński W. (1998) Mössbauer spectra of Fe^{3+}-poor schorls: reinterpretation on the basis of ordered structure model. Journal of the Czech Geological Society, 43, 69-74.

Prowatke, S., Ertl, A., and Hughes, J.M. (2003) Tetrahedrally-coordinated Al in Mn-rich, Li- and Fe-bearing olenite from Eibenstein an der Thaya, Lower Austria: A chemical and structural investigation. Neues Jahrbuch für Mineralogie, Monatshefte, 9, 385-395.

Saegusa, N., Price, D.X., and Smith, G. (1979) Analysis of the Mössbauer spectra of several iron-rich tourmalines (schorls). Journal de Physique, 40, C2-456-C2-459.

Schreyer, W., Hughes, J.M., Bernhardt, H.-J., Kalt, A., Prowatke, S., and Ertl, A. (2002) Reexamination of olenite from the type locality: detection of boron in tetrahedral coordination. European Journal of Mineralogy, 14, 935-942.

Selway, J.B., Novák, M., Hawthorne, F.C., Černý, P., Ottolini, L., and Kyser, T.K. (1998) Rossmanite, □$(LiAl_2)Al_6Si_6O_{18}(BO_3)_3(OH)_4$, a new alkali-deficient tourmaline: description and crystal structure. American Mineralogist, 83, 896-900.

Shannon, R.D. (1976) Revised effective ionic radii and systematic studies of interatomic distances in halides and chalcogenides. Acta Crystallographica, A32, 751-767.

Sheldrick, G.M. (2007) A short history of *SHELX*. Acta Crystallographica, A64, 112-122.

Wivel, C. and Mørup, S. (1981) Improved computational procedure for evaluation of overlapping hyperfine parameter distributions in Mössbauer spectra. Journal of Physics E: Scientific Instrumentation, 14, 605-610.

TABLE 1. Crystal data, data collection information and refinement details for (natural and heat-treated) Fe-rich and Mn-bearing schorl (BLS) from Blocherleitengraben, Lower Austria, and of (natural and heat-treated) a Mn-rich tourmaline (MNELB) from the island of Elba, Italy.

Sample	BLS1	BLS2	BLS2H1	BLS2H2	MNELB3	MNELB3H
a, *c* (Å)	16.039(1), 7.254(1)	16.043(2), 7.247(1)	15.917(2), 7.252(1)	15.918(2), 7.260(1)	15.951(2), 7.138(1)	15.852(2), 7.148(1)
V (Å^3)	1612.8(3)	1615.3(4)	1591.1(4)	1593.1(4)	1572.8(4)	1555.5(4)
Crystal dimensions (mm)	~0.15 x ~0.15 x ~0.15	0.08 x 0.10 x 0.12	0.08 x 0.10 x 0.12	0.08 x 0.10 x 0.12	0.13 x 0.17 x 0.22	0.13 x 0.17 x 0.22
Collection mode, $2\theta_{max}$ (°)	full sphere, 35.10	full sphere, 37.78	full sphere, 37.78	full sphere, 37.72	full sphere, 37.77	full sphere, 37.77
h, k, l ranges	-22/22, -22/22, -10/10	-27/27, -23/23, -12/12	-27/27, -23/23, -12/12	-27/27, -23/23, -12/12	-27/27, -23/23, -12/12	-27/27, -23/23, -12/12
Total reflections measured	3880	3855	3777	3783	3746	3713
Unique reflections	1156 (R_{int} 1.55%)	2087 (R_{int} 1.02%)	2045 (R_{int} 1.10%)	2046 (R_{int} 1.36%)	2025 (R_{int} 1.03%)	2008 (R_{int} 0.93%)
$R1(F)$, $wR2_{all}(F^2)$	1.27%, 3.33%	1.63 %, 4.08%	1.60 %, 4.13%	1.77 %, 4.37%	1.80 %, 4.82%	1.58 %, 4.20%
Flack *x* parameter	0.008(10)	0.009(9)	0.031(11)	0.023(12)	-0.096(19)	-0.12(2)
'Observed' refls. [$F_o > 4\sigma(F_o)$]	1155	2055	1998	1959	2010	1988
Extinct. coefficient	0.00015(10)	0.00401(16)	0.00064(10)	0.00045(11)	0.0042(2)	0.00072(17)
No. of refined parameters	94	96	92	92	95	96
GooF	1.117	1.124	1.187	1.130	1.127	1.043
$(\Delta/\sigma)_{max}$	0.001	0.001	0.000	0.001	0.001	0.002
$\Delta\sigma_{min}$, $\Delta\sigma_{max}$ (e/Å^3)	-0.26, 0.32	-0.42, 0.45	-0.43, 0.44	-0.48, 0.44	-0.98, 0.86	-0.41, 0.37

Note: Diffractometer: Nonius KappaCCD system except for BLS1 (Bruker Apex CCD); space group *R*3*m*; refinement on F^2. Unit-cell parameters have been refined from roughly 5500 reflections in each case.

TABLE 2. Table of positional parameters and their estimated standard deviations for (natural and heat-treated) Fe-rich and Mn-bearing schorl (BLS) from Blocherleitengraben, Lower Austria, and of (natural and heat-treated) a Mn-rich tourmaline (MNELB) from the island of Elba, Italy.

Site	*Sample*	*x*	*y*	*z*	U_{eq}	*Occ.*
X	BLS1	0	0	0.7500	0.0232(2)	$Na_{1.05(2)}$
	BLS2	0	0	0.2214(2)	0.0233(6)	$Na_{0.94(1)}Ca_{0.06}$
	BLS2H1	0	0	0.2193(2)	0.0207(6)	$Na_{0.97(1)}Ca_{0.03}$
	BLS2H2	0	0	0.2199(2)	0.0209(6)	$Na_{0.97(1)}Ca_{0.03}$
	MNELB3	0	0	0.7714(4)	0.0239(7)	$Na_{0.666(8)}$
	MNELB3H	0	0	0.7750(3)	0.0237(5)	$Na_{0.674(7)}$
Y	BLS1	-0.12322(2)	1/2x	0.3393(2)	0.0106(1)	$Fe_{0.829(5)}Al_{0.171}$
	BLS2	0.12338(2)	1/2x	0.63190(3)	0.00889(6)	$Fe_{0.819(4)}Al_{0.189}$
	BLS2H1	0.12621(2)	1/2x	0.63391(3)	0.00985(7)	$Fe_{0.724(4)}Al_{0.276}$
	BLS2H2	0.12583(2)	1/2x	0.63456(4)	0.00990(8)	$Fe_{0.676(4)}Al_{0.324}$
	MNELB3	0.87608(2)	1/2x	0.37180(5)	0.0094(1)	$Al_{0.589(4)}Mn_{0.411}$
	MNELB3H	0.87639(2)	1/2x	0.36624(4)	0.00820(9)	$Al_{0.706(3)}Mn_{0.294}$
Z	BLS1	0.70130(3)	0.73828(2)	0.3619(2)	0.00771(9)	$Al_{0.797(3)}Fe_{0.203}$
	BLS2	0.29875(2)	0.26174(2)	0.60992(3)	0.00578(7)	$Al_{0.818(2)}Fe_{0.182}$
	BLS2H1	0.29753(2)	0.25723(2)	0.60489(4)	0.00732(7)	$Al_{0.773(2)}Fe_{0.227}$
	BLS2H2	0.29741(2)	0.25699(2)	0.60442(4)	0.00767(7)	$Al_{0.751(3)}Fe_{0.249}$
	MNELB3	0.70199(2)	0.73879(2)	0.38810(4)	0.00538(6)	$Al_{1.00}$
	MNELB3H	0.70324(2)	0.74109(2)	0.39232(3)	0.00685(7)	$Al_{0.935(3)}Mn_{0.065}$
B	BLS1	0.88976(7)	2x	0.5194(3)	0.0102(3)	$B_{1.00}$
	BLS2	0.11031(5)	2x	0.4529(2)	0.0080(2)	$B_{1.00}$
	BLS2H1	0.11019(6)	2x	0.4533(2)	0.0071(2)	$B_{1.00}$
	BLS2H2	0.11011(6)	2x	0.4532(3)	0.0079(3)	$B_{1.00}$
	MNELB3	0.89002(5)	2x	0.5443(2)	0.0065(2)	$B_{1.00}$
	MNELB3H	0.89009(4)	2x	0.5463(2)	0.0066(2)	$B_{1.00}$
T	BLS1	0.80868(2)	0.81039(2)	0.9732(2)	0.0076(1)	$Si_{1.00}$
	BLS2	0.19142(2)	0.18967(2)	-0.00132(4)	0.00569(6)	$Si_{1.00}$
	BLS2H1	0.19113(2)	0.19027(2)	0.00136(4)	0.00554(6)	$Si_{1.00}$
	BLS2H2	0.19105(2)	0.19018(2)	0.00121(4)	0.00590(7)	$Si_{1.00}$
	MNELB3	0.80813(2)	0.81005(2)	0.99836(4)	0.00493(5)	$Si_{1.00}$
	MNELB3H	0.80860(1)	0.81006(1)	0.99750(3)	0.00519(5)	$Si_{1.00}$
H3	BLS1	-0.270(4)	1/2x	0.583(6)	0.08(2)	$H_{1.00}$
	BLS2	0.260(3)	1/2x	0.381(6)	0.06(1)	$H_{1.00}$*
	MNELB3	0.738(3)	1/2x	0.609(5)	0.029(9)	$H_{1.00}$
	MNELB3H	0.751(3)	1/2x	0.622(6)	0.08(1)	$H_{1.00}$**

O1	BLS1	0	0	0.1945(3)	0.0219(5)	$O_{1.00}$
	BLS2	0	0	0.7819(3)	0.0237(6)	$O_{0.70(5)}F_{0.30}$
	BLS2H1	0	0	0.7643(3)	0.0102(3)	$O_{1.00}$
	BLS2H2	0	0	0.7627(3)	0.0100(3)	$O_{1.00}$
	MNELB3	0	0	0.2193(4)	0.045(1)	$O_{0.43(7)}F_{0.57}$
	MNELB3H	0	0	0.2363(2)	0.0150(4)	$O_{0.86(4)}F_{0.14}$
O2	BLS1	0.93852(5)	2x	0.4919(3)	0.0144(3)	$O_{1.00}$
	BLS2	0.06156(4)	2x	0.4800(2)	0.0127(2)	$O_{1.00}$
	BLS2H1	0.06080(4)	2x	0.4850(2)	0.0095(2)	$O_{1.00}$
	BLS2H2	0.06072(4)	2x	0.4857(2)	0.0100(2)	$O_{1.00}$
	MNELB3	0.93850(4)	2x	0.5136(2)	0.0180(3)	$O_{1.00}$
	MNELB3H	0.93913(3)	2x	0.5110(1)	0.0115(2)	$O_{1.00}$
O3	BLS1	-0.2668(1)	1/2x	0.4614(3)	0.0171(3)	$O_{1.00}$
	BLS2	0.2678(1)	1/2x	0.5101(2)	0.0148(2)	$O_{1.00}$
	BLS2H1	0.26034(9)	1/2x	0.5224(2)	0.0105(2)	$O_{1.00}$
	BLS2H2	0.25949(9)	1/2x	0.5225(2)	0.0109(2)	$O_{1.00}$
	MNELB3	0.7320(1)	1/2x	0.4892(2)	0.0118(2)	$O_{1.00}$
	MNELB3H	0.74050(7)	1/2x	0.4849(1)	0.0117(1)	$O_{1.00}$
O4	BLS1	0.90743(5)	2x	0.9047(3)	0.0130(3)	$O_{1.00}$
	BLS2	0.09269(4)	2x	0.0675(2)	0.0107(2)	$O_{1.00}$
	BLS2H1	0.09408(4)	2x	0.0776(2)	0.0097(2)	$O_{1.00}$
	BLS2H2	0.09423(5)	2x	0.0779(2)	0.0102(2)	$O_{1.00}$
	MNELB3	0.90643(4)	2x	0.9285(2)	0.0091(2)	$O_{1.00}$
	MNELB3H	0.90523(3)	2x	0.9222(1)	0.0098(1)	$O_{1.00}$
O5	BLS1	-0.1846(1)	1/2x	0.8840(3)	0.0130(2)	$O_{1.00}$
	BLS2	0.18477(8)	1/2x	0.0879(2)	0.0106(2)	$O_{1.00}$
	BLS2H1	0.18202(9)	1/2x	0.0853(2)	0.0102(2)	$O_{1.00}$
	BLS2H2	0.18185(9)	1/2x	0.0853(2)	0.0106(2)	$O_{1.00}$
	MNELB3	0.81260(8)	1/2x	0.9066(2)	0.0095(2)	$O_{1.00}$
	MNELB3H	0.81440(7)	1/2x	0.9073(1)	0.0107(1)	$O_{1.00}$
O6	BLS1	0.80337(7)	0.81272(7)	0.1945(3)	0.0116(2)	$O_{1.00}$
	BLS2	0.19673(5)	0.18745(6)	0.7771(1)	0.0095(1)	$O_{1.00}$
	BLS2H1	0.19188(5)	0.18634(6)	0.7789(1)	0.0085(1)	$O_{1.00}$
	BLS2H2	0.19142(6)	0.18593(6)	0.7787(1)	0.0089(1)	$O_{1.00}$
	MNELB3	0.80269(5)	0.81281(6)	0.2233(1)	0.0081(1)	$O_{1.00}$
	MNELB3H	0.80696(4)	0.81508(4)	0.22339(8)	0.00814(9)	$O_{1.00}$
O7	BLS1	0.71602(7)	0.71574(6)	0.8939(3)	0.0123(2)	$O_{1.00}$
	BLS2	0.28411(5)	0.28447(5)	0.0780(1)	0.0100(1)	$O_{1.00}$
	BLS2H1	0.28586(6)	0.28515(5)	0.0767(1)	0.0086(2)	$O_{1.00}$
	BLS2H2	0.28587(6)	0.28509(6)	0.0763(1)	0.0090(1)	$O_{1.00}$
	MNELB3	0.71441(5)	0.71398(5)	0.9192(1)	0.0072(1)	$O_{1.00}$
	MNELB3H	0.71347(4)	0.71388(4)	0.92205(7)	0.00740(9)	$O_{1.00}$

O8	BLS1	0.79074(7)	0.72986(8)	0.5317(3)	0.0150(2)	$O_{1.00}$
	BLS2	0.20933(6)	0.27023(6)	0.4403(1)	0.0123(1)	$O_{1.00}$
	BLS2H1	0.20932(6)	0.27020(6)	0.4402(1)	0.0091(1)	$O_{1.00}$
	BLS2H2	0.20918(6)	0.26999(6)	0.4395(1)	0.0099(2)	$O_{1.00}$
	MNELB3	0.79000(5)	0.72921(6)	0.5579(1)	0.0085(1)	$O_{1.00}$
	MMELB3H	0.79026(4)	0.72920(4)	0.56059(8)	0.00797(9)	$O_{1.00}$

Note: Definition for U_{eq} see Fischer and Tillmanns (1988). * In BLS2H1 and BLS2H2 the H site was not present anymore. ** About the occupation of H site in MNELB3H see text.

TABLE 3. Selected interatomic distances (Å) in (natural and heat-treated) Fe-rich and Mn-bearing schorl (BLS) from Blocherleitengraben, Lower Austria, and (natural and heat-treated) a Mn-rich tourmaline (MNELB) from the island of Elba, Italy.

X-	**BLS1**	**BLS2**	**BLS2H1**	**BLS2H2**	**MNELB3**	**MNELB3H**
O2 (x3)	2.534(2)	2.537(2)	2.554(2)	2.555(2)	2.504(2)	2.521(2)
O5 (x3)	2.742(2)	2.743(2)	2.691(1)	2.691(1)	2.763(2)	2.718(1)
O4 (x3)	2.806(2)	2.807(1)	2.790(1)	2.795(1)	2.818(2)	2.807(1)
Mean	**2.694**	**2.696**	**2.678**	**2.680**	**2.695**	**2.682**
Y-						
O1	2.027(2)	2.030(3)	1.980(1)	1.968(1)	2.029(2)	1.9347(9)
O2 (x2)	2.037(1)	2.0358(8)	2.0215(8)	2.0189(8)	1.9833(9)	1.9766(6)
O6 (x2)	2.044(1)	2.0466(8)	1.9986(8)	1.9937(9)	2.0361(8)	1.9785(7)
O3	2.182(2)	2.192(1)	2.018(1)	2.014(1)	2.160(1)	2.049(1)
Mean	**2.062**	**2.064**	**2.006**	**2.001**	**2.038**	**1.982**
Z-						
O6	1.904(1)	1.9018(8)	1.9481(8)	1.9540(9)	1.8604(8)	1.8996(6)
O8	1.905(1)	1.9037(8)	1.9111(8)	1.9137(9)	1.8840(8)	1.8900(6)
O7	1.911(1)	1.9075(8)	1.9088(8)	1.9127(9)	1.8789(8)	1.8884(6)
O8’	1.946(1)	1.9449(9)	1.9314(8)	1.9337(9)	1.9178(8)	1.9092(6)
O7’	1.986(1)	1.9845(8)	2.0226(9)	2.0261(9)	1.9561(8)	1.9692(6)
O3	1.9913(7)	1.9895(6)	1.8978(6)	1.8968(6)	1.9739(6)	1.9416(5)
Mean	**1.941**	**1.939**	**1.937**	**1.940**	**1.912**	**1.916**
T-						
O7	1.6087(9)	1.6105(8)	1.6050(8)	1.6054(8)	1.6161(7)	1.6095(6)
O6	1.609(1)	1.6093(9)	1.6152(8)	1.6171(9)	1.6098(8)	1.6174(6)
O4	1.6270(5)	1.6288(5)	1.6253(5)	1.6259(5)	1.6245(5)	1.6208(4)
O5	1.6425(6)	1.6429(5)	1.6305(5)	1.6305(6)	1.6376(5)	1.6291(4)
Mean	**1.622**	**1.623**	**1.619**	**1.620**	**1.622**	**1.619**
B-						
O2	1.369(3)	1.369(2)	1.381(2)	1.382(2)	1.357(2)	1.370(2)
O8 (x2)	1.378(2)	1.379(1)	1.370(1)	1.369(1)	1.385(1)	1.3744(8)
Mean	**1.375**	**1.376**	**1.374**	**1.373**	**1.376**	**1.373**

TABLE 4. Composition of Fe-rich and Mn-bearing schorl from Blocherleitengraben, Lower Austria, and of a Mn-rich tourmaline from the island of Elba, Italy (wt.%).

	BLS1[1]	MNELB3[5]
SiO_2	32.99(23)	36.37(19)
TiO_2	1.06(3)	0.22(1)
B_2O_3	9.68[2]	10.60[2]
Al_2O_3	25.10(11)	37.05(14)
Cr_2O_3	0.01(1)	b.d.
FeO_{total}	21.66(22)	0.09(2)
FeO^*	14.95	-
$Fe_2O_3^*$	7.46	-
MnO^{**}	2.13(7)	9.28(13)
MgO	0.09(2)	b.d.
CaO	0.38(2)	0.04(1)
Li_2O	0.00[3]	0.70[6]
ZnO	0.17(3)	b.d.
Na_2O	2.51(7)	1.98(6)
K_2O	0.09(1)	b.d.
F	0.49(3)	0.98(12)
H_2O	2.70[4]	3.06[7]
O≡F	-0.21	-0.41
Sum	99.60	99.96
n	31	31
Si	5.92	5.96
$^{[4]}Al$	0.08	0.04
Sum T site	6.00	6.00
$^{[3]}B$	3.00	3.00
Al	5.23	7.12
Mn^{2+}	0.32	1.29
Fe^{2+}	2.25	0.01
Fe^{3+}	1.01	-
Mg	0.03	-
Li	-	0.46
Zn	0.02	-
Ti^{4+}	0.14	0.03
Sum Y, Z sites	9.00	8.91
Na	0.88	0.63
Ca	0.07	0.01
K	0.02	-
□	0.03	0.36
Sum X site	1.00	1.00
Sum cations	18.97	18.55
OH	3.23	3.35
F	0.28	0.51
Sum OH + F	3.51	3.86

Note: [1]Average of 8 EMP analyses. Standard deviation in brackets. [2]Calculated for B = 3.00 apfu. [3]The Li content (33 ppm) was determined by ICP-MS. [4]H_2O content calculated based on charge balance

assuming a normalization of Y + Z + T = 15.00 apfu. This value is consistent with the measured water content of 2.6(1) wt% as dermined by TGA. B.d.: below detection limit. [5]Average of 10 EMP analyses. Uncertainty (wt%) for Li_2O and H_2O: 0.11 and 0.05 respectively. [6]Determined by flame AAS. [7]Determined by TGA (details see text). *FeO and Fe_2O_3 were determined by Mössbauer spectroscopy (Table 6). **Total Mn calculated as MnO. Cl is below the detection limit.

TABLE 5. Mössbauer parameters for Fe-rich tourmaline (sample BLS) from Blocherleitengraben, Lower Austria.

	CS (mm/s)	QS (mm/s)	% Area
BLS (natural)			
Fe^{2+}	1.09	2.43	46.5
Fe^{2+}	1.06	1.58	8.5
ED Fe^{2+} - Fe^{3+}	0.93	1.17	28
Fe^{3+}	0.44	0.59	17
BLS (oxidized)			
Fe^{3+}	0.37	0.95	100

Note: Results are given in mm/s relative to the center point of a Fe foil calibration spectrum. The Lorentzian full peak width (γ) at half maximum intensity is held constant at 0.20 mm/s.

CS: the value of isomer shift, when the distributed hyperfine parameter has a value of zero

QS: the center of a Gaussian component of the Δ-distribution

% Area = the relative area of doublet

The ratio of Lorentzian heights of the two lines in an elemental quadrupole doublet, h_+/h_-,was constrained to have a value of 1 for all sub-components.

TABLE 6. References of tourmaline samples used in Fig. 7a and 7b.

1	Donnay and Barton (1972)
2	Donnay (1977)
3	Nuber and Schmetzer (1981)
4	Gorskaya et al. (1982)
5	Nuber and Schmetzer (1981)
6	Grice and Ercit (1993)
7-14	Burns et al. (1994)
15-16	MacDonald and Hawthorne (1995)
17	Ertl et al. (1997)
18	Selway et al. (1998)
19	Hughes et al. (2000)
20	Schreyer et al. (2002)
21	Cámara et al. (2002)
22-23	Marler et al. (2002)
24	Prowatke et al. (2003)
25-26	Ertl et al. (2003)
27	Ertl et al. (2004a)
28-32	Hughes et al. (2004)
33	Ertl et al. (2004b)
34-40	Bosi et al. (2005a)
41-42	Ertl et al. (2005)
43-49	Bosi et al. (2005b; samples: 66c -61Vbh)
50	Cempírek et al. (2006)
51-54	Ertl et al. (2006)

TABLE 7. Site-occupants and <Z-O> distances of tourmaline samples from the references, listed in table 6.

row	<Y–O>	Mg_Y	Fe^{2+}_Y	Mn_Y	Fe^{3+}_Y	Al_Y	Li_Y	Ti_Y	Zn_Y	<Z–O>	Alz	ΣY	Y-vac.	fit-54	fit-47	fit-45
1	2.0160	0.000	0.030	0.277	0.000	1.458	1.235	0.000	0.000	1.9050	6.000	3.000	0.000	1.9060	1.9057	1.9057
2	2.0010	0.000	0.030	0.275	0.000	1.466	1.230	0.000	0.000	1.9050	6.000	3.001	0.000	1.9060	1.9057	1.9057
3	2.0340	0.000	0.000	0.000	0.000	1.600	1.400	0.000	0.000	1.9090	6.000	3.000	0.000	1.9050	(1.9046)	(1.9045)
4	1.9690	0.000	0.000	0.220	0.020	2.180	0.530	0.005	0.000	1.9080	6.000	2.955	0.045	1.9090	1.9073	1.9072
5	2.0400	0.000	0.010	0.930	0.000	1.530	0.420	0.040	0.000	1.9100	6.000	2.930	0.070	1.9092	1.9092	1.9090
6	2.0190	0.000	0.030	0.410	0.000	1.530	1.030	0.000	0.000	1.9040	6.000	3.000	0.000	1.9069	1.9066	1.9066
7	2.0450	0.000	0.020	0.820	0.000	1.070	1.050	0.040	0.000	1.9100	6.000	3.000	0.000	1.9077	1.9077	(1.9075)
8	2.0460	0.000	0.160	0.740	0.000	1.010	1.030	0.040	0.000	1.9090	6.000	2.980	0.020	1.9076	1.9077	1.9076
9	2.0480	0.010	0.650	0.490	0.000	0.840	0.900	0.110	0.000	1.9080	6.000	3.000	0.000	1.9088	1.9092	1.9088
10	2.0400	0.000	0.000	0.800	0.000	1.110	1.040	0.030	0.000	1.9050	6.000	2.980	0.020	1.9074	1.9074	1.9073
11	2.0360	0.000	0.010	0.820	0.000	1.140	0.990	0.040	0.000	1.9040	6.000	3.000	0.000	1.9078	(1.9078)	(1.9077)
12	2.0430	0.000	0.050	0.860	0.000	1.050	1.000	0.040	0.000	1.9060	6.000	3.000	0.000	1.9079	1.9080	1.9078
13	2.0140	0.010	0.290	0.150	0.000	1.320	1.220	0.010	0.000	1.9020	6.000	3.000	0.000	1.9063	(1.9061)	(1.9061)
14	2.0030	0.000	0.000	0.050	0.000	1.610	1.340	0.000	0.000	1.9080	6.000	3.000	0.000	1.9052	(1.9049)	(1.9048)
15	1.9920	0.000	0.000	0.040	0.000	1.660	1.210	0.000	0.100	1.9040	6.000	3.010	0.000	1.9041	1.9055	1.9055
16	1.9870	0.000	0.000	0.080	0.000	1.710	1.160	0.000	0.050	1.9030	6.000	3.000	0.000	1.9050	1.9055	1.9055
17	1.9570	0.002	0.006	0.001	0.000	2.430	0.331	0.002	0.000	1.9050	6.000	2.772	0.228	1.9063	1.9061	1.9059
18	1.9660	0.000	0.000	0.000	0.000	2.170	0.710	0.000	0.000	1.9040	6.000	2.880	0.120	1.9061	1.9057	1.9056
19	1.9570	0.000	0.000	0.000	0.000	2.344	0.357	0.000	0.000	1.9020	6.000	2.701	0.299	1.9055	(1.9055)	(1.9053)
20	1.9690	0.000	0.042	0.087	0.000	2.073	0.630	0.000	0.000	1.9060	6.000	2.832	0.168	1.9061	1.9059	1.9058
21	2.0360	0.610	0.900	0.020	0.000	0.800	0.700	0.060	0.010	1.9110	6.000	3.100	0.000	1.9111	1.9110	1.9109
22	1.9270	0.000	0.000	0.000	0.000	2.900	0.000	0.000	0.000	1.9120	6.000	2.900	0.100	1.9085	(1.9079)	(1.9077)
23	1.9300	0.000	0.000	0.000	0.000	2.900	0.000	0.000	0.000	1.9080	6.000	2.900	0.100	1.9085	1.9079	1.9077
24	2.0290	0.002	0.227	0.676	0.000	1.349	0.517	0.038	0.002	1.9110	6.000	2.811	0.189	1.9077	(1.9080)	(1.9078)
25	2.0500	0.000	0.020	1.210	0.000	1.280	0.370	0.000	0.000	1.9080	6.000	2.880	0.120	1.9093	1.9093	1.9094
26	2.0450	0.000	0.020	1.140	0.000	1.230	0.480	0.010	0.000	1.9100	6.000	2.880	0.120	1.9088	1.9090	1.9089
27	2.0320	0.000	0.060	0.860	0.000	1.330	0.510	0.020	0.000	1.9080	6.000	2.780	0.220	1.9074	1.9077	1.9076
28	1.9640	0.005	0.084	0.009	0.000	2.338	0.365	0.005	0.000	1.9060	6.000	2.806	0.194	1.9066	1.9065	1.9062
29	1.9720	0.010	0.190	0.007	0.000	2.222	0.342	0.009	0.000	1.9090	6.000	2.780	0.220	1.9067	1.9066	(1.9064)
30	1.9740	0.011	0.336	0.015	0.000	2.116	0.272	0.010	0.000	1.9050	6.000	2.760	0.240	1.9069	1.9070	1.9068
31	1.9990	0.038	0.669	0.022	0.000	1.792	0.226	0.013	0.000	1.9070	6.000	2.760	0.240	1.9077	1.9080	1.9078
32	2.0180	0.086	1.202	0.024	0.000	1.320	0.190	0.028	0.000	1.9100	6.000	2.850	0.150	1.9095	1.9100	1.9099
33	2.0190	0.130	0.830	0.420	0.000	1.490	0.050	0.030	0.000	1.9130	6.000	2.950	0.050	1.9112	1.9113	1.9112
34	1.9960	0.000	0.041	0.045	0.000	1.666	1.249	0.000	0.000	1.9062	6.000	3.001	0.000	1.9056	1.9052	1.9052
35	2.0350	0.000	0.000	0.896	0.000	1.213	0.851	0.032	0.009	1.9084	6.000	3.001	0.000	1.9082	1.9083	1.9082
36	2.0380	0.000	0.000	0.976	0.000	1.199	0.781	0.034	0.011	1.9086	6.000	3.001	0.000	1.9086	1.9087	1.9086
37	2.0400	0.000	0.000	1.074	0.000	1.171	0.714	0.041	0.000	1.9094	6.000	3.000	0.000	1.9092	1.9091	1.9090
38	2.0390	0.000	0.000	1.163	0.000	1.225	0.572	0.039	0.000	1.9101	6.000	2.999	0.001	1.9097	1.9097	1.9096
39	2.0410	0.000	0.000	1.295	0.000	1.217	0.447	0.041	0.000	1.9108	6.000	3.000	0.000	1.9104	1.9104	1.9103
40	2.0420	0.000	0.000	1.312	0.000	1.200	0.447	0.041	0.000	1.9112	6.000	3.000	0.000	1.9104	1.9104	1.9103
41	1.9620	0.000	0.040	0.250	0.000	2.370	0.330	0.010	0.000	1.9080	6.000	3.000	0.000	1.9089	1.9083	1.9082
42	1.9640	0.000	0.040	0.280	0.000	2.350	0.320	0.010	0.000	1.9100	6.000	3.000	0.000	1.9090	1.9084	1.9083
43	2.0000	0.000	0.000	0.031	0.000	1.606	1.363	0.000	0.000	1.9064	6.000	3.000	0.000	1.9051	1.9048	1.9047
44	2.0018	0.000	0.000	0.029	0.000	1.587	1.385	0.000	0.000	1.9064	6.000	3.001	0.000	1.9051	1.9047	1.9046
45	2.0068	0.000	0.194	0.043	0.000	1.514	1.250	0.000	0.000	1.9066	6.000	3.001	0.000	1.9058	1.9055	1.9055
46	2.0114	0.044	0.121	0.096	0.000	1.456	1.282	0.000	0.000	1.9067	6.000	2.999	0.001	1.9058	1.9055	1.9055
47	2.0230	0.000	0.106	0.430	0.000	1.356	1.107	0.000	0.000	1.9070	6.000	2.999	0.001	1.9068	1.9066	1.9066

row	<Y–O>	Mg_Y	Fe^{2+}_Y	Mn_Y	Fe^{3+}_Y	Al_Y	Li_Y	Ti_Y	Zn_Y	<Z–O>	Alz	ΣY	Y-vac.	fit-54	fit-47	fit-45
48	2.0330	0.106	0.795	0.072	0.000	1.065	0.927	0.035	0.000	1.9075	6.000	3.000	0.000	1.9081	1.9083	1.9082
49	2.0380	0.000	0.932	0.149	0.030	1.075	0.649	0.015	0.150	1.9091	6.000	3.000	0.000	1.9084	1.9096	1.9096
50	1.9920	0.100	0.780	0.060	0.000	2.050	0.000	0.010	0.000	1.9100	6.000	3.000	0.000	1.9109	1.9106	1.9107
51	2.0200	0.000	0.000	0.070	0.000	1.410	1.330	0.000	0.000	1.9040	6.000	2.810	0.190	1.9036	1.9037	1.9035
52	2.0110	0.000	0.050	0.020	0.000	1.550	1.150	0.000	0.000	1.9040	6.000	2.770	0.230	1.9038	1.9039	1.9037
53	2.0040	0.000	0.020	0.040	0.000	1.620	1.090	0.000	0.000	1.9040	6.000	2.770	0.230	1.9040	1.9041	1.9038
54	1.9960	0.000	0.010	0.010	0.000	1.820	0.890	0.000	0.000	1.9060	6.000	2.730	0.270	1.9042	1.9043	1.9040

Note: "ΣY" – the sum of Y-cations, "Y-vac." – number of empty Y-sites in the Y-octahedra triad. Columns described as "fit-54"," fit-47" and "fit 45" show the modelled <Z–O> distance on the basis the multiple regression equations presented in the text for the initial set of data (n = 54), and for the final sets of data(n = 47 and n = 45). Results in brackets are values calculated for missing data in a respective model solution.

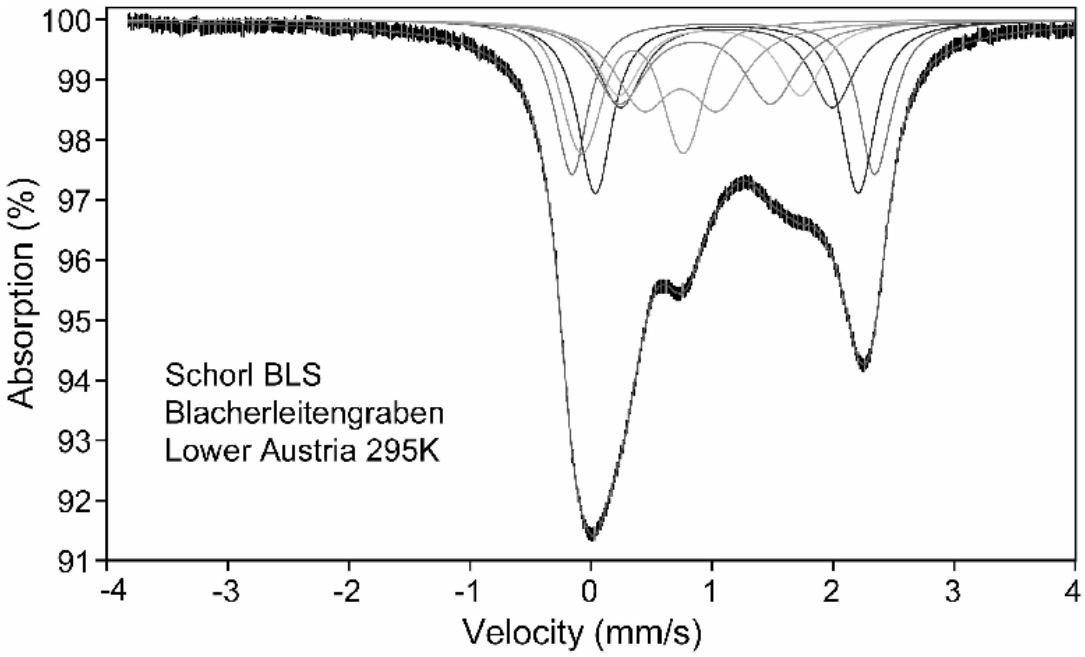

FIGURE 1. Room-temperature (295 K) Mössbauer spectrum of Fe-rich schorl from Blocherleitengraben, Lower Austria (sample BLS).

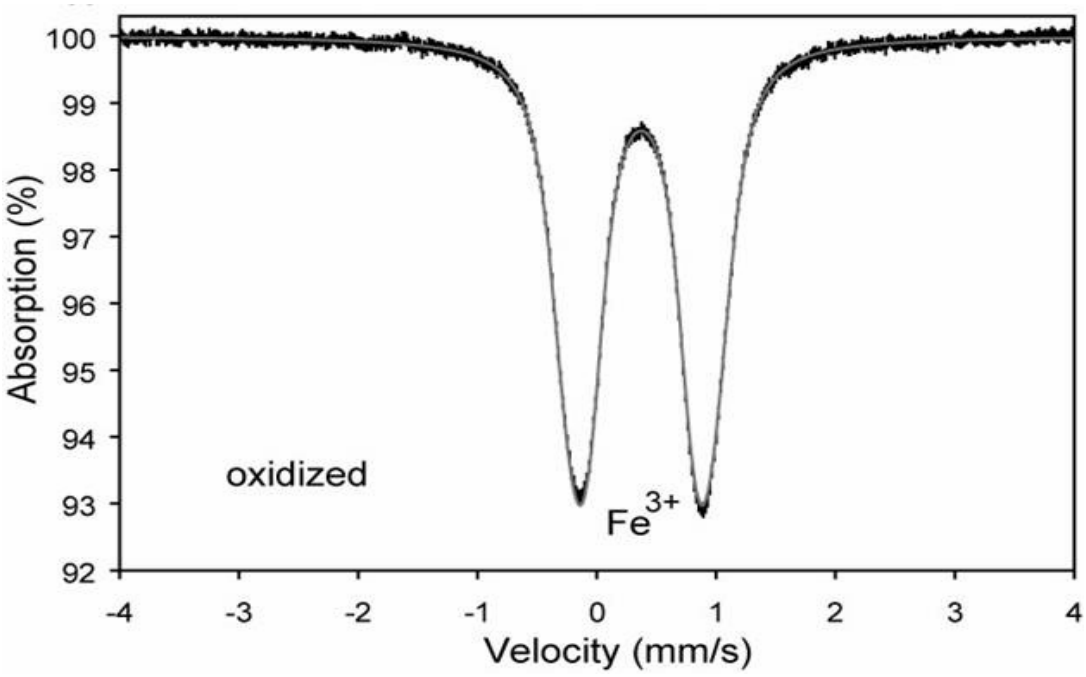

FIGURE 2. Room-temperature (295 K) Mössbauer spectrum of schorl from Blocherleitengraben, Lower Austria, which was oxidized at 750°C for 60 hours.

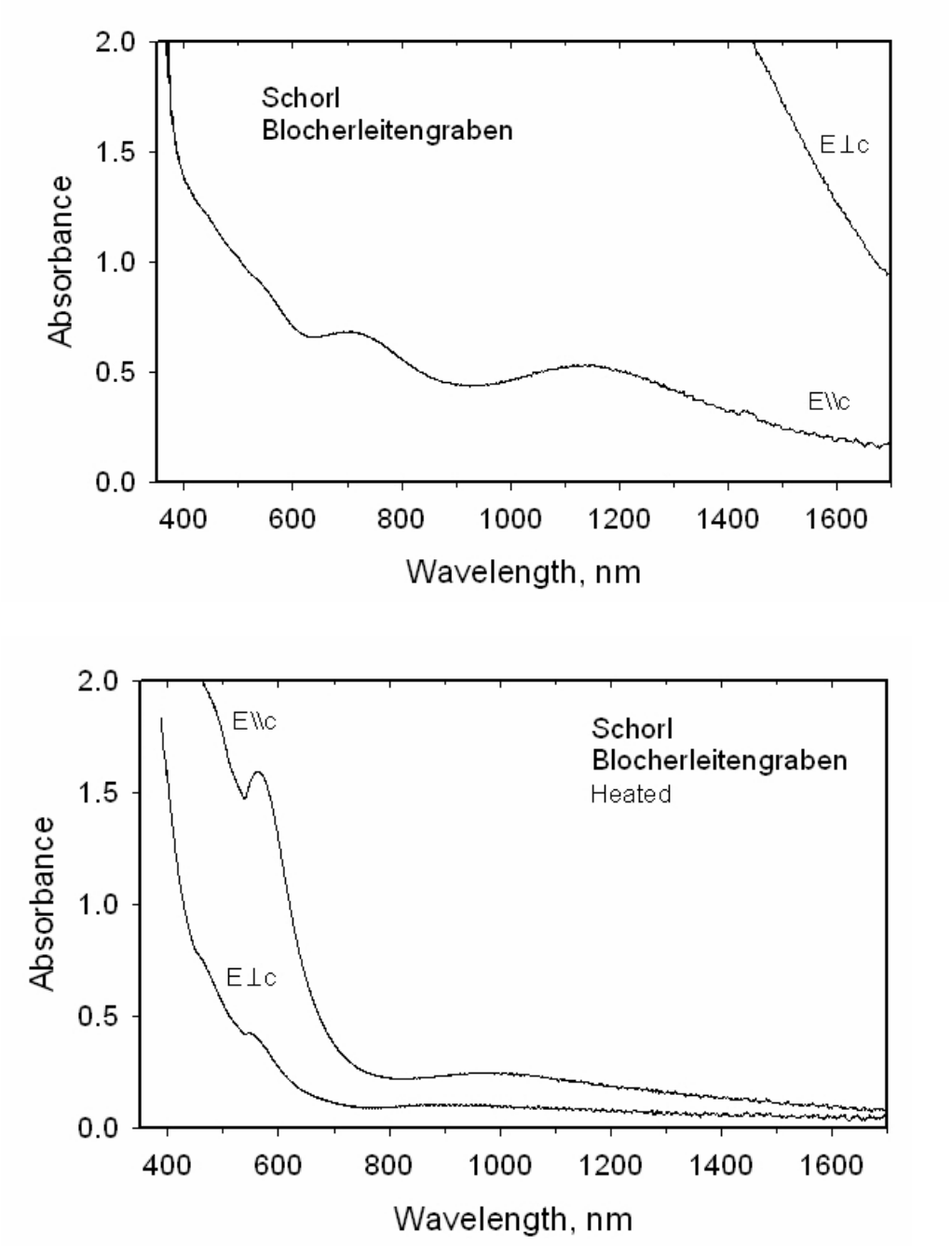

FIGURE 3. Optical absorption spectra of a 0.030 mm thick thin-sections of schorl from Blocherleitengraben, Lower Austria (BLS), before and after heating (750°C/60 hours) which show the dramatic loss of intensity of the Fe^{2+} bands in the E⊥c direction after heating (oxidation). Weak OH overtone bands can be seen near 1430 nm in the E\\c direction of the spectrum of the unheated sample but not in the spectrum of the heated sample.

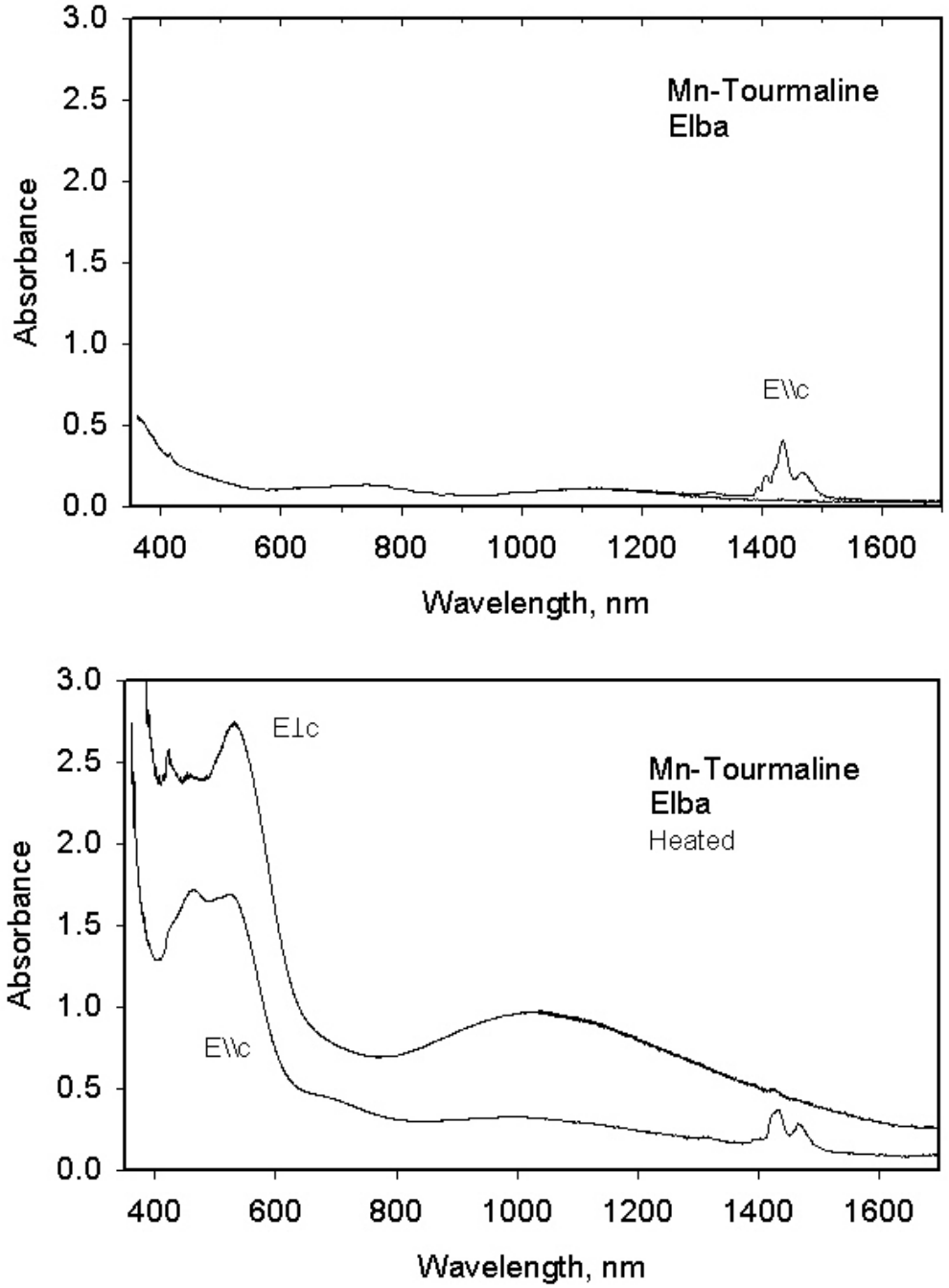

FIGURE 4. Optical absorption spectra of a ~0.6 mm thick crystal plate of unheated and heated (750°C/30 hours) Mn-rich tourmaline from Elba Island, Italy.

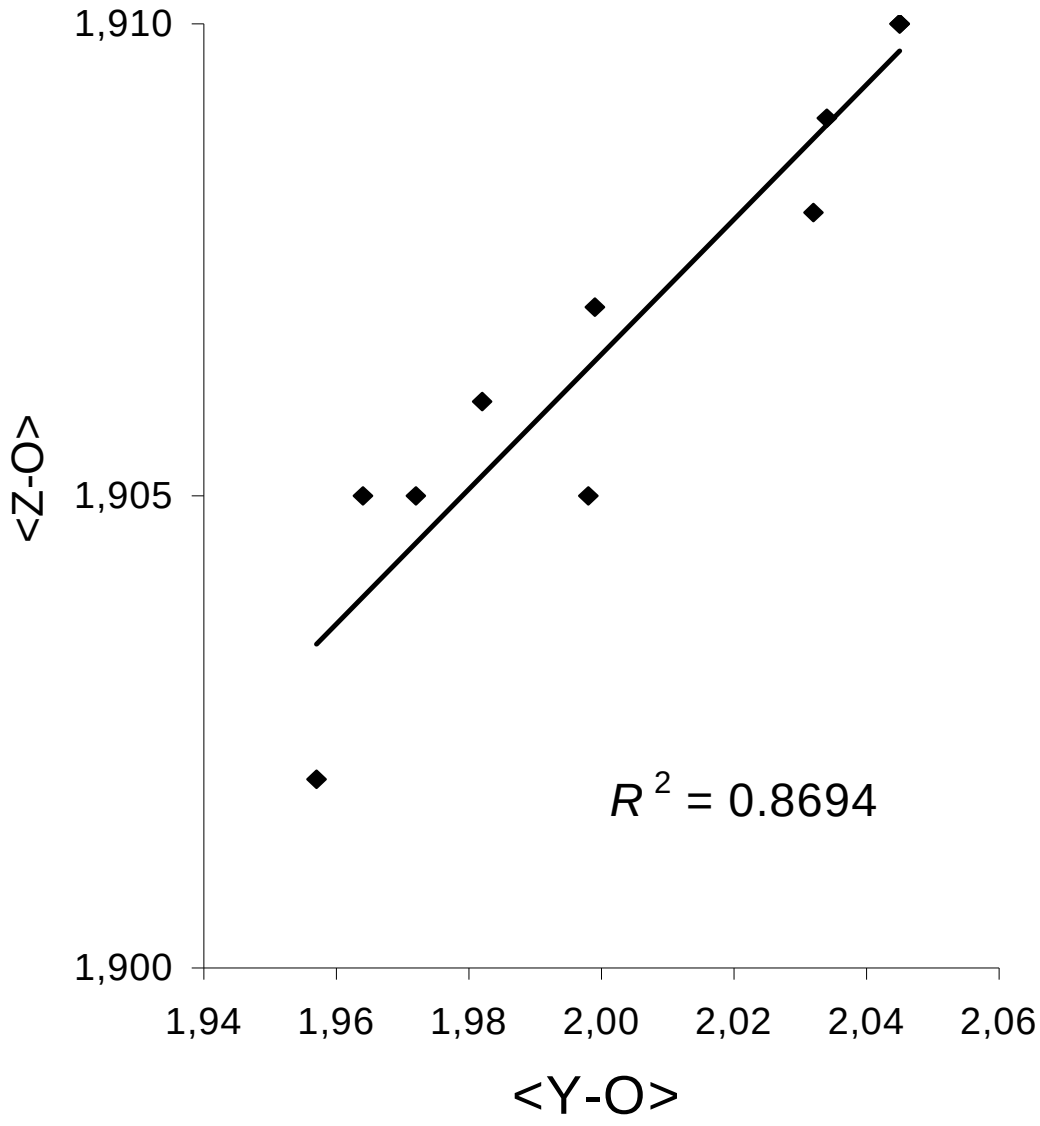

FIGURE 5. Relationship between <Y-O> and <Z-O> distances in Al-rich tourmalines (olenite, elbaite, liddicoatite), where we are sure that the Z site is occupied exclusively by Al. Structural data from Nuber & Schmetzer (1981), Hughes et al. (2000, 2001, 2004), and Ertl et al. (2002, 2003, 2004). There is no clear evidence for significant vacancies or Li at the Z site. Hawthorne (2002) showed by application of bond-valence theory that Li cannot occur at the Z site of tourmaline.

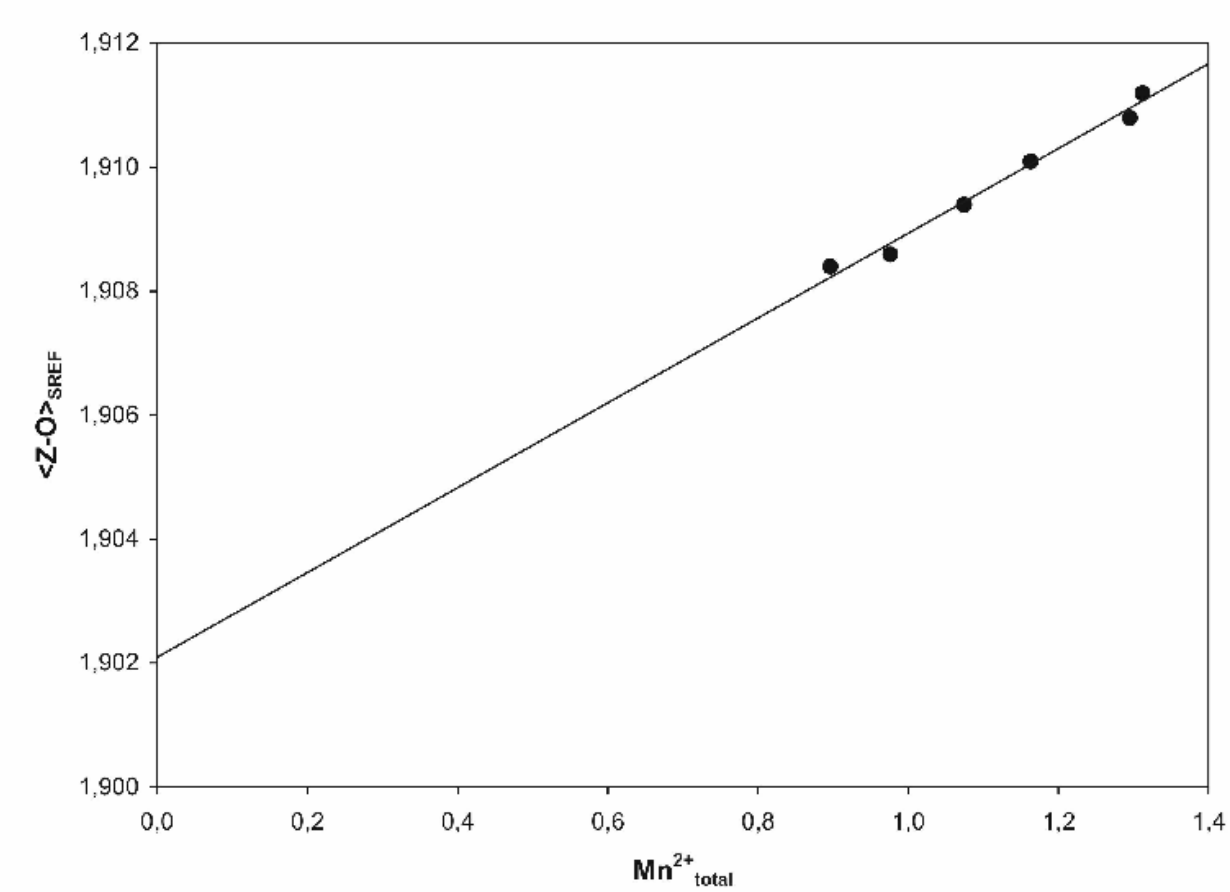

FIGURE 6. Correlation between Mn^{2+} and <Z-O> in Mn-rich tourmaline by using data from Bosi et al. (2005a).

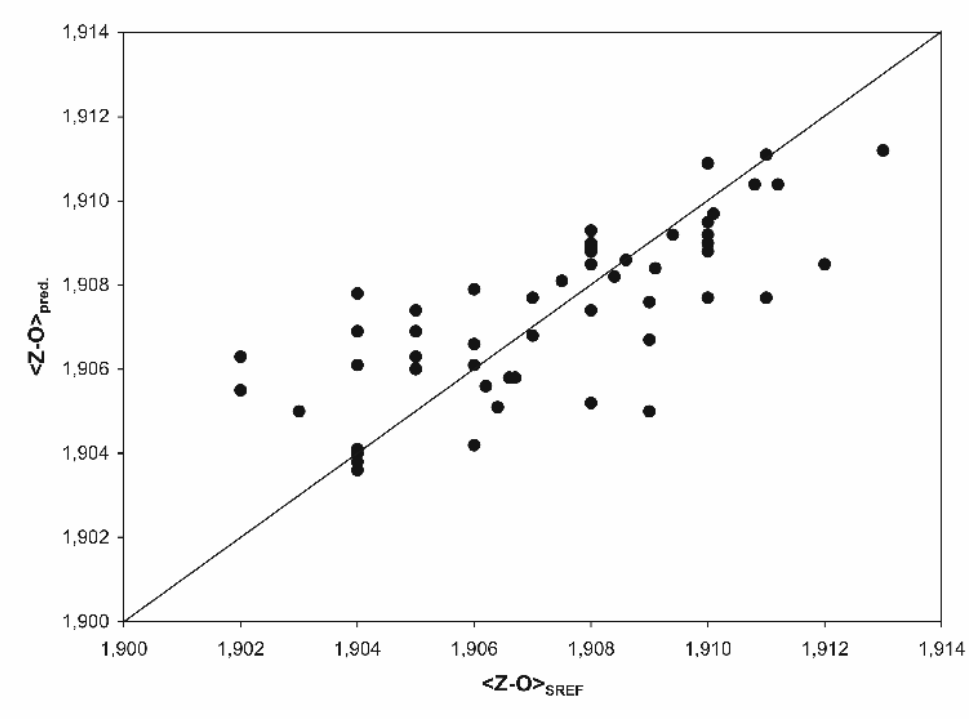

FIGURE 7a. Initial solution of the correlation between the calculated and the measured <Z-O> distances.

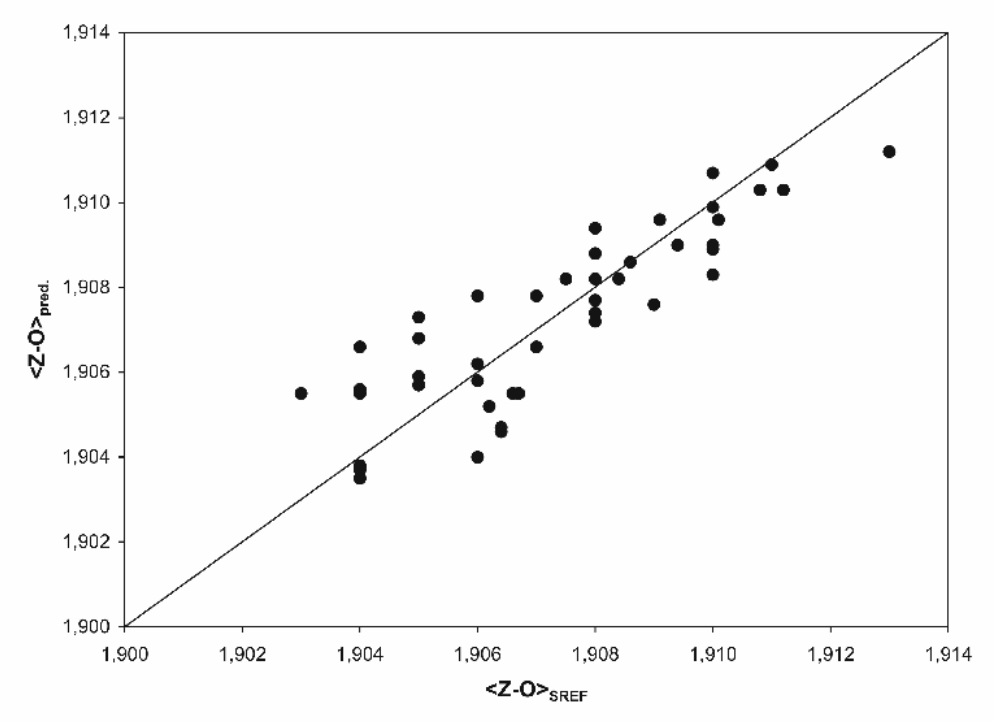

FIGURE 7b. Final solution of the correlation between the calculated and the measured <Z-O> distances.

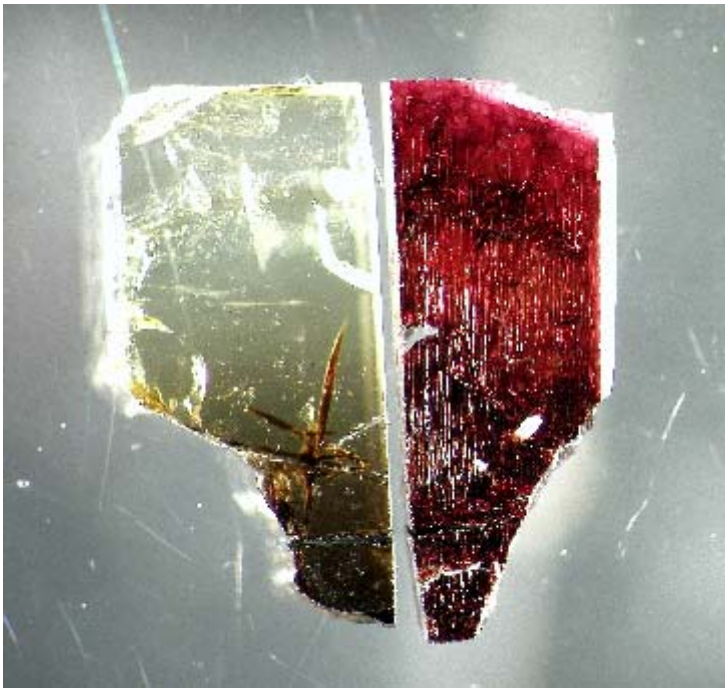

FIGURE 8. Unheated and heated (750°C/30 hours) piece of the same Mn-rich crystal from Elba Island, Italy. Both polished plates are ~8 mm in length and are ~0.6 mm thick.

5 Li-bearing, disordered Mg-rich tourmalines from the pegmatite-marble contact from the Austroalpine basement units (Styria, Austria)

5.1 Summary

Pale-blue to pale-green tourmalines from the contact zone of Permian pegmatitic rocks to micaschists and marbles from different localities of the Austroalpine basement units (Rappold Complex) in Styria, Austria, are characterized. All these Mg-rich tourmalines have small but significant Li contents, up to 0.29 wt% Li_2O, and can be characterized as dravite, with FeO contents of ~0.9-2.7 wt.-%. Their chemical composition varies from $^{X}(Na_{0.67}Ca_{0.19}K_{0.02}\square_{0.12})$ $^{Y}(Mg_{1.26}Al_{0.97}Fe^{2+}_{0.36}Li_{0.19}Ti^{4+}_{0.06}Zn_{0.01}\square_{0.15})$ $^{Z}(Al_{5.31}Mg_{0.69})$ $(BO_3)_3$ Si_6O_{18} $^{V}(OH)_3$ $^{W}[F_{0.66}(OH)_{0.34}]$, with a = 15.9220(3), c = 7.1732(2) Å to $^{X}(Na_{0.67}Ca_{0.24}K_{0.02}\square_{0.07})$ $^{Y}(Mg_{1.83}Al_{0.88}Fe^{2+}_{0.20}Li_{0.08}Zn_{0.01}Ti^{4+}_{0.01}\square_{0.09})$ $^{Z}(Al_{5.25}Mg_{0.75})$ $(BO_3)_3$ Si_6O_{18} $^{V}(OH)_3$ $^{W}[F_{0.87}(OH)_{0.13}]$, with a = 15.9354(4), c = 7.1934(4) Å, and they show a significant Al-Mg disorder between the Y and the Z sites ($R1$ = 0.013-0.015). There is a positive correlation between the Ca content and <Y-O> distance for all investigated tourmalines ($r^2 \approx$ 1.00), which may reflect short-range order configurations including Ca and Fe^{2+}, Mg, and Li. The tourmalines show X_{Mg} (X_{Mg} = Mg/Mg + Fe_{total}) values in the range 0.84-0.95. The REE pattern show more or less pronounced negative Eu and positive Yb anomalies. In comparison to tourmalines from highly-evolved pegmatites, the tourmaline samples from the border zone of the pegmatites of the Rappold Complex contain relatively low amounts of REE (~8-36 ppm) and Th (0.1-1.8 ppm) and low La_N/Yb_N ratios. There is a positive correlation ($r^2 \approx 0.82$) between MgO of the tourmalines and the surrounding micaschists. It can be concluded that the tourmalines may have crystallized in the contact between a pegmatitic melt formed by local anatexis and contact processes during the emplacement of the Permian pegmatites with carbonatic and metapelitic host rocks.

The MnO/TiO_2 ratio, as well as the Ce anomaly, the La_N/Ce_N to $Al_2O_3/(Al_2O_3+Fe_2O_3)$ relation, and the discrimination diagram Zr vs. TiO_2 indicate that the metamorphic sediments of the Rappold Complex derived from a variegated depositional area composed of shales, sandstones and greywackes in a hemipelagic to continental margin environment.

5.2 Introduction

In the contact zone of deformed pegmatitic rocks towards marbles and micaschists of the Rappold Complex (Austroalpine basement unit) in Styria, Austria, pale-blue to pale-green tourmalines occur at several localities. Tourmalines from pegmatites with such colours are usually designated as elbaite (Li-tourmaline). However, the tourmalines from the Rappold Complex bear smaller amounts of

Li and are rich in Mg. Such Li-bearing Mg-rich (>8 wt.% MgO) tourmalines are reported only from a very few localities worldwide, e.g. a tourmaline from Bližná, Czech Republic (Novák et al. 1999) and an unusual Li-rich, Fe- and Mg-bearing (~2 wt.% MgO) tourmaline crystal hosted in pegmatite from an unknown locality in Minas Gerais, Brazil (Dyar et al. 1998, 2001; Cámara et al. 2002).

To enlarge the data set on Li-bearing, Mg–rich tourmalines, the tourmalines from the Rappold Complex were characterised chemically (including light elements and REE) and structurally. Further, the REE signature of the tourmalines was compared to those of the surrounding mica schists to get more information about the formation of the tourmalines and also the pegmatites.

Tourmaline is the most important borosilicate mineral because of its ubiquity and diversity of petrologic information that it can yield (Henry and Dutrow 1996). Hawthorne and Henry (1999) gave the general chemical formula of the tourmaline-group minerals as $X\,Y_3\,Z_6\,[T_6O_{18}]\,(BO_3)_3\,V_3\,W$ [V site = O3 site, W site = O1 site]. The Z site can be occupied by Al, Mg, Fe^{3+}, and more rarely by V^{3+} and Cr^{3+}. The substitution of Mg for Al at the Z site was described by different authors (e.g., Grice and Ercit 1993; Hawthorne et al. 1993; MacDonald and Hawthorne 1995; Taylor et al. 1995; Bloodaxe et al. 1999; Cámara et al. 2002; Ertl et al. 2003; Bosi and Lucchesi 2004; Bosi et al. 2004). Hawthorne et al. (1993) asserted that the Mg content at the Z site cannot be determined on the basis of scattering power alone because of the similarity of Mg and Al with respect to X-ray scattering. Because of considerable differences in ionic radius between Al and Mg, their quantity can be determined more accurately from mean bond lengths. Hawthorne et al. (1993) and Grice and Ercit (1993) obtained linear relations between mean bond-lengths and the radii of constituent cations. Bloodaxe et al. (1999) used the method of Hawthorne et al. (1993) to determine the extent of order of Mg and Al between the two octahedral sites by minimizing the differences between grand mean octahedral bond length and bond lengths calculated from the radii of constituent cations. The final assignments in Bloodaxe et al. (1999) were made by minimizing the difference between the bond lengths on Y and Z.

5.3 Geology

Pegmatites and pegmatitic mobilisates are frequent in many Austroalpine basement units. Beside some Ordovican and a few Cretaceous pegmatitic rocks most of them are Permo-Triassic in age (Thöni 2002). The latter developed during a Permo-Triassic event of lithospheric extension that caused magmatic activity and a widespread high temperature/low pressure metamorphism with a geothermal field gradient of more than 45 °C/km (Schuster and Frank 2000; Thöni and Miller 2000; Schuster et al. 2001). Especially in the central part of the Koralpe-Wölz nappe system (Schmid et al. 2004), which consists of the Rappold, Saualpe-Koralpe, Plankogel, Strallegg, Sieggraben and Prijakt-Polinik complexes the Permian pegmatitic rocks are common (Thöni and Miller 2000; Schuster et al. 2001). All these complexes reached amphibolite to ganulite facies conditions, and also partly underwent local anatexis in Permian times (Habler and Thöni 2001; Schuster et al. 2001, 2004).

The tourmaline samples presented here were collected from four pegmatites of the Rappold Complex at the localities Gaberl (Stubalpe), Steinthaller (Gleinalpe), Dreiwasser (Gleinalpe) and Hohenwart (Pusterwald, Wölzer Tauern) (Fig. 1), which are all in Styria, Austria. The Rappold Complex is formed by graphitic, staurolithe and kyanite bearing micaschists, paragneisses and marbles. In addition, there are intercalations of calksilicates, quartzites and amphibolites, whereas granitic intrusions are not known until now.

From the microfabrics at least two amphibolite facies assemblages can be distinguished in the mineral-rich micaschists of the Rappold Complex: (1) The older one is defined by a mineral association including large staurolite1 and garnet1 porphyroblasts and a mineral phase which has been subsequently transformed into fine-grained kyanite. With respect to other Austroalpine units these aggregates are interpreted as former andalusite crystals. (2) The second assemblage consists of St2 + Grt2 + Ky + Ms + Bt + Pl + Qtz. St2 and Grt2 are present as tiny euhedral crystals in the matrix. Further Grt2 forms rims around Grt1, and together with kyanite also around St1. The latter developed by the prograde breakdown of St1 by the reaction St1 + Ms + Qtz = Ky + Grt2 + H_2O. Rarely, very large porphyroblasts of kyanite intergrown with St1 are present (Schuster et al. 2001).

Until now the age of the older assemblage was not definitely clear. It might have formed during a Variscan (Carboniferous) medium pressure event or during the early stages of the Permo-Triassic high temperature/low pressure event (Gaiges et al. 2006). At present the second possibility is preferred because there is one Sm-Nd isochron calculated from a garnet core (Grt1) together with the whole rock analysis that yielded a well defined Permian age of 286 ± 3 Ma (Schuster et al. 2001). However in other parts of the Rappold Complex Variscan garnet might also be present. Sm-Nd ages of pegmatitic veins, calculated from magmatic garnet, tourmaline and the whole rock are in the range of 260-290 Ma. Summarising the data, the older assemblage most likely formed in Permo-Triassic times at low pressures conditions within the andalusite stability field and during the emplacement of the pegmatites. The overprinting assemblage formed during the Eo-Alpine tectonothermal event in Cretaceous times. It reached conditions of 600-650 °C at 1.0-1.1 GPa (Faryad and Hoinkes 2003)

The pegmatitic veins of the Rappold Complex are a few centimetres to several meters in thickness. They exhibit ductile deformation at a various grade. In some regions the veins can be traced over several hundreds of meters and the deformation is restricted to the outer part, whereas in other regions they are boudinaged and characterised by a penetrative deformation of the pegmatitic bodies. Most of the pegmatitic rocks show a magmatic mineral area and are in contact to marbles and the tourmaline-rich pegmatitic zones described here were sampled from near to the contact to these marbles.

5.4 Experimental

5.4.1 Sample selection

Tourmaline samples were collected from outcrops in the Rappold Complex. Pale blue tourmaline (crystals up to ~5 mm in length and ~3 mm in diameter) occurs in a pegmatite at Gaberl, Stubalpe, Styria (sample GAB). This tourmaline is associated with albite, microcline, quartz, muscovite and apatite. Another locality of pale blue tourmaline (crystals up to ~7 mm in length and ~1.5 mm in diameter) is a pegmatite at Steinthaller, Gleinalpe, Styria (sample STE). This tourmaline is associated with microcline, quartz and muscovite. Olive-green tourmaline (crystals up to ~8 mm in length and ~0.5 mm in diameter) occurs in a pegmatite at Dreiwasser, Gleinalpe, Styria (sample GLE). It is associated with albite, quartz and minor muscovite. Tourmaline with pale blue colour (crystals up to ~7 mm in length and ~2.5 mm in diameter) occurs also in a pegmatite at Mt. Hohenwart, Pusterwald, Wölzer Tauern, Styria (sample HOH). It is associated with microcline, muscovite quartz and apatite. Representative samples of micaschist (in a distance of a few metres to the pegmatite) were collected at each locality.

5.4.2 Chemical composition

All elements of the tourmaline crystals (except B, Li, Be, Cr, Co, Ni, Zn, Rb, Sr, Cs, Ba, Sc, Y, REEs, Pb, Th, and U) were determined with a wavelength-dispersive ARL SEMQ electron microprobe at the Mineralogisch-Petrographische Abteilung, Naturhistorisches Museum, Vienna, Austria. The operating conditions were 15 kV accelerating voltage, sample current 15 nA (on benitoite), and spot size 5 x 5 μm^2 (defocused beam). Natural silicates and oxides were used as standards.

The sample preparation for the ICP-MS analyses was performed in a clean laboratory using ultrapure acids. Hand-picked concentrates of tourmaline crystals were used. To remove surface contamination, the tourmaline grains were leached in 2.5 N HCl for 15 minutes at about 80 °C. Chemical sample digestion was performed in tightly sealed Teflon beakers using a HF:HNO_3 mixture of 3:1. After about 2 weeks at ~150 °C the samples were evaporated and transformed into nitrate by HNO_3. Chemical sample digestion was further performed in Zr-cups by using NaOH (heating by a Bunsen burner). The ICP-MS analyses were performed on an ELAN 6100 (Perkin Elmer-SCIEX).

5.4.3 Crystal structure

Samples of the Mg-rich tourmalines were mounted on a Bruker Apex CCD diffractometer equipped with graphite-monochromated Mo *K*α radiation. Redundant data were collected for a sphere of reciprocal space, and absorption was corrected using semi-empirical methods as implemented in the programs SADABS (Bruker AXS, Inc. 2003). A total of 4500 frames were collected for each sample, at

0.20 ° frame width, and a scan time of 15 s, and a detector distance of 5 cm; data from 0-30 ° θ were used in the refinement.

The structure was refined using a tourmaline starting model and the Bruker SHELXTL V. 6.10 package of programs, with neutral-atom scattering factors and terms for anomalous dispersion. Refinement was performed with anisotropic displacement parameters for all non-hydrogen atoms, and the structure was refined on F^2. In Table 4 the refined cell-parameters and details of the refinement are listed, in Table 5 the atom coordinates and equivalent-isotropic displacement parameters are listed, and in Table 6 selected interatomic distances are presented.

B, O1-O8, and H3 were constrained to fully occupy their respective sites, and the tourmaline *Y* site was modeled with Mg and Fe scattering factors because significant amounts of Fe occur in each sample beside the dominant cations Mg and Al. The *Z* site was modeled with Al and Mg because a released *Z*-site occupancy, modeled only with Al, gave no evidence for significant amounts of Fe at this site. Occupancy of the *T* site was constrained to fully occupy this site with Si, because there was no indication for $^{[4]}$B. The H atom associated with O3 (H3) was easily located in the difference map, and subsequently refined.

5.5 Results

5.5.1 Discussion of the tourmaline structure

The optimized structural formula of the investigated tourmaline samples, which were derived by using chemical and structural data (details see Table 1), are:

GAB: $^{X}(Na_{0.78}Ca_{0.13}K_{0.02}\square_{0.07})$ $^{Y}(Mg_{1.44}Al_{1.24}Fe^{2+}_{0.12}Li_{0.02}Zn_{0.02}Ti^{4+}_{0.01}\square_{0.15})$ $^{Z}(Al_{5.00}Mg_{0.98})$ $(BO_3)_3$ $^{T}(Si_{5.97}Al_{0.03})$ O_{18} $^{V}(OH)_3$ $^{W}[F_{0.81}(OH)_{0.19}]$

STE: $^{X}(Na_{0.67}Ca_{0.24}K_{0.02}\square_{0.07})$ $^{Y}(Mg_{1.83}Al_{0.88}Fe^{2+}_{0.20}Li_{0.08}Zn_{0.01}Ti^{4+}_{0.01}\square_{0.09})$ $^{Z}(Al_{5.25}Mg_{0.75})$ $(BO_3)_3$ Si_6O_{18} $^{V}(OH)_3$ $^{W}[F_{0.87}(OH)_{0.13}]$

GLE: $^{X}(Na_{0.67}Ca_{0.19}K_{0.02}\square_{0.12})$ $^{Y}(Mg_{1.26}Al_{0.97}Fe^{2+}_{0.36}Li_{0.19}Ti^{4+}_{0.06}Zn_{0.01}\square_{0.15})$ $^{Z}(Al_{5.31}Mg_{0.69})$ $(BO_3)_3$ Si_6O_{18} $^{V}(OH)_3$ $^{W}[F_{0.66}(OH)_{0.34}]$

HOH: $^{X}(Na_{0.77}Ca_{0.14}K_{0.02}\square_{0.07})$ $^{Y}(Mg_{1.31}Al_{1.28}Fe^{2+}_{0.36}Li_{0.03}Zn_{0.01}Ti^{4+}_{0.01})$ $^{Z}(Al_{4.94}Mg_{1.06})$ $(BO_3)_3$ Si_6O_{18} $^{V}(OH)_3$ $^{W}[(OH)_{0.48}F_{0.27}O_{0.25}]$

The *X* site in all is samples mainly occupied by Na but additionally contains significant amounts of Ca (≥0.13 apfu). Only relatively small amounts of K have been found in these samples (~0.1 wt.% K_2O; Table 1). The *X*-site vacancies, which are in the range 0.07-0.12 pfu, are relatively small. There is an interesting positive correlation, with $r^2 \approx 1.00$, between the Ca content and <*Y*-O> distance for all investigated tourmaline samples (Fig. 2). It is not absolutely clear, but perhaps Ca^{2+}

(contrary to Na^{1+} and K^{1+}) is favoured at the *X* sites in these tourmalines with occupants with lower valence states than 3 (Al^{3+}) at the *Y* site, occupants such as Mg^{2+}, Fe^{2+} and Li^{1+}. Possible short-range order configurations including Ca are given in Table 7.

The *Y* site is in all samples dominantly occupied by Mg (~1.3-1.8 apfu). Because of a significant Mg-Al disorder between the *Y* and *Z* site, also a relatively high amount of Al occupies the *Y* site. A significant amount of Fe (0.12-0.36 apfu) was also found by chemical analyses and supported by structural refinement. Three tourmaline samples (GAB, STE, HOH) have a pale-blue colour and one sample has an olive-green colour (GLE). The pale-blue colour most likely comes from absorption by Fe^{2+}, whereas the olive-green colour can be derived from Fe^{2+}-Ti^{4+} intervalence charge transfer, together with light absorption by Fe^{2+}, which would be consistent with the higher amount of TiO_2 (~0.5 wt.%) in the olive-green tourmaline (sample GLE) contrary to the relatively small amounts of TiO_2 (~0.1 wt.%) in the pale blue tourmalines (Mattson and Rossman 1987, 1988; Cempírek et al. 2006; Rossman 2008). Hence, the investigated tourmalines show no indication of significant amounts of Fe^{3+} (>10% relative to total Fe). Interestingly all investigated tourmaline samples have a significant amount of Li (Li_2O: 0.02-0.29 wt.%). Usually Mg-rich tourmalines contain only small amounts of Li with ≤50 ppm (e.g., Grice and Ercit 1993; Dyar et al. 1998; Pertlik et al. 2003).

The *Z* site is mainly occupied by Al but contains also relatively high amounts of Mg. The refinement of Al⇔Mg is not very accurate because Al^{3+} and Mg^{2+} are isoelectronic. Therefore the <*Z*-O> distances, which are in the range 1.921-1.929 Å (Table 6), were used to estimate the ^{Z}Mg content. The Mg content was distributed between the *Y* and the *Z* site by minimizing the error between the average ionic radius of the *Y*-site and *Z*-site occupants in relation to the observed bond lengths. As a good approximation for the average ionic radius of the *Y*-site and *Z*-site occupants the sum of ^{Y}Mg, Fe^{2+}, Li, Ti^{4+} and Zn (for the *Y* site) and the amount of ^{Z}Mg (for the *Z* site) can be used (Figs. 3-5). For the final assigned *Y*-site and *Z*-site occupants, $r^2 \approx 0.98$ for the positive correlation of ^{Y}<r> to <*Y*-O> (Fig. 4) as well as for the correlation ^{Z}Mg to <*Z*-O> (Fig. 5). The latter correlation is of course only valid if there are no significant amounts of Fe^{3+} at *Z* site. The investigated tourmalines contain relatively low amounts of Fe (~1-3 wt.% FeO) and there is no evidence for significant amounts of Fe^{3+} at the *Z* site of these samples (Tables 1, 5). There is a positive correlation ($r^2 \approx 0.82$) between MgO of the tourmalines and the surrounding micaschists (Fig. 6).

The <*T*-O> distances of ~1.620 Å (Table 6), are in agreement with occupancy of this position essentially by Si atoms (MacDonald and Hawthorne 1995; Hawthorne 1996; Ertl et al. 2001). A H atom (= H3) at the site associated with O3 was easily located in this refinement.

Ertl et al. (2002) showed that the bond-angle distortion (σ_{oct}^2) of the ZO_6 octahedron in a tourmaline is largely a function of the <*Y*-O> distance of that tourmaline, although the occupant of the O3 site (*V* site) also affects that distortion. The covariance, *r*, of <*Y*-O> and the σ_{oct}^2 of the ZO_6 octahedron is -0.991 for all investigated tourmalines that are occupied by 3 (OH) groups, including the samples from Hughes et al. (2004). The investigated tourmalines lie exactly on the *V* site = 3 (OH) line. Hence, the *V* site is occupied completely by 3(OH). The *W* site of the samples GAB, STE and

GLE is mainly occupied by F (Table 1). The relatively high amounts of F are in agreement with the low vacancies at the *X* site (Henry 2005).

5.5.2 REEs and trace elements in the tourmalines

As noted in the literature, trace elements in tourmaline yield information on the genesis of tourmalines and their host rocks. For this reason also the REEs and some trace elements in the investigated tourmaline samples were analyzed.

The chondrite-normalized REE patterns of the Mg-rich tourmalines from the Rappold Complex (Table 3; Figures 7-10) exhibit minor enrichment of LREEs in comparison to HREEs (La_N/Yb_N ratios of 1.5, 2.1, 2.2, and 3.9.) and they contain relatively low sums of REEs in the range 8.3-36.5 ppm. The REE signatures of these tourmalines show, in addition to a negative Eu anomaly, a more-or-less significantly-developed positive Yb anomaly. The Th contents are in the range of 0.1-1.8 ppm (Table 3).

5.5.3 Discussion of the Eu and Yb anomaly in the tourmalines

As mentioned above the REE signatures of these tourmalines show, in addition to a negative Eu anomaly, a more or less significantly-developed positive Yb anomaly (Fig. 7-10). Yb and Eu are relatively volatile elements compared to the other REEs (Lodders and Fegley 1993). Hsu (2003) proposes a mechanism for a Yb anomaly. In nature, REEs usually occur in trivalent state. Under highly reducing conditions, Eu and Yb can be divalent because of the enhanced stability of the half-filled (Eu^{2+}) and completely filled (Yb^{2+}) 4f subshell. Divalent REEs have larger ionic radii than trivalent ones and will behave different during anatexis, igneous fractionation and crystallization. This results in Yb and Eu anomalies. With respect to Raith et al. (2004), who concluded that tourmaline does not preferentially fractionate specific REEs or groups of REEs during crystallization and that tourmaline REE patterns mirror the REE distribution of their immediate host rock, it can be supposed that the Eu and Yb anomaly of the tourmalines reflect the REE pattern of the pegmatitic melt during crystallisation of the tourmalines. Therefore these anomalies are a signature of the rocks that were affected by anatexis or that originated during the process of local anatexis (see also Martins and Janasi 2005).

5.5.4 Discussion of the origin of the tourmalines and their pegmatitic host rocks

According to Ertl et al. (2006), tourmalines from pegmatites that originated from highly-fractionated granitic melts are strongly enriched in LREEs compared to HREEs (La_N/Yb_N ratio of ~350-420) and exhibit negative Eu anomalies. Furthermore, they have relatively high REE (~70-150 ppm) and Th contents (~3-4 ppm). Higher Th contents conform to the enrichment in LREE that are

geochemical analogues of Th. Conversely, tourmalines from pegmatites, which are not related to conventional processes of late-stage fractionation of granitic magmas, show relatively low REE (~3-4 ppm) and low La_N/Yb_N ratios of 1.2-1.8 (Kontak et al. 2002).

The chondrite-normalized REE patterns as well as the low REE and Th contents of the Mg-rich tourmalines described here clearly show a different signature in comparison to tourmalines from pegmatites that originated from highly fractionated granitic melts. This fact can be explained in several ways: (1) The pegmatitic host rocks are not crystallised from highly fractionated granitic melts. (2) The crystallisation of the tourmaline-rich zone is highly influenced by contact phenomena with the country-rock, especially the marbles and micaschists, or (3) a combination of both effects.

The first possibility is supported by the regional geology. As mentioned above Permian pegmatitic rocks are widely distributed and frequent in many Austroalpine basement units, whereas Permian granitic rocks are scarce and restricted to a few units. On the basis of isotopic data, the observed Permian granites are not the parent melts of the pegmatites (Thöni and Miller 2002). In parts of the Rappold Complex there are indications for the breakdown of white mica and the formation of alumosilicate (andalusite) during the Permian event. In some places (the area of St. Radegund, southern part of the Niedere Tauern mts.), a network of millimeters to a few centimeters wide pegmatitic veins is preserved. These observations indicate that parts of the Rappold Complex have been a source region for the pegmatitic melts. Conversely, there are localities (e.g., Hohenwart area) where pegmatitic veins with minor internal deformation can be traced for several hundreds meters and in these areas the spodumene-bearing pegmatites also occur. It can be suggested that the pegmatitic rocks represent relatively small patches of melt formed by muscovite breakdown reactions. These melts rose in the crust, perhaps for several hundreds of meters up to a few kilometers, but they did not pass through a stage in a large magma chamber with crystallisation of a granite.

An influence of contact phenomena is very likely because of the following evidence: Mn-poor tourmalines from granitic rocks (differentiated pegmatites which are not associated with marbles) normally have relatively low Ca contents (e.g., Selway et al. 1999, 2000, 2002) except when they are associated with marbles (e.g., Ertl et al. 2006), whereas metamorphic tourmalines can contain up to 1 apfu (in calc-silicates and marbles; Henry and Dutrow 1996). Furthermore, the X_{Mg} values are usually similar to that of the host rock and depend also on the grade of the metamorphism (e.g., Raith et al. 2004; Henry and Dutrow 1996). The investigated tourmalines have significant Ca contents up to ~0.24 apfu and high X_{Mg} values, atypical for granitic melts. Their X_{Mg} is well-correlated to that of the surrounding metasediments, and the wt% MgO of the tourmalines and the surrounding micaschists show positive correlation ($r^2 \approx 0.82$) (Fig. 6).

On the basis of these arguments, the tourmalines described here may have crystallized in the contact between a pegmatitic melt formed by local anatexis and contact processes with carbonatic and metapelitic host rocks. In this contact zone B and Li came from the pegmatitic melt whereas significant amounts of Ca, Mg and Fe derived from the country-rocks.

5.5.5 Discussion of formation temperatures

Henry and Dutrow (1996) reported correlations between the mineral chemistry and metamorphic conditions in metamorphic tourmaline from Al-rich metapelites. Although the investigated tourmalines have not grown directly in a metapelite but in a pegmatitic rocks that may have formed due to local anatexis of metapelites, they formed by contact processes during the emplacement of these pegmatites, and may be influenced by the surrounding micaschists, as suggested by a positive correlation ($r^2 \approx 0.82$) between wt% MgO of the tourmalines and the surrounding micaschists (Fig. 5).

All of the Mg-rich tourmalines show X_{Mg} (X_{Mg} = Mg/Mg + Fe_{total}) values in the range 0.84-0.95. By using the X_{Mg} to *X*-site vacancy correlation of Fig. 11 in Henry and Dutrow (1996), they plot in the fields of medium and high-grade tourmalines. Using their Fig. 12, which shows a correlation of Ca to *X*-site vacancy for tourmalines from metapelites and calcareous metasediments, the tourmalines samples from the Rappold Complex plot between the fields of medium- and high-grade metamorphic tourmalines. By using Fig. 13 of Henry and Dutrow (1996), which shows a correlation of X_{Mg} to Ca, the Mg-rich tourmalines plot in the field for high-grade metapelites. Hence, it can be concluded that the tourmalines formed at (minimum) temperatures of ~600±50 °C. These temperatures are in agreement with those determined for the Permo-Triassic HT/LP event in the Rappold Complex (Faryad and Honikes 2003).

5.5.6 Geochemistry of the micaschists

Because the investigated tourmalines crystallised in pegmatitic rocks in contact to micaschists and marbles of the Rappold Complex, also the surrounding micaschists were chemically characterised, including REE elements. The major and minor element composition of the micaschist samples is shown in Table 2, the trace elements are shown in Table 3. The SiO_2 content of the micaschist samples ranges from ~45 to ~64 wt.%, and the Al_2O_3 content is between ~15 and ~26 wt.%. The Fe_2O_3 content is in the range ~7-10 wt.%, the MgO content is in the range ~2.2 - 2.9 wt.% and the TiO_2 content between ~0.7 and ~1.7 wt.%. The CaO content is in the range ~2-6 wt.%, whereas the Na_2O content is between ~0.9 to ~2.5 wt.% and the K_2O content between ~3 and ~6 wt.%. With respect to the average pelite from Symmes and Ferry (1991) the investigated rocks show no homogeneous trend. The samples GAB, GLE and HOH are enriched in Al_2O_3, Fe_2O_3, K_2O, but the SiO_2, CaO, Na_2O values are scattered around the values of the average metapelite. In the discrimination diagram Zr vs. TiO_2 from Garcia et al. (1991) the sample GAP plots in the field of shales whereas all other samples are classified as sandstones and greywackes.

The MnO/TiO_2 ratio can be an indicator of the depositional environment (Sugisaki et al. 1982; Yamamoto 1983; Sugisaki 1984; Sugitani 1996). These authors suggested that the MnO/TiO_2 ratio can be used to distinguish pelagic and continental sources of siliceous sediments. Sugitani (1996) studied

the MnO/TiO_2 ratios of marine sediments at various distances from land. He divided these values into two groups: sediments <110 km away from land are hemipelagic, and those >600 km are pelagic. Fukukawa et al. (2004) defined the boundary of these two groups at 400 km, which corresponds to a MnO/TiO_2 ratio of ~0.5. This value can be used for classifying sediments into the hemipelagic and pelagic origins. The MnO/TiO_2 ratio of the samples studied here varies from 0.05 to 0.39 (data from table 2). If these values were used which were obtained from the mica schist samples of the Rappold Complex, the former sediments would be classified as hemipelagic. Fukukawa et al. (2004) suggested a high mobility of Mn, confirmed by depth profiles of Mn abundances in sediments. It is necessary to consider a metamorphic effect when employing the MnO/TiO_2 ratio to characterise sedimentary rocks, as has been shown by Murray (1994) and references therein. However, no MnO/TiO_2 ratio > 0.5 was observed.

The chondrite-normalized REE patterns (Fig. 7-10) and the REE concentrations (Table 3) of the investigated micaschists are typical for argillaceous schists (Taylor and McLennan 1985). The most striking feature recorded in the REE patterns of sediments is the degree of the Ce anomaly, noted as Ce/Ce* (Shimizu and Masuda 1977):

$Ce/Ce^* = Ce_N/(La_N \times Pr_N)^{1/2}$, where N indicates the normalized abundance with chondrite. A negative Ce anomaly implies that the sediment was formed under a pelagic environment, whereas a positive or no Ce anomaly implies formation at the continental margin. For the metamorphic sediments of the Rappold Complex a small positive Ce anomaly with ~1.0 was calculated for all samples, which implies formation at the continental margin.

Murray (1994) summarized the abundances of REE and other elements and provided a discrimination diagram by a bivariate plot of La_N/Ce_N and $Al_2O_3/(Al_2O_3+Fe_2O_3)$. The continental margin sediments contain relatively high amounts of Ce, leading to a low La_N/Ce_N ratio, and the pelagic sediments, depleted in Ce, show a high La_N/Ce_N ratio. The present data are concentrated near the boundary of the two fields of the pelagic and the continental margin. This indicates that the metamorphic sediments of the Rappold Complex derived from a variegated depositional area composed of shales, sandstones and greywackes in a pelagic to continental margin environment.

5.6 Acknowledgements

Special thanks to W. Zirbs, Vienna, Austria, for fluorine determination and to A. Wagner, Vienna, Austria, for sample preparation work. This work was supported by Österreichischer Fonds zur Förderung der wissenschaftlichen Forschung (FWF) project no. P20509.

5.7 References

Bloodaxe ES, Hughes JM, Dyar MD et al (1999) Linking structure and chemistry in the Schorl-Dravite series. Am Mineral 84: 922-928.

Bosi F, Lucchesi S (2004) Crystal chemistry of the schorl-dravite series. Eur J Mineral 16: 335-344.

Bosi F, Lucchesi S, Reznitskii L (2004) Crystal chemistry of the dravite-chromdravite series. Eur J Mineral 16: 345-352.

Cámara F, Ottolini L, Hawthorne FC (2002) Chemistry of three tourmalines by SREF, EMPA, and SIMS. Am Mineral 87: 1437-1442.

Cempírek J, Novák M, Ertl A et al (2006) Fe-bearing olenite with tetrahedrally coordinated Al from an abyssal pegmatite at Kutná Hora, Czech Republic: Structure, crystal chemistry, optical and XANES spectra. Can Mineral, 44: 23-30.

Dyar MD, Taylor ME, Lutz TM et al (1998) Inclusive chemical characterization of tourmaline: Mössbauer study of Fe valence and site occupancy. Am Mineral 83: 848-864.

Dyar MD, Wiedenbeck M, Robertson D et al (2001) Reference minerals for the microanalysis of light elements. Geostand Newsl 25: 441-463.

Ertl A, Hughes JM, Marler B (2001) Empirical formulae for the calculation of <T-O> and X-O2 bond lengths in tourmaline and relations to tetrahedrally-coordinated boron. N Jb Miner Mh 2001: 548-557.

Ertl A, Hughes JM, Brandstätter F et al (2003) Disordered Mg-bearing olenite from a granitic pegmatite from Goslarn, Austria: A chemical, structural, and infrared spectroscopic study. Can Mineral 41: 1363-1370.

Ertl A, Hughes JM, Prowatke S et al (2006) Tetrahedrally-coordinated boron in tourmalines from the liddicoatite-elbaite series from Madagascar: Structure, chemistry, and infrared spectroscopic studies. Am Mineral 91: 1847-1856.

Faryad SW, Hoinkes G (2003) P-T gradient of Eo-Alpine metamorphism within the Austroalpine basement units east of the Tauern Window (Austria). Mineralogy and Petrology 77: 129-159.

Fischer RX, Tillmanns E (1988) The equivalent isotropic displacement factor. Acta Cryst. C44: 775-776.

Fukukawa M, Takahashi Y, Hayasaka Y et al (2004) 4. Geochemical Study of ODP Leg 191 Site 1179 Sediments: Direct Observation of Mn and Ce Oxidation States. In: Sager, WW, Kanazawa T, Escutia C (eds.), Proc ODP, Sci Results 191: 1-24, College Station TX (Ocean Drilling Program).

Gaiges F, Abart R, DeCapitani C et al (2006) Characterisation of polymetamorphism in the Austroalpine basement east of the Tauern Window using garnet isopleth thermobarometry. J metam Geol 24: 451-475.

Garcia D, Coelho J, Perrin M (1991) Fractionation between TiO_2 and Zr as a measure of sorting within shale and sandstone series (Northern Portugal). Eur J Mineral 3: 401-414.

Grice JD, Ercit TS (1993) Ordering of Fe and Mg in the tourmaline crystal structure: The correct formula. N Jb Miner Abh 165: 245-266.

Habler G, Thöni M (2001) Preservation of Permo-Triassic low-pressure assemblages in the Cretaceous high-pressure metamorphic Saualpe crystalline basement (Eastern Alps, Austria). J metam Geol 19: 679-697.

Hawthorne FC (1996) Structural mechanisms for light-element variations in tourmaline. Can Mineral 34: 123-132.

Hawthorne FC, Henry DJ (1999) Classification of the minerals of the tourmaline group. Eur J Mineral 11: 201-215.

Hawthorne FC, MacDonald DJ, Burns PC (1993) Reassignment of cation site-occupancies in tourmaline: Al-Mg disorder in the crystal structure of dravite. Am Mineral 78: 265-270.

Henry DJ (2005) Fluorine – X-site vacancy avoidance in natural tourmaline: internal vs. external control. 2005 Goldschmidt Conference, May 20-25, Moscow, Idaho, USA, Abstracts Volume, abstract no. 1318.

Henry DJ, Dutrow BL (1996) Metamorphic tourmaline and its petrologic applications. In: Grew ES, Anovitz LM (eds.) (1996) Boron: Mineralogy, petrology and geochemistry. Rev Mineral 33: 505-557.

Hsu W (2003) Rare earth element geochemistry and petrogenesis of Miles (IIE) silicate inclusions. Geochim Cosmochim Acta 67: 4807-4821.

Kontak DJ, Dostal J, Kyser TK et al (2002) A petrological, geochemical, isotopic and fluid inclusion study of 370 Ma pegmatite-aplite sheets, Peggys Cove, Nova Scotia, Canada. Can Mineral 40: 1249-1286.

Lodders K, Fegley B (1993) Lanthanide and actinide chemistry at high C/O ratios in the solar nebula. Earth Planet Sci Lett 177: 125–145.

MacDonald DJ, Hawthorne FC (1995) The crystal chemistry of Si ⇔ Al substitution in tourmaline. Can Mineral 33: 849-858.

Mali H (2004) Die Spodumenpegmatite von Brettstein und Pusterwald (Wölzer Tauern, Steiermark, Österreich). Joannea - Mineralogie 2: 5-53.

Martins L, Janasi VA (2005) Trace-element zonation in monazite from garnet-bearing migmatites and associated granites, SE Brazil: Implications for crustal anatexis. Goldschmidt Conference Abstracts 2005, Accessory Mineral Geochemistry II, A30.

Mattson SM, Rossman GR (1987) Fe^{2+}-Fe^{3+} interactions in tourmaline. Phys Chem Minerals 14: 163-171.

Mattson SM, Rossman GR (1988) Fe^{2+}-Ti^{4+} charge transfer absorption in stoichiometric Fe,Ti minerals. Phys Chem Minerals 16: 78-82.

McDonough WF, Sun SS (1995) Composition of the Earth. Chem Geol 120: 223-253.

Murray RW (1994) Chemical criteria to identify the depositional environment of chert: general principles and applications. Sediment Geol 90: 213–232.

Novák M, Selway JB, Černý P et al (1999) Tourmaline of the elbaite-dravite series from an elbaite-subtype pegmatite at Bližná, southern Bohemia, Czech Republic. Eur J Mineral 11: 557-568.

Palme H (1988) Chemical abundances in meteorites. In Cosmic Chemistry (G Klare, ed.), Rev Modern Astron 1: 28-51. Springer, Berlin Heidelberg.

Pertlik F, Ertl A, Körner W et al (2003) Na-rich dravite in the marbles from Friesach, Carinthia, Austria: Chemistry and crystal structure. N Jb Miner Mh 2003: 277-288.

Raith JG, Riemer N, Meisel T (2004) Boron metasomatism and behavior of rare earth elements during formation of tourmaline rocks in the eastern Arunta Inlier, central Australia. Contrib Mineral Petrol 147: 91-109.

Rossman GR (2008) The tourmaline group. Tourmaline colors. http://minerals.gps.caltech.edu/FILES/Visible/tourmaline/Index.html Accessed 29 March 2008

Schmid SM, Fügenschuh B, Kissling E et al (2004) Tectonic map and overall architecture of the Alpine orogen. Eclogae geologicae Helveticae 97/1: 93-117.

Schuster R, Frank W (2000) Metamorphic evolution of the Austroalpine units east of the Tauern Window: indications for Jurassic strike slip tectonics. Mitt Ges Geol Bergbaustudenten Österreich 42: 37-58.

Schuster R, Scharbert S, Abart R et al (2001) Permo-Triassic extension and related HT/LP metamorphism in the Austroalpine - Southalpine realm. Mitt Ges Geol Bergbaustudenten Österreich 44: 111-141.

Schuster R, Koller F, Hoeck V et al (2004) Explanatory notes to the map: Metamorphic structure of the Alps - Metamorphic evolution of the Eastern Alps. Mitt Österr Miner Ges 149: 175-199.

Selway JB, Novák M, Černý P et al (1999) Compositional evolution of tourmaline in lepidolite-subtype pegmatites. Eur J Mineral 11: 569-584.

Selway JB, Černý P, Hawthorne FC et al (2000) The Tanco pegmatite at Bernic Lake, Manitoba. XIV. Internal tourmaline. Can Mineral 38: 877-891.

Selway JB, Smeds S-A, Černý P et al (2002) Compositional evolution of tourmaline in the petalite-subtype Nyköpingsgruvan pegmatites, Utö, Stockholm Archipelago, Sweden. GFF 124: 93-102.

Shimizu H, Masuda A (1977) Cerium in chert as an indication of marine environment of its formation. Nature 266: 346-348.

Sugisaki R (1984) Relation between chemical composition and sedimentation rate of Pacific ocean-floor sediments deposited since the middle Cretaceous: basic evidence for chemical constraints on depositional environments of ancient sediments. J Geol 92: 235-259.

Sugisaki R, Yamamoto K, Adachi M (1982) Triassic bedded cherts in central Japan are not pelagic. Nature 298: 644-647.

Sugitani K (1996) Study of sedimentary paleoenvironments of siliceous sedimentary rocks using some geochemical indicators. Geochemistry 30: 75-89 (in Japanese).

Symmes GH, Ferry JM (1991) Evidence from mineral assemblages for infiltration of pelitic schists by aqueous fluids during metamorphism. Contrib Mineral Petrol 108: 419-438.

Taylor MC, Cooper MA, Hawthorne FC (1995) Local charge-compensation in hydroxyl-deficient uvite. Can Mineral 33: 1215-1221.

Taylor SR, McLennan SM (1985) The Continental Crust: its Composition and Evolution. Blackwell Scientific Publications, Oxford, 312 pp.

Thöni M (1999) A review of geochronological data from the Eastern Alps. Schweiz Mineral Petrogr Mitt 79/1: 209-230.

Thöni M (2002) Sm-Nd isotope systematics in garnet from different lithologies (Eastern Alps): age results, and an evaluation of potential problems for garnet Sm-Nd chronometry. Chem Geol 185: 255-281.

Thöni M, Miller C (2000) Permo-Triassic pegmatites in the eo-Alpine eclogite-facies Koralpe complex, Austria: age and magma source constraints from mineral chemical, Rb-Sr and Sm-Nd isotopic data. Schweiz Mineral Petrogr Mitt 80: 169-186.

Wasson JT, Kallemeyn GW (1988) Composition of chondrites. Phil Trans Roy Soc London, Ser A, Math Phys Sci: 352(1587), 535-544.

Yamamoto K (1983) Geochemical study of Triassic bedded cherts from Kamiaso, Gifu Prefecture. Chishitsugaku Zasshi 89: 143–162 (in Japanese).

Table 1. Composition of pegmatitic Mg-rich tourmalines from different localities in the Rappold Complex (Austroalpine basement units), Styria, Austria (wt.%).

	GAB[1]	GAB[2]	STE[1]	STE[2]	GLE[1]	GLE[2]	HOH[1]	HOH[2]
SiO_2	37.28	37.28	37.32	37.32	37.33	37.24	37.39	37.06
TiO_2	0.09	0.09	0.11	0.11	0.50	0.50	0.06	0.06
B_2O_3	10.45	10.86	10.45	10.82	10.59	10.79	10.54	10.74
Al_2O_3	33.30	33.30	31.95	31.76	33.69	33.07	32.74	32.59
Cr_2O_3	0.01	0.01	0.01	0.01	0.02	0.02	0.01	0.01
FeO*	0.86	0.86	1.50	1.50	2.69	2.69	2.66	2.66
MnO*	0.01	0.01	0.02	0.02	0.01	0.01	0.06	0.06
MgO	10.12	10.12	10.74	10.74	8.12	8.12	9.82	9.82
CaO	0.78	0.78	1.37	1.37	1.08	1.08	0.83	0.83
ZnO	0.16	0.16	0.08	0.08	0.12	0.12	0.05	0.05
Li_2O	0.03	0.03	0.13	0.13	0.29	0.29	0.05	0.05
Na_2O	2.51	2.51	2.14	2.14	2.13	2.13	2.46	2.46
K_2O	0.08	0.08	0.09	0.09	0.08	0.08	0.08	0.08
F	1.59	1.59	1.72	1.72	1.29	1.29	0.53	0.53
H_2O[3]	2.97	2.99	2.90	2.91	3.13	3.11	2.99	3.48
O≡F	-0.67	-0.67	-0.72	-0.72	-0.54	-0.54	-0.22	-0.22
Sum	99.57	100.00	99.81	100.00	100.53	100.00	100.05	100.00
N	31	31	31	31	31	31	31	31
Si (apfu)	6.00	5.97	6.02	6.00	5.99	6.00	6.06	6.00
[4]Al	-	0.03	-	-	0.01	-	-	-
Sum T site	6.00	6.00	6.02	6.00	6.00	6.00	6.06	6.00
[3]B	2.90	3.00	2.91	3.00	2.93	3.00	2.95	3.00
Mg	2.43	2.42	2.58	2.58	1.94	1.95	2.37	2.37
Al	6.33	6.26	6.08	6.03	6.36	6.28	6.25	6.22
Fe^{2+}	0.12	0.12	0.20	0.20	0.36	0.36	0.36	0.36
Mn^{2+}	-	-	-	-	-	-	0.01	-
Li	0.02	0.02	0.08	0.08	0.19	0.19	0.03	0.03
Zn	0.02	0.02	0.01	0.01	0.01	0.01	0.01	0.01
Ti^{4+}	0.01	0.01	0.01	0.01	0.06	0.06	0.01	0.01
Sum Y, Z sites	8.93	8.85	8.96	8.91	8.92	8.85	9.04	9.00
Ca	0.13	0.13	0.24	0.24	0.19	0.19	0.14	0.14
Na	0.78	0.78	0.68	0.67	0.66	0.67	0.77	0.77
K	0.02	0.02	0.02	0.02	0.02	0.02	0.02	0.02
□	0.07	0.07	0.06	0.07	0.13	0.12	0.07	0.07
Sum X site	0.93	0.93	0.94	0.93	0.87	0.88	0.93	0.93
Sum cations	18.76	18.78	18.83	18.84	18.79	18.73	18.98	18.93
OH	3.19	3.19	3.12	3.13	3.35	3.34	3.33	3.48
F	0.81	0.81	0.88	0.87	0.65	0.66	0.27	0.27
Sum OH + F	4.00	4.00	4.00	4.00	4.00	4.00	3.50	3.75

Note: Average of 10 EMP analyses. B_2O_3, Li_2O and ZnO determined by ICP-MS analysis and F determined by F-sensitive electrodes on the tourmaline bulk samples. [2]Weight percent of B_2O_3, Al_2O_3 and SiO_2 calculated for an optimized formula (with a total oxide sum of 100%) by

considering the <T-O> distances (Table 6), by taking care that Si ≤ 6 apfu. $^{3}H_2O$ was calculated for (OH) + F = 4.00, except for sample HOH, where it was calculated for (OH) + F = 3.50 [see normalization procedure of Novák et al. (2004) for F-poor tourmalines]. For the optimized formula of sample HOH the H_2O content was calculated considering a charge-balanced formula and a cation sum of Y + Z +w T = 18 apfu. * Total Fe and Mn calculated as FeO and MnO (see text).

Table 2. Major and minor elements (ICP-MS analyses) of micaschists (which surround the tourmaline-bearing pegmatitic rocks) from different localities in the Rappold Complex (Austroalpine basement units), Styria, Austria (wt.%).

	Mica Schist GAB	Mica Schist STE	Mica Schist GLE	Mica Schist HOH
SiO_2	44.63	64.15	60.30	54.40
P_2O_5	0.24	0.15	0.16	0.16
TiO_2	1.74	0.78	0.71	0.89
Al_2O_3	26.30	15.20	18.00	18.85
$Fe_2O_3^*$	10.15	7.04	7.95	7.94
MnO	0.08	0.10	0.14	0.35
MgO	2.88	2.90	2.15	2.41
CaO	1.78	3.11	1.80	5.80
Li_2O	0.02	0.02	0.01	0.06
Na_2O	1.30	2.48	1.42	0.91
K_2O	6.20	2.56	4.71	4.80
Rb_2O	0.03	0.01	0.02	0.02
Sr_2O_3	0.04	0.02	0.01	0.07
BaO	0.09	0.04	0.11	0.07
ZnO	0.02	0.02	0.01	0.02
LOI	3.77	1.06	2.34	2.74
CO_2	0.37	n.d.	n.d.	n.d.
Sum	99.27	99.64	99.84	99.49

Note: LOI: loss on ignition. N.d.: not determined. * Total Fe as Fe_2O_3.

Table 3. Trace elements (ICP-MS analyses) of Mg-rich tourmaline and micaschists (which surround the tourmaline-bearing pegmatitic rocks) from different localities in the Rappold Complex (Austroalpine basement units), Styria, Austria (ppm).

	Tourmaline GAB	Tourmaline STE	Tourmaline GLE	Tourmaline HOH	Mic aschist GAB	Micaschist STE	Micaschist GLE	Micaschist HOH	Chondrite
Be	1.80	4.40	4.90	3.30	4.65	2.43	3.30	7.3	-
Cr	110.0	13.0	31.5	39.0	150.0	126.0	119.0	150.0	-
Co	1.40	1.20	22.0	0.90	10.2	19.2	21.7	7.6	-
Ni	170.0	61.0	70.0	72.0	69.0	79.0	53.0	59.0	-
Cu	-	-	-	-	48.0	28.0	46.0	45.0	
Rb	18.0	18.0	1.50	1.80	275.0	128.0	185.0	164.0	-
Sr	130.0	142.0	53.0	80.0	309.0	154.0	94.0	553.0	-
Zr	-	-	-	-	302.0	194.0	185.0	132.0	-
Cs	1.00	0.70	0.70	0.90	7.5	7.0	9.5	27.0	-
Ba	77.2	49.2	15.8	33.5	835.0	373.0	1005.0	598.0	-
Sc	0.90	1.20	33.4	4.70	21.5	16.0	20.0	19.5	-
Y	5.33	3.85	7.90	2.18	42.0	18.0	37.0	37.5	-
Pb	57.0	68.0	57.0	45.0	3.00	26.0	20.0	75.0	-
Bi	-	-	-	-	0.14	0.16	0.14	0.38	-
Th	1.75	1.38	1.00	0.12	21.0	15.0	15.0	13.5	-
U	0.55	0.32	1.20	0.15	2.50	1.55	2.70	2.30	-
La	3.30	1.42	8.2	3.50	76.0	31.0	57.0	48.0	0.236
Ce	4.50	2.70	12.3	1.90	155.0	63.0	108.0	89.0	0.616
Pr	0.56	0.31	1.25	0.23	17.0	6.9	12.5	9.5	0.0929
Nd	2.25	1.20	5.55	0.93	70.0	30.0	54.0	39.0	0.457
Sm	0.72	0.40	1.45	0.32	12.9	5.60	9.5	6.7	0.149
Eu	0.21	0.10	0.19	0.10	2.60	1.30	1.90	1.50	0.056
Gd	0.77	0.45	1.50	0.41	12.0	5.30	8.5	6.3	0.197
Tb	0.16	0.09	0.29	0.08	1.73	0.78	1.25	0.95	0.0355
Dy	0.87	0.58	1.80	0.45	8.6	3.70	6.6	5.40	0.245
Ho	0.19	0.12	0.31	0.07	1.65	0.70	1.30	1.25	0.0546
Er	0.52	0.37	0.85	0.17	4.50	1.90	3.90	3.90	0.166
Tm	0.08	0.06	0.13	0.03	0.62	0.30	0.63	0.65	0.0247
Yb	0.57	0.45	2.50	1.55	3.30	2.00	4.10	4.30	0.159
Lu	0.10	0.06	0.18	0.08	0.44	0.32	0.62	0.61	0.0245
ΣREE	14.80	8.31	36.49	9.82	366.34	152.80	261.25	217.06	

Note: Errors for oxides and elements ≤5%. Chondrite values compiled by T. Meisel from Raith et al. (2004) (all REE exclusive of Ho and Er: Wasson and Kallemeyn 1988; Ho: McDonough and Sun 1995; Er: Palme 1988).

Table 4. Crystal data and results of structure refinement of Mg-rich tourmalines from different localities in the Rappold Complex (Austroalpine basement units), Styria, Austria.

Space group: *R*3*m*

Unit cell parameters (Å):

GAB: a = 15.9307(4), c = 7.2074(3) STE: a = 15.9354(4), c = 7.1934(4)

GLE: a = 15.9220(3), c = 7.1732(2) HOH: a = 15.9354(3), c = 7.2076(2)

Frame width, scan time, number of frames, detector distance: 0.20 **º**, 15 s, 4500, 5 cm

Measured reflections, full sphere:

GAB: 11,641 STE: 11,584

GLE: 11,481 HOH: 11,560

Unique reflections; refined parameters:

GAB: 1,135; 94 STE: 1,135; 94

GLE: 1,131; 94 HOH: 1,133; 94

*R*1*****, $F_o > 4\sigma_{(Fo)}$:

GAB: 0.0151 STE: 0.0143

GLE: 0.0128 HOH: 0.0130

Difference peaks (+,-):

GAB: 0.38, -0.24 STE: 0.38, -0.27

GLE: 0.28, -0.22 HOH: 0.31, -0.24

Goodness-of-Fit**§**:

GAB: 1.103 STE: 1.143

GLE: 1.191 HOH: 1.196

---

* $R1 = \Sigma| |F_o| - |F_c| | / \Sigma|F_o|$.

§ GooF = $S = \{\Sigma[w(F_o^2 - F_c^2)^2] / (n-p)\}^{1/2}$.

Table 5. Table of atom parameters in Mg-rich tourmalines from different localities in the Rappold Complex (Austroalpine basement units), Styria, Austria.

GAB:

Atom	***x***	***y***	***Z***	U_{eq}	**refined occ.***
X	0	0	¼	0.0212(4)	$Na_{1.073(8)}$
T	0.19185(2)	0.18996(2)	0.0113(2)	0.00708(9)	$Si_{1.00}$
B	0.10964(7)	2*x*	0.4668(3)	0.0090(3)	$B_{1.00}$
Y	0.12540(4)	1/2*x*	-0.3560(2)	0.0092(2)	$Mg_{0.950(3)}Fe_{0.050}$
Z	0.29802(3)	0.26160(3)	-0.3763(2)	0.0067(3)	$Al_{0.69(5)}Mg_{0.31}$
O1	0	0	-0.2164(3)	0.0131(4)	$O_{1.00}$
O2	0.06071(5)	2*x*	0.4972(3)	0.0140(3)	$O_{1.00}$
O3	0.2638(1)	1/2*x*	-0.4764(3)	0.0156(3)	$O_{1.00}$
O4	0.09295(5)	2*x*	0.0824(3)	0.0126(2)	$O_{1.00}$
O5	0.1835(1)	1/2*x*	0.1033(3)	0.0126(2)	$O_{1.00}$
O6	0.19546(6)	0.18543(6)	-0.2108(2)	0.0109(2)	$O_{1.00}$
O7	0.28503(6)	0.28477(6)	0.0910(2)	0.0107(2)	$O_{1.00}$
O8	0.20930(6)	0.26997(7)	0.4528(2)	0.0120(2)	$O_{1.00}$
H3	0.260(2)	1/2*x*	0.416(5)	0.037(9)	$H_{1.00}$

STE:

Atom	***x***	***y***	***Z***	U_{eq}	**refined occ.***
X	0	0	¾	0.0169(4)	$Na_{1.122(8)}$
T	0.80812(2)	0.80997(2)	0.9839(2)	0.00678(9)	$Si_{1.00}$
B	0.89027(7)	2*x*	0.5293(3)	0.0086(3)	$B_{1.00}$
Y	0.87449(4)	1/2*x*	0.3529(2)	0.0102(3)	$Mg_{0.935(3)}Fe_{0.065}$
Z	0.70201(3)	0.73844(3)	0.3712(2)	0.0061(3)	$Al_{0.68(5)}Mg_{0.32}$
O1	0	0	0.2099(3)	0.0104(4)	$O_{1.00}$
O2	0.93923(5)	2*x*	0.5015(3)	0.0133(3)	$O_{1.00}$
O3	0.7342(1)	1/2*x*	0.4717(3)	0.0139(3)	$O_{1.00}$
O4	0.90722(5)	2*x*	0.9128(3)	0.0118(3)	$O_{1.00}$
O5	0.8166(1)	1/2*x*	0.8919(3)	0.0119(2)	$O_{1.00}$
O6	0.80409(6)	0.81374(6)	0.2063(2)	0.0104(2)	$O_{1.00}$
O7	0.71497(6)	0.71522(6)	0.9034(2)	0.0101(2)	$O_{1.00}$
O8	0.79043(7)	0.72966(7)	0.5420(2)	0.0112(2)	$O_{1.00}$
H3	0.740(2)	1/2*x*	0.575(5)	0.032(9)	$H_{1.00}$

GLE:

Atom	***x***	***y***	***Z***	U_{eq}	**refined occ.***
X	0	0	¼	0.0196(4)	$Na_{1.023(8)}$
T	0.19185(2)	0.18996(2)	0.0178(2)	0.00685(9)	$Si_{1.00}$
B	0.10973(7)	2*x*	0.4722(3)	0.0087(3)	$B_{1.00}$
Y	0.12451(4)	1/2*x*	-0.3504(2)	0.0092(2)	$Mg_{0.892(3)}Fe_{0.108}$
Z	0.29781(3)	0.26137(3)	-0.3703(2)	0.0065(3)	$Al_{0.77(5)}Mg_{0.23}$
O1	0	0	-0.2074(3)	0.0143(4)	$O_{1.00}$
O2	0.06090(5)	2*x*	0.5019(3)	0.0139(3)	$O_{1.00}$
O3	0.2653(1)	1/2*x*	-0.4710(3)	0.0145(3)	$O_{1.00}$
O4	0.09315(5)	2*x*	0.0890(3)	0.0118(2)	$O_{1.00}$
O5	0.1844(1)	1/2*x*	0.1103(3)	0.0119(2)	$O_{1.00}$
O6	0.19586(6)	0.18595(6)	-0.2052(2)	0.0104(2)	$O_{1.00}$
O7	0.28519(6)	0.28506(6)	0.0975(2)	0.0100(2)	$O_{1.00}$
O8	0.20961(6)	0.27043(7)	0.4589(2)	0.0110(2)	$O_{1.00}$
H3	0.261(2)	1/2*x*	0.423(5)	0.038(9)	$H_{1.00}$

HOH:

Atom	***x***	***y***	***Z***	U_{eq}	**refined occ.***
X	0	0	¾	0.0207(4)	$Na_{1.067(7)}$
T	0.80820(2)	0.81009(2)	0.9872(2)	0.00723(8)	$Si_{1.00}$
B	0.89030(6)	2*x*	0.5318(3)	0.0090(3)	$B_{1.00}$
Y	0.87499(3)	1/2*x*	0.3540(2)	0.0094(2)	$Mg_{0.879(3)}Fe_{0.121}$
Z	0.70194(2)	0.73839(2)	0.3750(2)	0.0073(2)	$Al_{0.82(5)}Mg_{0.18}$
O1	0	0	0.2147(3)	0.0146(4)	$O_{1.00}$
O2	0.93923(4)	2*x*	0.5012(2)	0.0142(3)	$O_{1.00}$
O3	0.7363(1)	1/2*x*	0.4749(3)	0.0160(2)	$O_{1.00}$
O4	0.90704(4)	2*x*	0.9161(2)	0.0126(2)	$O_{1.00}$
O5	0.81650(9)	1/2*x*	0.8953(2)	0.0127(2)	$O_{1.00}$
O6	0.80454(6)	0.81454(6)	0.2093(2)	0.0111(2)	$O_{1.00}$
O7	0.71502(6)	0.71525(5)	0.9077(2)	0.0109(2)	$O_{1.00}$
O8	0.79071(6)	0.73001(6)	0.5460(2)	0.0122(2)	$O_{1.00}$
H3	0.740(2)	1/2*x*	0.588(5)	0.046(9)	$H_{1.00}$

Note: * Optimized occupancies in Table 1. Definition for U_{eq} see Fischer and Tillmanns (1988).

Table 6. Selected interatomic distances in Mg-rich tourmalines from different localities in the Rappold Complex (Austroalpine basement units), Styria, Austria.

	GAB	STE	GLE	HOH
X-				
O2 x3	2.446(2)	2.451(2)	2.468(2)	2.456(2)
O5 x3	2.743(2)	2.729(2)	2.734(1)	2.740(1)
O4 x3	2.835(2)	2.816(2)	2.818(1)	2.832(1)
Mean	**2.675**	**2.665**	**2.673**	**2.676**
Y-				
O1	2.001(1)	2.014(1)	2.001(1)	1.996(1)
O2 x2	2.0052(9)	2.0129(9)	2.0023(9)	2.0052(8)
O6 x2	1.995(1)	2.009(1)	2.0051(9)	1.9966(9)
O3	2.097(2)	2.116(2)	2.126(2)	2.103(1)
Mean	**2.016**	**2.029**	**2.024**	**2.017**
Z-				
O6	1.893(1)	1.882(1)	1.8798(10)	1.8941(9)
O8	1.8959(9)	1.892(1)	1.8901(9)	1.8958(9)
O7	1.9064(9)	1.9020(9)	1.8981(9)	1.9061(8)
O8’	1.929(1)	1.927(1)	1.9232(9)	1.9303(9)
O7’	1.9577(9)	1.9593(9)	1.9574(9)	1.9586(8)
O3	1.9901(7)	1.9844(7)	1.9829(7)	1.9905(6)
Mean	**1.929**	**1.924**	**1.922**	**1.929**
T-				
O7	1.6040(9)	1.6053(9)	1.6044(10)	1.6042(8)
O6	1.6043(10)	1.6033(10)	1.6063(9)	1.6046(9)
O4	1.6271(5)	1.6274(5)	1.6262(5)	1.6270(5)
O5	1.6426(6)	1.6432(6)	1.6417(6)	1.6422(6)
Mean	**1.6195**	**1.6198**	**1.6197**	**1.6195**
B-				
O2	1.368(2)	1.366(2)	1.364(2)	1.369(2)
O8 (x2)	1.379(1)	1.381(1)	1.381(1)	1.378(1)
Mean	**1.375**	**1.376**	**1.375**	**1.375**

Table 7. Possible short-range order configurations in Mg-rich tourmalines of the Rappold Complex (Austroalpine basement units), Styria, Austria.

X site	*Y* site	*Z* site	*W* site
Na	Mg_2Al	Al_5Mg	F,OH
Na	Mg_3	Al_6	F,OH
Na	$MgFe^{2+}Al$	Al_5Mg	F,OH
Na	MgAlLi	Al_6	F,OH
Na	$Fe^{2+}AlLi$	Al_6	F,OH
Na	Al_2Mg	Al_5Mg	O
Na	Al_2Li	Al_6	O
Na	Al_2Fe^{2+}	Al_5Mg	O
Ca	Mg_2Fe^{2+}	Al_5Mg	F,OH
Ca	MgAlLi	Al_5Mg	F,OH
Ca	$Fe^{2+}AlLi$	Al_5Mg	F,OH
Ca	Li_2Al	Al_6	F,OH
Ca	Mg_2Al	Al_5Mg	O
Ca	Mg_3	Al_6	O
Ca	$MgFe^{2+}Al$	Al_5Mg	O

Note: The *T* site of all listed short-range order configurations is occupied by Si_6. The *V* site (O3 sites) is occupied by $(OH)_3$.

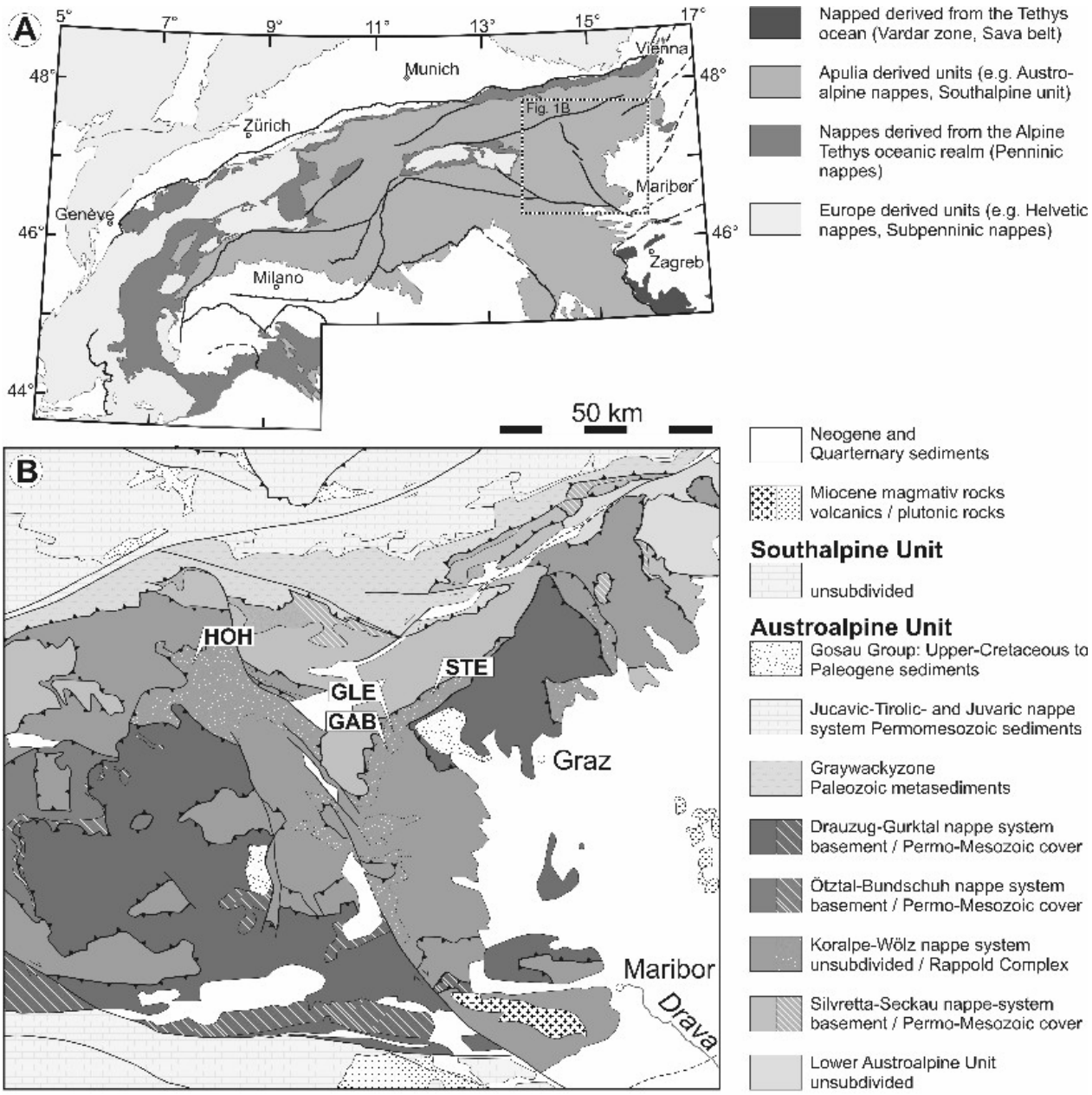

Fig. 1

FIGURE 1. A) Map showing the major tectonic units of the Alps and their paleogeographic origin. B) Geologic map of the Easten Alps showing the distribution of the Rappold Complex and the sample localities: GLE (Drei Wasser, Gleinalpe: E 14.9684° / N 47.1461), GAB (Schlossreihe, Stubalpe: E 14.9573° / N 47.1077°), STE (Steinthaller, Übelbach, Gleinalpe: E 15.1893°Ost / N 47.2315°), HOH (Hohenwart, Wölzer Tauern: E 14.2469° / N 47.3322°) (All coordinates are WSG 84).

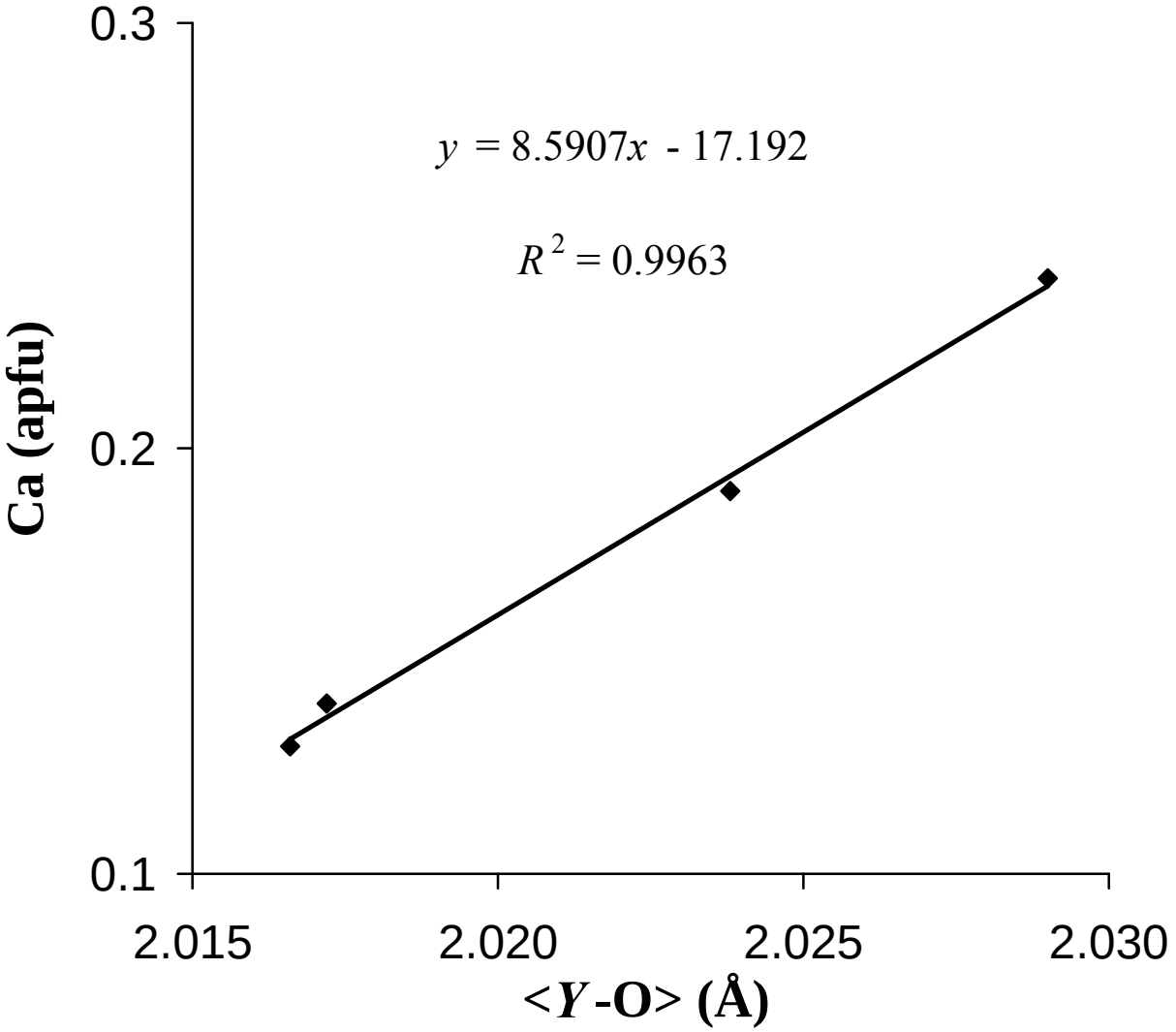

FIGURE 2. Relationship between the average *Y*-O bond length (Å) and the Ca content at the *X* site (apfu) in pale-blue to pale-green Mg-rich tourmalines from pegmatitic rocks of the Rappold Complex (Austroalpine basement units), Austrian Alps, Styria, Austria.

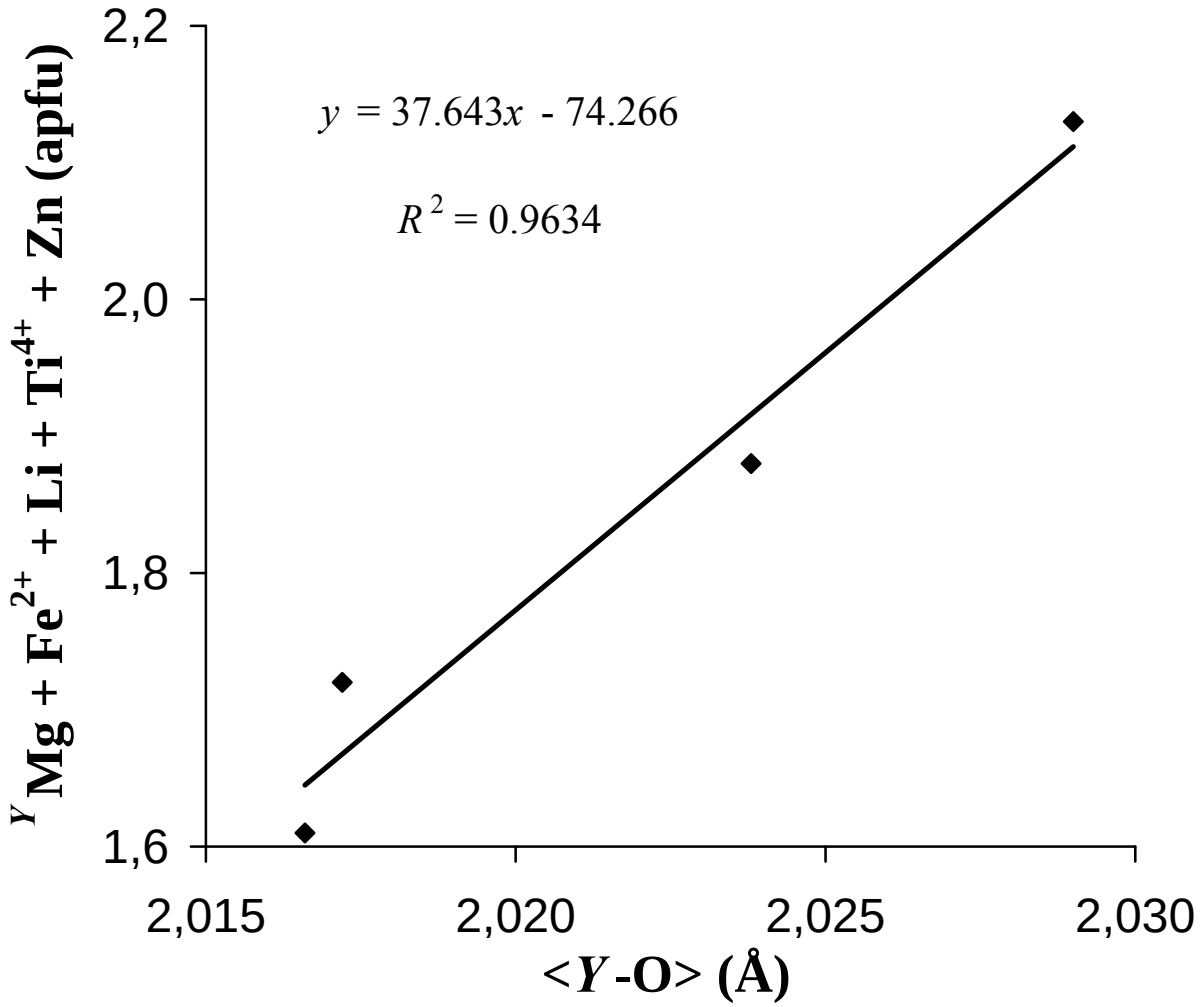

FIGURE 3. Relationship between the average *Y*-O bond length (Å) and the amounts of (^{Y}Mg + Fe^{2+} + Li + Ti^{4+} + Zn) at the *Y* site (apfu) of the optimized formulae of pale-blue to pale-green Mg-rich tourmalines from pegmatitic rocks of the Rappold Complex (Austroalpine basement units), Austrian Alps, Styria, Austria.

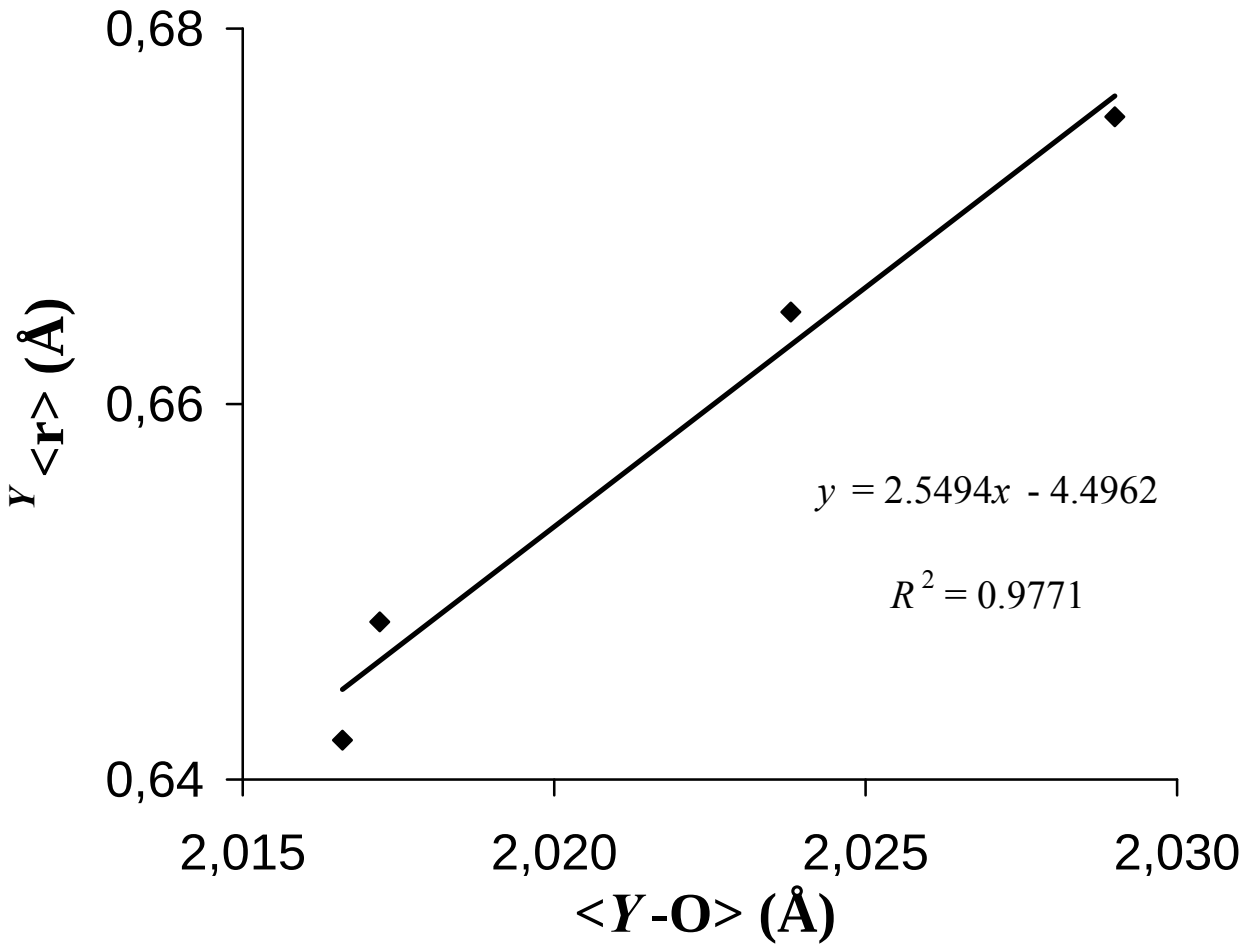

FIGURE 4. Relationship between the average *Y*-O bond length (Å) and the average ionic radius of the *Y*-site occupants (Å) of the optimized formulae of pale-blue to pale-green Mg-rich tourmalines from pegmatitic rocks of the Rappold Complex (Austroalpine basement units), Austrian Alps, Styria, Austria.

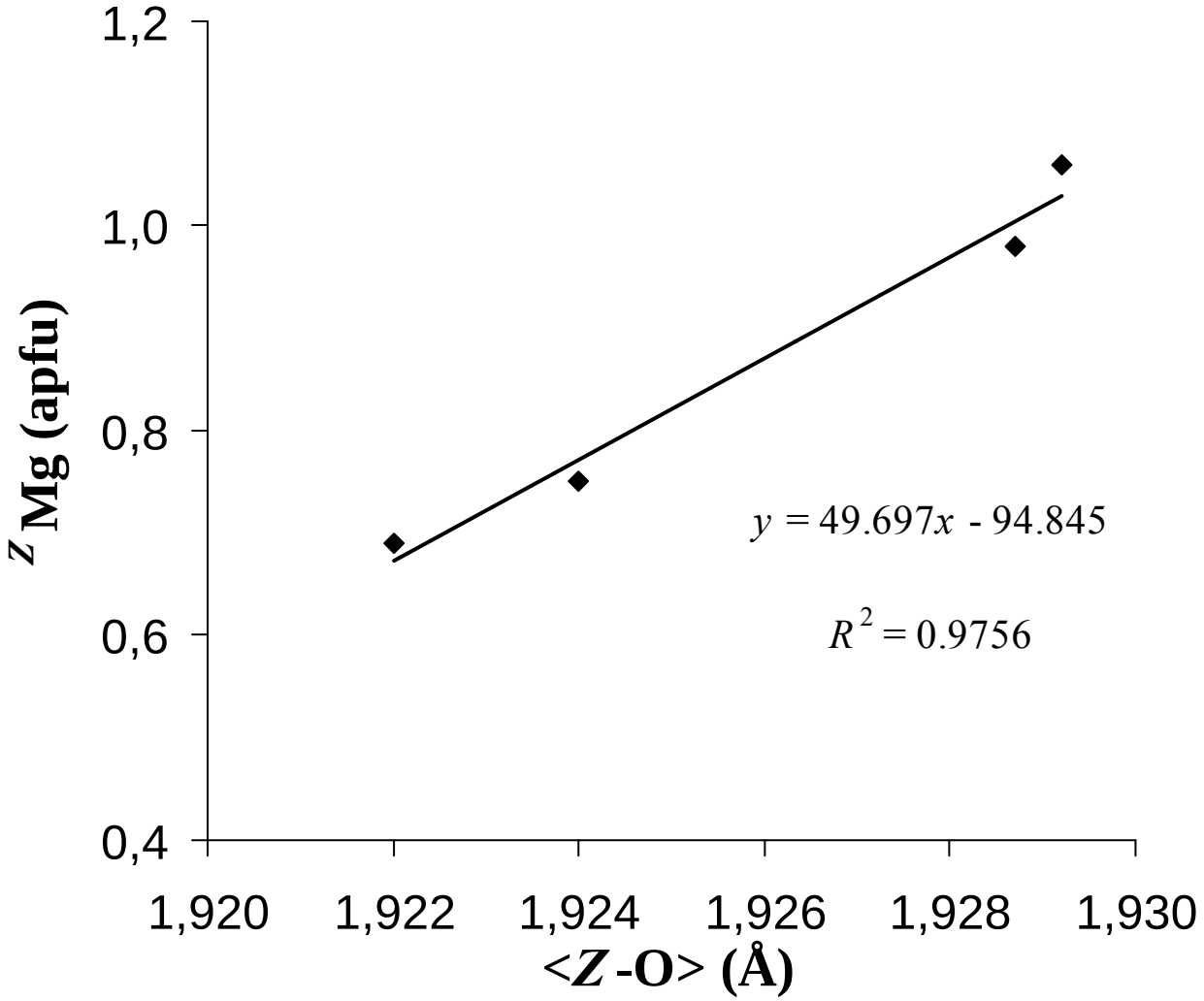

FIGURE 5. Relationship between the average *Z*-O bond length (Å) and the ^{Z}Mg content (apfu) of the optimized formulae of pale-blue to pale-green Mg-rich tourmalines from pegmatitic rocks of the Rappold Complex (Austroalpine basement units), Austrian Alps, Styria, Austria.

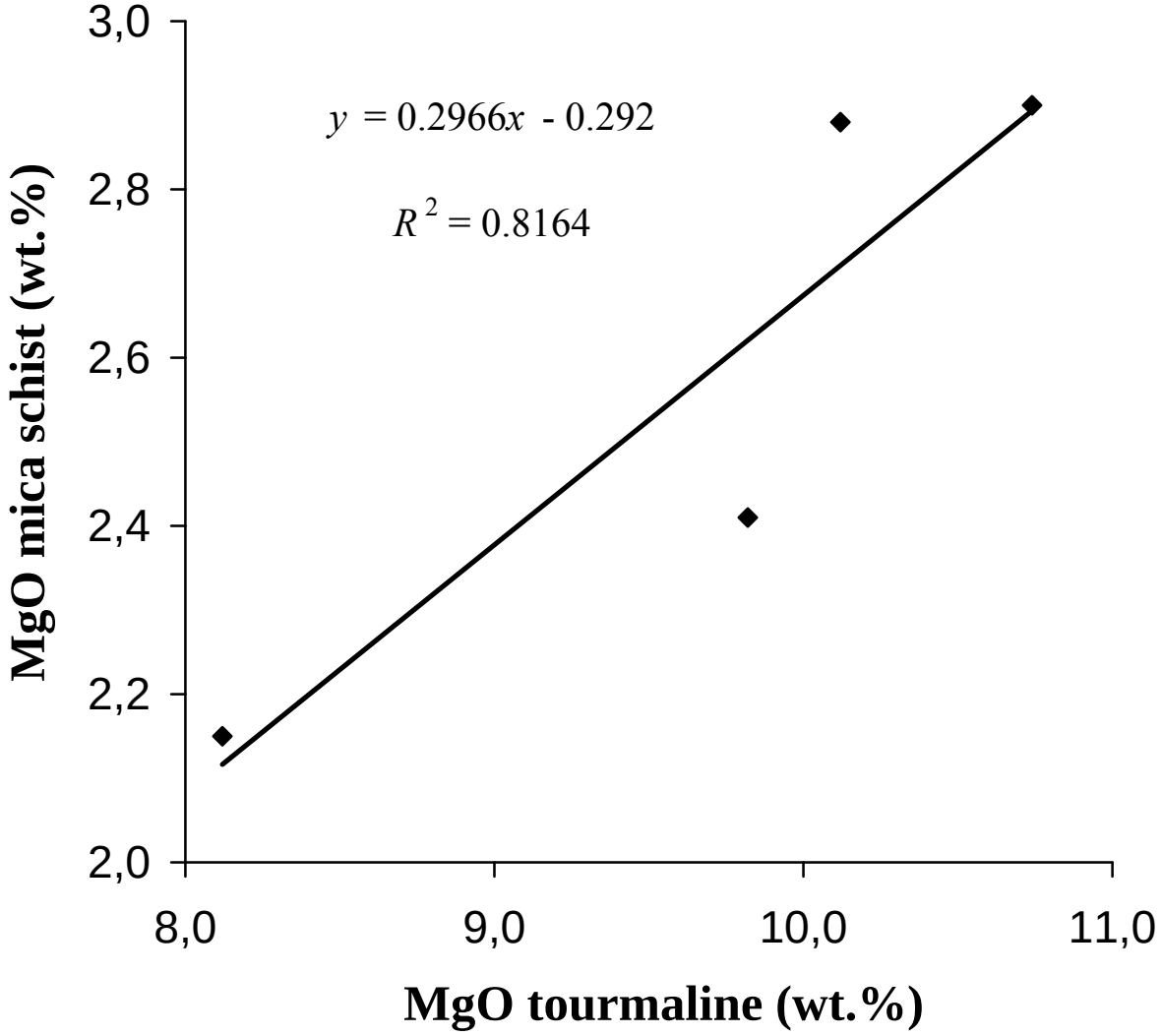

FIGURE 6. Relationship between the MgO content (wt.%) of pale-blue to pale-green Mg-rich tourmalines from pegmatitic rocks and of the surrounding micaschists of the Rappold Complex (Austroalpine basement units), Austrian Alps, Styria, Austria.

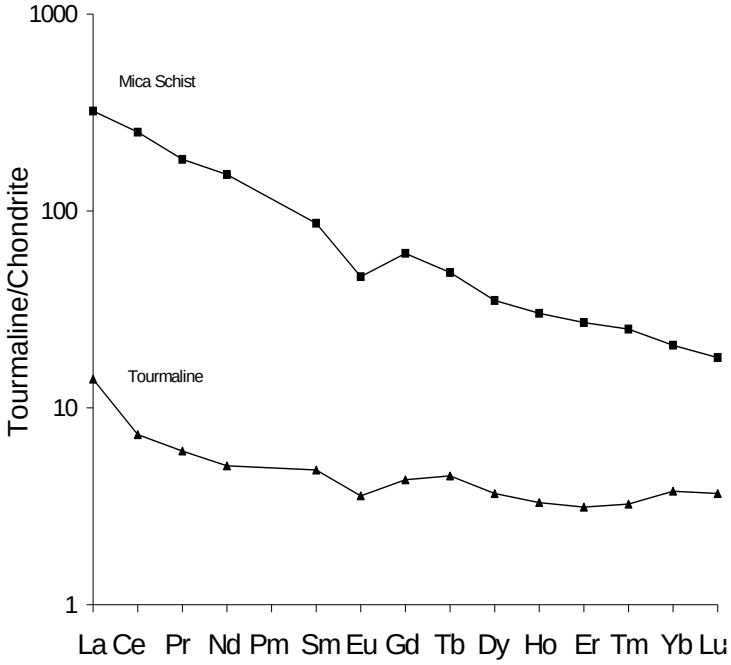

FIGURE 7. Chondrite-normalized REE patterns of the pale blue tourmaline from Gaberl, Stubalpe, Styria (sample GAB) and of the micaschist surrounding the tourmaline-bearing pegmatitic rock.

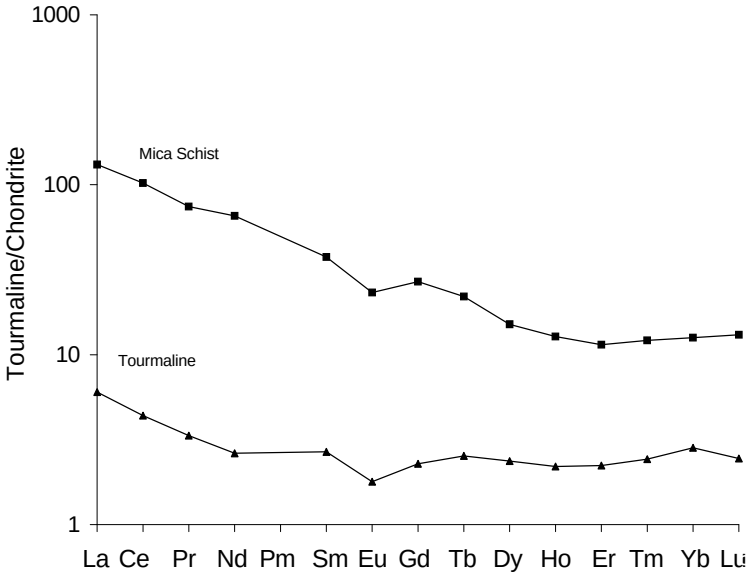

FIGURE 8. Chondrite-normalized REE patterns of the pale blue tourmaline from Steinthaller, Gleinalpe, Styria (sample STE) and of the micaschist surrounding the tourmaline-bearing pegmatitic rock.

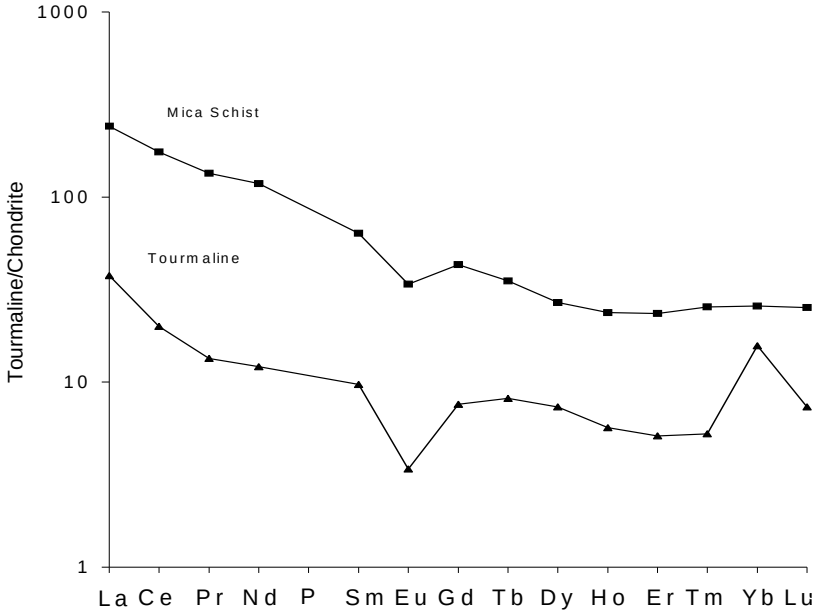

FIG. 9. Chondrite-normalized REE patterns of the olive-green tourmaline from Dreiwasser, Gleinalpe, Styria (sample GLE) and of the micaschist surrounding the tourmaline-bearing pegmatitic rock.

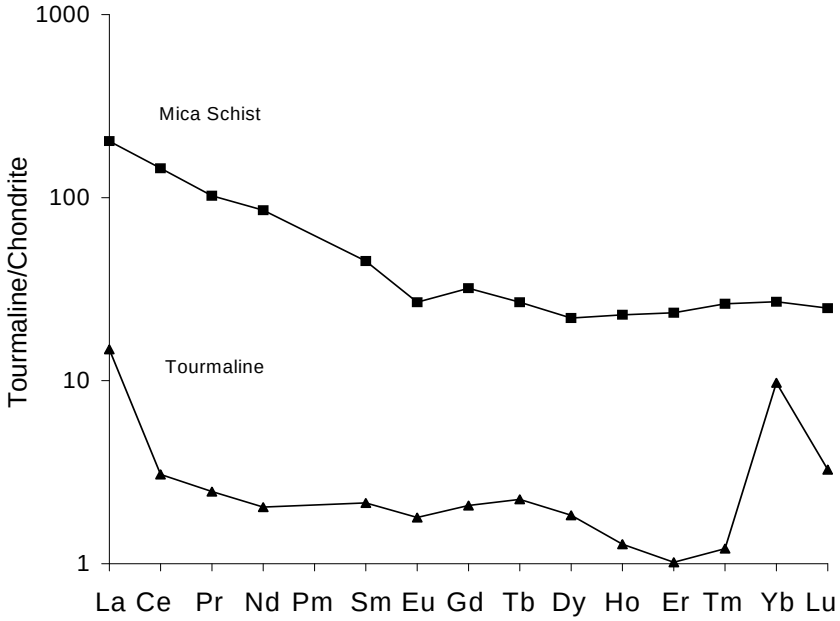

FIGURE 10. Chondrite-normalized REE patterns of the pale blue tourmaline from Hohenwart, Pusterwald, Wölzer Tauern, Styria (sample HOH) and of the micaschist surrounding the tourmaline-bearing pegmatitic rock.

6 Metamorphic ultra-high-pressure tourmalines: Structure, chemistry, and correlations to *PT* conditions

6.1 ABSTRACT

Tourmalines from metamorphic rocks occurring in three ultra high-pressure (UHP) metamorphic localities were structurally and chemically characterized to generate accurate structural formulae and to test for any systematic response related to varying temperatures and pressures. Dravite from the Parigi, Dora Maira, Western Alps, Italy locality (~3.7 GPa, 800ºC) has a formula of $^{X}(Na_{0.90}Ca_{0.05}K_{0.01}\square_{0.04})$ $^{Y}(Mg_{1.78}Al_{0.99}Fe^{2+}_{0.12}Ti^{4+}_{0.03}\square_{0.08})$ $^{Z}(Al_{5.10}Mg_{0.90})$ $(BO_3)_3$ $^{T}Si_{6.00}O_{18}$ $^{V}(OH)_3$ $^{W}[(OH)_{0.72}F_{0.28}]$, with a cell dimensions of a = 15.935(1), c = 7.201(1) Å. Dravite from the Lago di Cignana, Western Alps, Italy locality (~2.7-2.9 GPa, 600-630 ºC) has a formula of $^{X}(Na_{0.84}Ca_{0.09}K_{0.01}\square_{0.06})$ $^{Y}(Mg_{1.64}Al_{0.79}Fe^{2+}_{0.48}Mn^{2+}_{0.06}Ti^{4+}_{0.02}Ni_{0.02}Zn_{0.01})$ $^{Z}(Al_{5.00}Mg_{1.00})$ $(BO_3)_3$ $^{T}(Si_{5.98}Al_{0.02})O_{18}$ $^{V}(OH)_3$ $^{W}[(OH)_{0.65}F_{0.35}]$ with a cell dimension of a = 15.945(1), c = 7.210(1) Å. "Oxy-schorl" from the Saxony Ore Mountains, Germany locality (>2.9 GPa, 870 ºC) has a formula of $^{X}(Na_{0.86}Ca_{0.02}K_{0.02}\square_{0.10})$ $^{Y}(Al_{1.63}Fe^{2+}_{1.23}Ti^{4+}_{0.11}Mg_{0.03}Zn_{0.01})$ $^{Z}(Al_{5.05}Mg_{0.95})$ $(BO_3)_3$ $^{T}(Si_{5.96}Al_{0.04})O_{18}$ $^{V}(OH)_3$ $^{W}[O_{0.81}F_{0.10}(OH)_{0.09}]$ with a cell dimension of a = 15.929(1), c = 7.183(1) Å. There is no structural evidence for significant substitution of Si by Al or B in the UHP tourmalines (<T-O> distances ~1.620 Å), even in tourmaline from the highest temperature sample from Saxony Ore Mountains. This contrasts with tourmalines formed at high grade, but lower pressure conditions having significant amounts of $^{[4]}$Al. For this limited data set there is an excellent positive correlation (r^2 = 1.00) between the sum of $^{[6]}$Al (Sum of Al at the Y and Z site) in the UHP tourmalines and the determined temperature conditions of tourmaline formation of the different localities. Further there is a highly negative correlation (r^2 = 0.94) between the <Y-O> distances of the UHP tourmalines and the temperature conditions of tourmaline formation. This correlation is most compatible with a temperature-related increase of ^{Y}Al content resulting from significant Al-Mg disorder between the Y and Z sites. Hence, such Al-Mg disorder appears to be dependent on the temperature during crystallization. Additional temperature-related features includes a negative correlation (r^2 = 0.92) with the average charge at the X site of the tourmalines and a negative correlation (r^2 = 0.97) with F content of the tourmalines.

6.2 INTRODUCTION AND PREVIOUS WORK

Tourmaline can be formed in different geochemical environments that have undergone magmatic, metasomatic, diagenetic or metamorphic processes (e.g., Henry and Guidotti 1985; Deer et al. 1992; Henry and Dutrow 1992, 1996; Slack 1996; Dutrow et al. 1999; Henry et al. 1999, 2008; Ertl et al. 2008b; Marschall et al. 2009). The general chemical formula of the tourmaline-group minerals was given as $XY_3Z_6[T_6O_{18}](BO_3)_3V_3W$ by Hawthorne and Henry (1999). The X site is usually occupied by Na, Ca, and rarely by K, but can also be vacant. The elements Fe^{2+}, Fe^{3+}, Mn^{2+}, Mg, Li,

Cu, Ti^{4+}, V^{3+} and Cr^{3+} are typically ordered into the Y site. Most tourmalines show also a significant amount (>5%) of Al at this site. The Z site in tourmaline is usually occupied by Al, but sometimes contains significant amounts of Mg, Fe^{3+}, and more rarely V^{3+} and Cr^{3+}. The substitution of Al for Mg at the *Z* site was described by Grice and Ercit (1993), Hawthorne et al. (1993), MacDonald and Hawthorne (1995), Taylor et al. (1995), Bloodaxe et al. (1999), Ertl et al. (2003a, 2008a), Bosi and Lucchesi (2004), Bosi et al. (2004) and Marschall et al. (2004). The T site is usually occupied by Si, but can also incorporate significant amounts of Al (e.g., Foit and Rosenberg 1979; MacDonald and Hawthorne 1995) and B (Ertl et al. 1997, 2008, and references therein).

Tourmaline compositions in metamorphic rocks are strongly related to the local bulk composition and mineral assemblages, but there are some general trends that are apparently a function of metamorphic grade. Based on a survey of natural tourmaline data, Henry and Dutrow (1996) suggested there are increases in tetrahedral Al via the $Al_2Si(R^{2+}Si)_{-1}$ exchange vector and in F contents at the W site, and decrease of X-site vacancies via the $^{X}\square Al(NaR^{2+})_{-1}$ exchange vector while the metamorphic grade increases (R^{2+}= Fe^{2+}, Mn^{2+}, Mg). In contrast, the experimental study of van Goerne et al. (2001) suggested that for a fixed Na content in the fluid phase, the latter exchange vector increases with temperature. A further trend noted in natural tourmaline is the increase in Ti contents as a function of grade (e.g., Thompson 2006). Probably the most robust tourmaline compositional feature is the compositional polarity (sector zoning) such that tourmaline of significantly different compositions develops at the opposite poles of the c-axis of the tourmaline (Henry and Dutrow 1996; van Hinsberg and Schumacher 2007). This compositional polarity diminishes as a function of temperature and disappears at medium grades of metamorphism and has been suggested as a geothermometer.

6.3 TOURMALINE STABILITY, REGIONAL GEOLOGY OF THE ULTRA HIGH PRESSURE (UHP) MASSIFS AND SAMPLE CHARACTERISTICS

The temperature and pressure stability of tourmaline is very large. It ranges from diagenetic/epigenetic to high-grade metamorphic conditions up to magmatic conditions (e.g. ~150-850°C at ~100-400 MPa; Robbins and Yoder 1962; Manning and Pichavant 1983). The *PT* stability of dravite was established in experiments by Werding and Schreyer (2002) at pressures of 3-5 GPa and temperatures with >950°C (Fig. 1). These studies reported the breakdown of dravite to different Al-Mg phases at pressures as high as 6-8 GPa (Krosse 1985; Werding and Schreyer 2002; Fig. 1). In the presence of coesite natural tourmaline breaks down at a pressure of 4 GPa in the temperature range of 800-850°C and 4.5-5 GPa at a lower temperature of 700°C (Ota et al. 2008; Fig. 1).

In this study natural tourmalines that developed under well-established ultrahigh pressure (UHP) metamorphic conditions are considered. The UHP gneisses from the Kokchetav Massif, Kazakhstan (Dobretsov et al. 1995) were not considered because it is unclear whether these

tourmalines crystallized during UHP conditions in that there are no coesite inclusions but only quartz inclusions without any expansion cracks and palisade quartz textures (Marschall et al. 2009).

Tourmalines were obtained from two UHP localities in the Western Alps. The pyrope quartzites from Parigi, Dora Maira, contain dravite inclusions in coesite-bearing pyrope megacrysts, in kyanite and in phlogopite-kyanite-quartzpseudomorphs after pyrope (Schreyer 1985; Schertl et al. 1991). Optically continuous tourmaline inclusions in pyrope were interpreted as evidence for growth pyrope and kyanite at the expense of tourmaline (Schreyer 1985; Schertl et al. 1991). Geothermobarometry and petrogenetic phase relations of mineral inclusion establish that the peak conditions of the UHP metamorphism was ~3.7 GPa/~800°C (Schertl et al. 1991). Similar peak conditions of ~4.5 GPa/~750°Cof the pyrope quartzite were revealed by the experimental work of Hermann (2003). The second location in which Mg-rich tourmaline was reported in UHP rocks is in the Western Alps at Lago di Cignana (Reinecke 1991, 1998; Bebout and Nakamura 2003). These UHP metasediments formed at *PT* conditions of ~2.7-2.9 GPa/~600-630°C (Reinecke 1991, 1998). Reinecke (1991) described inclusions of relict coesite, hematite, rutile and braunite in tourmalines from Lago di Cignana (Fig. 2).

A third UHP locality with tourmaline is located in the Erzgebirge at the northwestern border of the Bohemian Massif, which is part of the Devonian-Carboniferous metamorphic basement of the Mid-European Variscides exposed in Saxony (Saxony Ore Mountains) and the northern Czech Republic. It is characterized by a stack of five tectonometamorphic units with a distinct PT history (Willner et al. 1997; Rötzler et al. 1998). The investigated sample R6b is from the diamond- and coesite-bearing Gneiss-Eclogite Unit (GEU). PT estimates of the eclogite revealed conditions of >2.9 GPa at 870°C (Schmädicke and Müller 2000), but the occurrence of diamond in the felsic gneisses requires pressures in excess of 4 GPa (Massonne 2003; Massonne et al. 2007). PT estimates with 8 GPa at >1050°C have been published for the GEU by Massonne (2003). Samples were collected as loose decimetre-sized blocks from a small creek 5 km ENE of the village of Saidenbach. Sample R6b is a felsic medium-grained mylonitic granulite displaying strongly elongated quartz and feldspar with black tourmaline porphyroclasts.Tourmaline crystals are short-prismatic and up to 3 mm in length. In thin sections, cut perpendicular to the c-axis, they show three distinct color zones which display diffuse boundaries: a blue core, a brownish mantle, and a greenish-grey anhedral rim zone, which is intimately intergrown with quartz, feldspar and phengite from the matrix. Different inclusions in tourmalines from these UHP massifs were described: Reinecke (1991) described inclusions of relic coesite, hematite, rutile and braunite in tourmalines from Lago di Cignana. An idiomorphic tourmaline crystal from this locality with a relic coesite inclusion is shown in Figure 2. Marschall et al. (2009) observed coesite and kyanite inclusions in the mantle zone of tourmaline from the Saxony Ore Mountains (in phengite-quartz gneiss sample R6b).

In the UHP tourmaline samples under investigation additional inclusions which were identified by Raman spectroscopy and electron microprobe analysis (EMPA). In the sample from Dora Maira a phengite inclusion (~2 μm in diameter) was observed. In the tourmaline from Lago di Cignana

talc (~12 μm in length), zircon (a crystal with ~3 μm in diameter), and a mineral from the epidote group (~15 μm in diameter) with the composition $(Ca_{1.75}Mn^{2+}_{0.25})(Al_{2.02}Mn^{3+}_{0.49}Fe^{3+}_{0.49})(O/OH/SiO_4/Si_2O_7)$ was found. This phase belongs to the piemontite-epidote series with a sursassite component of ~13 mol% (similar to the chemical data of piemontite described by Reinecke 1991). In the tourmaline sample from the Saxony Ore Mountains a kyanite inclusion (~3 μm in length) was identified.

6.4 EXPERIMENTAL DETAILS

6.4.1 Sample selection

Tourmaline samples from the UHP units in the Western Alps (Lago di Cignana and Dora Maira) and from the Saxony Ore Mountains were separated. A ~5 cm piece of the piemontite- and talc-bearing garnet-phengite-coesite-schist (investigated and described by Reinecke 1998) from Lago di Cignana was crushed and reddish tourmaline crystals were hand-picked under the microscope. After optical inspections the clearest fragment (sample Laci) ~0.15 x 0.20 x 0.24 mm in dimension was used for single-crystal structure refinements and subsequent for chemical analyses. Similar tourmalines from this locality contain coesite inclusions (Reinecke 1991). Another fragment from the Dora Maira locality (sample Domai; 0.12 x 0.15 x 0.25 mm) of an idiomorphic, very pale brown tourmaline, included in a small pyrope crystal (~1 cm) was separated. The pyrope in this sample also contains coesite (Schreyer 1985; Schertl et al. 1991). A third fragment from the Saxony Ore Mountains (sample R6b; 0.15 x 0.22 x 0.22 mm) was separated of the coesite-bearing mantle (Marschall et al. 2009) of a macroscopically black tourmaline crystal.

6.4.2 Crystal structure refinements

Two tourmaline fragments from the Western Alps (samples R6b and Domai) and the idiomorphic reddish tourmaline crystal from Lago di Cignana (sample Laci) were mounted on a Kappa APEX II CCD X-ray-single crystal-diffractometer from Bruker AXS equipped with graphite-monochromatic Mo $K\alpha$ radiation (Universität Wien). Data were collected at room temperature with six-fold redundancy (up to 80° 2θ), were integrated and corrected for Lorentz and polarization factors and absorption correction by evaluation of multiscans. The structure was refined with SHELXL-97 (Sheldrick 1997) using scattering factors for neutral atoms and a tourmaline starting model from Ertl et al. (2006). The H atom bonded to the O3 atom was located from a difference-Fourier map and subsequently refined. Refinement was performed with anisotropic thermal parameters for all non-hydrogen atoms. Site occupancies were refined according to well-known characteristics of the tourmaline structure (Na was refined at the X site, Mg and Fe were refined at the Y site; for other details see Table 2; the correlation coefficients do not show significant correlations in the refinement, *e.g.,* between site occupancy and overall scale factor). The refinement converged at a $R1(F)$ values of

1.3-2.0 %. Table 1 provides crystal data and details of the structure refinement. In Table 2, the atomic parameters are listed, and in Table 3 selected interatomic distances are presented.

6.4.3 Chemical analyses

The three single crystals which were used for the crystal structure determination were subsequently analyzed with a Cameca SX-100 electron microprobe (EMP) at the Department of Lithospheric Research, Geozentrum, Universität Wien, Austria, equipped with four wavelength-dispersive spectrometers (Table 4). We used the following (natural and synthetic) standards and X-ray lines for calibration: albite (Na*K*α), olivine (Mg*K*α, Si*K*α, Fe*K*α), almandine (Al*K*α), rutile (Ti*K*α), orthoclase (K*K*α), wollastonite (Ca*K*α), spessartine (Mn*K*α), gahnite (Zn*K*α), NiO (Ni*K*α) and apatite-(CaF) (F*K*α). Matrix corrections were performed using the PAP correction procedure provided by the latest Cameca's PeakSight version 4.0 software. An accelerating voltage of 20 keV and a beam current of 20 nA were used for all elements except for F (10 keV/20 nA). The method of peak to background ratio with counting time 20 seconds on peak position and 10 seconds on each background position peak position were used. A defocused beam with 5 μm in diameter was used. Under the described conditions, analytical errors are ±2% relative for major elements and ±5% relative for minor elements. All investigated tourmaline fragments were very homogeneous as indicated by low standard deviations (Tab. 4).

6.5 RESULTS

Crystal structures. The general structural formula of tourmaline is given by Hawthorne and Henry (1999) as $XY_3Z_6(BO_3)_3(T_6O_{18})V_3W$, where the V and W sites are anion sites. In the following section the occupation of the different sites is discussed.

X-site occupancy. In all samples the X site is occupied mainly by Na (0.84-0.90 apfu; Table 4), by small amounts of Ca (0.02-0.09 apfu), and by minor amounts of K (0.01-0.02 apfu). X-site vacancies are 0.04-0.10 pfu.

Y-site occupancy. The Y site is predominantly occupied by Mg in samples Domai and Laci, but they also contain significant amounts of ^{Y}Al. Only sample R6b has Al dominant at the Y site, as indicated by the relatively low <Y-O> distance of 2.010 Å (Table 3). The other samples (Domai and Laci) have larger <Y-O> distances with 2.023-2.027 Å indicative of significant amounts of (Mg + Fe^2) at the Y site (Table 3). Different samples contain variable amounts of Fe^{2+} at the Y site, 0.12-1.23 apfu (Table 4). Although no Mössbauer spectroscopy was performed on these samples, the very pale brown color of the tourmaline from Dora Maira and on the deep brown color (using a thicksection) of the mantle zone of the investigated tourmaline from the Saxony Ore Mountains, which can be explained by intervalence charge transfer of Fe^{2+}-Ti^{4+} (Rossman 2008), a significant percentage of Fe^{3+} in these samples is not likely. Only sample Laci contains a significant amount of Mn^{2+} (0.06 apfu). This sample may also contain some Mn in the valence state 3+, as indicated by the reddish color (Reinitz and Rossman 1988; Ertl et al. 2003b). All samples show small amounts of Ti^{4+} (0.02-0.11 apfu).

Samples Laci and R6b show have minor amounts of Zn (ZnO: 0.06-0.09 wt%; Table 4). Only tourmaline sample Laci shows a significant amount of Ni (NiO: 0.15 wt%; Table 4). This is not surprising because associated minerals (phlogopite and clinochlore) from these oceanic sediments show also some Ni (0.07-0.18 wt% NiO; Reinecke 1991).

Z-site occupancy. Because of enlarged <Z-O> bond-length distances (relative to tourmalines with only Al at the Z site, having <Z-O> distances of 1.906±0.004 Å; Donnay and Barton 1972; Burns et al. 1994; Hughes et al. 2000; Ertl et al. 2003b, 2005, 2006, 2008b) some Al will be substituted by ions with a larger ionic radius. Releasing the Z-site occupancy of the structure refinements did not give an evidence for a substitution of Al by Fe, because the occupancy (within a 3σ error) did show only Al (and Mg) at the Z site. However, it cannot be excluded that a small amount of Fe (≤0.10 apfu) occupies the Z site. Considering the results of crystal chemical investigations on the schorl-dravite series by Bloodaxe et al. (1999) and Bosi and Lucchesi (2004) and based on the <Z-O> distances (1.626-1.629 Å; Table 3), 0.9-1.0 apfu Mg was assigned to the Z site of the investigated samples.

T-site occupancy. Although B was not measured directly, there is no compelling evidence for a substitution of Si by B (within a 3σ error) on the T site. The <T-O> distances (~1.620 Å, Table 3) for all samples, give no indication for a significant (>2 atom% Al) substitution of Si by Al or B (Foit and Rosenberg 1979; McDonald and Hawthorne 1995; Ertl et al. 1997, 2001, 2005, 2006, 2008b). Small amounts of Al (≤0.04 apfu), which were assigned to the T site, are possibly a result of uncertainty in the chemical analyses or normalization procedures (Table 4), and are not proven by single crystal X-ray data.

V-site and W-site occupation. Ertl et al. (2002) showed that the bond-angle distortion (σ_{oct}^2) of the ZO_6 octahedron in a tourmaline is largely a function of the <Y-O> distance of that tourmaline, although the V-site occupant also affects that distortion. The covariance, *r*, of <Y-O> and the σ_{oct}^2 of the ZO_6 octahedron is -0.99 for all investigated tourmalines of Ertl et al. (2002) that are occupied by 3 (OH) groups, including the samples from Hughes et al. (2004). The investigated UHP-tourmaline samples don't show a significant deviation of the V site = 3 (OH) line in figure 3 from Ertl et al. (2002). It is, however, only possible to get a semi-quantitative estimation of the OH content of the O3 site by using this relationship. Hence, it can be assumed that the V site in all investigated samples is filled by ~3.0 (OH). The W site of the investigated tourmalines is occupied by low to moderate F contents (0.10-0.35 apfu; Table 4). H_2O data are available for tourmaline from the Saxony Ore Mountains (sample R6b) (SIMS data from a similar sample from Marschall et al. 2008). Therefore, the complete W site occupancy is estimated to be~$[O_{0.8}F_{0.1}(OH)_{0.1}]$. For the other samples, which exhibit higher F contents, in absence of H_2O data, the OH content was calculated as 4 – F = OH. The good total sums (of the chemical data in Table 4) by using these calculated H_2O contents are an indication that these values could be a good approximation to the actual OH contents.

Because the <T-O> distance is ~1.620 Å for all samples (Table 5), which is a typical bond-length for tourmalines where the T site is almost completely occupied by Si (MacDonald & Hawthorne 1995; Bloodaxe et al. 1999; Ertl et al. 2001; Bosi and Lucchesi 2004, average value for all

samples with Si ≥ 5.95 apfu), the formulae were calculated by assuming B = 3 apfu and on the basis of (O, OH, F) = 31 (Table 4):

Domai: $^{X}(Na_{0.90}Ca_{0.05}K_{0.01}\square_{0.04})$ $^{Y}(Mg_{1.78}Al_{0.99}Fe^{2+}_{0.12}Ti^{4+}_{0.03}\square_{0.08})$ $^{Z}(Al_{5.10}Mg_{0.90})$ $(BO_3)_3$ $^{T}Si_{6.00}O_{18}$ $^{V}(OH)_3$ $^{W}[(OH)_{0.72}F_{0.28}]$

Laci: $^{X}(Na_{0.84}Ca_{0.09}K_{0.01}\square_{0.06})$ $^{Y}(Mg_{1.64}Al_{0.79}Fe^{2+}_{0.48}Mn^{2+}_{0.06}Ti^{4+}_{0.02}Ni_{0.02}Zn_{0.01})$ $^{Z}(Al_{5.00}Mg_{1.00})$ $(BO_3)_3$ $^{T}(Si_{5.98}Al_{0.02})O_{18}$ $^{V}(OH)_3$ $^{W}[(OH)_{0.65}F_{0.35}]$

R6b: $^{X}(Na_{0.86}Ca_{0.02}K_{0.02}\square_{0.10})$ $^{Y}(Al_{1.63}Fe^{2+}_{1.23}Ti^{4+}_{0.11}Mg_{0.03}Zn_{0.01})$ $^{Z}(Al_{5.05}Mg_{0.95})$ $(BO_3)_3$ $^{T}(Si_{5.96}Al_{0.04})O_{18}$ $^{V}(OH)_3$ $^{W}[O_{0.81}F_{0.10}(OH)_{0.09}]$

6.6 DISCUSSION

There is a very good negative correlation (r^2 = 0.99) between the average charge of the X-site occupants and the F content of the investigated UHP tourmalines (Fig. 3). Henry (2000) found a strong negative correlation between the X-site vacancy and the F content in all generations of magmatic to hydrothermal tourmaline from the Cruzeiro Mine, Minas Gerais, Brazil. Henry (2005) showed in an evaluation of ~600 chemical analyses of different tourmaline varieties that tourmalines with more than 0.5 *X*-site vacancies there is little or no F present in the tourmaline. Both relations, using the X-site vacancies orusing the average charge of the X-site occupants are very similar, but the latter approach might be more advantageous.

Henry and Dutrow (1996) pointed out that in metamorphic tourmalines from metapelitic rocks and metaquartzites the X-site vacancies decrease from 0.6±0.2 to 0.3±0.05 as temperature decreases from 200°C to 650°C and then futher decrease to 0.05±0.05 above 750°C. In the UHP tourmalines the X-site charges are negatively correlated with temperature of tourmaline formation (r^2 = 0.92; Fig. 4). A possible explanation might be a different trend of the T-site occupation in UHP tourmalines relative to low-medium pressure tourmalines. While Henry and Dutrow (1996) found that in (diagenetic to high grade) metamorphic tourmalines (from metapelitic rocks and metaquartzites) there is little or no $^{[4]}$Al below 450°C, it increases progressively up to an average of 0.25 $^{[4]}$Al apfu above 750°C. In the investigated UHP tourmalines which crystallized at temperatures up to ~870°C there are no indications for significant $^{[4]}$Al contents. A substitution of Si by Al would increase the tetrahedral site size. At UHP conditions it is likely that this substitution would not be favored, even at relatively high temperatures. Because F is coupled with the average charge of the X-site occupants (Fig. 3), the F content of the UHP tourmalines shows a good negative correlation (r^2 = 0.97) with the temperature of tourmaline formation (Fig. 5).

It is interesting that there is a very good correlation (r^2 = 1.00; Fig. 6) between the average charge of the X-site occupants and <Y-O> distances (Table 3). This can only be explained by an increasing $^{Y}Al^{3+}$ content (while <Y-O> distances decrease), which is essentially charge-balanced by decreasing local charge at the X site. There is also a high negative correlation (r^2 = 0.94) between the <Y-O>

distance and the temperature conditions of tourmaline formation (Fig. 7). This correlation can be explained by an increasing ^{Y}Al content (by simultaneously increasing temperature), as a result of significant Al-Mg disorder between the Y and Z sites. Hence, such a disorder is considered to be dependent on the temperature during crystallization. It is interesting to note that the black colored Fe-rich and Mg-bearing tourmaline from the Saxony Ore Mountains with the final formula $^{X}(Na_{0.86}Ca_{0.02}K_{0.02}\square_{0.10})$ $^{Y}(Al_{1.63}Fe^{2+}_{1.23}Ti^{4+}_{0.11}Mg_{0.03}Zn_{0.01})$ $^{Z}(Al_{5.05}Mg_{0.95})$ $(BO_3)_3$ $^{T}(Si_{5.96}Al_{0.04})O_{18}$ $^{V}(OH)_3$ $^{W}[O_{0.81}F_{0.10}(OH)_{0.09}]$ is Al dominant at the Y site.

There is an excellent positive correlation (r^2 = 0.99) between the $^{[6]}$Al content (Sum of Al at the Y and Z site) of the investigated UHP tourmalines and the temperature of tourmaline formation (Figs 8, 9). The increase of octahedral Al in the UHP tourmalines can be explained via the (simplified) exchange vector $^{[6]}AlOH(NaR^{2+}F)_{-1}$ (with R^{2+}: Fe^{2+}, Mn^{2+}, Mg), which is a modified version to the exchange vector suggested by Henry and Dutrow (1996) for diagenetic to high grade metamorphic tourmalines.

Because of the very limited localities with the occurrence of UHP tourmalines more extensive detailed studies are not currently possible. Consequently, to further elucidate the relations between metamorphic conditions and the crystal chemistry of tourmalines, efforts should be concentrated on diagenetic to high-grade metamorphic tourmalines from petrologic well characterized environments.

6.7 ACKNOWLEDGMENTS

Special thanks to A. Wagner, Vienna, Austria, for preparing the tourmaline samples and Olaf Medenbach for extracting pieces of the tourmaline from Dora Maira. This work was supported by Österreichischer Fonds zur Förderung der wissenschaftlichen Forschung (FWF) project no. P20509.

6.8 REFERENCES

Bebout, G.E. and Nakamura, E. (2003) Record in metamorphic tourmaline of subduction-zone devolatilization and boron cycling. Geology, 31, 407-410.

Bloodaxe, E.S., Hughes, J.M., Dyar, M.D., Grew, E.S., and Guidotti, C.V. (1999) Linking structure and chemistry in the schorl-dravite series. American Mineralogist, 84, 922-928.

Bohlen, S.R. and Boettcher, A.L. (1982) The quartz-coesite transformation: A pressure determination and the effects of other components. Journal of Geophysical Research, 87, 7073-7078.

Bosi, F. and Lucchesi, S. (2004) Crystal chemistry of the schorl-dravite series. European Journal of Mineralogy, 16, 335-344.

Bosi, F., Lucchesi, S., and Reznitskii, L. (2004) Crystal chemistry of the dravite–chromdravite series. European Journal of Mineralogy, 16, 345-352.

Bruker AXS Inc. (2001) SaintPlus. Bruker AXS Inc., Madison, Wisconsin, USA.

Bundy, F.P. (1980) The P,T phase and reaction diagram for elemental carbon. Journal of Geophysical Research, 88, 6930-6936.

Burns, P.C., MacDonald, D.J., and Hawthorne, F.C. (1994) The crystal chemistry of manganese-bearing elbaite. Canadian Mineralogist, 32, 31-41.

Deer, W.A., Howie, R.A., and Zussman, J. (1992) An introduction to the rock-forming minerals. 2nd edition, 712 pp. Longman Scientific & Technical, London.

Dobretsov, N.L., Sobolev, N.V., Shatsky, V.S., Coleman, R.G. and Ernst, W.G. (1995) Geotectonic evolution of diamondiferous paragneisses of the Kokchetav complex, Northern Kazakhstan - the geologic enigma of ultrahigh-pressure crustal rocks within Phanerozoic foldbelt. The Island Arc, 4, 267-279.

Donnay, G. and Barton, P. Jr. (1972) Refinement of the crystal structure of elbaite and the mechanism of tourmaline solid solution. Tschermaks Mineralogisch Petrographische Mitteilungen, 18, 273-286.

Dutrow, B. and Henry, D. J. (2000) Complexly zoned fibrous tourmaline, Cruzeiro mine, Minas Gerais, Brazil: A record of evolving magmatic and hydrothermal fluids.

Dutrow, B., Foster, C. T., Jr., and Henry, D. J. (1999) Tourmaline-rich pseudomorphs in sillimanite zone metapelites: Demarcation of an infiltration front. American Mineralogist, 84, 794-805

Ertl, A., Pertlik, F., and Bernhardt, H.-J. (1997) Investigations on olenite with excess boron from the Koralpe, Styria, Austria. Österreichische Akademie der Wissenschaften, Mathematisch-Naturwissenschaftliche Klasse, Abt. I, Anzeiger, 134, 3-10.

Ertl, A., Hughes, J.M., and Marler, B. (2001) Empirical formulae for the calculation of <*T*-O> and *X*-O2 bond lengths in tourmaline and relations to tetrahedrally-coordinated boron. Neues Jahrbuch Mineralogie Monatshefte, 12, 548-557.

Ertl, A., Hughes, J.M., Pertlik, F., Foit F.F. Jr., Wright, S.E., Brandstätter, F., and Marler, B. (2002) Polyhedron distortions in tourmaline. Canadian Mineralogist, 40, 153-162.

Ertl, A., Hughes, J.M., Brandstätter, F., Dyar, M.D., and Prasad, P.S.R. (2003a): Disordered Mg-bearing olenite from a granitic pegmatite from Goslarn, Austria: A chemical, structural, and infrared spectroscopic study. Canadian Mineralogist, 41, 1363-1370.

Ertl, A., Hughes, J.M., Prowatke, S., Rossman, G.R., London, D., and Fritz, E.A. (2003b): Mn-rich tourmaline from Austria: structure, chemistry, optical spectra, and relations to synthetic solid solutions. American Mineralogist, 88, 1369-1376.

Ertl, A., Rossman, G.R., Hughes, J.M., Prowatke, S., and Ludwig, T. (2005) Mn-bearing "oxy-rossmanite" with tetrahedrally-coordinated Al and B from Austria: structure, chemistry, and infrared and optical spectroscopic study. American Mineralogist, 90, 481-487.

Ertl, A., Hughes, J.M., Prowatke, S., Ludwig, T., Prasad, P.S.R., Brandstätter, F., Körner, W., Schuster, R., Pertlik, F., and Marschall, H. (2006) Tetrahedrally-coordinated boron in tourmalines from the liddicoatite-elbaite series from Madagascar: Structure, chemistry, and infrared spectroscopic studies. American Mineralogist, 91, 1847-1856.

Ertl, A., Rossman, G.R., Hughes, J.M., Ma, C., and Brandstätter, F. (2008a) V^{3+}-bearing, Mg-rich, strongly disordered olenite from a graphite deposit near Amstall, Lower Austria: A structural, chemical and spectroscopic investigation. Neues Jahrbuch Mineralogie Abhandlungen, 184, 243-253.

Ertl, A., Tillmanns, E., Ntaflos, T., Francis, C., Giester, G., Körner, W., Hughes, J.M., Lengauer, C., and Prem, M. (2008b) Tetrahedrally coordinated boron in Al-rich tourmaline and its relationship to the pressure–temperature conditions of formation. European Journal of Mineralogy, 20, 881-888.

Foit, F.F. and Rosenberg, P.E. (1979) The structure of vanadium-bearing tourmaline and its implications regarding tourmaline solid solutions. American Mineralogist, 64, 788-798.

Grice, J.D. and Ercit, T.S. (1993) Ordering of Fe and Mg in the tourmaline crystal structure: the correct formula. Neues Jahrbuch Mineralogie Abhandlungen, 165, 245-266.

Hawthorne, F.C. (2002) Bond-valence constraints on the chemical composition of tourmaline. Canadian Mineralogist, 40, 789-797.

Hawthorne, F.C. and Henry, D.J. (1999) Classification of the minerals of the tourmaline group. European Journal of Mineralogy, 11, 201-215.

Hawthorne, F.C., MacDonald, D.J., and Burns, P.C. (1993) Reassignment of cation site-occupancies in tourmaline: Al-Mg disorder in the crystal structure of dravite. American Mineralogist, 78, 265-270.

Henry, D.J. (2005) Fluorine – X-site vacancy avoidance in natural tourmaline: internal vs. external control. 2005 Goldschmidt Conference, May 20-25, Moscow, Idaho, USA, Abstracts Volume, abstract no. 1318.

Henry, D.J. and Dutrow, B. (1996) Metamorphic tourmaline and its petrologic applications. In E.S. Grew and L.M. Anovitz, Eds., Boron: Mineralogy, Petrology, and Geochemistry. Reviews in

Mineralogy and Geochemistry, 33, 503-557. Mineralogical Society of America, Washington, D.C.

Henry, D.J. and Dutrow, B.L. (1992) Tourmaline in a low grade clastic metasedimentary rocks: an example of the petrogenetic potential of tourmaline: Contributions to Mineralogy and Petrology, 112, 203-218.

Henry, D.J. and Guidotti, C.V. (1985) Tourmaline in the staurolite grade metapelites of NW Maine: a petrogenetic indicator mineral. American Mineralogist, 70, 1-15.

Henry, D.J., Kirkland, B.L., and Kirkland, D.W. (1999) Sector-zoned tourmaline from the cap rock of a salt dome. European Journal of Mineralogy, 11, 263-280.

Henry, D. J., Sun, H., Slack, J., and Dutrow, B. L. (2008) Tourmaline in meta-evaporites and highly magnesian rocks: perspectives from Namibian tourmalinites. European Journal of Mineralogy, 20, 973-993.

Hermann, J. (2003) Experimental evidence for diamond-facies metamorphism in the Dora-Maira massif. Lithos, 70, 163-182.

Hughes, J.M., Ertl, A., Dyar, M.D., Grew, E.S., Shearer, C.K., Yates, M.G., and Guidotti, C.V. (2000) Tetrahedrally coordinated boron in a tourmaline: boron-rich olenite from Stoffhütte, Koralpe, Austria. Canadian Mineralogist, 38, 861-868.

Hughes, J.M., Ertl, A., Dyar, M.D., Grew, E.S., Wiedenbeck, M., and Brandstätter, F. (2004) Structural and chemical response to varying $^{[4]}$B content in zoned Fe-bearing olenite from Koralpe, Austria. American Mineralogist, 89, 447-454.

Krosse, S. (1995) Hochdrucksynthese, Stabilität und Eigenschaften der Borsilikate Dravit und Kornerupin sowie Darstellung und Stabilitätsverhalten eines neuen Mg-Al-Borates. Dr. rer. nat. thesis, Ruhr-Universität Bochum, Germany.

MacDonald, D.J. and Hawthorne, F.C. (1995) The crystal chemistry of Si $\Leftrightarrow$ Al substitution in tourmaline. Canadian Mineralogist, 33, 849-858.

Manning, D.A.C. and Pichavant, M. (1983) The role of fluorine and boron in the generation of granitic melts. In: Atherton, M.P. and Gribble, C.D. (eds.) Migmatites, Melting and Metamorphism, chapter 7, 94-109, Shiva Publications, Cheshire.

Marschall, H.R., Ertl, A., Hughes, J.M., and McCammon, C. (2004) Metamorphic Na- and OH-rich disordered dravite with tetrahedral boron, associated with omphacite, from Syros, Greece: chemistry and structure. European Journal of Mineralogy, 16, 817-823.

Marschall, H.R., Korsakov, A.V., Luvizotto, G.L., Nasdala, L., and Ludwig, T. (2009) On the occurrence and boron isotopic composition of tourmaline in (ultra)high-pressure metamorphic rocks. Journal of the Geological Society, (in press).

Massonne, H.J. (2003) A comparison of the evolution of diamondiferous quartz-rich rocks from the Saxonian Erzgebirge and the Kokchetav massif: are so-called diamondiferous gneisses magmatic rocks? Earth and Planetary Science Letters, 216, 347-364.

Massonne, H.J., Kennedy, A., Nasdala, L., and Theye, T. (2007) Dating of zircon and monazite from diamondiferous quartzofeldspathic rocks of the Saxonian Erzgebirge – hints at burial and exhumation velocities. Mineralogical Magazine, 71, 407-425.

Ota, T., Kobayashi, K., Katsura, T., and Nakamura, E. (2008) Tourmaline breakdown in a pelitic system: implications for boron cycling through subduction zones. Contributions to Mineralogy and Petrology, 155, 19-32.

Reinecke, T. (1991) Very-high-pressure metamorphism and uplift of coesite-bearing metasediments from the Zermatt-Saas zone, Western Alps. European Journal of Mineralogy, 3, 7-17.

Reinecke, T. (1998) Prograde high- to ultrahigh-pressure metamorphism and exhumation of oceanic sediments at Lago di Cignana, Zermatt-Saas Zone, western Alps. Lithos, 42, 147-189.

Reinitz, I.L. and Rossman, G.R. (1988) Role of natural radiation in tourmaline coloration. American Mineralogist, 73, 822-825.

Robbins, C.R. and Yoder, H.S., Jr. (1962) Stability relations of dravite, a tourmaline. Carnegie Institution of Washington Ybk, 61, 106-108.

Rossman, G.R. (2008) Colors in minerals caused by Intervalence Charge Transfer (IVCT). http://minerals.gps.caltech.edu/COLOR_Causes/IVCT/Index.htm (Dec. 18th, 2008).

Rötzler, K., Schumacher, R., Maresch, W.V. and Willner, A.P. (1998) Characterization and geodynamic implications of contrasting metamorphic evolution in juxtaposed high-pressure units of the western Erzgebirge (Saxony, Germany). European Journal of Mineralogy, 10, 261-280.

Schmädicke, E. and Müller, W.F. (2000) Unusual exsolution phenomena in omphacite and partial replacement of phengite by phlogopite plus kyanite in an eclogite from the Erzgebirge. Contributions to Mineralogy and Petrology, 139, 629-642.

Schertl, H.P., Schreyer, W., and Chopin, C. (1991) The pyrope-coesite rocks and their country rocks at Parigi, Dora Maira Massif,Western Alps: detailed petrography, mineral chemistry and $P - T$ path. Contribution to Mineralogy and Petrology, 108, 1-21.

Schreyer, W. (1985) Metamorphism of crustal rocks at mantle depth: high pressure minerals and mineral assemblages in metapelites. Fortschritte der Mineralogie, 63, 227-261.

Sheldrick, G.M. (1997) SHELXL-97, a program for crystal structure refinement. University of Göttingen, Germany.

Slack, J. F. (1996) Tourmaline associations with hydrothermal ore deposits. In: Grew, E. S. and Anovitz, L. M. (editors) Boron: Mineralogy, Petrology and Geochemistry. MSA Reviews in Mineralogy, 33, 559-644.

Taylor, M.C., Cooper, M.A., and Hawthorne, F.C. (1995) Local charge-compensation in hydroxyl-deficient uvite. Canadian Mineralogist, 33, 1215-1221.

Thomson, J.A. (2006) A rare garnet-tourmaline-sillimanite-biotite-ilmenite-quartz assemblage form the granulite facies of south-central Massachusetts. American Mineralogist, 91, 1730-1738.

van Hinsberg, V.J. and Schumacher, J.C. (2007) Intersector element partitioning in tourmaline: a potentially powerful single crystal thermometer. Contributions to Mineralogy and Petrology, 153(3), 289-301.

von Goerne, G., Franz, G., and Heinrich, W. (2001) Synthesis of tourmaline solid solutions in the system Na_2O-MgO-Al_2O_3-SiO_2-B_2O_3-H_2O-HCl and the distribution of Na between tourmaline and fluid at 300 to 700 °C and 200 MPa. Contributions to Mineralogy and Petrology, 141, 160-173.

Werding, G. and Schreyer, W. (2002) Experimental studies on borosilicates and selected borates. In: Grew, E.S. and Anovitz, L.M. (eds.) Boron: mineralogy, petrology and geochemistry. Reviews in Mineralogy, 33, 117-163, Mineralogical Society of America, 2nd edition.

Willner, A.P., Rötzler, K. and Maresch, W.V. (1997) Pressure-temperature and fluid evolution of quartzo-feldspathic metamorphic rocks with a relic high-pressure, granulite-facies history from the Central Erzgebirge (Saxony, Germany). Journal of Petrology, 38, 307-336.

Table 1. Crystal data, data collection information and refinement details for UHP tourmalines.

Sample	R6b	Domai	Laci
a, c (Å)	15.929(1), 7.183(1)	15.935(1), 7.201(1)	15.945(1), 7.210(1)
V (Å^3)	1578.4(4)	1583.5(4)	1587.5(4)
Crystal dimensions (mm)	0.15 x 0.22 x 0.22	0.12 x 0.15 x 0.25	0.15 x 0.20 x 0.24
Collection mode, $2\theta_{max}$ (°)	full sphere, 91.40	full sphere, 90.78	full sphere, 87.93
h, k, l ranges	-31/32, -30/31, -13/14	-31/30, -30/31, -14/13	-31/31, -31/30, -13/13
Total reflections measured	43951	42893	43361
Unique reflections	3139 (R_{int} 1.86%)	3026 (R_{int} 2.93%)	2935 (R_{int} 2.09%)
$R_1(F)$, $wR_2(F^2)$	1.31%, 3.55%	2.01%, 4.41%	1.36%, 3.45%
Flack *x* parameter	0.058(21)	0.053(48)	0.040(18)
'Observed' refls. [$F_o > 4\sigma_{(Fo)}$]	3098	2803	2884
Extinct. coefficient	0.00371(15)	0.00371(13)	0.00371(12)
No. of refined parameters	95	95	95
GooF	0.831	0.949	0.819
$\Delta\sigma_{min}$, $\Delta\sigma_{max}$ (e/Å^3)	-0.36, 0.47	-0.41, 0.49	-0.28, 0.36

TABLE 2. Table of atom parameters in UHP tourmalines.

Site	*Sample*	*x*	*y*	*z*	U_{eq}	*Occ.*
X	R6b	0	0	0.2250(2)	0.0219(3)	$Na_{0.91(1)}$
	Domai	0	0	0.2396(2)	0.0214(3)	$Na_{1.02(1)}$
	Laci	0	0	0.2325(1)	0.0204(2)	$Na_{1.00(1)}$
Y	R6b	0.12241(1)	1/2x	0.63418(3)	0.00765(4)	$Mg_{0.609(1)}Fe_{0.391}$
	Domai	0.12571(3)	1/2x	0.63044(5)	0.0081(2)	$Mg_{0.933(1)}Fe_{0.067}$
	Laci	0.12426(2)	1/2x	0.63250(3)	0.00810(6)	$Mg_{0.808(1)}Fe_{0.192}$
Z	R6b	0.29781(1)	0.26128(1)	0.60853(2)	0.00541(4)	$Al_{1.00}$
	Domai	0.29806(2)	0.26164(2)	0.61163(3)	0.00622(4)	$Al_{1.00}$
	Laci	0.29802(1)	0.26159(1)	0.61070(2)	0.00545(3)	$Al_{1.00}$
B	R6b	0.10999(3)	2x	0.4526(1)	0.0068(1)	$B_{1.00}$
	Domai	0.10979(4)	2x	0.4546(2)	0.0069(1)	$B_{1.00}$
	Laci	0.10987(3)	2x	0.4536(1)	0.0065(2)	$B_{1.00}$
T	R6b	0.19157(1)	0.18968(1)	-0.00115(2)	0.00525(3)	$Si_{1.00}$
	Domai	0.19191(1)	0.19000(1)	-0.00089(3)	0.00548(3)	$Si_{1.00}$
	Laci	0.19175(1)	0.18990(1)	-0.00135(2)	0.00520(3)	$Si_{1.00}$
H3	R6b	0.252(2)	1/2x	0.397(4)	0.042(7)	$H_{1.00}$
	Domai	0.259(2)	1/2x	0.400(4)	0.049(9)	$H_{1.00}$
	Laci	0.256(2)	1/2x	0.400(3)	0.045(7)	$H_{1.00}$
O1	R6b	0	0	0.7708(2)	0.0224(4)	$O_{0.81(1)}F_{0.19}$
	Domai	0	0	0.7720(2)	0.0144(4)	$O_{0.68(1)}F_{0.32}$
	Laci	0	0	0.7712(2)	0.0135(2)	$O_{0.61(1)}F_{0.39}$
O2	R6b	0.06101(2)	2x	0.48628(9)	0.0130(1)	$O_{1.00}$
	Domai	0.06094(3)	2x	0.4848(1)	0.0111(1)	$O_{1.00}$
	Laci	0.06106(2)	2x	0.48347(9)	0.01023(9)	$O_{1.00}$

Site	*Sample*	*x*	*y*	*z*	U_{eq}	*Occ.*
O3	R6b	0.26269(7)	1/2x	0.50873(9)	0.0158(1)	$O_{1.00}$
	Domai	0.26529(8)	1/2x	0.5106(1)	0.0127(1)	$O_{1.00}$
	Laci	0.26510(6)	1/2x	0.50989(9)	0.0125(1)	$O_{1.00}$
O4	R6b	0.09338(3)	2x	0.07027(9)	0.01067(9)	$O_{1.00}$
	Domai	0.09305(3)	2x	0.0694(1)	0.0107(1)	$O_{1.00}$
	Laci	0.09310(3)	2x	0.06931(9)	0.01017(9)	$O_{1.00}$
O5	R6b	0.18558(5)	1/2x	0.09176(9)	0.01051(9)	$O_{1.00}$
	Domai	0.18401(7)	1/2x	0.0909(1)	0.0106(1)	$O_{1.00}$
	Laci	0.18433(5)	1/2x	0.09025(9)	0.01010(9)	$O_{1.00}$
O6	R6b	0.19525(3)	0.18501(3)	0.77532(6)	0.00927(6)	$O_{1.00}$
	Domai	0.19604(4)	0.18586(4)	0.77669(8)	0.00877(8)	$O_{1.00}$
	Laci	0.19581(3)	0.18592(3)	0.77662(6)	0.00840(6)	$O_{1.00}$
O7	R6b	0.28521(3)	0.28528(3)	0.07611(6)	0.00885(6)	$O_{1.00}$
	Domai	0.28501(4)	0.28490(4)	0.07900(8)	0.00867(8)	$O_{1.00}$
	Laci	0.28489(3)	0.28483(3)	0.07811(6)	0.00850(6)	$O_{1.00}$
O8	R6b	0.20931(3)	0.27011(3)	0.43816(7)	0.01020(6)	$O_{1.00}$
	Domai	0.20952(4)	0.27018(4)	0.44103(8)	0.00961(8)	$O_{1.00}$
	Laci	0.20927(3)	0.27006(3)	0.44018(6)	0.00962(6)	$O_{1.00}$

Note: Definition for U_{eq} see Fischer and Tillmanns (1988).

TABLE 3. Selected interatomic distances in tourmalines from the UHP tourmalines (Standard deviation in brackets).

	R6b	**Domai**	**Laci**
X-			
O2 x3	2.521(1)	2.439(1)	2.473(1)
O5 x3	2.733(1)	2.756(1)	2.7443(8)
O4 x3	2.8060(9)	2.846(1)	2.8278(8)
Mean	**2.687(1)**	**2.680(1)**	**2.682(1)**
Y-			
O1	1.9531(8)	2.0120(9)	1.9861(7)
O2 x2	1.9929(5)	2.0051(6)	2.0122(5)
O6 x2	1.9938(5)	2.0026(6)	2.0064(5)
O3	2.1348(9)	2.111(1)	2.1362(8)
Mean	**2.0102(6)**	**2.0231(7)**	**2.0266(6)**
Z-			
O6	1.8963(5)	1.8843(6)	1.8912(5)
O7	1.8987(5)	1.9031(6)	1.9055(5)
O8	1.8959(5)	1.8943(6)	1.8986(5)
O8’	1.9242(5)	1.9263(6)	1.9296(5)
O7’	1.9571(5)	1.9573(6)	1.9610(5)
O3	1.9880(4)	1.9885(5)	1.9893(4)
Mean	**1.9267(5)**	**1.9256(6)**	**1.9292(5)**
T-			
O7	1.6066(4)	1.6047(6)	1.6053(4)
O6	1.6097(5)	1.6057(6)	1.6046(5)
O4	1.6245(3)	1.6259(4)	1.6262(3)
O5	1.6400(3)	1.6414(4)	1.6414(3)
Mean	**1.6202(4)**	**1.6194(5)**	**1.6194(4)**
B-			
O2	1.373(1)	1.366(1)	1.365(1)
O8 (x2)	1.3740(6)	1.3797(8)	1.3760(6)
Mean	**1.374(1)**	**1.375(1)**	**1.372(1)**

TABLE 4. Composition of UHP tourmalines (wt%, standard deviation in brackets).

	R6b	Domai	Laci
SiO_2 wt.%	35.85(9)	37.40(13)	36.80(11)
TiO_2	0.87(1)	0.21(4)	0.13(2)
B_2O_3[1]	10.46	10.85	10.70
Al_2O_3	34.32(6)	32.23(18)	30.35(17)
Cr_2O_3	0.01(1)	b. d.	0.02(1)
FeO	8.87(7)	0.91(4)	3.55(12)
MnO	0.02(1)	b. d.	0.42(14)
MgO	3.96(4)	11.21(15)	10.92(7)
ZnO	0.09(1)	b. d.	0.06(1)
NiO	b. d.	b. d.	0.15(1)
CaO	0.12(1)	0.29(3)	0.50(3)
Na_2O	2.67(5)	2.90(5)	2.68(4)
K_2O	0.08(1)	0.05(1)	0.05(1)
H_2O[2]	2.79*	3.48	3.37
F	0.20(2)	0.55(7)	0.67(9)
O≡F	-0.08	-0.23	-0.28
Sum	100.23	99.85	100.09
Si *apfu*	5.96	6.00	5.98
$^{[4]}$Al	0.04	-	0.02
Sum T site	6.00	6.00	6.00
$^{[3]}$B	3.00	3.00	3.00
Al	6.68	6.09	5.79
Fe^{2+}	1.23	0.12	0.48
Mn^{2+}	-	-	0.06
Mg	0.98	2.68	2.64
Ti^{4+}	0.11	0.03	0.02
Zn	0.01	-	0.01
Ni	-	-	0.02
Sum Y, Z sites	9.01	8.92	9.02
Ca	0.02	0.05	0.09
Na	0.86	0.90	0.84
K	0.02	0.01	0.01
□	0.10	0.04	0.06
Sum X site	1.00	1.00	1.00
Sum cations	18.91	18.88	18.96
OH	3.09	3.72	3.65
F	0.10	0.28	0.35
Sum OH + F	3.19	4.00	4.00

Note: Average of 6 EMP analyses for R6b, 8 EMP analyses for Domai and 15 EMP analyses for Laci. [1]B_2O_3 calculated as B = 3.00 apfu (see text). [2]H_2O content was calculated as OH + F = 4 pfu, except for sample R6b: *H_2O SIMS data from Marschall et al. (2008). Total Mn and Fe calculated as MnO and FeO. Cl is below the detection limit in all samples. A component is not considered significant unless its value exceeds the uncertainty. B. d.: below detection limit.

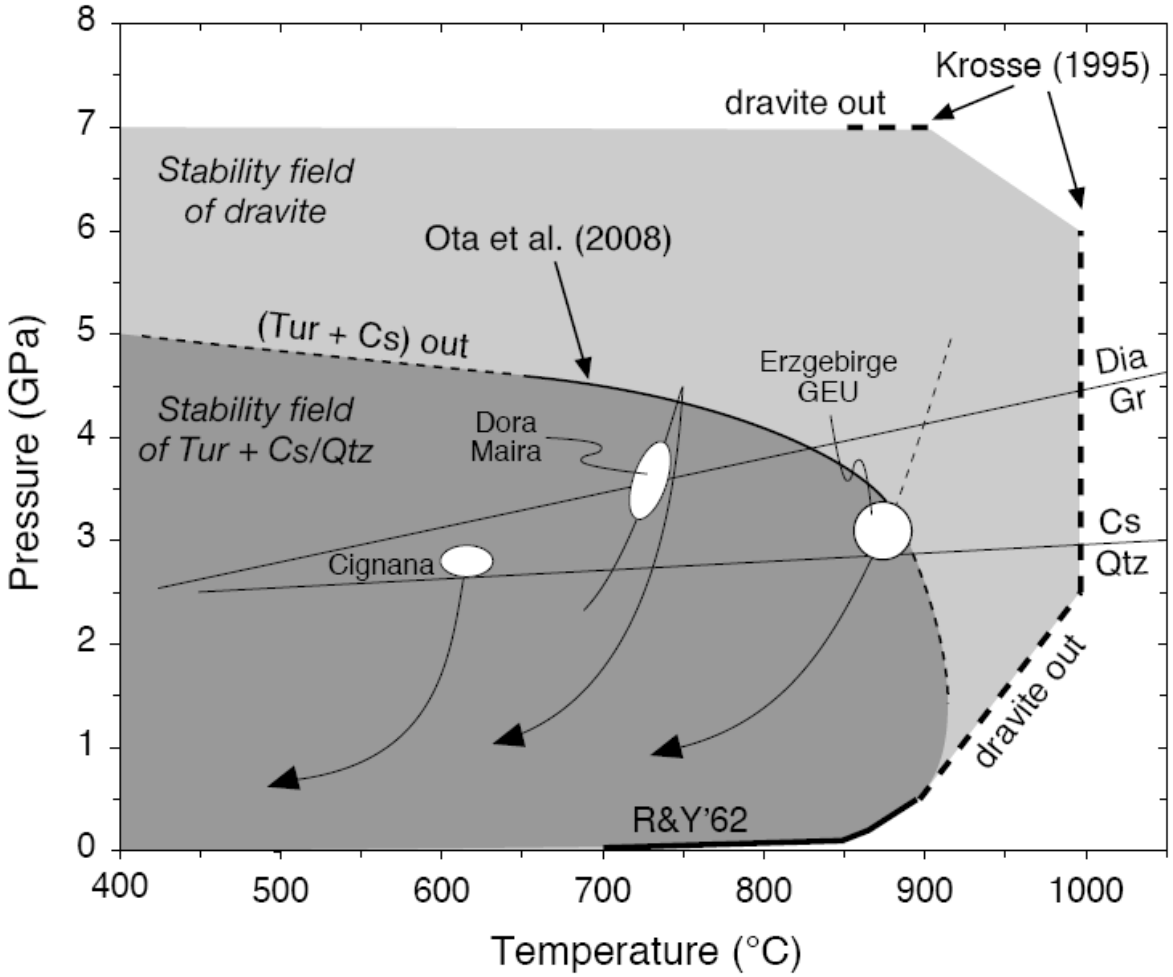

FIGURE 1. *PT* diagram showing (1) the experimentally determined stability of dravitic tourmaline (light grey field) (Robbins and Yoder 1962; Krosse 1995; Werding and Schreyer 2002) and tourmaline + coesite/quartz (dark grey field) (Ota et al. 2008), and (2) peak metamorphic conditions of the different tourmaline-bearing UHP rocks (from which the tourmalines were investigated) with most likely conditions of tourmaline formation marked by white ellipses: Diamond- and coesite-bearing gneisses from the Gneiss-Eclogite Unit (GEU) of the Saxony Ore Mountains, Germany (Schmädicke and Müller 2000; Massonne 2003; Massonne et al. 2007); Coesite-pyrope-kyanite quartzite from the Dora Maira massif, Western Alps, Italy (Schreyer 1985; Schertl et al. 1991); Coesite-bearing metasediments from Lago di Cignana, Western Alps, Italy (Reinecke 1991, 1998; Bebout and Nakamura 2003). Equilibria of quartz-coesite after Bohlen and Boettcher (1982) and graphite-diamond after Bundy (1980).

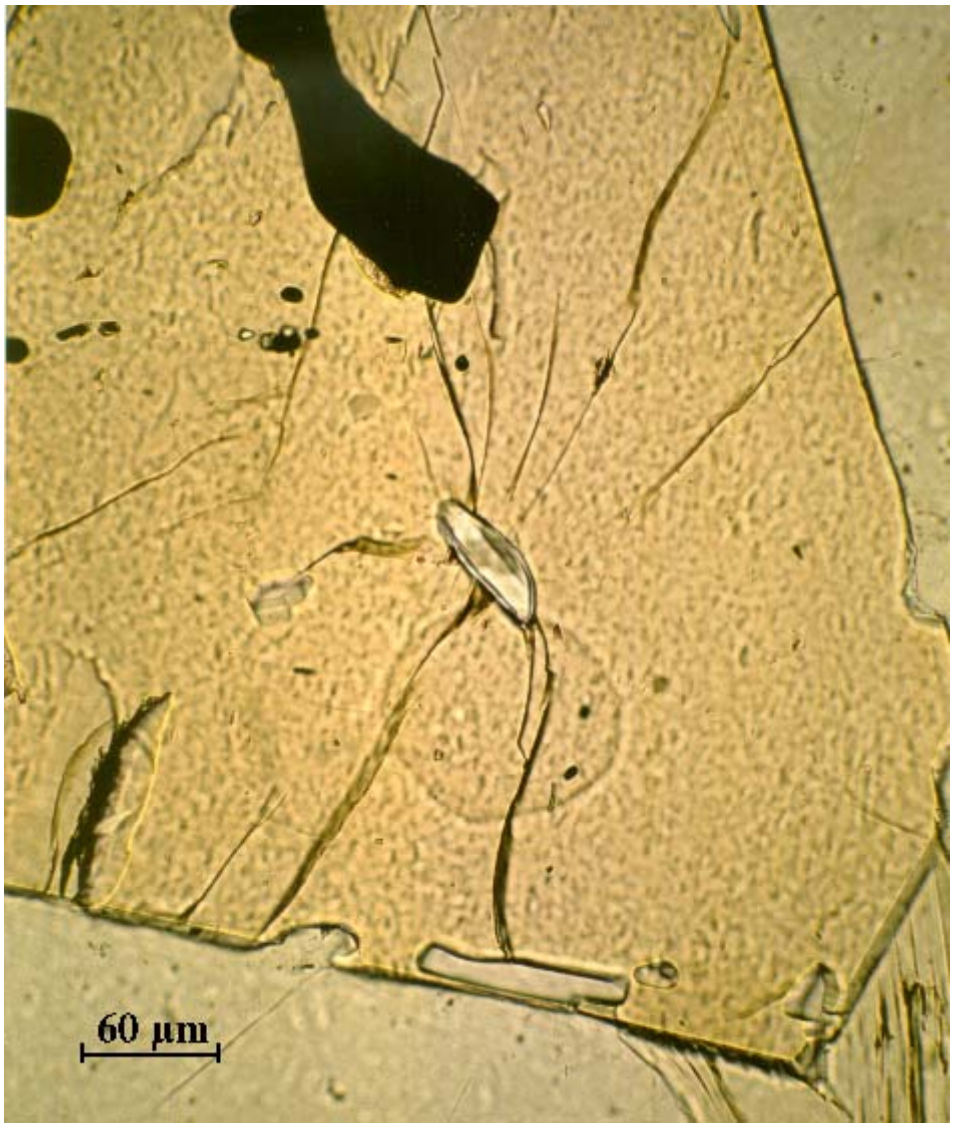

FIGURE 2. Relic coesite inclusion (confirmed by Raman spectroscopy; Reinecke 1991) in an idiomorphic tourmaline crystal from Lago di Cignana, Western Alps, Italy.

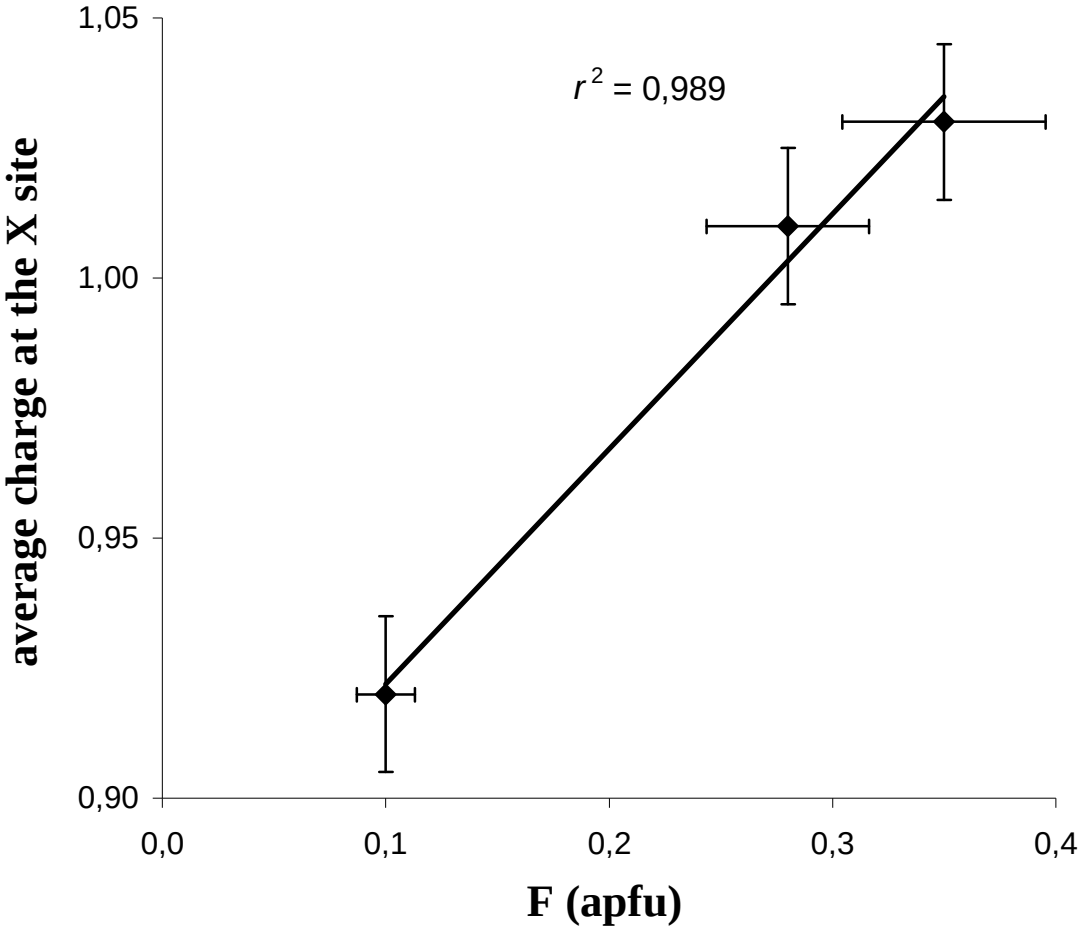

FIGURE 3. Relationship between the average charge of the X-site occupants and the F content of the investigated UHP tourmalines (EMPA data from Table 4). Bars: average estimated standard deviation (±1σ).

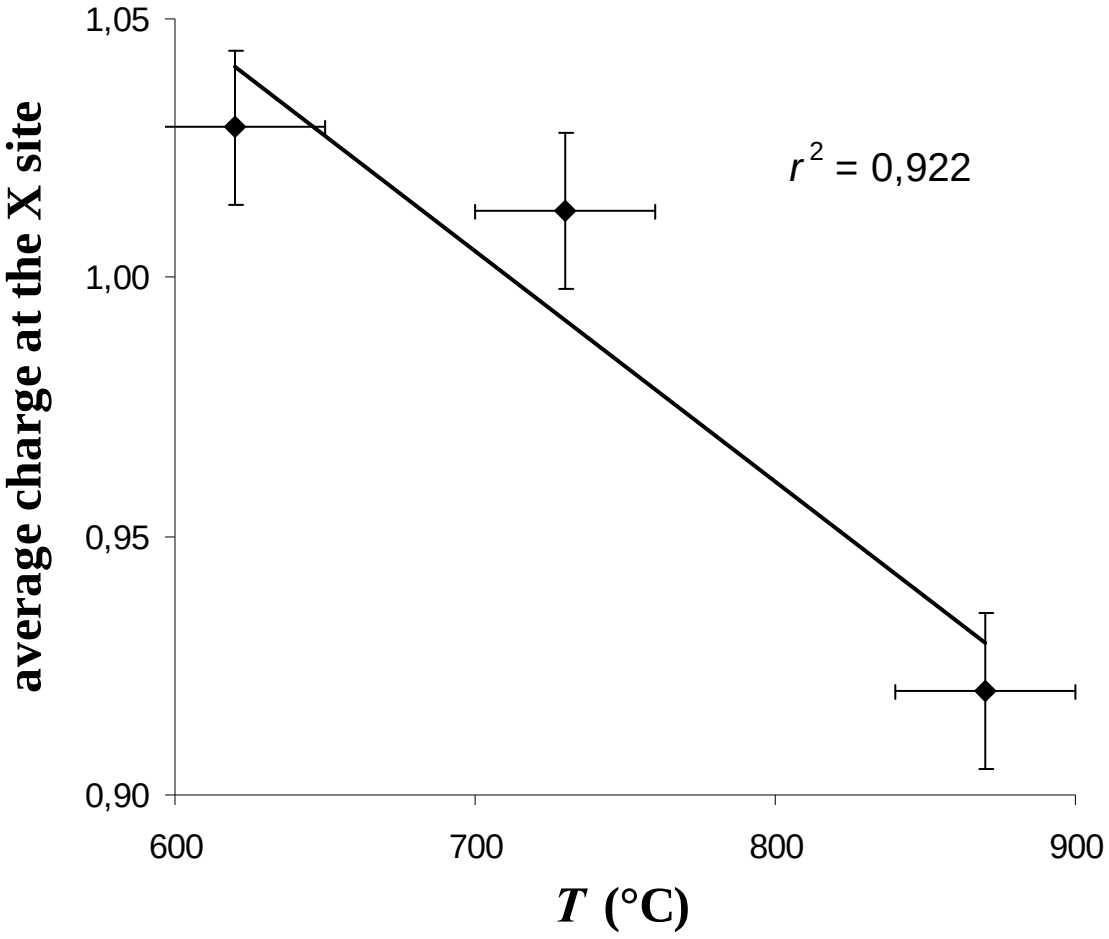

FIGURE 4. Relationship between the average charge of the X-site occupants of the investigated UHP tourmalines and the temperature conditions of tourmaline formation. Bars: average estimated standard deviation (±1σ).

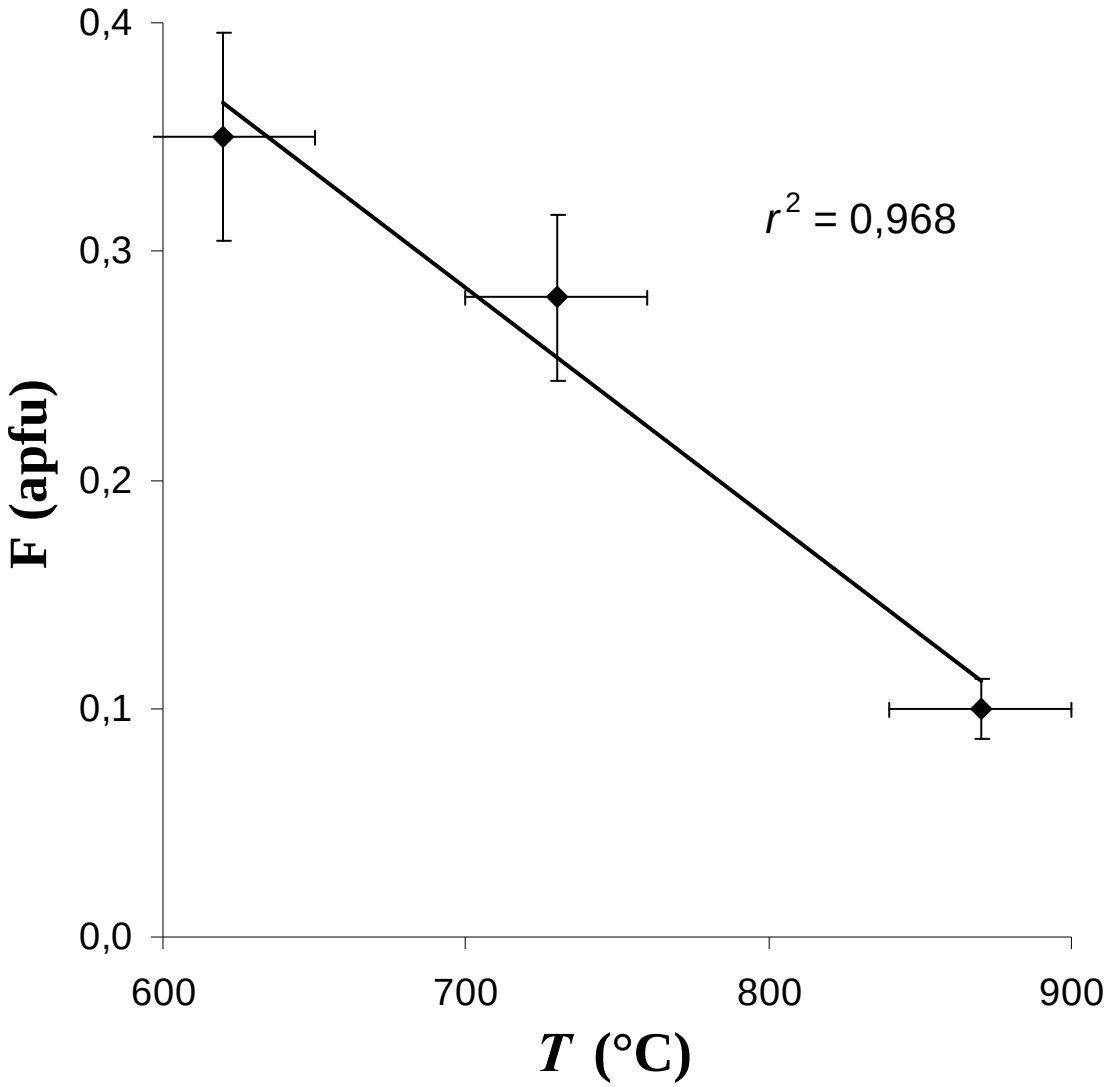

FIGURE 5. Relationship between the F content (EMPA data from Table 4) of the investigated UHP tourmalines and the temperature conditions of tourmaline formation. By using the refined F data (Table 2) the correlation coefficient $r^2 = 1.00$. Bars: average estimated standard deviation (±1σ).

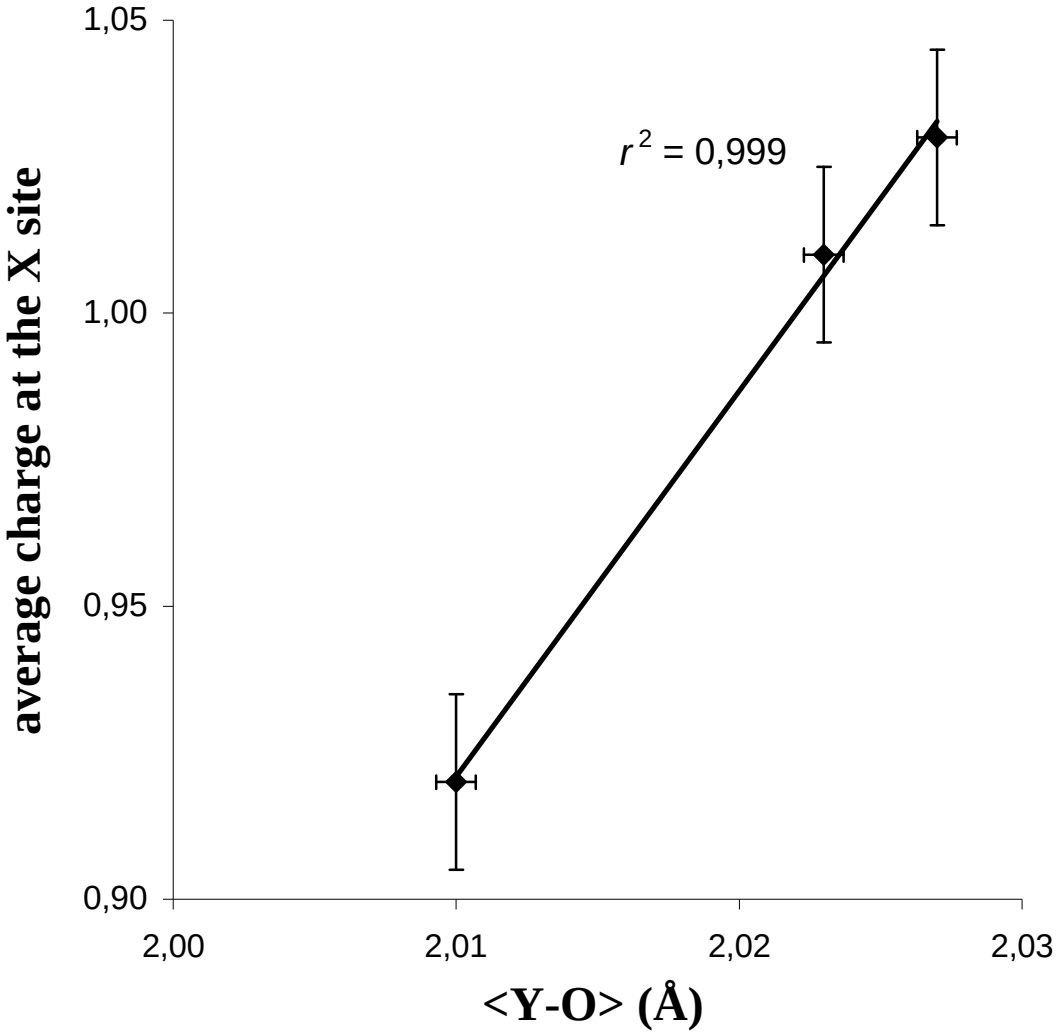

FIGURE 6. Relationship between the average charge of the X-site occupants of the investigated UHP tourmalines and the <Y-O> distance (Table 3). Bars: average estimated standard deviation (±1σ).

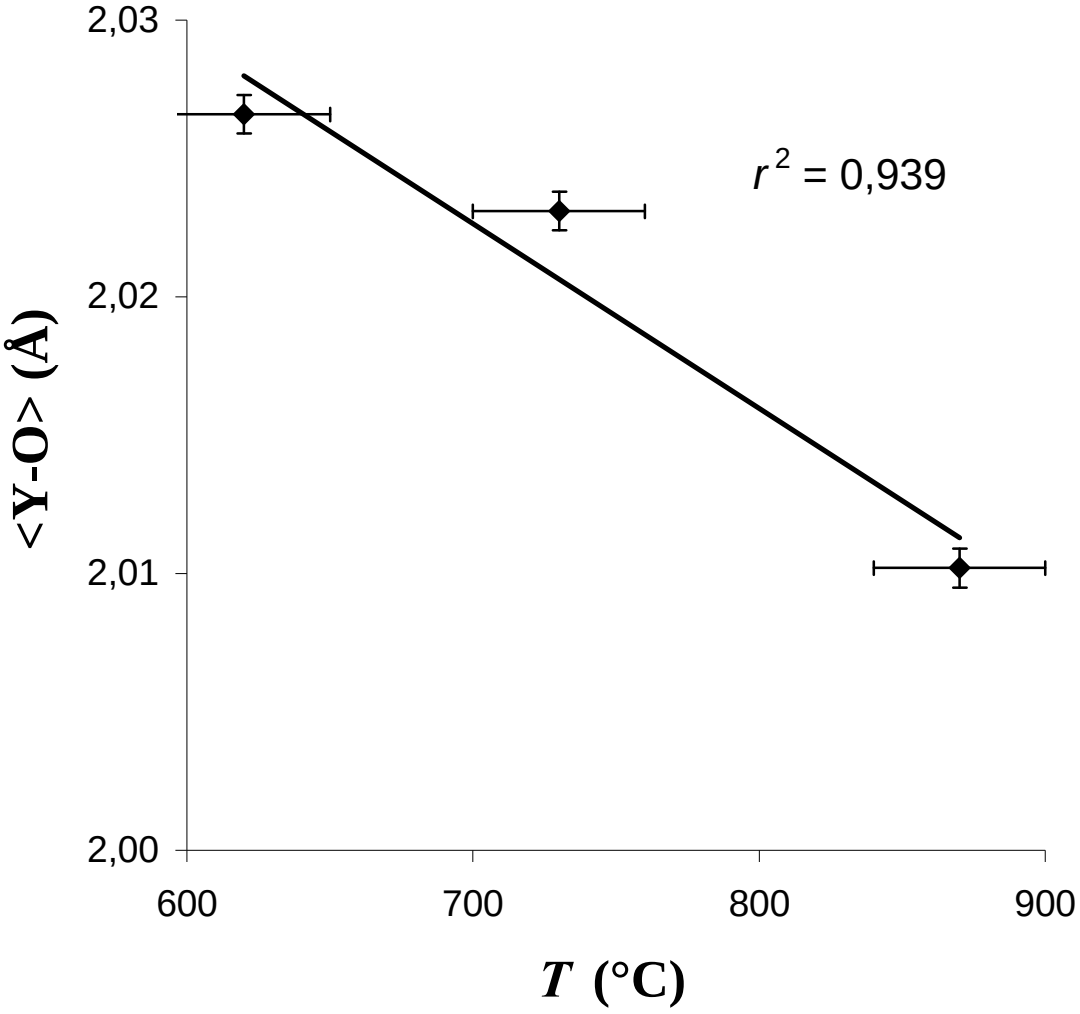

FIGURE 7. Relationship between the <Y-O> distance of the investigated UHP tourmalines and the temperature conditions of tourmaline formation. Bars: average estimated standard deviation (±1σ).

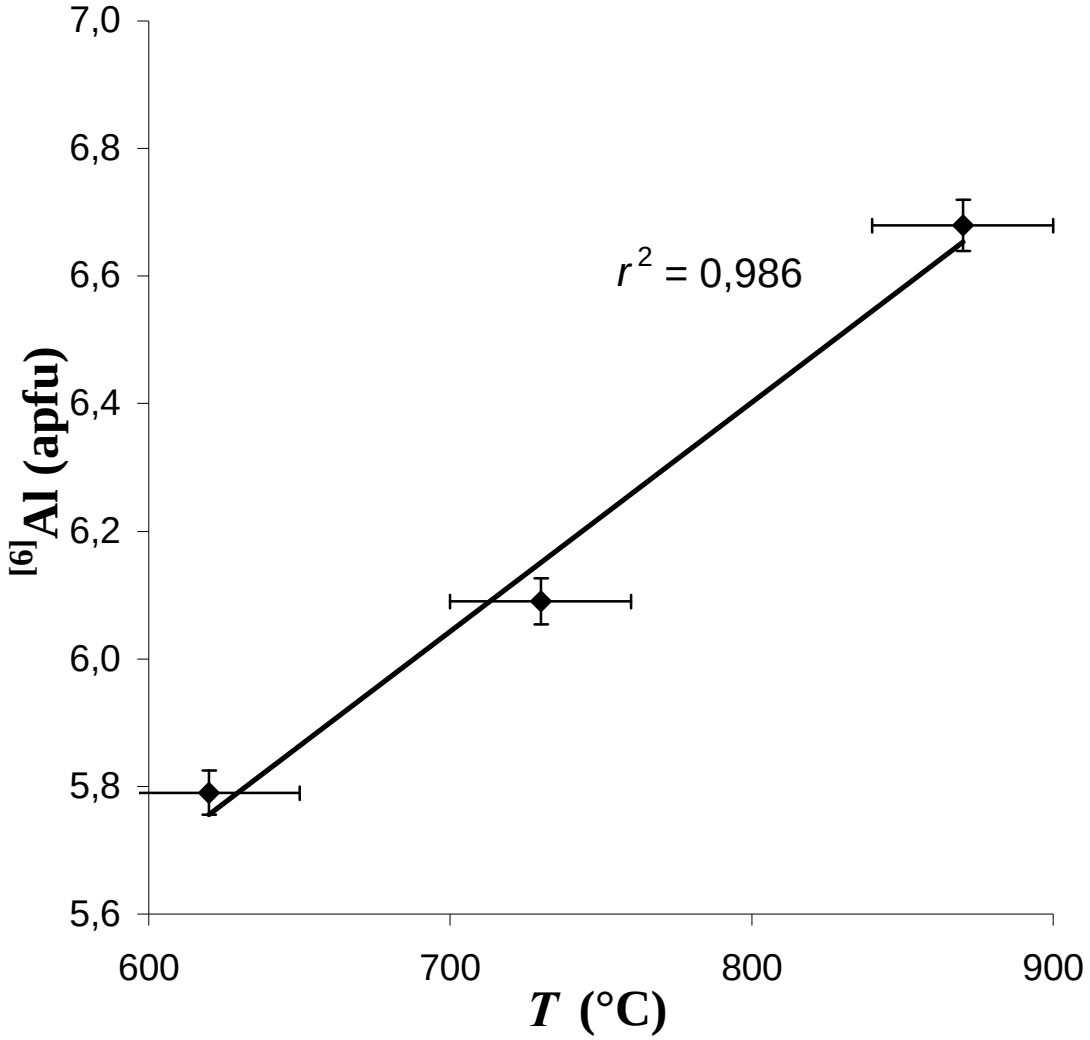

FIGURE 8. Relationship between the [6]Al content (Sum of Al at the Y and Z site) of the investigated UHP tourmalines and the temperature conditions of tourmaline formation. Bars: average estimated standard deviation (±1σ).

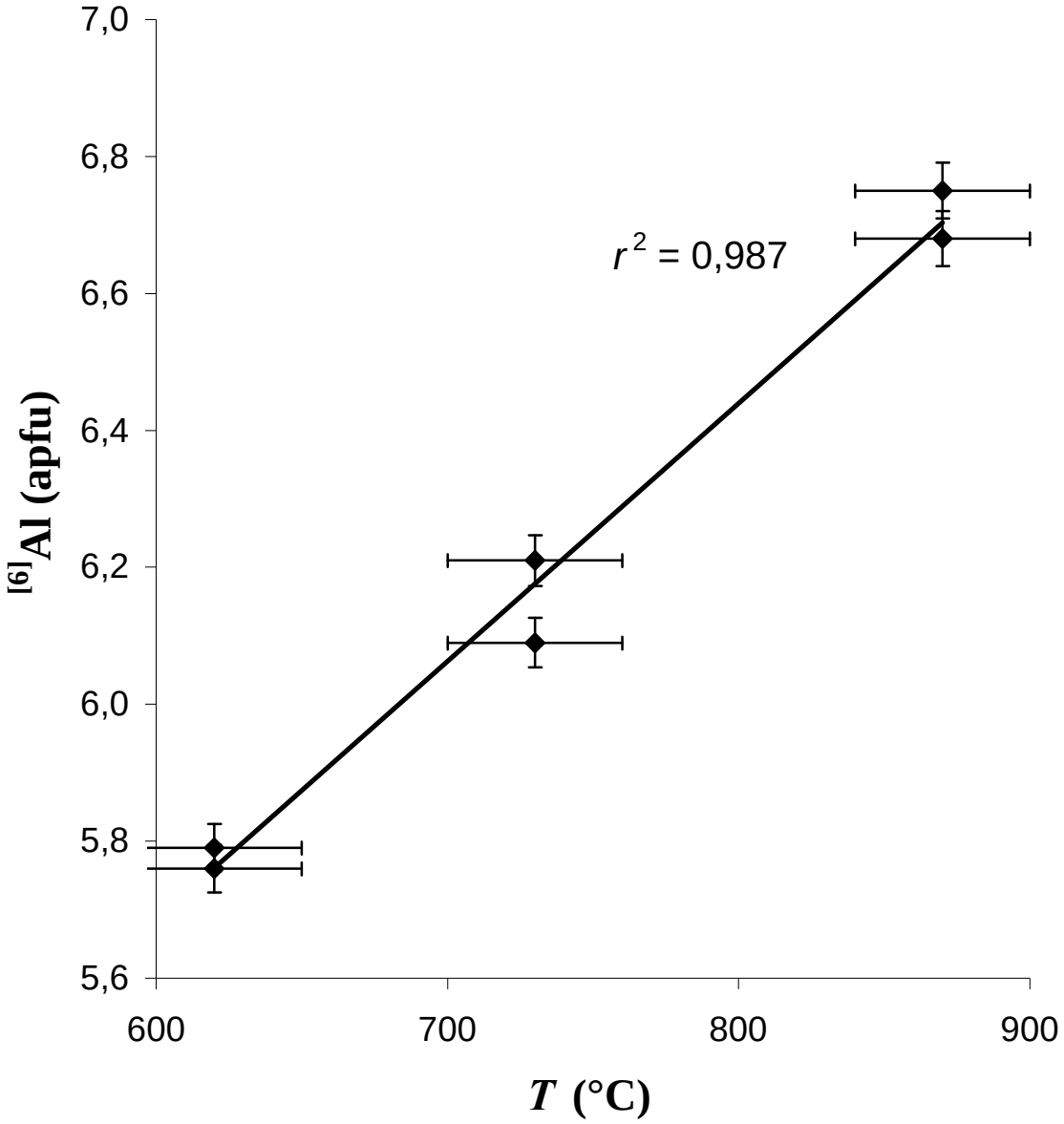

FIGURE 9. Relationship between the [6]Al content (Sum of Al at the Y and Z site) of the UHP tourmalines and the temperature conditions of tourmaline formation. Plotted are also samples R6b (coesite bearing mantle of the tourmaline), Erzgebirge, Germany (Marschall et al. 2009), dravite (inclusion from a small pyrope crystal) from Dora Maira (Schreyer 1985), and the tourmaline from Lago di Cignana, Zermatt-Saas zone, Western Alps (Reinecke 1991). Bars: average estimated standard deviation (±1σ).

7 Summary

In this work, investigations on tourmalines of different chemistry and formation were conducted. The general chemical formula of the tourmaline-group minerals can be written as $XY_3Z_6[T_6O_{18}](BO_3)_3V_3W$. At first, tourmalines of the elbaite-schorl and "fluor-elbaite"-rossmanite series, including Mn-rich elbaites, were investigated. Such samples are common in Li-pegmatites and often show interesting zonations. Tourmalines with unusual, high concentrations of Fe^{2+} and Mn^{2+} were investigated to find out if Fe^{2+} and Mn^{2+} also occupy the *Z* site. Later, these samples were oxidized and subsequently structurally characterised. Very unusual are pale-blue to pale-green Mg-rich tourmalines which also contain significant amounts of Li. Such samples were characterised from pegmatites which all occur in the Austroalpine basement units in Styria. Mg-rich and V-bearing olenites from a graphite deposit, as well as Mg-bearing tourmalines from ultra-high pressure (UHP) metamorphic rocks, where Mg and Al are strongly disordered between the *Y* and the *Z* site, were characterised. Further, an Al-rich tourmaline (from Madagascar) with relatively low lattice parameters was chemically and structurally characterised, because tourmalines with relatively high amounts of tetrahedrally coordinated B are not that common.

Detailed chemical, Mössbauer, infrared, optical (absorption) and structural data were obtained on 12 tourmaline samples from gem pockets in the Himalaya mine, San Diego County, California, U.S.A. One of these tourmalines shows strong color zonation from core to rim and correspondingly strong compositional zonation. The elements Li and F that are normally coupled are decoupled in this zoned tourmaline. When lepidolite starts crystallizing, the F content in tourmaline decreases. The black core of this crystal is an Al-rich, Mn-bearing "oxy-schorl". A yellowish green, intermediate Mn-rich "fluor-elbaite" zone contains a relatively-high Mn content with ~6 wt.% MnO. There is an inverse correlation between the lattice parameter *a* and the Li content (r^2 = 0.96). There is an excellent positive correlation between the lattice parameter *a* and the (Fe^{2+} + Mn^{2+}) content in tourmalines from the elbaite-schorl series (r^2 = 0.99). Lower values than 15.84 Å for lattice parameter *a* can be derived by an increasing $^{[4]}$B content in samples which usually have a (Fe^{2+} + Mn^{2+}) content of <0.1 apfu. There is an inverse correlation between <*Y*-O> and the Al and Fe^{3+} content at the *Y* site in tourmalines from the elbaite-schorl series (r^2 = 0.98). Within the core of the crystal, the *T* site contains ~0.3 apfu $^{[4]}$Al whereas in the Al- and Li-rich tourmalines it contains ~0.2 apfu $^{[4]}$B. The intermediate zones contain mixed occupations of Si, Al and B. Similar to $^{[4]}$B-bearing tourmalines from other localities, a positive correlation between Al at the *Y* site and $^{[4]}$B was found (r^2 = 0.93) in tourmalines from the Himalaya Mine. Another positive correlation was found between (Mn^{2+} + Fe^{2+}) and $^{[4]}$Al in tourmalines from this locality (r^2 = 0.99). These correlations indicate that, in the short-range order configurations, ^{Y}Al is coupled with $^{[4]}$B, whereas Mn^{2+} and Fe^{2+} are coupled with $^{[4]}$Al. The chemical analyses indicate that some elbaites contain a mixed occupation of F, OH and O at the W site. The conclusion is that the assumption OH = 4 – F is only valid for elbaitic tourmalines with FeO + MnO < 8 wt%.

A very Fe^{2+}- and Mn^{2+}-rich tourmaline (from Blocherleitengraben, Lower Austria) was used to test whether Fe^{2+} and Mn^{2+} substitute on the *Z* site of tourmaline to a detectable degree. On basis of the chemical data, the structural refinement and the spectroscopic data, the first proposed formula for schorl was determined by assigning the entire amount of Fe^{3+} and Ti^{4+} to the *Z* site and the amount of Fe^{2+} and

Fe^{3+} from delocalized electrons to the *Y*-*Z* electron charge delocalization (ED) doublet. This first possibilty would be consistent with a lack of Fe^{2+} at the *Z* site, apart from that connected with delocalized electrons. A second possibilty is discussed, with two ED doublets (delocalized electrons between *Y*-*Z* and *Y*-*Y*) of the Mössbauer spectra, and where the Z site is occupied by small amounts of static Fe^{2+} (~0.3 apfu).

A Mn-rich tourmaline (~1.3 apfu Mn^{2+}) from a pegmatite at Elba Island, Italy, was characterised by crystal structure determination, chemical analyses and optical spectroscopy. Within a 3σ error there is no clear evidence for Mn at the *Z* site by a tentative refinement of Al↔Mn. The problems of inaccuracies in determination of site occupancy and enlarged <*Z*-O> distances in tourmaline because of large cations at the *Y* site are discussed. A positive correlation (r^2 = 0.87) was found between <*Y*-O> and <*Z*-O> distances in tourmalines where the *Z* site is only occupied by Al. During heating of these Fe^{2+}- and Mn^{2+}-rich tourmalines at 750°C, some Fe and Mn of the *Y* site was exchanged with some Al of the *Z* site, during oxidizing to Fe^{3+}/Mn^{3+}. The refined ^{Z}Fe content grew larger (by ~37%) after heating and oxidation. Simultaneously, the refined ^{Y}Fe content was smaller and the <*Y*-O> distance was significantly reduced. A similar observation was made by oxidizing the Mn^{2+}-rich tourmaline. Simultaneously, OH was released in both samples as was indicated by structural refinements and by optical absorption spectra. The final product after heating the schorl was a buergerite with approximately all Fe^{2+} oxidized to Fe^{3+} as was indicated by structural and spectroscopic data. After heating the Mn^{2+}-rich tourmaline at 750°C for 30 hours, the yellow sample was red, as expected for the oxidation of Mn^{2+} to Mn^{3+}.

Tourmaline samples from Wolkenburg, Saxony, Germany, were chemically (including light elements) and structurally characterised. The crystal chemical formulae of these three investigated samples range from a “fluor-elbaite” dominant composition to Na-rich rossmanite. When the rossmanite component increases, while the “fluor-elbaite” component decreases, the olenite component also increases. In a pegmatitic system where essentially no Fe, Mn, Ti and Mg are available, the Li content is an important factor, which seems to control the amount of Si in tourmaline (r^2 = 1.00 for samples from the “fluor-elbaite”-rossmanite-“oxy-rossmanite” series). Once the Li^{1+} content is lower, Al^{3+} cations (with a higher oxidation state) must occupy the *Y* site. For a charge-balanced formula, other cation sites must therefore have lower bulk charges. This can be achieved by increasing vacancies at the *X* site and increasing amounts of trivalent cations at the *T* site. In the Wolkenburg tourmalines of the “fluor-elbaite”-rossmanite series both substitutions are observed. For the investigated tourmalines a modified (coupled) Tschermaks’ substitution with $^{X}\square + {}^{Y}Al^{3+} + {}^{T}(Al, B)^{3+} \leftrightarrow {}^{X}Na^{+} + {}^{Y}Li^{+} + {}^{T}Si^{4+}$ can be proposed. The F content is dependent on the charge of the *X*-site occupants (r^2 = 1.00). There is also a good negative correlation between the charge of the *X*-site occupants and the *X*-O2 distance (r^2 = 1.00), which can be used in the future to draw some conclusions about the *X*-site occupancy when only single-crystal structure data are available.

Three tourmalines from ultra high-pressure metamorphic rocks were structurally and chemically characterised. Tourmaline from Parigi, Dora Maira, as well as from Lago di Cignana, Western Alps, Italy, belong to the dravite-olenite series. Tourmaline from the village of Saidenbach in the Saxony Ore Mountains, Germany, can be assigned to “oxy-schorl”. There is no structural evidence for a significant substitution of Si by Al or B in the UHP tourmalines, not even in tourmaline from the Saxony Ore Mountains, where the temperature reached ~870°C. This is in contrast to tourmalines from high grade

lithologies (at lower pressures), which usually contain significant amounts of $^{[4]}$Al. There is an excellent positive correlation (r^2 = 1.00) between the sum of $^{[6]}$Al in the UHP tourmalines and the temperature conditions of tourmaline formation of the different units. Further there is a high negative correlation (r^2 = 0.94) between the <*Y*-O> distances of the UHP tourmalines and the temperature conditions of tourmaline formation. This correlation can be explained by an increasing ^{Y}Al content (by simultaneously increasing temperature conditions), as a result from a significant Al-Mg disorder between the *Y* and *Z* sites. Hence, such a disorder could be dependent on the temperature during crystallization. There is a good negative correlation (r^2 = 0.92) between the average charge of the *X*-site occupants in the tourmalines and the temperature conditions of tourmaline formation. Further, there is an excellent negative correlation (r^2 = 0.97) between the F content of the tourmalines and the temperature conditions of tourmaline formation.

Pale-blue to pale-green tourmalines from the contact zone of Permian pegmatitic rocks to micaschists and marbles from different localities of the Austroalpine basement units (Rappold Complex) in Styria, Austria, are characterized. All these Mg-rich tourmalines have small but significant Li contents up to 0.29 wt% Li_2O and can be characterised as Fe-bearing dravite. They show a significant Al-Mg disorder between the *Y* and the *Z* sites. These tourmalines may have crystallized in the contact between a pegmatitic melt formed by local anatexis and contact processes during the emplacement of the Permian pegmatites with carbonatic and metapelitic host rocks.

Structural, chemical and spectroscopic data of green V- and Cr-bearing tourmaline from the graphite deposit at Weinberg Mountain, west of the village of Amstall, Lower Austria, were obtained. Whereas the V^{3+} and Cr^{3+} contents stay constant, Mg decreases from the core to the rim. The relative short <*Y*-O> distances and the enlarged <*Z*-O> distances show that Al and Mg are strongly disordered between the *Y* and *Z* sites in this tourmaline. An explanation of the strong Mg-Al disorder between the *Y* and the *Z* sites in this tourmaline could be that this disorder, derived from a high-*T* overprint during crystallization, is supported by a relatively high amount of $^{[4]}$Al and low vacancies at the *X* site.

An Al-rich tourmaline from the Sahatany Pegmatite Field in Manjaka, Sahatany Valley, Madagascar, was structurally and chemically characterised. The combination of chemical and structural data yields an optimized formula of $\sim^{X}(Na_{0.5}Ca_{0.1}\square_{0.4})^{Y}(Al_{2.0}Li_{0.9}Mn^{2+}_{0.1})^{Z}Al_6(BO_3)_3{}^{T}[Si_{5.6}B_{0.4}]O_{18}{}^{V}(OH)_3{}^{W}[(OH)_{0.6}O_{0.4}]$, with relatively low lattice parameters of a = 15.777(1), c = 7.086(1) Å. The <*T*-O> distance of ~1.611 Å is one of the smallest distances observed in natural tourmalines. Together with other natural and synthetic Al-rich tourmalines, a very good inverse correlation (r^2 = 1.00) between $^{[4]}$B and the unit cell volume was found. $^{[4]}$B increases with the Al content at the *Y* site approximately as a power function with a linear term up until $^{[4]}$B ≈ Si ≈ 3 apfu and ^{Y}Al ≈ 3 apfu, respectively, in natural and synthetic Al-rich tourmalines. Short-range order considerations would not allow $^{[4]}$B in solid solution between schorl and elbaite, but would in solid solutions between schorl, "oxy-schorl", elbaite, liddicoatite, or rossmanite and hypothetical $^{[4]}$B-rich tourmaline end members with only Al^{3+} at the *Y* site. Plots of $^{[4]}$B content of synthetic and natural Al-rich tourmalines which crystallized at elevated *PT* conditions show that higher $^{[4]}$B contents are found in tourmaline at lower temperatures. This is consistent with previous investigations on the coordination of B in melts. Above a pressure of ~1000-1500 MPa (depending on the temperature) the highest observed $^{[4]}$B content does not change significantly at a given temperature.

Zusammenfassung

In dieser Arbeit wurden kristallchemische Untersuchungen an Turmalinen mit unterschiedlichem Chemismus und unterschiedlicher Entstehung durchgeführt. Die allgemeine chemische Formel für Minerale der Turmalingruppe lautet $XY_3Z_6[T_6O_{18}](BO_3)_3V_3W$. Zum einen wurden Glieder der Elbait-Schörl- und „Fluor-Elbait"-Rossmanit-Reihe, einschließlich Mn-reicher Elbaite, untersucht. Solche Turmaline kommen häufig in Li-Pegmatiten vor und zeigen oft interessante Zonierungen. Turmaline mit ungewöhnlich hohen Anteilen von Fe^{2+} und Mn^{2+} wurden ebenso charakterisiert, um herauszufinden, ob Fe^{2+} und Mn^{2+} auch die *Z*-Position besetzen. Diese Proben wurden auch an Luft oxidiert und danach strukturell charakterisiert. Ungewöhnlich ist das Vorkommen von hellblau bis hellgrün gefärbten Mg-reichen Turmalinen aus Pegmatiten der ostalpinen Grundgebirgseinheit der Steiermark, die signifikante Anteile von Li enthalten. Außerdem wurden noch Mg-reiche und V-haltige Olenite der Graphitlagerstätte Amstall und Mg-haltige Turmaline von Ultrahochdruck- (UHP) metamorphen Gesteinen charakterisiert, wobei Mg und Al eine ausgeprägte Unordnung zwischen der *Y*- und der *Z*-Position aufweisen. Weiters wurde ein Al-reicher Turmalin (von Madagaskar) mit relativ niedrigen Gitterparametern und relativ viel B chemisch und strukturell untersucht, da solch hohe Anteile von tetraedrisch koordiniertem B nicht sehr häufig sind.

Detaillierte chemisch-analytische, Mössbauer- und infrarotspekroskopische, sowie optische (Absorptionsspektren) und strukturelle Daten wurden von 12 Turmalin-Proben aus Pegmatit-Hohlräumen der Himalaya Mine, Kalifornien, U.S.A., gemessen. Ein Kristall zeigt eine starke Farbzonierung vom Kern zum Rand, die mit einer starken Zonierung der chemischen Zusammensetzung korrespondiert. Die Elemente Li und F, welche normalerweise miteinander gekoppelt sind, sind in diesem Turmalinkristall entkoppelt. Wenn Lepidolith zu kristallisieren beginnt, nimmt der F-Gehalt des Turmalins ab. Der schwarze Kern dieses Kristalls ist ein Al-reicher, Mn-haltiger „Oxy-Schörl". Eine gelblich-grüne Zwischenzone von „Fluor-Elbait" weist einen relativ hohen Mn-Gehalt von ~6 Gew.-% MnO auf. Es existiert eine inverse Korrelation zwischen der Gitterkonstante *a* (für ≥15.84 Å) und dem Li-Anteil (r^2 = 0.96). Weiters gibt es eine sehr gute positive Korrelation zwischen der Gitterkonstante *a* und dem (Fe^{2+} + Mn^{2+})-Anteil in Turmalinen der Elbait-Schörl Mischkristallreihe (r^2 = 0.99). Niedrigere Werte als 15.84 Å für die Gitterkonstante *a* können durch einen zunehmenden Anteil von $^{[4]}$B erreicht werden. Zwischen dem <*Y*-O>-Abstand und dem Al- und Fe^{3+}-Anteil der Y-Position gibt es in Turmalinen der Elbait-Schörl-Mischkristallreihe eine inverse Korrelation (r^2 = 0.98). Vergleichbar zu anderen $^{[4]}$B-haltigen Turmalinen, zeigt sich auch in den Turmalinen der Himalaya Mine eine positive Korrelation zwischen Al auf der *Y*-Position und $^{[4]}$B (r^2 = 0.93). Eine weitere positive Korrelation wurde zwischen dem (Fe^{2+} + Mn^{2+})-Gehalt und $^{[4]}$Al in Turmalinen dieser Lokalität beobachtet (r^2 = 0.99). Diese Korrelationen weisen darauf hin, dass in Nahordnungs-Konfigurationen ^{Y}Al mit $^{[4]}$B, sowie Fe^{2+} und Mn^{2+} mit $^{[4]}$Al gekoppelt sind. Die chemischen Analysen zeigen, dass einige Elbaite eine gemischte Besetzung von F, OH und O auf der *W*-Position haben. Die Schlussfolgerung ist, dass die Annahme von OH = 4 – F nur für elbaitische Turmaline mit FeO + MnO < 8 Gew.-% gültig ist.

Ein sehr Fe^{2+}- und Mn^{2+}-reicher Schörl vom Blocherleitengraben, Niederösterreich, wurde untersucht, um zu testen, ob Fe^{2+} und Mn^{2+} die *Z*-Position besetzen können. Auf Basis der chemischen

Daten, Strukturverfeinerungen und spektroskopischen Daten wurde einerseits für diesen Schörl vorgeschlagen, die gesamte Menge von Fe^{3+} und Ti^{4+} der *Z*-Position zuzuordnen, sowie den Anteil von Fe^{2+} und Fe^{3+} der delokalisierten Elektronen des *Y*-*Z*-Doublets des Mössbauer Spektrums diesen Positionen zuzuordnen. Dies würde bedeuten, dass bis auf die delokalisierten Elektronen kein statisches Fe^{2+} auf der *Z*-Position vorhanden sein würde. Weiters wird eine zweite Möglichkeit diskutiert, wobei zwei ED-Doubletten (delokalisierte Elektronen zwischen *Y*-*Z* und *Y*-*Y*) angenommen werden, sowie außerdem etwas statisches Fe^{2+} (~0.3 apfu) die *Z*-Position besetzt.

Ein Mn-reicher pegmatitischer Turmalin (~1.3 apfu Mn^{2+}) von der Insel Elba, Italien, wurde mittels Kristallstrukturverfeinerung, chemischer Analyse und optischer Spektroskopie untersucht. Innerhalb eines 3σ-Fehlers gibt es keinen eindeutigen Beweis für Mn auf der *Z*–Position anhand einer Verfeinerung des Al:Mn-Verhältnisses. Weiters werden mögliche Ungenauigkeiten bei der Bestimmung der Besetzungsdichte einer Position diskutiert, sowie die Vergrößerung der <*Z*-O>-Bindungslänge durch den Einfluss von größeren Kationen auf der *Y*-Position. Es wurde eine positive Korrelation (r^2 = 0.87) zwischen den <*Y*-O>- und <*Z*-O>-Abständen in Turmalinen gefunden, bei denen die *Z*-Position nur von Al besetzt ist. Durch Erhitzen der Fe^{2+}- und Mn^{2+}-reichen Turmaline auf 750°C an Luft wechselten während der Oxidation zu Fe^{3+}/Mn^{3+} signifikante Anteile dieser Elemente von der *Y*- zur *Z*-Position, wobei gleichzeitig Anteile von Al von der *Z*- zur *Y*-Position wechselten. Der verfeinerte ^{Z}Fe-Anteil war nach der Erhitzung signifikant (~37%) größer, als vor der Erhitzung. Gleichzeitig verkleinerte sich der verfeinerte ^{Y}Fe-Anteil und es verringerte sich die <*Y*-O>-Distanz deutlich. Eine ganz ähnliche Beobachtung konnte durch die Oxidation von Mn^{2+}-reichen Turmalinen der Insel Elba gemacht werden. Gleichzeitig wurde von allen oxidierten Turmalinproben H_2O abgegeben, was auch durch die Resultate der Strukturverfeinerung sowie der optischen Absorptionsspektren bestätigt wurde. Als Ergebnis der Erhitzung vom Schörl wurde ein Buergerit erhalten, bei dem praktisch das gesamte Fe^{2+} zu Fe^{3+} oxidiert wurde, belegt durch Strukturdaten und spektroskopische Ergebnisse. Bei der Erhitzung des Mn^{2+}-reichen Turmalins auf 750°C für 30 h veränderte sich die ursprünglich gelbe Farbe zu einer roten Färbung, in Übereinstimmung mit einer Oxidation von Mn^{2+} zu Mn^{3+}.

Von drei schwach gefärbten bis farblosen Al- und Li-reichen pegmatitischen Turmalinen von Wolkenburg, Sachsen, Deutschland, wurden Fragmente durch Einkristallstrukturen und chemischen Daten (EMPA, SIMS, TGA) charakterisiert. Die Zusammensetzung dieser untersuchten Proben reicht von „Fluor-Elbait“ bis zu Na-reichem Rossmanit. Wenn in einem pegmatitischen System praktisch kein Fe, Mn, Ti und Mg verfügbar ist, ist der Li-Gehalt ein wichtiger Faktor, welcher anscheinend den Si-Anteil der Turmaline bestimmt (r^2 = 1.00 für Proben der “Fluor-Elbait”-Rossmanit-“Oxy-Rossmanit”-Serie). Wenn der Li^+-Anteil niedriger ist, müssen Al^{3+}-Kationen (mit einer höheren Oxidationsstufe) die *Y*-Position besetzen. Für eine ladungsausgeglichene Formel müssen daher andere Kationpositionen niedrigere Ladungen aufweisen. Dies kann durch mehr Leerstellen auf der *X*-Position und durch eine steigende Anzahl von dreiwertigen Kationen an der *T*-Position erreicht werden. In den Wolkenburg-Turmalinen der “Fluor-Elbait”-Rossmanit-Serie werden beide Substitutionen beobachtet. Für die untersuchten Turmaline kann eine modifizierte (gekoppelte) Tschermak-Substitution mit $^{X}\square + {}^{Y}Al^{3+} + {}^{T}(Al, B)^{3+} \leftrightarrow {}^{X}Na^{+} + {}^{Y}Li^{+} + {}^{T}Si^{4+}$ beobachtet werden. Der F-Anteil ist von der Ladung der Besetzungen der *X*-Position abhängig (r^2 = 1.00). Es gibt auch eine gute negative Korrelation zwischen der Ladung der Besetzungen der *X*-Position und der *X*-O2

Bindungslänge (r^2 = 1.00), welche in Zukunft auch dafür verwendet werden kann, um Hinweise über die Besetzung der *X*-Position zu erhalten, wenn nur Daten einer Einkristallstruktur vorhanden sind.

Drei nahezu farblose bis schwarze Turmaline von Ultrahochdruck- (UHP) metamorphen Gesteinen wurden strukturell und chemisch charakterisiert. Turmaline von Parigi, Dora Maira, sowie von Lago di Cignana, Westalpen, Italien, können der Dravit-Olenit-Reihe zugeordnet werden. Turmalin („Oxy-Schörl“) von Saidenbach aus dem Sächsischen Erzgebirge, Deutschland, weist einen großen Anteil von ^{Y}Al auf. Es gibt keine strukturelle Evidenz für eine signifikante Substitution von Si durch Al oder B in den UHP-Turmalinen, auch nicht im Turmalin vom Sächsischen Erzgebirge, wo die Temperatur ~870°C erreichte. Dies steht im Gegensatz zu $^{[4]}$Al-reichen Turmalinen von hochgradig metamorphen (granulitfaziellen) Lithologien. Es gibt eine ausgezeichnete positive Korrelation (r^2 = 1.00) zwischen der Summe des $^{[6]}$Al in den UHP-Turmalinen und der Temperaturbedingungen der Turmalinbildung der verschiedenen Einheiten. Weiters gibt es eine hohe negative Korrelation (r^2 = 0.94) zwischen den <*Y*-O>-Abständen der UHP-Turmaline und den Temperaturbedingungen der Turmalinbildung. Diese Korrelation kann durch einen ansteigenden ^{Y}Al-Gehalt (bei gleichzeitig ansteigenden Temperaturbedingungen) erklärt werden, resultierend aus einer signifikanten Al-Mg-Unordnung zwischen den *Y*- und *Z*-Positionen. Daher ist zu vermuten, dass eine solche Unordnung von der Temperatur während der Turmalin-Kristallisation abhängig ist. Es gibt eine gute negative Korrelation (r^2 = 0.92) zwischen der mittleren Ladung der Kationen auf der *X*-Position und den Temperaturbedingungen der Turmalinbildung. Ferner gibt es noch eine exzellente negative Korrelation (r^2 = 0.97) zwischen dem F-Anteil der Turmaline und den Temperaturbedingungen der Turmalinbildung.

Hellblaue bis -grüne Turmaline aus der Kontaktzone von permischen pegmatitischen Gesteinen zu Gimmerschiefern und Marmoren verschiedener Lokalitäten der Austroalpinen Grundgebirgseinheit (Rappold-Komplex) der Steiermark, Österreich, wurden chemisch und strukturell charakterisiert. All diese Mg-reichen Turmaline haben kleine, aber signifikante Li-Anteile bis zu 0.29 Gew.-% Li_2O und können als Fe-haltige Dravite bezeichnet werden, wobei diese Turmaline eine signifikante Al-Mg-Unordnung zwischen der *Y*- und der *Z*-Position zeigen.

Weiters wurden strukturelle, chemische und spektroskopische Daten von grünen V- und Cr-haltigen Turmalinen der Graphitlagerstätte am Weinberg, westlich der Ortschaft Amstall, Niederösterreich, aufgenommen. Während V^{3+} und Cr^{3+} konstant bleiben, nimmt der Mg-Anteil vom Kern- zum Randbereich ab. Die relativ kurzen <*Y*-O>-Abstände und die vergrößerten <*Z*-O>-Distanzen zeigen, dass eine starke Unordnung von Al und Mg zwischen den *Y*- und den *Z*-Positionen auftritt. Eine mögliche Erklärung dieser starken Mg-Al-Unordnung wäre, dass diese durch die hoch-Temperatur-Überprägung während der Kristallisation ausgbildet wurde, wobei auch der relativ hohe Anteil von $^{[4]}$Al und die niedrigen Leerstellen an der *X*-Position diese Vermutung stützen würden.

Ein Al- und B-reicher Turmalin vom Sahatany Pegmatit-Feld in Manjaka, Sahatany Valley, Madagaskar, wurde strukturell und chemisch charakterisiert. Die Kombination von chemischen und strukturellen Daten ergab die Formel $\sim^{X}(Na_{0.5}Ca_{0.1}\square_{0.4})^{Y}(Al_{2.0}Li_{0.9}Mn^{2+}_{0.1})^{Z}Al_6(BO_3)_3{}^{T}[Si_{5.6}B_{0.4}]O_{18}{}^{V}(OH)_3{}^{W}[(OH)_{0.6}O_{0.4}]$, mit relativ niedrigen Gitterkonstanten von a = 15.777(1), c = 7.086(1) Å. Die <*T*-O>-Bindungslänge von ~1.611 Å ist eine der niedrigsten, welche bislang in natürlichen Turmalinen beobachtet wurde. Zusammen mit anderen natürlichen und synthetischen Al-reichen Turmalinen wurde eine sehr gute

inverse Korrelation (r^2 = 1.00) zwischen $^{[4]}$B und dem Elementarzellenvolumen gefunden. Der maximal beobachtete Anteil von $^{[4]}$B (in natürlichen und synthetischen Turmalinen) nimmt gleichzeitig mit dem Al-Anteil der *Y*-Position zu, bis $^{[4]}$B ≈ Si ≈ 3 apfu und ^{Y}Al ≈ 3 apfu, wobei sich diese Korrelation annähernd durch eine quadratische Funktion mit einem linearen Term darstellen lässt. Betrachtungen der Nahordnung zeigen, dass kein $^{[4]}$B in der Schörl-Elbait-Mischkristallreihe auftreten kann, sehr wohl aber in Mischkristallreihen zwischen Schörl, „Oxy-Schörl“, Elbait, Liddicoatit oder Rossmanit und hypothetischen $^{[4]}$B-reichen Turmalin-Endgliedern, in welchen die *Y*-Position ausschließlich mit Al^{3+} besetzt ist. Anhand einer graphischen Darstellung der $^{[4]}$B-Anteile von synthetischen und natürlichen Al-reichen Turmalinen, welche bei verschiedenen *PT*-Bedingungen kristallisiert sind, ist ersichtlich, dass es ausgeprägte Korrelationen zwischen den *PT*-Bedingungen und dem $^{[4]}$B-Anteil gibt. In Richtung niedrigerer Temperaturen wurden höhere Anteile von $^{[4]}$B in Turmalin gefunden, konsistent mit bisherigen Beobachtungen bezüglich der Koordinationen von B in Schmelzen. Oberhalb von Druckbedingungen mit ~1000-1500 MPa (temperaturabhängig) zeigt sich keine signifikante Änderung des höchsten beobachteten $^{[4]}$B-Gehalts bei einer bestimmten Temperatur.

References

Adeoye, M.O. & Adewoye, O.O. (2004): Investigation of hardness anisotropy in tourmaline. J. Minerals & Materials Characterization & Engineering 3, 2, 99-103.

Bloodaxe, E.S., Hughes, J.M., Dyar, M.D., Grew, E.S. & Guidotti, C.V. (1999): Linking structure and chemistry in the Schorl-Dravite series. American Mineralogist, 84, 922-928.

Bosi, F. & Lucchesi, S. (2004): Crystal chemistry of the schorl-dravite series. European Journal of Mineralogy 16, 335-344.

Dirlam, D.M., Laurs, B.M., Pezzotta, F. & Simmons, W.B. (2002): Liddicoatite tourmaline from Anjanabonoina, Madagascar. Gems and Gemology 38, 28-53.

Dietrich, R. (1985): The tourmaline group. 1st ed., Van Nostrand Reinhold Company, New York, 300 pp.

Donnay, G. & Barton, P.Jr. (1972): Refinement of the crystal structure of elbaite and the mechanism of tourmaline solid solution. Tschermaks Mineralogisch Petrographische Mitteilungen, 18, 273-286.

Donnay, G. & Buerger, M.J. (1950): The determination of the crystal structure of tourmaline. Acta Crystallographica, 3, 5-12.

Dutrow, B. & Henry, D.J. (2000): Complexly zoned fibrous tourmaline: A record of evolving magmatic and hydrothermal fluids. Canadian Mineralogist, 38, 131-143.

Dyar, M.D., Guidotti, C.V., Core, D.P., Weam, K.M., Wise, M.A., Francis, C.A., Johnson, K., Brady, J.B., Robertson, J.D. & Cross, L.R. (1999): Stable isotope and crystal chemistry of tourmaline across pegmatite – country rock boundaries at Black Mountain and Mount Mica, southwestern Maine, USA. European Journal of Mineralogy, 11, 281-294.

Ertl, A. & Brandstätter, F. (1998): Olenit mit Borüberschuß aus einem Metapegmatit östlich der Stoffhütte, Koralpe, Steiermark, Österreich. Mitteilungen der Abteilung für Mineralogy des Landesmuseum Joanneum, 62/63, 3-21, Graz.

Ertl, A. & Hughes, J.M. (2002): The crystal structure of an aluminum-rich schorl overgrown by boron-rich olenite from Koralpe, Styria, Austria. Mineralogy and Petrology, 75, 1-2, 69-78.

Ertl, A., Pertlik, F. & Bernhardt, H.-J. (1997): Investigations on olenite with excess boron from the Koralpe, Styria, Austria. Österreichische Akademie der Wissenschaften, Mathematisch-naturwissenschaftliche Klasse, Abteilung I, Anzeiger, 134, 3-10, Wien.

Ertl, A., Hughes, J.M. & Marler, B. (2001a): Empirical formulae for the calculation of <T-O> and X-O2 bond lengths in tourmaline and relations to tetrahedrally-coordinated boron. Neues Jahrbuch für Mineralogie Monatshefte, 2001(12), 548-557.

Ertl, A., Marler, B. & Pertlik, F. (2001b): Kristallchemische Überlegungen zur Besetzung „nichttetraedrischer“ Kationenpositionen durch Silizium im Strukturtyp Turmalin. Mitteilungen der Österreichischen Mineralogischen Gesellschaft, 146, 72-74.

Ertl, A., Pertlik, F. & Bernhardt, H.-J. (2001c): Hellblaue Olenit-Schörl-Dravit Mischkristalle von Ebersdorf, Niederösterreich: Chemismus und Kristallstruktur. Mitteilungen der Österreichischen Mineralogischen Gesellschaft, 146, 75-77.

Ertl, A., Hughes, J.M., Pertlik, F., Foit, F.F. Jr., Wright, S.E., Brandstätter, F. & Marler, B. (2002): Polyhedron distortions in tourmaline. Canadian Mineralogist, 40, 153-162.

Ertl, A., Hughes, J.M., Brandstätter, F., Dyar, M.D. & Prasad, P.S.R. (2003a): Disordered Mg-bearing olenite from a granitic pegmatite from Goslarn, Austria: A chemical, structural, and infrared spectroscopic study. Canadian Mineralogist, 41, 1363-1370.

Ertl, A., Hughes, J.M., Prowatke, S., Rossman, G.R., London, D. & Fritz, E.A. (2003b): Mn-rich tourmaline from Austria: structure, chemistry, optical spectra, and relations to synthetic solid solutions. American Mineralogist, 88, 1369-1376.

Ertl, A., Pertlik, F., Dyar, M.D., Prowatke, S., Hughes, J.M., Ludwig, T. & Bernhardt, H.-J. (2004a): Olenite with tetrahedrally coordinated Fe^{3+} from Eibenstein, Austria: structural, chemical, and Mössbauer data. Canadian Mineralogist, 42, 1057-1063.

Ertl, A., Schuster, R., Prowatke, S., Brandstätter, F., Ludwig, T., Bernhardt, H.-J., Koller, F. & Hughes, J.M. (2004b): Mn-rich tourmaline and fluorapatite in a Variscan pegmatite from Eibenstein an der Thaya, Bohemian massif, Lower Austria. Eur European Journal of Mineralogy, 16, 551-560.

Ertl, A., Rossman, G.R., Hughes, J.M., Prowatke, S. & Ludwig, T. (2005): Mn-bearing "oxy-rossmanite" with tetrahedrally-coordinated Al and B from Austria: structure, chemistry, and infrared and optical spectroscopic study. American Mineralogist, 90, 481-487.

Ertl, A., Hughes, J.M., Prowatke, S., Ludwig, T., Prasad, P.S.R., Brandstätter, F., Körner, W., Schuster, R., Pertlik, F. & Marschall, H. (2006a): Tetrahedrally-coordinated boron in tourmalines from the liddicoatite-elbaite series from Madagascar: Structure, chemistry, and infrared spectroscopic studies. American Mineralogist, 91, 1847-1856.

Ertl, A., Kolitsch, U., Prowatke, S., Dyar, M.D. & Henry, D.J. (2006b): The F-analogue of schorl from Grasstein, Trentino – South Tyrol, Italy: crystal structure and chemistry. European Journal of Mineralogy, 18, 583-588.

Ertl, A., Rossman, G.R., Hughes, J.M., Wang, Y., O'Leary, J., Dyar, M.D., Prowatke, S. & Ludwig, T. (2006c): Elbaite from the Himalaya Mine, Mesa Grande, California. Gems and Gemology, 42, 96.

Ertl, A., Hughes, J.M., Prowatke, S., Ludwig, T., Brandstätter, F., Körner, W. & Dyar, M.D. (2007): Tetrahedrally-coordinated boron in Li-bearing olenite from "mushroom" tourmaline from Momeik, Myanamar: Structure and chemistry. Canadian Mineralogist, 45, (in press).

Galbraith, C. (2007): Tourmaline compositions as an indicator of emerald mineralization at Tsa da Glisza, Yukon Territory. Book of Abstracts, Atlantic Geoscience Society Colloquium & Annual General Meeting, February 2-3, 2007, Delta Beausejour Hotel, Moncton, New Brunswick.

Gaweda, A., Pieczka, A. & Kraczka, J. (2002): Tourmalines from the Western Tatra Mountains (W-Carpathians, S-Poland): Their characteristics and petrogenetic importance. European Journal of Mineralogy, 14, 943 - 955.

Goerne, G.v. (1998): Turmalin als petrogenetischer Indikator für Fluid-Gestein-Wechselwirkungen. Experimentelle Untersuchungen zum Einbau von Na und Ca in Turmalin. Technical University, Dissertation, 151 pp., Berlin.

Grice, J.D. & Ercit, T.S. (1993): Ordering of Fe and Mg in the tourmaline crystal structure: The correct formula. Neues Jahrbuch für Mineralogie Abhandlungen, 165, 245-266.

Hawkins, K.D., Mackinnon, I.D.R. & Schneeberger, H. (1995): Influence of chemistry on the pyroelectric effect in tourmaline. American Mineralogist, 80, 491-501.

Hawthorne, F.C. & Henry, D.J. (1999): Classification of the minerals of the tourmaline group. European Journal of Mineralogy, 11, 201-215.

Hawthorne, F.C., MacDonald, D.J. & Burns, P.C. (1993): Reassignment of cation site-occupancies in tourmaline: Al-Mg disorder in the crystal structure of dravite. Am American Mineralogist, 78, 265-270.

Henry, D. J. (2003): Tourmaline as a geochemical tape recorder in metamorphic rocks. Geological Society of America Abstracts with Program, 35.

Henry, D.J. & Guidotti, C.V. (1985): Tourmaline as a petrogenetic indicator mineral: an example from the staurolite-grade metapelites of NW Maine. American Mineralogist, 70, 1-15.

Hughes, J.M., Ertl, A., Dyar, M.D., Grew, E.S., Shearer, C.K., Yates, M.G. & Guidotti, C.V. (2000): Tetrahedrally coordinated boron in a tourmaline: boron-rich olenite from Stoffhütte, Koralpe, Austria. Canadian Mineralogist, 38, 861-868.

Hughes, J.M., Ertl, A., Dyar, M.D., Grew, E.S., Wiedenbeck, M. & Brandstätter, F. (2004): Structural and chemical response to varying $^{[4]}$B content in zoned Fe-bearing olenite from Koralpe, Austria. American Mineralogist, 89, 447-454.

Ikuta, D., Kawame, N., Banno, S., Hirajima, T., Ito, K., Rakovan, J.F., Downs, R.T. & Tamada, O. (2007): First in situ X-ray identification of coesite and retrograde quartz on a glass thin section of an ultrahigh-pressure metamorphic rock and their crystal structure details. American Mineralogist, 92, 57-63.

Jolliff, B.L., Papike, J.J. & Shearer, C.K. (1986): Tourmaline as a recorder of pegmatite evolution: Bob Ingersoll pegmatite, Black Hills, South Dakota. American Mineralogist, 71, 472-500.

Kalt, A., Schreyer, W., Ludwig, T., Prowatke, S., Bernhardt, H.-J. & Ertl, A. (2001): Complete solid solution between magnesian schorl and lithian excess-boron olenite in a pegmatite from Koralpe (eastern Alps, Austria). European Journal of Mineralogy, 13, 1191-1205.

Lally, J. & Cummiskey, D. (2003): Dynamic pressure calibration. Sensors, 20, 4, 15.

London, D., Ertl, A., Hughes, J.M., Morgan VI, G.B., Fritz, E.A. & Harms, B.S. (2006): Synthetic Ag-rich tourmaline: structure and chemistry. American Mineralogist, 91, 680-684.

MacDonald, D.J. & Hawthorne, F.C. (1995): The crystal chemistry of Si ⇔ Al substitution in tourmaline. Canadian Mineralogist, 33, 849-858.

Marler, B. & Ertl, A. (2002): Nuclear magnetic resonance and infrared spectroscopic study of excess-boron olenite from Koralpe, Styria, Austria. American Mineralogist, 87, 364-367.

Marschall, H.R., Ertl, A., Hughes, J.M. & McCammon, C. (2004): Metamorphic Na- and OH-rich disordered dravite with tetrahedral boron, associated with omphacite, from Syros, Greece: chemistry and structure. European Journal of Mineralogy, 16, 817-823.

Novák, M., Selway, J.B., Černý, P., Hawthorne, F.C. & Ottolini, L. (1999): Tourmaline of the elbaite-dravite series from an elbaite-subtype pegmatite at Bližná, southern Bohemia, Czech Republic. European Journal of Mineralogy, 11, 557-568.

Oliveira, E.F., Castañeda, C., Eeckhout, S.G., Gilmar, M.M., Kwitko, R.R., De Grave, E. & Botelho, N.F. (2002): Infrared and Mössbauer study of Brazilian tourmalines from different geological environment. American Mineralogist, 87, 1154-1163.

Pertlik, F., Ertl, A., Körner, W., Brandstätter, F. & Schuster, R. (2003): Na-rich dravite in the marbles from Friesach, Carinthia, Austria: Chemistry and crystal structure. Neues Jahrbuch für Mineralogie Monatshefte, 2003(6), 277-288.

Pieczka, A. (2000): Modelling of some structural parameters of tourmalines on the basis of their chemical composition. I. Ordered structure model. European Journal of Mineralogy, 12, 589-596.

Prasad, S.E., Waechter, D.F., Blacow, R.G., King, H.W. & Yaman, Y. (2005): Application of piezoelectrics to smart structures. In: Mota Soares, C.A., Holnicki-Szulc, J., Suleman, A. & Mota Soares, C.M. (Eds.): II ECCOMAS Thematic Conference on SMART Structures and Materials. Book of Abstracts, 1-16, Instituto Superior Técnico, IDMEC/IST, July 18-21, 2005, Lisbon, Portugal.

Prowatke, S., Ertl, A. & Hughes, J.M. (2003): Tetrahedrally-coordinated Al in Mn-rich, Li- and Fe-bearing olenite from Eibenstein an der Thaya, Lower Austria: A chemical and structural investigation. Neues Jahrbuch für Mineralogie Monatshefte, 2003(9), 385-395.

Roda-Robles, E., Pesquera, Al, Gil, P.P., Torres-Ruiz, J. & Fontan, F. (2004): Tourmaline from the rare-element Pinilla pegmatite, (Central Iberian Zone, Zamora, Spain): chemical variation and implications for pegmatitic evolution. Mineralogy and Petrology, 81, 249-263.

Schreyer, W., Wodara, U., Marler, B., van Aken, P.A., Seifert, F. & Robert, J.L. (2000): Synthetic tourmaline (olenite) with excess boron replacing silicon in the tetrahedral site: I. synthesis conditions, chemical and spectroscopic evidence. European Journal of Mineralogy, 12, 529-541.

Schreyer, W., Ertl, A., Hughes, J., Bernhardt, H.-J., Kalt, A. & Prowatke, S. (2002a): Tetrahedral boron in olenite from the type locality: A chemical and structural investigation. EMPG IX, Ninth International Symposium on Experimental Mineralogy, Petrology and Geochemistry, Zürich, Switzerland, 24.-27.3., Journal of Conference Abstracts 7(1), 97.

Schreyer, W., Hughes, J.M., Bernhardt, H.-J., Kalt, A., Prowatke, S. & Ertl, A. (2002b): Reexamination of olenite from the type locality: detection of boron in tetrahedral coordination. European Journal of Mineralogy, 14, 935-942.

Selway, J.B. (1999): Compositional evolution of tourmaline in granitic pegmatites. Ph.D thesis of Manitoba University, 363 pp.

Taylor, M.C., Cooper, M.A. & Hawthorne, F.C. (1995): Local charge-compensation in hydroxyl-deficient uvite. Canadian Mineralogist, 33, 1215-1221.

Wilson, J.S. (2003): Pressure measurement: Principles and practice. Sensors, 20, 1, 25.

Zhenggang, Z., Fang, L., Yin Sheng, W. & Cuiping, Y. (2004): Research on the craft of the tourmaline powder process and its application in functional fiber. Materials Review, 18, 2, 253-254.

Acknowledgements

I would like to thank my supervisor Prof. Dr. Ekkehart Tillmanns for the possibility to work in a project which focuses on my favourite mineral group – the tourmalines, and for scientific discussions and his kind help in all situations.

I also want to thank the following colleagues (in alphabetical order) for their help and for stimulating discussions: Dr. Franz Brandstätter, Prof. Dr. M. Darby Dyar, Prof. Dr. Gerald Giester, Prof. Dr. John M. Hughes, Priv.-Doz. Dr. Uwe Kolitsch, Dr. Wilfried Körner, Prof. Dr. David London, Dipl. Phys. Thomas Ludwig, Dr. Hans-Peter Meyer, Prof. Dr. Lutz Nasdala, Prof. Dr. Theodoros Ntaflos, Prof. Dr. Adam Pieczka, Dr. Stefan Prowatke, Prof. Dr. George R. Rossman and Dr. Ralf Schuster.

Further, I am grateful to my colleagues (in alphabetical order) of the Institut für Mineralogie und Kristallographie, Wien, for their support, help and interest: Prof. Dr. Anton Beran, Prof. Dr. Herta Effenberger, Dr. Michael Götzinger, Dr. Christian L. Lengauer, Prof. Dr. Eugen Libowitzky, Prof. Dr. Manfred Wildner, Mag. Markus Prem, Dr. Maria Wierzbicka-Wieczorek and Prof. Dr. Josef Zemann.

I also want to thank Prof. Dr. Lutz Nasdala, Prof. Dr. Hans-Peter Schertl, Prof. Dr. Thomas Reinecke, Dr. Horst Marschall, Prof. Dr. Darrell Henry and Dipl.-Ing. Dr. Heinrich Mali for providing me different tourmaline samples and for helpful discussions.

Special thanks also to Mr. Andreas Wagner for his excellent preparation work, Ing. Wolfgang Zirbs and Mr. Thomas Rosen for their help with computer problems and all kind of other problems. Thanks also to Mag. Olga Vepritzky for taking care of all my correspondence and packets.

Finally, I am very grateful to my mother Gerda Dobretsberger, her husband Friedrich Dobretsberger and my father Rudolf Ertl, for every possible support and for their interest in my work.

This work was financially supported by the Austrian Science Foundation (FWF), project no. P20509.

Curriculum Vitae

Name:	Andreas Gerhard Ertl
Date of Birth:	July 5th, 1965
Place of Birth:	Vienna, Austria
Martial Status:	not married
Nationality:	Austria

Education

1975 – 1979	Grammar school in Gänserndorf, Lower Austria
1979 – 1984	TGM, Höhere Lehranstalt für Elektronik und Biomedizinische Technik (High School for Electronics and Biomedical Technique), Vienna
June 1984	Abitur (with distinction) at the TGM in Vienna.
1984 – 1985	Military service in the Austrian Army (and member of the military teaching stuff for electronics and communication technique)
1985 – 1990	Study *Elektrotechnik* (Electrotechnology), Technical University Vienna
1991 – 1994	Study *Erdwissenschaften* (Geoscience), University of Vienna
1994 – 2001	Study *Mineralogie und Kristallographie* (Mineralogy and crystallography), University of Vienna
1995 – 2005	Scientific work in the field of mineralogy and crystallography in Austria and in the U.S.A., different publications
2005 – 2006	Bachelor's study – Geoscience, University of Vienna.
Oct. 2006	Bachelor's degree (Bakk. rer. nat.)
2006 – 2007	Master's study – Geoscience, University of Vienna
May 2007	Master's degree (with distinction) (Mag. rer. nat.)
2007 – 2009	Ph. D. study at the Institute of Mineralogy and Crystallography, University of Vienna

Scientific Activities

March 2008	Employed at the Institute of Mineralogy and Crystallography, University of Vienna, Austria in the FWF research project "A new method for the determination of novel tourmalines"

Professional Affiliations

- Member of the ÖMG (Austrian Mineralogical Association)
- Member of Subcommittee on Tourmaline Nomenclature (STN) of the International Mineralogical Association's Commission on New Minerals, Nomenclature and Classification (CNMNC)

Languages

- German, English

Publication List (in chronological order)

Ertl, A., Libowitzky, E. & Pertlik, F. (1994): Chemische und röntgenographische Untersuchungen an Eskimoit (~$Ag_7Pb_{10}Bi_{15}S_{36}$) und Heyrovskyit (~$AgPb_{10}Bi_5S_{18}$) vom „Rauriser Goldberg", Hüttwinkeltal, Land Salzburg. Mitt. Österr. Miner. Ges., 139, 135-142, Wien.

Ertl, A. (1994): Mineralienregister Österreich, Stand Nov. 1994. 21 pp., Eigenverlag, Strasshof.

Ertl, A. (1995): Elbait, Olenit, Dravit-Buergerit-Mischkristalle, Dravit, Uvit und ein neuer Al-Turmalin (?) von österreichischen Fundstellen. Mitt. Österr. Miner. Ges., 140, 55-72, Wien.

Ertl, A., Pertlik, F. & Bernhardt, H.-J. (1997): Investigations on olenite with excess boron from the Koralpe, Styria, Austria. Österr. Akad. Wiss., Math.-naturw. Kl., Abt. I, Anzeiger, 134, 3-10, Wien.

Bernhardt, H.-J., Brandstätter, F., Ertl, A., Körner, W., Mikenda, W. & Pertlik, F. (1999): Untersuchungen an einem borhaltigen Muskovit-$2M_1$ von der Koralpe, Steiermark. - Ann. Naturhist. Mus. Wien, 100 A (1998), 1-11, Wien.

Ertl, A. & Brandstätter, F. (1998): Olenit mit Borüberschuß aus einem Metapegmatit östlich der Stoffhütte, Koralpe, Steiermark, Österreich. Mitt. Abt. Miner. Landesmuseum Joanneum, 62/63, 3-21, Graz.

Ertl, A. (1999): Nachruf auf Hofrat Dr. Peter Beck-Mannagetta. Mitt. Österr. Geol. Ges., 90 (1997), 207-212, Wien.

Ertl, A. (2000): Druckabschätzungen in Metabasiten und Metapeliten mittels des Pyropanteiles in Granaten (engl. transl.: Pressure determination from metabasites and metapelites by using the pyrope component of garnets). 21 pp., Eigenverlag, Wien.
http://members.a1.net/andreas.ertl/ertl(2000).pdf

Ertl., A. & Brandstätter, F. (2000): Über den „Protopartzit" bzw. „Thrombolith" aus dem Magnesitsteinbruch Veitsch, Sattlerkogel, Steiermark, Österreich. Joannea Min., 1, 27-30, Graz.

Ertl, A. & Heede, H.-U. (2000): Haben einige Eklogite der Typuslokalität in der Sau- und Koralpe außer der eo-Alpinen Metamorphose auch eine permische und eine variszische Metamorphose erlebt? Joannea Min., 1, 5-22, Graz.

Ertl, A. & Postl, W. (2000): In memoriam Peter Beck-Mannagetta 1917-1998. Joannea Min., 1, 91-94, Graz.

Ertl, A., Brandstätter, F., Schuster, R. & Thöni, M. (2000): Ein ungewöhnlich großer, magmatisch gebildeter, idiomorpher Granat aus einem mylonitisierten permischen Pegmatit aus dem Plattengneis bei Stainz, Steiermark, Österreich. Joannea Min., 1, 23-26, Graz.

Hughes, J.M., Ertl, A., Dyar, M.D., Grew, E.S., Shearer, C.K., Yates, M.G. & Guidotti, C.V. (2000): Tetrahedrally coordinated boron in a tourmaline: boron-rich olenite from Stoffhütte, Koralpe, Austria. Can. Mineral., 38, 861-868.

Ertl, A. & Wagner, A. (2001): Fluorit und Magnetit von der Loja bei Persenbeug, NÖ. – MEFOS (Vereinsmitteilungen VOÖM), 22, 17-18, Wien.

Ertl, A., Hughes, J.M. & Marler, B. (2001): Empirical formulae for the calculation of <T-O> and X-O2 bond lengths in tourmaline and relations to tetrahedrally-coordinated boron. N. Jb. Miner. Mh., 2001(12), 548-557.

Ertl, A., Marler, B. & Pertlik, F. (2001): Kristallchemische Überlegungen zur Besetzung „nichttetraedrischer“ Kationenpositionen durch Silizium im Strukturtyp Turmalin. Mitt. Österr. Miner. Ges., 146, 72-74.

Ertl, A., Pertlik, F. & Bernhardt, H.-J. (2001): Hellblaue Olenit-Schörl-Dravit Mischkristalle von Ebersdorf, Niederösterreich: Chemismus und Kristallstruktur. Mitt. Österr. Miner. Ges., 146, 75-77.

Kalt, A., Schreyer, W., Ludwig, T., Prowatke, S., Bernhardt, H.-J. & Ertl, A. (2001): Complete solid solution between magnesian schorl and lithian excess-boron olenite in a pegmatite from Koralpe (eastern Alps, Austria). Eur. J. Mineral., 13, 1191-1205.

Ertl, A. & Hughes, J.M. (2002): The crystal structure of an aluminum-rich schorl overgrown by boron-rich olenite from Koralpe, Styria, Austria. Mineral. Petrol., 75, 1-2, 69-78.

Ertl, A. & Wagner, A. (2002): Bläulicher Turmalin (Olenit) und Gipskristalle aus einem Pegmatit bei Ebersdorf, NÖ. MEFOS (Vereinsmitteilungen VOÖM), 25, 7-8, Wien.

Ertl, A., Hughes, J.M., Pertlik, F., Foit F.F. Jr., Wright, S.E., Brandstätter, F. & Marler, B. (2002): Polyhedron distortions in tourmaline. Can. Mineral., 40, 153-162.

Marler, B. & Ertl, A. (2002): Nuclear magnetic resonance and infrared spectroscopic study of excess-boron olenite from Koralpe, Styria, Austria. Am. Mineral., 87, 364-367.

Niedermayr, G., Bojar, H.-P., Brandstätter, F., Ertl, A., Ettinger, K., Hollerer, Ch.E., Leikauf., B., Moser, B., Postl, W., Taucher, J. & Walter, F. (2002): Neue Mineralfunde aus Österreich LI. Carinthia II, 192/112, 215-244.

Schreyer, W., Hughes, J.M., Bernhardt, H.-J., Kalt, A., Prowatke, S. & Ertl, A. (2002): Reexamination of olenite from the type locality: detection of boron in tetrahedral coordination. Eur. J. Mineral., 14, 935-942.

Ertl, A., Hughes, J.M., Brandstätter, F., Dyar, M.D. & Prasad, P.S.R. (2003): Disordered Mg-bearing olenite from a granitic pegmatite from Goslarn, Austria: A chemical, structural, and infrared spectroscopic study. Can. Mineral., 41, 1363-1370.

Ertl, A., Hughes, J.M., Prowatke, S., Rossman, G.R., London, D. & Fritz, E.A. (2003): Mn-rich tourmaline from Austria: structure, chemistry, optical spectra, and relations to synthetic solid solutions. Am. Mineral., 88, 1369-1376.

Niedermayr, G., Bojar, H.-P., Brandstätter, F., Ertl, A., Leikauf., B., Moser, B., Postl, W., Schuster, R. & Schuster, W. (2003): Neue Mineralfunde aus Österreich LII. Carinthia II, 193/113, 195-216.

Pertlik, F., Ertl, A., Körner, W., Brandstätter, F. & Schuster, R. (2003): Na-rich dravite in the marbles from Friesach, Carinthia, Austria: Chemistry and crystal structure. N. Jb. Miner. Mh., 2003(6), 277-288.

Prowatke, S., Ertl, A. & Hughes, J.M. (2003): Tetrahedrally-coordinated Al in Mn-rich, Li- and Fe-bearing olenite from Eibenstein an der Thaya, Lower Austria: A chemical and structural investigation. N. Jb. Miner. Mh., 2003(9), 385-395.

Ertl, A., Hughes, J.M. & Wagner, A. (2004): Mn-reicher Olenit, Mn-reicher Fluorapatit, Topas, Kassiterit und rosa Muskovit aus einem Pegmatit bei Eibenstein an der Thaya, NÖ. MEFOS (Vereinsmitteilungen VOÖM), 28, 6-9, Wien.

Ertl, A., Pertlik, F., Dyar, M.D., Prowatke, S., Hughes, J.M., Ludwig, T. & Bernhardt, H.-J. (2004): Fe-rich Olenite with tetrahedrally coordinated Fe^{3+} from Eibenstein, Austria: Structural, chemical, and Mössbauer data. Can. Mineral., 42, 1057-1063.

Ertl, A., Schuster, R., Prowatke, S., Brandstätter, F., Ludwig, T., Bernhardt, H.-J., Koller, F. & Hughes J.M. (2004): Mn-rich tourmaline and fluorapatite in a Variscan pegmatite from Eibenstein an der Thaya, Bohemian massif, Lower Austria. Eur. J. Mineral., 16, 551-560.

Hughes, J.M., Ertl, A., Bernhardt, H.-J., Rossman, G.R. & Rakovan, J. (2004): Mn-rich fluorapatite from Austria: Crystal structure, chemical analysis, and spectroscopic investigations. Am. Mineral., 89, 629-632.

Hughes, J.M., Ertl, A., Dyar, M.D., Grew, E.S., Wiedenbeck, M. & Brandstätter, F. (2004): Structural and chemical response to varying $^{[4]}B$ content in zoned Fe-bearing olenite from Koralpe, Austria. Am. Mineral., 89, 447-454.

Marschall, H.R., Ertl, A., Hughes, J.M. & McCammon, C. (2004): Metamorphic Na- and OH-rich disordered dravite with tetrahedral boron, associated with omphacite, from Syros, Greece: chemistry and structure. Eur. J. Mineral., 16, 817-823.

Niedermayr, G., Bernhard, F., Bojar, H.-P., Brandstätter, F., Ertl, A., Ettinger, K., Hammer, V.M.F., Hauzenberger, C., Kickmayer, B., Leikauf., B., Moser, B., Postl, W., Sabor, M. & Walter, F. (2004): Neue Mineralfunde aus Österreich LII. Carinthia II, 194/114, 217-257.

Ertl, A., Pertlik, F., Prem, M., Post, J.E., Kim, S.J., Brandstätter, F. & Schuster, R. (2005): Ranciéite crystals from Friesach, Carinthia, Austria. Eur. J. Mineral., 17, 163-172.

Ertl, A., Rossman, G.R., Hughes, J.M., Prowatke, S. & Ludwig, T. (2005): Mn-bearing "oxy-rossmanite" with tetrahedrally-coordinated Al and B from Austria: structure, chemistry, and infrared and optical spectroscopic study. Am. Mineral., 90, 481-487.

Fuchs, Y., Ertl, A., Hughes, J.M., Prowatke, S., Brandstätter, F. & Schuster, R. (2005): Dumortierite from the Gföhl unit, Lower Austria: chemistry, structure, and infra-red spectroscopy. Eur. J. Mineral., 17, 173-183.

Niedermayr, G., Auer, C., Bernhard, F., Bojar, H.-P., Brandstätter, F., Ertl, A., Ettinger, K., Hammer, V.M.F., Leikauf., B., Postl, W., Sabor, M., Schuster, R., Seemann, R. & Walter, F. (2005): Neue Mineralfunde aus Österreich LIV. Carinthia II, 195/115, 277-315.

Cempírek, J., Novák, M., Ertl, A., Hughes, J.M., Rossman, G.R. & Dyar, M.D. (2006): Fe-bearing olenite with tetrahedrally coordinated Al from an abyssal pegmatite of the Bohemian massif at Kutná Hora: Structure, crystal chemistry, and optical spectra. Can. Mineral., 44, 23-30.

Ertl, A. (2006): Über die Etymologie und die Typlokalitäten des Minerals Schörl. Mitt. Österr. Miner. Ges., 152, 7-16.

Ertl, A. & Wagner, A. (2006): Topas, Beryll und Ferrotantalit aus einem Pegmatit bei Heidenreichstein, Niederösterreich. Eigenverlag, Wien. http://members.a1.net/andreas.ertl/ertl&wagner(2006).pdf

Ertl, A., Hughes, J.M., Prowatke, S., Ludwig, T., Prasad, P.S.R., Brandstätter, F., Körner, W., Schuster, R., Pertlik, F. & Marschall, H. (2006): Tetrahedrally-coordinated boron in tourmalines from the liddicoatite-elbaite series from Madagascar: Structure, chemistry, and infrared spectroscopic studies. Am. Mineral., 91, 1847-1856.

Ertl, A., Kolitsch, U., Prowatke, S., Dyar, M.D. & Henry, D.J. (2006): The F-analogue of schorl from Grasstein, Trentino – South Tyrol, Italy: crystal structure and chemistry. Eur. J. Mineral., 18, 583-588.

Ertl, A., Rossman, G.R., Hughes, J.M., Wang, Y., O'Leary, J., Dyar, M.D., Prowatke, S. & Ludwig, T. (2006): Elbaite from the Himalaya Mine, Mesa Grande, California. Gems & Gemol., 42, 96.

London, D., Ertl, A., Hughes, J.M., Morgan VI, G.B., Fritz, E.A. & Harms, B.S. (2006): Synthetic Ag-rich tourmaline: structure and chemistry. Am. Mineral., 91**,** 680-684**.**

Ulrych, J., Nižňanský, D., Pertlik, F., Giester, G., Ertl, A. & Brandstätter, F. (2006): Clinopyroxene from an alkali pyroxenite xenolith, Loučná-Oberwiesenthal Volcanic Centre, Bohemian Massif: crystal chemistry and structure. Geol. Quart., 50, 257-264.

Ertl, A. (2007): Über die Typlokalität und die Nomenklatur des Minerals Dravit. Mitt. Österr. Miner. Ges., 153, 23-29.

Ertl, A. & Prem, M. (2007): Late-stage hydrothermal alteration products occurring in the Stewart Mine, San Diego Co., California, U.S.A. Mitt. Österr. Miner. Ges., 153, 11-12.

Ertl, A. & Rossmann, G.R. (2007): Preliminary study of higher-temperature treatment of canary tourmaline. Gems & Gemol., 44, 322.

Ertl, A., Hughes, J.M., Prowatke, S., Ludwig, T., Brandstätter, F., Körner, W. & Dyar, M.D. (2007): Tetrahedrally-coordinated boron in Li-bearing olenite from "mushroom" tourmaline from Momeik, Myanamar: Structure and chemistry. Can. Mineral., 45, 891-899.

Ertl, A., Prem, M. & Lein, R. (2007): Beobachtungen zum Mineralbestand und zur Magnesitgenese im Salzbergbau Bad Ischl (Oberösterreich). Mitt. Österr. Miner. Ges., 153, 13-16.

Ertl, A. (2008): About the nomenclature and the type locality of elbaite: A historical review. Mitt. Österr. Miner. Ges., 154, 35-44.

Ertl, A. (2008): Röntgenographische Untersuchungen an Turmalinen mit tetraedrisch koordiniertem Bor. Mitt. Österr. Miner. Ges., 154, 103-104.

Ertl, A. (2008): Die Turmaline des Waldviertels. In: Steininger, F.F. (Ed.): Waldviertel – Kristallviertel. Die steinerne Schatzkammer Österreichs – Gesteine und Mineralien des Waldviertels. Waldviertler Heimatbund, 47, 103-105, Horn – Waidhofen/Thaya.

Ertl, A. & Hamilton, M. (2008): Der Magnesit vom Eichberg bei Gloggnitz (Niederösterreich) und dessen Begleitminerale: Eine Mineralogische Studie. Mitt. Österr. Miner. Ges., 154, 53-57.

Ertl, A., Brandstätter, F. & Prem, M. (2008): Moldanubische Korundvorkommen mit Rubin und Saphir bei Drosendorf, Waldviertel, Niederösterreich. Mitt. Österr. Miner. Ges., 154, 45-51.

Ertl, A., Dyar, M.D., Hughes, J.M., Brandstätter, F., Gunter, M.E., Prem, M. & Peterson, R.C. (2008): Pertlikite, a new tetragonal Mg-rich member of the voltaite group from Madeni Zakh, Iran. Can. Mineral., 46, 823-832.

Ertl, A., Rossman, G.R., Hughes, J.M., Ma, C. & Brandstätter, F. (2008): V^{3+}-bearing, Mg-rich, strongly disordered olenite from a graphite deposit near Amstall, Lower Austria: A structural, chemical and spectroscopic investigation. N. Jb. Miner. Abh., 184, 243-253.

Ertl, A., Tillmanns, E., Ntaflos, T., Francis, C., Giester, G., Körner, W., Hughes, J.M., Lengauer, C. & Prem, M. (2008): Tetrahedrally-coordinated boron in Al-rich tourmaline and its relationship to the pressure-temperature conditions of formation. Eur. J. Mineral., 20, 881-888.

Post, J.E., Heaney, P.J. & Ertl, A. (2008): Rietveld refinement of the ranciéite structure using synchrotron powder diffraction data. Powder Diffraction, 23, 10-14.

Abstracts

Ertl, A. & Pertlik, F. (1998): Replacement of silicon by boron in the tetrahedral positions of phyllosilicate structures. Scripta Fac. Sci. Nat. Univ. Masaryk. Brun., 26 (1996), 67-68, Brno.

Ertl, A. (1999): Replacement of aluminum by silicon in the Z-octahedra in the structure of tourmaline. 2nd European Workshop on Tourmaline and Borosilicates, Laboratoire de Minéralogie - Cristallographie, Abstracts, September 22-24, 1999, 8, Paris.

Ertl, A. (1999): Replacement of aluminum by silicon in the Z-octahedra in the structure of tourmaline. Bull. Liaison S.F.M.C., 11, No. 3, 114-115, Paris.

Ertl, A. & Pertlik, F. (1999): Replacement of silicon by boron in tourmaline- and mica-type structures. 2nd European Workshop on Tourmaline and Borosilicates, Laboratoire de Minéralogie - Cristallographie, Abstracts, September 22-24, 1999, 9, Paris.

Ertl, A. & Pertlik, F. (1999): Replacement of silicon by boron in tourmaline- and mica-type structures. Bull. Liaison S.F.M.C., 11, No. 3, 115, Paris.

Ertl, A., Kudjelka, A., Lenitz, H. & Pertlik, F. (1999): Synopsis der Leiter des Mineralogischen Museums (= Mineralogisches Institut) der Universität Wien im 19. Jahrhundert. - Ber. Deutsch. Mineral. Ges., Beih. z. Eur. J. Mineral., 11, No. 1, 65, Stuttgart.

Hughes, J.M., Ertl, A., Dyar, M.D., Grew, E.S., Shearer, C.K. & Yates, M.G. (1999): Boron in the tourmaline tetrahedral site: Chemistry and structure of a boron-rich olenite. 2nd European Workshop on Tourmaline and Borosilicates, Laboratoire de Minéralogie - Cristallographie, Abstracts, September 22-24, 1999, 12, Paris.

Hughes, J.M., Ertl, A., Dyar, M.D., Grew, E.S., Shearer, C.K. & Yates, M.G. (1999): Boron in the tourmaline tetrahedral site: Chemistry and structure of a boron-rich olenite. Bull. Liaison S.F.M.C., 11, No. 3, 117, Paris.

Kalt, A., Schreyer, W., Bernhardt, H.-J. & Ertl, A. (1999): Complete solid solution between magnesian schorl and lithian excess-boron olenite in the Koralpe pegmatite. 2nd European Workshop on Tourmaline and Borosilicates, Laboratoire de Minéralogie - Cristallographie, Abstracts, September 22-24, 1999, 13-14, Paris.

Kalt, A., Schreyer, W., Bernhardt H.-J. & Ertl, A. (1999): Complete solid solution between magnesian schorl and lithian excess-boron olenite in the Koralpe pegmatite. Bull. Liaison S.F.M.C., 11, No. 3, 117-118, Paris.

Ertl, A. & Pertlik, F. (2000): Tetraedrisch koordiniertes Bor in natürlichem Turmalin und Muskovit. Ber. Deutsch. Mineral. Ges., Beih. z. Eur. J. Mineral., 12, No. 1, 42, Stuttgart.

Kalt, A., Schreyer, W., Ludwig, T., Prowatke, S., Bernhardt, H.-J. & Ertl, A. (2000): Complete solid solution between magnesian schorl and lithian excess-boron olenite in the Koralpe pegmatite (Austria). Ber. Deutsch. Mineral. Ges., Beih. z. Eur. J. Mineral., 12, No. 1, 91, Stuttgart.

Marler, B., Ertl, A., Wolf, I., Löffler, E. (2001): NMR and infrared spectroscopic study of excess-boron tourmaline from Koralpe, Styria, Austria. Ber. Deutsch. Mineral. Ges., Beih. z. Eur. J. Mineral., 13, No. 1, 117, Stuttgart.

Hughes, J., Ertl, A., Dyar, D., Grew, E. & Brandstätter, F. (2002): Structural and chemical response to varying $^{[4]}$B content in olenite from Koralpe, Austria. EMPG IX, Ninth International Symposium on Experimental Mineralogy, Petrology and Geochemistry, Zürich, Switzerland, 24.-27.3., Journal of Conference Abstracts, 7 (1), 47-48.

Schreyer, W., Ertl, A., Hughes, J., Bernhardt, H.-J., Kalt, A. & Prowatke, S. (2002): Tetrahedral boron in olenite from the type locality: A chemical and structural investigation. EMPG IX, Ninth International Symposium on Experimental Mineralogy, Petrology and Geochemistry, Zürich, Switzerland, 24.-27.3., Journal of Conference Abstracts, 7 (1), 97.

Ertl. A. (2003): *Contribution to* „Festschrift Josef Zemann". Mitt. Österr. Miner. Ges., 148, 36.

Ertl, A. & Hughes, J.M. (2003): Tetrahedrally-coordinated boron in liddicoatite from Madagascar. LERM 2003, International Symposium on Light Elements in Rock-forming Minerals, Nové Město na Moravě, Czech Republic, 20.-25.6., Book of Abstracts, 16.

Hughes, J.M., Ertl, A. & Prowatke, S. (2003): Mn-rich tourmaline from the Moldanubicum in Austria: Structure and chemistry. LERM 2003, International Symposium on Light Elements in Rock-forming Minerals, Nové Město na Moravě, Czech Republic, 20.-25.6., Book of Abstracts, 32.

Ertl, A. & Pertlik, F. (2007): Wechselwirkung zwischen dem Al-Gehalt der Y-Position und dem B-Gehalt der T-Position in Turmalinen: Ein Beitrag zur Kristallchemie. Mitt. Österr. Miner. Ges., 153, MinPet 2007, ÖMG & Geologischer Dienst der Autonomen Provinz Bozen, 16.-21. Sept., Meran, Italy, 41.

Ertl, A. & Tillmanns, E. (2007): Werner Schreyer's experiments on synthetic B-rich high-pressure tourmalines and micas. Journal of Conference Abstracts, Goldschmidt Conference, Goldschmidt 2007, August 20-24, University of Cologne, A261.

Ertl, A. & Tillmanns, E. (2008): Al- and $^{[4]}$B-Rich tourmaline from the Sahatany Pegmatite Field, Madagascar, and its relevance on a new barometer. Journal of Conference Abstracts, Goldschmidt 2008 - "from Sea to Sky", July 13-18, Vancouver, Canada, A247.

Posters and Talks

1998, 13. Nov.: Lecture (in German) at the ***University Graz, Graz, Styria, Austria,*** Institut für Mineralogie-Kristallographie und Petrologie for the *„1. Kor-Saualm Workshop"* about boron-rich olenite from Koralpe: *„Interpretation der Mineralogie von Turmalin mit Relevanz zur metamorphen Entwicklung des Koralpen Kristallins" (Interpretation of the chemical composition from tourmaline in relation to the metamorphic evolution of the Koralpe).*

1999, 22. Sept.: Lecture (in Englisch) at the ***Université Pierre et Marie Curie, Paris***, ***France,*** Laboratoire de Minéralogie – Cristallographie, for the *„2nd European Workshop on Tourmaline and Borosilicates"* about *„Replacement of silicon by boron in tourmaline- and mica type structures"*.

1999, 23. Sept.: Lecture (in Englisch) at the ***Université Pierre et Marie Curie, Paris***, ***France,*** Laboratoire de Minéralogie – Cristallographie, for the *„2nd European Workshop on Tourmaline and Borosilicates“* about *„Replacement of aluminum by silicon in the Z-octahedra in the structure of tourmaline“*.

2000, 28. Sept.: Lecture (in German) and posterpresentation at the ***University Heidelberg, Heidelberg, Germany***, for the *DMG-Tagung* about *„Tetraedrisch koordiniertes Bor in natürlichem Turmalin und Muskovit“ (tetrahedrally-coordinated boron in natural tourmaline and muscovite)*.

2001, 27. May: Lecture (in German) at the ***University Vienna, Vienna, Austria,*** Geozentrum, about *„Pegmatite in der Koralpe – Vierkoordiniertes Bor im Turmalin“ (Pegmatites from the Koralpe – four-coordinated boron in tourmaline)*.

2001, 25. Sept.: Posterpresentation at the ***University Vienna, Vienna, Austria,*** Geozentrum, for the *MinPet Tagung 2001* about *„Hellblaue Olenit-Schörl-Dravit Mischkristalle von Ebersdorf, Niederösterreich“ (lightblue olenite-schorl-dravite tourmaline crystals from Ebersdorf, Lower Austria)* (Ertl, Pertlik & Bernhardt).

2002, 25. March: Posterpresentation at the ***Eidgenössische Technische Hochschule (ETH), Zürich, Switzerland,*** for the *„Ninth International Symposium on Experimental Mineralogy, Petrology and Geochemistry – EMPG IX“* about *„Tetrahedral boron in olenite from the type locality“* (Schreyer, Ertl, Hughes, Bernhardt, Kalt & Prowatke) and co-author of the poster *„Structural and chemical response to varying $^{[4]}$B content in olenite from the Koralpe“* (Hughes, Ertl, Dyar, Grew & Brandstätter).

2002, 13. Nov.: Lecture (in Englisch) at the ***Miami University, Oxford, Ohio, U.S.A.,*** Shideler Hall, about *„Tetrahedral boron in tourmalines, where it is, and how to find it“*.

2003, 20.-23. June: Posterpresentation at the *„International Symposium on Light Elements in Rock-forming Minerals – LERM 2003“* in ***Nové Město na Moravě, Moravia, Czech Republic****,* about *„Tetrahedrally-coordinated boron in liddicoatite from Madagascar”* (Ertl & Hughes) and co-author of the poster *„Mn-rich tourmaline from the Moldanubicum in Austria: Structure and chemistry”* (Hughes, Ertl, Prowatke & Rossman).

2003, 20. Nov.: Lecture (in Englisch) at the ***Comenius University, Bratislava, Slovakia,*** Mlynská dolina, Faculty of Natural Sciences, Room B1-501, about *“Tourmaline – unusual compositions and interesting structural details”*.

2004, 30. March: Lecture (in Englisch) at the ***Miami University, Oxford, Ohio, U.S.A.,*** Shideler Hall (12:00 am), about “*Tourmaline – News from the tourmaline group”*.

2004, 5. April: Lecture (in Englisch) at the ***University of Massachusetts, South Hadley, Massachusetts, U.S.A.,*** Morrell Science Building (10:10 am), about "*Tourmaline – News from the tourmaline group".*

2004, 12. April: Lecture (in Englisch) at the ***American Museum of Natural History, New York City, New Jersey, U.S.A.,*** (1:00 pm), about "*Tourmaline – News from the tourmaline group".*

2004, 14. April: Lecture (in Englisch) at the ***Smithsonian Institution, National Museum of Natural History, Washington, D.C., U.S.A.,*** NMNH, Fourth Floor East Wing, Mineral Sciences Seminar Room, E410 (10:00 am), about "*Tourmaline – News from the tourmaline group".*

2004, 20. April: Lecture (in Englisch) at the ***Louisiana State University, Baton Rouge, Louisiana, U.S.A.,*** Howe-Russell Geoscience Complex, E208 (3:30 pm), about "*Tourmaline – News from the tourmaline group".*

2004, 23. April: Lecture (in Englisch) at the ***University of Oklahoma, Norman, Oklahoma, U.S.A.,*** Sarkeys Energy Center, Room 830 (9:00 am), about "*Tourmaline – News from the tourmaline group".*

2004, 30. April: Lecture (in Englisch) at the ***Pasadena City College, Pasadena, California, U.S.A.,*** Building E, Room 220 (7:30 pm), for the Mineralogical Society of Southern California, about "*Tourmaline – News from the tourmaline group".*

2005, 3. June: Lecture (in German) at the ***University of Vienna, Vienna, Austria,*** Geozentrum, Room 2A122 (11:15 am), about *"Zur Struktur Al-reicher Turmaline" (About the structure of Al-rich tourmaline)*.

2006, 5. May: Lecture (in German) at the ***University of Vienna, Vienna, Austria,*** Geozentrum, Room 2A122 (11:15 am), about *"Dumortierit und seine Substitutionen" (Dumortierite and its substitutions)*.

2006, 26. Aug.: Lecture (in English) at the ***Manchester Grand Hyatt San Diego Hotel, San Diego, California, U.S.A.,*** Randle Ballroom A/B (11:50 am), for the *"Gemological Research Conference (GRC)"* (hosted by GIA) about *"Elbaite from the Himalaya Mine, Mesa Grande, California"* (General Gemology).

2006, 1. Dec.: Lecture (in German) at the ***University of Vienna, Vienna, Austria,*** Geozentrum, Room 2A122 (11:15 am), about *"Turmaline der Liddicoatit-Elbait Reihe" (Tourmalines from the liddicoatite-elbaite series).*

2007, 31. May: Lecture (in German) at the ***University of Vienna, Vienna, Austria,*** Geozentrum, Room 2B204 (Eberhard Clar-Saal) (3:30 pm), about *"Al- und B-reiche Turmaline: Mineralogie und Vorkommen" (Al- and B-rich tourmalines: Mineralogy and occurrence)*.

2007, 23. Aug.: Lecture (in English) at the ***University of Cologne, Cologne, Germany,*** Room A3 (16:00 am), for the 17th V. M. Goldschmidt Conference (19th – 24th Aug. 2007) about *"Werner Schreyer's experiments on synthetic B-rich high-pressure tourmalines and micas"* (Ertl & Tillmanns).

2007, 18. Sept.: Posterpresentation at the ***Hotel Steigenberger Therme Meran, Meran, South Tyrol, Italy,*** for the MinPet2007 (16th – 21st Sept. 2007), about "*Wechselwirkung zwischen dem Al-Gehalt der Y-Position und dem B-Gehalt der T-Position in Turmalinen: Ein Beitrag zur Kristallchemie"* (Ertl & Pertlik).

2007, 24. Sept.: Lecture (in English) at the ***McGill University, Montréal, Québec, Canada,*** Earth & Planetary Sciences, Frank Dawson Adams Building, Room 232 (3:15 pm), about *"The wide range of tourmaline chemical composition and what it tells us about the environment of crystallization"*.

2007, 25. Sept.: Lecture (in English) at the ***University of Vermont, Burlington, Vermont, U.S.A.,*** Department of Geology, Delehanty Hall, Room 219 (12:15 pm), about *"The wide range of tourmaline chemical composition and what it tells us about the environment of crystallization"*.

2007, 28. Sept.: Lecture (in English) at the ***University of Maine, Orono, Maine, U.S.A.,*** Department of Earth Sciences, Edward Bryand Global Sciences Center, Room 100 (3:00 pm), about *"The wide range of tourmaline chemical composition and what it tells us about the environment of crystallization"*.

2007, 1. Oct.: Lecture (in English) at the ***Smithsonian Institution, National Museum of Natural History, Washington, D.C., U.S.A.,*** Department of Mineral Sciences, Fourth Floor East Wing, Conference Room (10:15 am), about *"Tourmaline minerals"*.

2008, 21. April: Lecture (in German) at the ***University of Heidelberg, Heidelberg, Germany***, Mineralogisches Institut, INF 235, Großer Hörsaal (5:15 pm)**,** about *"Turmaline unterschiedlicher Lithologien: Neuigkeiten über die Turmalingruppe und interessante Korrelationen"* (Geowissenschaftliches Kolloquium).

2008, 23. April: Lecture (in German) at the ***Ruhr-University Bochum, Bochum, Germany****,* Institut für Mineralogie, Gebäude NA, Hörsaal 3/99 (12:15 am)**,** about *"Turmaline unterschiedlicher Lithologien: Neuigkeiten über die Turmalingruppe und interessante Korrelationen"* (Geowissenschaftliches Kolloquium - GMG Kolloquium).

2008, 17. July: Poster at the ***University of British Columbia, Vancouver, Canada,*** for the 18th V. M. Goldschmidt Conference (13th – 18th July 2008) about *"Al- and $^{[4]}$B-rich tourmaline from the Sahatany pegmatite field, Madagascar and its relationship to the pressure-temperature conditions"* (Ertl & Tillmanns).

2008, 24. Oct.: Lecture (in German) at the ***University of Vienna, Vienna, Austria,*** Geozentrum, Room 2A120 (11:15 am), about *"Metamorphe Turmaline und deren Bedeutung" (Metamorphic tourmalines and their significance)*.

2009, 15. Jan.: Lecture (in German) at the ***University Karlsruhe (TH), Karlsruhe, Germany,*** about ***"****Turmaline - eine bedeutende Mineralgruppe" (Tourmaline – an important mineral group).*

PART 2 – Publications

This part contains the following papers, focusing on the characterisation of tourmalines, which were published in international refereed journals. These papers were submitted and published within the time of my Ph.D. study. The right column shows the amount of contribution to each paper by A. Ertl in percent.

Publication	percent-age
Ertl, A., Rossman, G.R., Hughes, J.M., Ma, C. & Brandstätter, F. (2008): V^{3+}-bearing, Mg-rich, strongly disordered olenite from a graphite deposit near Amstall, Lower Austria: A structural, chemical and spectroscopic investigation. N. Jb. Miner. Abh., 184, 243-253.	90%
Ertl, A., Tillmanns, E., Ntaflos, T., Francis, C., Giester, G., Körner, W., Hughes, J.M., Lengauer, C. & Prem, M. (2008): Tetrahedrally-coordinated boron in Al-rich tourmaline and its relationship to the pressure-temperature conditions of formation. Eur. J. Mineral., 20, 881-888.	95%

N. Jb. Miner. Abh.
2008, Vol. 184/3, p. 243–253, Stuttgart, March 2008, published online 2008

V^{3+}-bearing, Mg-rich, strongly disordered olenite from a graphite deposit near Amstall, Lower Austria: A structural, chemical and spectroscopic investigation

Andreas Ertl, George R. Rossman, John M. Hughes, Chi Ma and Franz Brandstätter

With 4 figures and 6 tables

Abstract: An optical absorption spectrum, structural and chemical data of green V- and Cr-bearing tourmaline from the graphite deposit at Weinberg Mountain, west of the village of Amstall, Lower Austria, were obtained. To address the role of V and Cr in the spectrum of tourmaline, examination of additional samples of V- and Cr-containing tourmalines was conducted. This study confirmed that V and Cr produce similar spectra in tourmalines. However, the wavelengths of the 600 nm region band (E\\c), and the 440 nm region band (E⊥c) varied in relation to the proportion of Cr in the sample. Likewise, the intensity of the 680 nm region spin-forbidden bands varies in proportion to the absolute amount of Cr in the sample. Molar absorption coefficients for both V and Cr in tourmaline were determined for the 600 nm region. For the E⊥c band, ε(V) = 12.3 ± 0.7; ε(Cr) = 39.7 ± 1.4; and for the E\\c band, ε(V) = 11.9 ± 2.0; ε(Cr) =15.9 ± 2.8. In each case the Cr bands are more intense than the corresponding V band.

These features can be used to confirm that the spectroscopic features of the Amstall tourmaline come dominantly from V. The optimized formula, calculated using structural and chemical data for the core of a 4 mm wide crystal, is $^{X}(Na_{0.69}Ca_{0.16}K_{0.01}\square_{0.14})$ $^{Y}(Al_{1.46}Mg_{1.34}V^{3+}_{0.11}Ti^{4+}_{0.05}Cr^{3+}_{0.02}Fe_{0.02})$ $^{Z}(Al_{4.77}Mg_{1.23})$ $(BO_3)_3$ $^{T}(Si_{5.70}Al_{0.30})$ O_{18} $[(OH)_{3.87}O_{0.13}]$, with a = 15.984(2), c = 7.222(2) Å, R = 0.017. The optimized formula, calculated using structural and chemical data for the rim, is $^{X}(Na_{0.67}Ca_{0.24}K_{0.01}\square_{0.08})$ $^{Y}(Al_{1.57}Mg_{1.24}V^{3+}_{0.11}Ti^{4+}_{0.05}Cr^{3+}_{0.02}Fe_{0.01})$ $^{Z}(Al_{4.84}Mg_{1.16})$ $(BO_3)_3$ $^{T}(Si_{5.90}Al_{0.10})$ O_{18} $[(OH)_{3.35}O_{0.65}]$, with a = 15.9175(5), c = 7.1914(4) Å, R = 0.014. Whereas the V^{3+} and Cr^{3+} contents stay constant, Mg decreases from the core to the rim. This is reflected by decreasing <*Y*-O> (from 2.013 to 2.003 Å) and <*Z*-O> distances (from 1.938 to 1.930 Å). The relative short <*Y*-O> distances and the enlarged <*Z*-O> distances show that Al and Mg are strongly disordered between the *Y* and *Z* sites in this tourmaline. We assume that the strong Mg-Al disorder between the *Y* and the *Z* sites in this tourmaline derived from a high-*T* overprint (~750 °C, ~6–9 kbar) during crystallization, which is supported by a relatively high amount of $^{[4]}$Al and low vacancies at the *X* site.

Key words: V-bearing, Mg-rich olenite, optical spectrum, crystal structure, chemical analyses, disorder.

Introduction

Green, vanadium-bearing, magnesium-rich tourmaline from the mountain Weinberg, approximately 500 m west of the village of Amstall, Lower Austria, occurs in small quartz-feldspar dikes in graphite schist. Ertl (1995), in his summary of the mineral paragenesis from this large graphite deposit, gave unit-cell parameters and the results of semi-quantitative chemical analyses, but in the preliminary report those author did not note that these tourmaline samples are vanadium-bearing. From the same locality, Hughes et al. (Submitted) described V-rich $2M_1$ muscovite with the highest reported V^{3+} content noted in that phase to date (V_2O_3 = 11.35 wt%).

Hawthorne & Henry (1999) gave the general chemical formula of the tourmaline-group minerals as $X\ Y_3\ Z_6\ [T_6O_{18}]\ (BO_3)_3\ V_3\ W$ [*V* site = O3 site, *W* site = O1 site]. The *Z* site in tourmaline can be occupied by Al, Mg, Fe^{3+}, V^{3+} and Cr^{3+}. The substitution of Al for Mg at the *Z* site was described by Grice & Ercit (1993), Hawthorne et al. (1993), MacDonald & Hawthorne (1995), Taylor et al. (1995), Bloodaxe et al. (1999), Ertl et al. (2003a), Bosi & Lucchesi (2004), and Bosi et al. (2004).

Vanadium-containing tourmalines, including gem varieties, have previously been described from Kenya and Tanzania (Bassett 1953, Zwaan 1974). Their spectroscopy and other properties were studied in detail by Schmetzer (1978, 1982), Schmetzer & Bank (1979), and Platonov & Tarashchan (1973).

DOI: 10.1127/0077-7757/2008/0100
0077-7757/08/0100 $ 2.75

The structure of V-rich dravite was first described by Foit & Rosenberg (1979). Structures and chemistry of V-bearing to V-rich (and Cr-rich) tourmalines from Siberia, Russia, were recently described by Bosi & Lucchesi (2004) and Bosi et al. (2004).

Regional geology and description of mineralogy of the quartz-feldspar dikes

The graphite deposit near Amstall occurs within the Bunte Series (tectonic Drosendorf unit) of the Austrian part of the Moldanubian zone (see sampling area in Fig. 1). Petrakakis et al. (1999) suggested that the Bunte Series is an old segment of crust containing a composite Proterozoic gneissic basement overlain by a late Proterozoic and/to Silurian, shelf and slope-derived, pelite- and carbonate-rich, volcano-sedimentary succession. Graphite from this deposit, which is silica-rich, originated due to metamorphosis of sapropel and shows a higher degree of crystallinity (Holzer 1963, 1964, Holzer & Zirkl 1962, Zirkl 1961). Graphite is also a characteristic mineral in the gneisses, quarzites, and marbles of the Bunte Serie (Petrakakis et al. 1999). *PT* estimates of the metamorphic conditions derived from typical Grt+Sil+Kfs+Bt-gneisses and some Grt+Opx-amphibolites were given

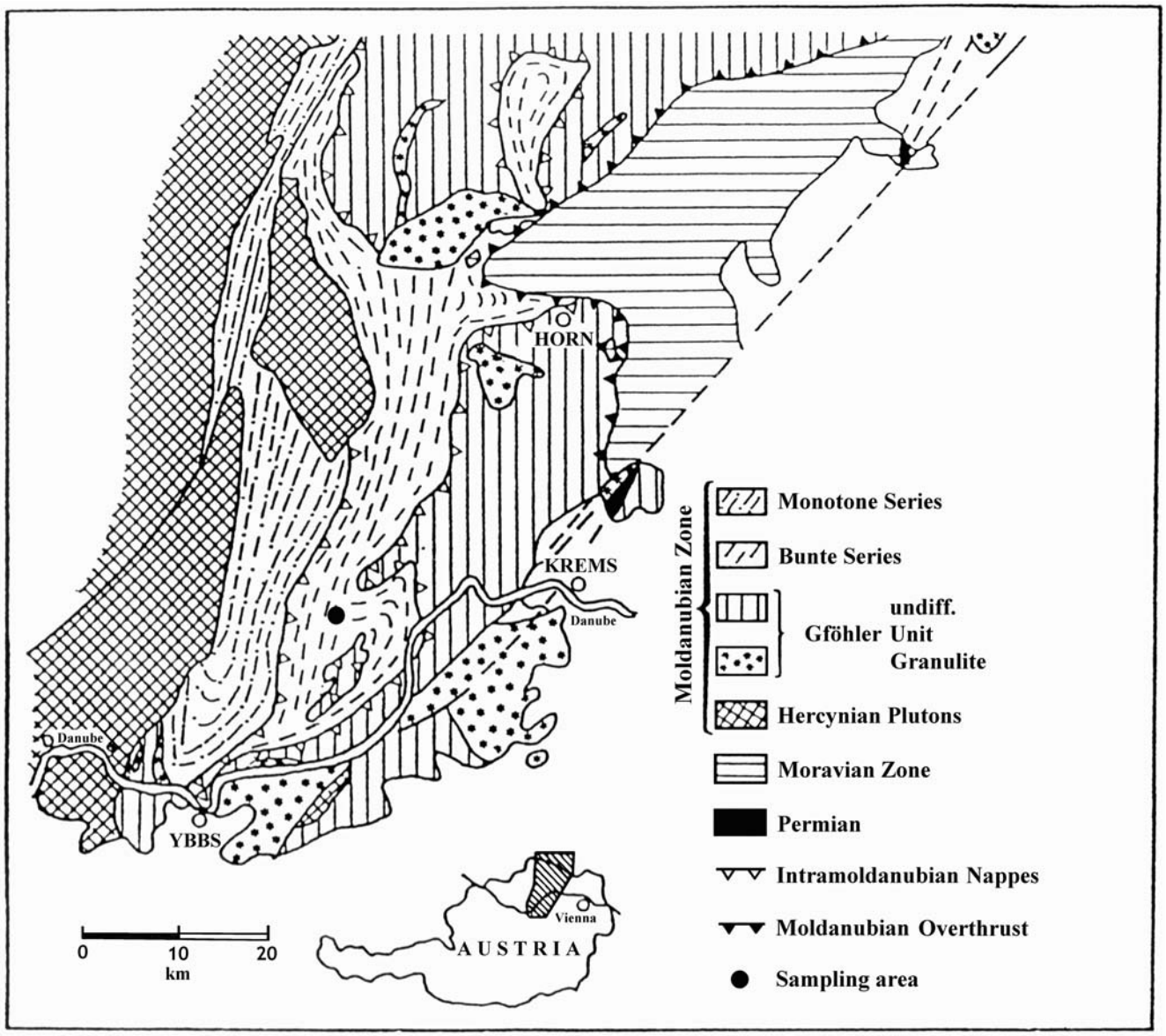

Fig. 1. Simplified geological map of the Austrian part of the Moldanubian zone after Scharbert & Fuchs (1981) and Petrakakis & Jawecki (1995).

from PETRAKAKIS (1997) and PETRAKAKIS et al. (1999) as 7–11 kbar/700–800 °C (a_{H2O}<<1; see also PETRAKAKIS & JAWECKI 1995). This Variscan MP/HT event (around 340 Ma) was accompanied by strong decompression-induced anatexis of fertile lithologies (PETRAKAKIS et al. 1999). An overview of the geochronological data is given by KLÖTZLI et al. (1999). Although the graphite deposit is also assumed to be of Proterozoic origin, the quartz-feldspar dikes (containing tourmaline) within the graphite schist could be related to a decompression-induced anatexis during a younger (Variscan?) metamorphic event.

The quartz-feldspar dikes contain albite, oligoclase, orthoclase, quartz, muscovite (V-bearing to V-rich), sillimanite, pyrite, jarosite, natrojarosite, rutile, titanite, apatite, vivianite, xenotime-(Y), monazite-(Ce?), allanite-(Ce), amstallite, siderite, calcite, and laumontite, (summarized by Ertl 1995). Tourmaline crystals (usually up to 2 mm in length, rarely up to 2 cm) occur sometimes in pyrite-rich quartz-feldspar dikes.

Experimental details

Sample selection

A green short prismatic tourmaline crystal (VDR0, ~1 mm in width; ~2 mm in length) from the described graphite deposit near Amstall, Lower Austria, was used for the spectroscopic investigations. Pieces from the rim (VDR1) and from the core (VDR2) were separated from a second green short prismatic tourmaline crystal (~4 mm in width, ~7 mm in length). These euhedral crystals are intergrown with feldspar and graphite and show the forms {101}, {120} and {010}. The two pieces (VDR1, VDR2) were first used for structure refinements and subsequently for chemical analysis. Samples of a variety of other green to yellow-green tourmalines from East Africa and Myanmar containing both V and Cr were selected for optical absorption studies (Table 1). They were generally clear, transparent fragments of crystals. The sample of GRR 2128 was obtained by slicing off the outermost 2 mm clear rim of an otherwise turbid crystal.

Table 1. V- and Cr-bearing tourmaline samples from different localities.

Sample	Locality and description
VDR0	Green, prismatic crystal from a graphite quarry, Amstall, west of Mühldorf, Waldviertel, Lower Austria, Austria
GRR 768	Fragments of a dark green fluor-rich uvite from an unspecified locality in Kenya
GRR 1719	Fragments of a dark green dravite crystal from an unspecified locality in Tanzania
GRR 2128	A 1.5 cm cluster of green, euhedral crystals of V-containing uvite from the Mogok region, Myanmar
GRR 2467	Fragments of a yellow-green uvite crystal from an unspecified locality in Tanzania.
GRR 2396	Crystal sections of a dark, yellowish-green fluor-rich uvite from an unspecified locality in Kenya

Optical spectra

Optical absorption spectra were obtained on a microspectrometer consisting of a 1024 element silicon diode array connected to a highly modified SpectraTech NicPlan® infrared microscope using a pair of conventional 10× objectives as objective and condenser. Polarized spectra were obtained with a calcite polarizer at a spectroscopic resolution of about 1 nm using a sampling area of 100 ×100 µm in the clearest central portion of the crystal. Doubly-polished slabs of each crystal were prepared that contained the *c*-axis in the plane of the slab. The thicknesses of the samples used for measurements are: VDR0, 0.629 mm; GRR768, 1.204 mm; GRR 1719, 2.076 mm; GRR 2128, 1.111 mm; GRR 2467, 2.258 mm. The spectrum of a synthetic, Cr-doped olenite originally presented by TARAN et al. (1993), retaken on a 0.278 mm thick sample, was provided by M.N. Taran.

Near-infrared spectra

The near-infrared spectrum of VDR0 was obtained on a Thermo-Nicolet Magna 860 FTIR using a CaF_2 beamsplitter and a LN_2-cooled MCT-A detector. The spectrum was obtained over the 9000–2500 cm^{-1} range in a 1 mm diameter region of the crystal dominated by the core portion of the crystal. Total integrated absorbance was determined in the region of the first overtone of the OH stretch using the formula $Abs_{total} = 2\times \int Abs_{(\perp c)} + \int Abs_{(\parallel c)}$. The water content was determined from an ongoing, currently unpublished study of the correlation between the integrated near-IR intensities and the total "water" contents of the tourmaline group.

Crystal structure

The same crystals (VDR1, VDR2; ~50 µm in diameter) that were used for chemical analyses were mounted on a Bruker Apex CCD diffractometer equipped with graphite-monochromated Mo $K\alpha$ radiation. Refined cell-parameters and other crystal data are listed in Table 2. Redundant

Table 2. Crystal data and results of structure refinement for V-bearing, Mg-rich olenite from Amstall, Lower Austria.

Space group: *R*3*m*	
Unit cell parameters (Å):	
VDR1: a = 15.9175(5), c = 7.1914(4)	VDR2: a = 15.984(2), c = 7.222(2)
Frame width, scan time, number of frames, detector distance: 0.20^0, 15 s, 4500, 5 cm	
Measured reflections, full sphere:	
VDR1: 11,593	VDR2: 11,527
Unique reflections; refined parameters:	
VDR1: 1,133; 94	VDR2: 1,145; 94
$R1$, $I > 4\sigma_I$:	
VDR1: 0.0136	VDR2: 0.0172
Difference peaks (+,–):	
VDR1: 0.34, 0.22	VDR2: 0.42, 0.36
Goodness-of-Fit:	
VDR1: 0.439	VDR2: 1.190

data were collected for an approximate sphere of reciprocal space, and were integrated and corrected for Lorentz and polarization factors using the Bruker program SAINT-PLUS (Bruker AXS Inc. 2001).

The structure was refined using tourmaline starting models and the Bruker SHELXTL v. 6.10 package of programs, with neutral-atom scattering factors and terms for anomalous dispersion. Refinement was performed with anisotropic thermal parameters for all non-hydrogen atoms. In Table 3, we list the atom parameters, and in Table 4, we present selected interatomic distances.

Chemical analysis

The two single crystals used for the structure refinement were analyzed with a wavelength-dispersive ARL SEMQ electron microprobe (EMP) at the Natural History Museum, Vienna, Austria (Table 5). Accelerating voltage was

Table 3. Atomic positions equivalent isotropic U for atoms in V-bearing, Mg-rich olenite from Amstall, Lower Austria.

VDR1 (rim):

ATOM	*X*	*Y*	*Z*	U_{EQ}	*OCC.*
Na	0	0	3/4	0.0179(4)	$Na_{1.030(7)}$
Si	0.80836(2)	0.81025(2)	0.9768(2)	0.00674(9)	$Si_{1.00}$
B	0.89035(6)	0.7807(1)	0.5230(3)	0.0082(3)	$B_{1.00}$
AlY	0.87652(3)	0.93826(2)	0.3416(2)	0.0110(2)	$Al_{1.014(4)}$
AlZ	0.70236(2)	0.73867(2)	0.3660(2)	0.0074(1)	$Al_{0.991(3)}$
O1	0	0	0.2073(3)	0.0115(3)	$O_{1.00}$
O2	0.93955(4)	0.87910(8)	0.4908(2)	0.0130(2)	$O_{1.00}$
O3	0.7385(1)	0.86925(5)	0.4661(2)	0.0153(2)	$O_{1.00}$
O4	0.90662(4)	0.81325(9)	0.9044(2)	0.0122(2)	$O_{1.00}$
O5	0.81610(9)	0.90805(4)	0.8835(2)	0.0125(2)	$O_{1.00}$
O6	0.80560(5)	0.81561(6)	0.1998(2)	0.0105(2)	$O_{1.00}$
O7	0.71466(5)	0.71503(5)	0.8986(2)	0.0104(2)	$O_{1.00}$
O8	0.79089(5)	0.73001(6)	0.5371(2)	0.0116(2)	$O_{1.00}$
H3	0.742(2)	0.871(1)	0.584(4)	0.039(8)	$H_{1.00}$

VDR2 (core):

ATOM	*X*	*Y*	*Z*	U_{EQ}	*OCC.*
Na	0	0	1/4	0.02086(11)	$Na_{0.996(1)}$
Si	0.19165(2)	0.18976(2)	0.0213(2)	0.0074(1)	$Si_{1.00}$
B	0.10974(7)	0.2195(1)	0.4756(3)	0.0087(3)	$B_{3.00}$
AlY	0.12378(4)	0.06189(2)	–0.3442(2)	0.0120(2)	$Al_{1.020(1)}$
AlZ	0.29770(2)	0.26139(3)	–0.3678(2)	0.0082(1)	$Al_{0.996(3)}$
O1	0	0	–0.2083(3)	0.0120(4)	$O_{1.00}$
O2	0.06066(5)	0.12132(9)	0.5077(3)	0.0136(3)	$O_{1.00}$
O3	0.2617(1)	0.13087(6)	–0.4681(3)	0.0160(3)	$O_{1.00}$
O4	0.09339(5)	0.1868(1)	0.0933(3)	0.0129(2)	$O_{1.00}$
O5	0.1841(1)	0.09203(5)	0.1142(3)	0.0131(2)	$O_{1.00}$
O6	0.19465(6)	0.18456(6)	–0.2015(2)	0.0109 (2)	$O_{1.00}$
O7	0.28527(6)	0.28488(6)	0.0996(2)	0.0110(2)	$O_{1.00}$
O8	0.20915(6)	0.27003(7)	0.4611(2)	0.0122(2)	$O_{1.00}$
H3	0.260(2)	0.130(1)	0.417(5)	0.038(9)	$H_{1.00}$

Table 4. Selected interatomic distances (Å) in V-bearing, Mg-rich olenite from Amstall, Lower Austria.

	VDR1 (rim)	**VDR2** (core)
X-		
O2 (x3)	2.501(1)	2.507(2)
O5 (x3)	2.711(1)	2.730(2)
O4 (x3)	2.804(1)	2.823(2)
Mean	**2.672**	**2.687**
Y-		
O1	1.957(1)	1.974(1)
O6 (x2)	1.9802(9)	1.992(1)
O2 (x2)	1.9973(8)	2.0057(9)
O3	2.103(1)	2.109(2)
Mean	**2.003**	**2.013**
Z-		
O8	1.8967(8)	1.9037(9)
O6	1.9015(9)	1.908(1)
O7	1.9054(8)	1.9135(9)
O8'	1.9271(8)	1.935(1)
O7'	1.9542(8)	1.9628(9)
O3	1.9933(6)	2.0021(7)
Mean	**1.930**	**1.938**
T-		
O7	1.6054(7)	1.6109(9)
O6	1.6076(9)	1.6127(11)
O4	1.6265(4)	1.6323(5)
O5	1.6422(5)	1.6480(6)
Mean	**1.6204**	**1.6260**
B-		
O2	1.375(1)	1.378(2)
O8 (x2)	1.376(2)	1.380(1)
Mean	**1.376**	**1.379**

15 kV, beam current 15 nA, and spot size 2 µm. Natural silicates and oxides were used as standards. Under the described conditions, analytical errors on all analyses are ± 3 % relative for major elements and 5 % relative for minor elements.

The amount of B_2O_3 was calculated as B = 3.00 *apfu* by assuming that there is no $^{[4]}$B in this tourmaline sample. This assumption is supported by the structure refinements and also by the <*T*-O> distances of ≥1.620 Å (Table 3). The ideal <*T*-O> bond length (*T* site fully occupied with Si) has been determined to be ~1.620 Å by various structural studies (MacDonald & Hawthorne 1995, Bloodaxe et al. 1999, Ertl et al. 2001).

The amount of H_2O was calculated based on (OH+F) = 3.5 *pfu* following the results of Novák et al. (2004) who found that the normalization of electron-microprobe data of (Fe,Mg)-rich, (Ca,Li,F)-poor tourmalines from granitic pegmatites is generally satisfied based on $(OH,F)_{3.5}O_{0.5}$. The OH content in the optimized formulae was calculated for charge-balanced formulae (see also Bosi & Lucchesi 2004). The near-infrared spectrum confirms the validity of this calculation.

Analyses of the other tourmalines were conducted with a JEOL 8200 electron microprobe at the California Institute of Technology. To optimize the analysis of the low concentrations of V and Cr, beam current of 40 nA was employed at 15 kV accelerating voltage and 10 µm defocused spot size. Standards for the analysis were albite (Na*K*α), anorthite (Ca*K*α, Al*K*α, Si*K*α), forsterite (Mg*K*α), fayalite (Fe*K*α), Cr_2O_3 (Cr*K*α), V_2O_3 (V*K*α), phlogopite (F*K*α), Mn-olivine (Mn*K*α), TiO_2 (Ti*K*α) and ZnO (Zn*K*α). Spectral interferences of V *K*α by Ti and Cr Kα by V were corrected. Analyses were processed with the CITZAF correction procedure (Armstrong 1995).

Optimization of site occupancies

Using quadratic programming methods, Wright et al. (2000) offer a method of optimizing the site occupancies of cation sites in minerals with multiply occupied cation sites; the optimized formula essentially minimizes the differences between the formula obtained from the results of the chemical analysis and that obtained by SREF. Using that method with the structure refinement and chemical data obtained in this study, the structural formulae of these tourmaline samples are:

VDR1 (rim): $^{X}(Na_{0.67}Ca_{0.24}K_{0.01}\square_{0.08})\ ^{Y}(Al_{1.57}Mg_{1.24}V^{3+}_{0.11}Ti^{4+}_{0.05}Cr^{3+}_{0.02}Fe_{0.01})\ ^{Z}(Al_{4.84}Mg_{1.16})\ (BO_3)_3\ ^{T}(Si_{5.90}Al_{0.10})\ O_{18}\ [(OH)_{3.35}O_{0.65}]$

VDR2 (core): $^{X}(Na_{0.69}Ca_{0.16}K_{0.01}\square_{0.14})\ ^{Y}(Al_{1.46}Mg_{1.34}V^{3+}_{0.11}Ti^{4+}_{0.05}Cr^{3+}_{0.02}Fe_{0.02})\ ^{Z}(Al_{4.77}Mg_{1.23})\ (BO_3)_3\ ^{T}(Si_{5.70}Al_{0.30})\ O_{18}\ [(OH)_{3.87}O_{0.13}]$

The valence state of Fe could not be obtained by Mössbauer spectroscopy due to the very low FeO content (Table 1).

Results and discussion

Cause of color. The optical spectrum of VDR0 (Fig. 2) contains absorption bands with maxima at about 438 and 608 nm (E⊥c) and 438 and 608 nm (E\\c). These positions are consistent with those observed previously in vanadium-containing tourmalines (Schmetzer 1982). The spectrum and the dominance of vanadium in the chemical analysis suggest that vanadium is the primary cause of color and is present in the 3+ oxidation state in an approximately octahedral site.

A potential complication comes from the fact that chromium is also present in the Amstall tourmaline in

Table 5. Composition of V-bearing, Mg-rich olenite from Amstall, Lower Austria (wt.%).

	VDR1 (rim)[1]	VDR1 (rim)[2]	VDR2 (core)[1]	VDR2 (core)[2]
SiO_2 wt.%	36.47	36.66	35.40	35.52
TiO_2	0.44	0.41	0.41	0.41
B_2O_3	10.82[3]	10.80	10.76[3]	10.83
Al_2O_3	34.36	34.33	34.76	34.52
Cr_2O_3	0.17	0.16	0.13	0.16
V_2O_3	0.84	0.85	0.85	0.85
FeO	0.11	0.07	0.14	0.15
MnO	0.03	–	0.03	–
MgO	10.24	10.01	10.66	10.74
CaO	1.30	1.39	0.74	0.93
Na_2O	1.94	2.15	2.11	2.22
K_2O	0.05	0.05	0.06	0.05
H_2O	3.27[4]	3.12	3.24[4]	3.62
Sum	100.04	100.00	99.29	100.00
Si *apfu*	5.85	5.90	5.73	5.70
[4]Al	0.15	0.10	0.27	0.30
Sum *T* site	6.00	6.00	6.00	6.00
[3]B	3.00	3.00	3.00	3.00
Al	6.35	6.41	6.36	6.23
Cr^{3+}	0.02	0.02	0.02	0.02
V^{3+}	0.11	0.11	0.11	0.11
Fe^{2+}	0.01	0.01	0.02	0.02
Mn	0.00	–	0.00	–
Mg	2.45	2.40	2.57	2.57
Ti	0.05	0.05	0.05	0.05
Sum *Y*, *Z* sites	8.99	9.00	9.13	9.00
Ca	0.22	0.24	0.13	0.16
Na	0.60	0.67	0.66	0.69
K	0.01	0.01	0.01	0.01
Sum *X* site	0.83	0.92	0.80	0.86
Sum cations	18.82	18.92	18.93	18.86
Sum OH	3.50[4]	3.35[5]	3.50[4]	3.87[5]

Note: [1] Average of 3 EMP analyses. [2] Wt. percent calculated from optimal site occupancies and normalized to 100%. A component is not considered significant unless its value exceeds the uncertainty. [3] B_2O_3 calculated as B = 3.00. [4] H_2O was calculated for (OH + F) = 3.5 (Novák et al. 2004). F was below the detection limit. [5] OH in the optimized formulae was calculated for charge-balanced formulae.

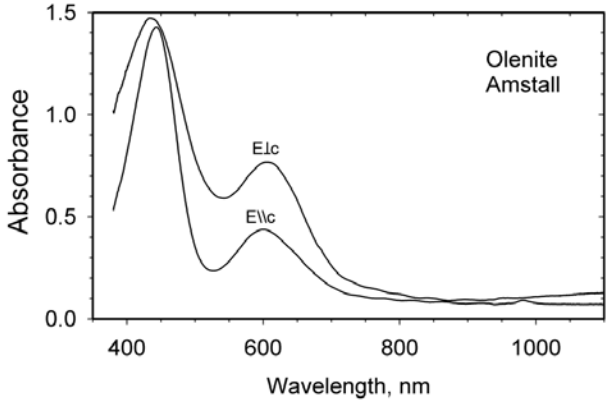

Fig. 2. Optical absorption spectrum of a 0.629 mm thick crystal of the V^{3+}-bearing, Mg-rich olenite from Amstall, Lower Austria, plotted normalized to 1.0 mm thickness.

lesser amounts. In tourmalines, chromium occurs in the 3+ oxidation state and has an optical absorption spectrum that closely resembles V^{3+} in band position. No information is available about the quantitative intensities of absorption of V^{3+} and Cr^{3+} in tourmaline.

A significant difference is the frequent obvious presence of a series of sharp bands in the 680–690 nm region (from spin-forbidden transitions) in Cr^{3+} spectra that are barely visible in V^{3+} spectra. Low intensities in the spin-forbidden region suggest that V^{3+} is the dominate cause of color in the Amstall olenite.

To address the issues regarding the role of V and Cr in the spectrum of tourmaline, examination of additional samples of V- and Cr-containing tourmalines was conducted (Table 1). Samples were chosen in the uvite-drav-

ite-olenite series that contained different concentrations of V and Cr that ranged from V-dominant to Cr-dominant. This study confirmed that V and Cr produce similar spectra in tourmalines (Fig. 3). However, the wavelengths of the 600 nm region band (E\\c), and the 440 nm region band (E⊥c) varied in relation to the proportion of Cr in the sample (Fig. 4a,b). Likewise, the intensity of the 680 nm region spin-forbidden bands varies in proportion to the absolute amount of Cr in the sample. These features are sufficiently diagnostic that they can be used to confirm that the spectroscopic features of the Amstall tourmaline come dominantly from V.

Also relevant is a spectrum of a synthetic tourmaline containing Cr^{3+} that is presented by Taran et al. (1993). Although it bears much similarity to the spectra of V^{3+} in tourmalines, there are some differences that distinguish it from the spectrum of the Amstall tourmaline. A prominent band in the Cr^{3+} spectrum is centered at 596 nm compared to 610 nm in the Amstall tourmaline as well as vanadian tourmalines from Tanzania. The sharp, spin forbidden band of Cr^{3+} occurs at 686 nm in all of the Cr^{3+} and mixed Cr^{3+} /V^{3+} tourmalines. It is significantly more intense in the synthetic Cr-containing tourmaline than it is in the Amstall tourmaline even though the Amstall tourmaline contains twice the amount of V than the synthetic tourmaline contains Cr.

This study also makes it possible to determine the molar absorption coefficient (epsilon values) for both V and Cr in the uvite-dravite-olenite series of tourmalines. Using pairs of spectra, simultaneous linear equations involving Cr and V concentrations and total absorption intensities of the E\\c and E⊥c bands in the 600 nm region were solved that yielded the epsilon values for both elements. Multiple pairs from the overdetermined equations were selected that, gratifyingly, yielded nearly the same answers for both epsilon values. For the E⊥c band, ε(V) = 12.3 ± 0.7; ε(Cr) = 39.7 ± 1.4; and for the E\\c band, the values are not as well constrained, but ε(V) = 11.9 ± 2.0; ε(Cr) =15.9 ± 2.8. In each case the Cr bands are more intense than the corresponding V band.

OH Content. The total integrated absorbance of the near-infrared OH overtones in the 7400 cm^{-1} region excluding the ~7600 cm^{-1} band, is 1270 cm^{-2}. Using this value and the calculated density (3.051) and correlations between OH content in tourmalines (Ertl et al. 2006), we estimate that the Amstall tourmaline (VDR0) has 3.32 wt% H_2O. This value lies between the calculated H_2O content (by charge balance) for the core (3.62 wt%; VDR2, Table 5) and the rim composition (3.12 wt%; VDR1, Table 5) of the larger crystal from this locality.

Compositional and structural trends. Using valid current tourmaline end-member species (Hawthorne & Henry 1999), we can describe the tourmaline samples from Amstall essentially as a solid solution of olenite and dravite components. The core sample (VDR2) consists of 49 mol% olenite and 45 mol% dravite. The rim sample (VDR1) consists of 52 mol% olenite and 41 mol% dravite. Whereas the olenite component decreases from the core to the rim, the dravite component increases.

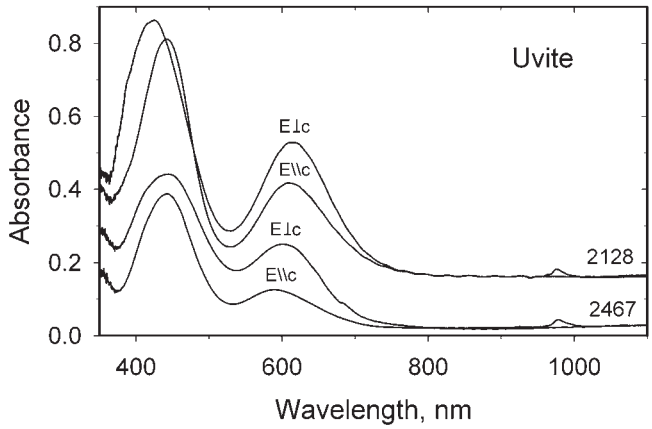

Fig. 3. Comparison of the spectra of Cr-dominant uvite (GRR 2467), and V-dominant uvite (GRR 2128), showing that the 440 nm band (E⊥c) occurs at shorter wavelength than the corresponding Cr band. Also, weak, spin-forbidden bands near 680 nm are apparent in the spectrum of the Cr-dominant uvite. All spectra plotted normalized to 1.0 mm thickness. The spectra of GRR 2128 are offset vertically for clarity.

The CaO content increases from the core to the rim (from 0.74 to 1.30 wt%; Table 1), whereas the Na_2O content does not change significantly. Also the <*X*-O> distance decreases from the core to the rim (from 2.687 to 2.672 Å). An increasing Ca content from the Fe-rich core to the Fe-poor rim was also observed in B-rich olenite (Hughes et al. 2004). Contrary to this investigation, the Fe content in our samples is constantly very low, whereas the Mg content is decreasing from the core to the rim.

Based on optical spectroscopic data, Schmetzer (1982) concluded that "in the tourmaline lattice, [there is] a preference for the smaller Al-site [*Z* site] (rather than the greater Mg-site [*Y* site]) by V^{3+}". However, the optimized formulae show that V^{3+} only occupies the *Y* sites in our tourmalines. Significant V^{3+} contents at the *Z* site were only described from a few tourmalines in the past (up to 0.22–0.38 *apfu*; Foit & Rosenberg 1979, Bosi & Lucchesi 2004, Bosi et al. 2004), whereas usually the major or the whole V^{3+} contents were assigned to the *Y* site (Foit & Rosenberg 1979, McDonald & Hawthorne 1995, Bosi & Lucchesi 2004, Bosi et al. 2004). In all these papers the <*Y*-O> distance was higher (2.020–2.048 Å) than in our samples (2.013 to 2.003 Å; Table 4), ex-

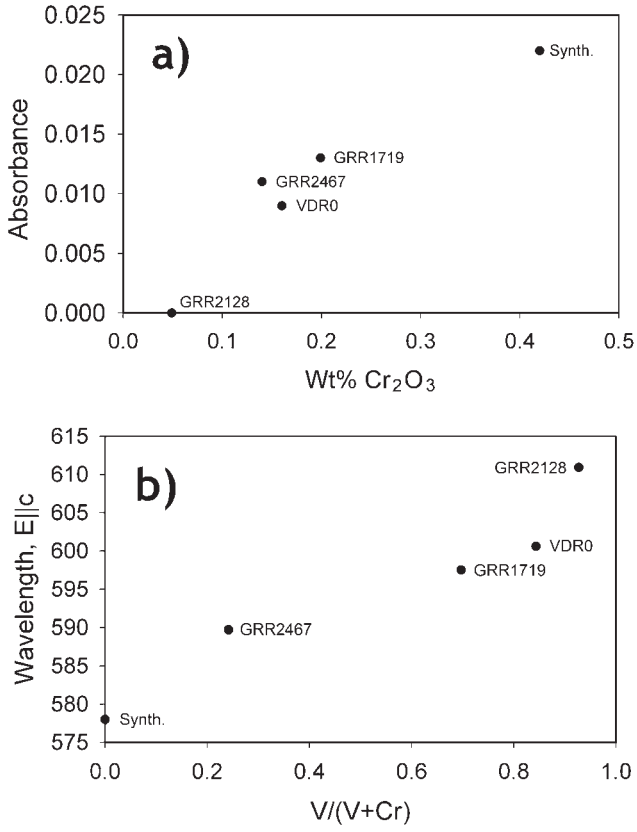

Fig. 4. Dependence of spectral features on the Cr and V content of tourmalines;
a) Absorbance normalized to 1.0 mm thickness of the spin-forbidden band (~680 nm); b) Wavelength position of the 600 nm region band (E\\c) in relation to the proportion of Cr in the tourmaline samples used for the correlations: VDR0, Synthetic, GRR 1719, GRR 2128, GRR 2467.

cept in the $^{Y}Cr^{3+}$-rich tourmalines from Bosi et al. (2004) (1.999–2.002 Å). While the small <*Y*-O> distance in our samples can be explained by relatively high Al contents, the tourmalines from Bosi et al. (2004) have no or very small amounts of Al at the *Y* site (up to 0.097 *apfu*) but are enriched in Cr^{3+} (1.740 to 2.298 *apfu* at the *Y* site). The V^{3+} content does not change significantly from the core to the rim in our Mg-rich olenite from Amstall.

The Si value of the core sample (VDR2; Table 1) with ~5.7 *apfu* is relatively low, but no tetrahedral B was found by crystal structure determination. During refinement no significant change of the scattering value could be observed by releasing the occupancy of the *T* site. In combination with the relatively high <*T*-O> distance of ~1.626 Å we conclude that, in addition to Si, only Al can occupy the *T* site in this Mg-rich tourmaline (cf. MacDonald & Hawthorne 1995). The value of ~0.3 *apfu* $^{[4]}$Al is in good agreement with the observed <*T*-O> distance (Foit & Rosenberg 1979, Ertl et al. 2001, Prowatke et al. 2003). Henry & Dutrow (1996) described 0.25 $^{[4]}$Al *apfu* from tourmalines which have been crystallized above 750 °C. Such tourmalines from high grade metapelites have relatively low vacancies (0.05±0.05) at the *X* site when they crystallized above 750 °C (Henry & Dutrow 1996). Hence, we conclude that these V-bearing tourmalines started crystallizing at temperatures ~750 °C. This is in agreement with the intensive high-*T* overprint of the rocks of the Moldanubian Bunte Series in the range 700–800 °C and 8–11 kbar (Petrakakis 1997). After an approximately isobar decompression down to ~6 kbar isotherm cooling down to ~500 °C followed (see Fig. 7 and 8 in Petrakakis 1997).

The total Mg content decreases from the core to the rim, and is reflected by decreasing <*Y*-O> (from 2.013 to 2.003 Å) and <*Z*-O> distances (from 1.938 to 1.930 Å). The relatively short <*Y*-O> distances and the enlarged <*Z*-O> distances ($^{Z}Al_{6.0}$ produces <*Z*-O> distances in the range 1.902–1.911 Å; Grice & Ercit 1993, Hughes et al. 2000, Ertl et al. 2003b, Prowatke et al. 2003), show that Al and Mg are strongly disordered in these V-bearing tourmaline samples. The tourmaline from Amstall shows the greatest amount of Mg-Al disorder between the *Y* and the *Z* sites of all investigated tourmalines to date. Tourmalines with a large amount of Mg-Al disorder between the *Y* site and the *Z* site were further reported by Ertl et al. (2003a) [up to $Al_{1.58}Mg_{0.91}$ at the *Y* site (<*Y*-O> = 2.006 Å) and $Al_{4.90}Mg_{1.10}$ at the *Z* site (<*Z*-O> = 1.926 Å)], by Bosi & Lucchesi (2004) [V-bearing tourmaline 9840f: $Al_{1.25}Mg_{1.22}$ at the *Y* site (<*Y*-O> = 2.011 Å) and $Al_{4.99}Mg_{0.99}$ at the *Z* site (<*Z*-O> = 1.930 Å)], and by Bloodaxe et al. (1999) [sample LCW 2356: $Al_{1.09}Mg_{1.52}$ at the *Y* site (<*Y*-O> = 2.022 Å) and $Al_{4.98}Mg_{1.02}$ at the *Z* site (<*Z*-O> = 1.926 Å)]. Different methods for the approximate estimation of the Mg content at the *Z* site have been published: Bloodaxe et al. (1999) described a negative correlation between Fe^{2+} on the *Y* site and Mg on *Z*. By using figure 3 from Bloodaxe et al. (1999), ~1.14 *apfu* Mg were assigned to the *Z* site for the tourmaline samples from Amstall. Ertl et al. (2003a) gave another method for approximating the Mg content at the *Z* site. Each lattice parameter for the *c-axis* corresponds to a particular Mg content at the *Z* site. The estimated ^{Z}Mg contents for the tourmaline samples from Amstall are in the range ~1.0–1.3 *apfu* Mg. By using figure 5 (variation in *c* cell constant as a function of <*Z*-O>) of Bosi & Lucchesi (2004), the estimated <*Z*-O> distances for tourmaline sample VDR1 gives ~1.927 Å (measured distance: 1.930 Å; Table 4), and for sample VDR2 it gives ~1.937 Å (measured distance: 1.938 Å; Table 4). By using the measured <*Z*-O> distances and by applying figure 3 (relationship between <*Z*-O> and *Z*-site population) of Bosi &

Table 6. Electron microprobe analyses (wt.%) of other V- and Cr-bearing tourmalines used in this study.

	GRR2128	GRR2396	GRR1719	GRR768	GRR2467	Synthetic*
Na_2O	1.19	0.98	1.51	1.25	1.13	2.17
CaO	3.29	3.46	1.15	3.26	3.16	0.00
MgO	12.61	13.24	9.68	13.74	11.31	0.03
FeO	0.011	0.064	0.002	0.004	0.033	0.15
Cr_2O_3	0.049	0.098	0.199	0.140	0.140	0.42
V_2O_3	0.614	0.294	0.452	0.244	0.044	n.a.
Al_2O_3	30.02	27.53	32.77	26.69	30.40	51.77
SiO_2	35.59	36.39	36.75	36.52	36.04	31.70
F	1.03	1.589	0.25	1.66	0.13	n.a.
MnO	0.001	0.004	0.008	0.010	0.001	0.02
TiO_2	0.16	0.49	0.28	1.02	0.898	0.00
ZnO	0.02	0.04	0.01	0.02	0.019	n.a.
Sum	84.58	84.18	83.05	84.56	83.27	86.26
V/(V+Cr)	0.92	0.75	0.67	0.64	0.22	0.00

Note: * Data (sample no. 10) from Taran et al. (1993) and personal communication (2007). n.a. = not analyzed. The localities of these samples are described in Table 1. The Mg-Al disorder between the Y and the Z sites can not be estimated in these samples without structural data.

Formula proportions

GRR2128:
$(Ca_{0.584}Na_{0.383}\square_{0.033})\ (Mg_{2.889}V^{3+}_{0.082}Ti^{4+}_{0.020}Cr^{3+}_{0.006}Fe_{0.002}Zn_{0.002})\ (Al_{5.771}Mg_{0.229})\ (BO_3)_3\ [Si_{5.902}Al_{0.098}O_{18}]\ (OH)_3\ [F_{0.54}O_{0.31}(OH)_{0.15}]$

GRR2396
$(Ca_{0.611}Na_{0.313}\square_{0.076})\ (Mg_{2.603}Ti^{4+}_{0.061}V^{3+}_{0.039}Cr^{3+}_{0.013}Fe_{0.009}Mn_{0.001}\square_{0.274})\ (Al_{5.349}Mg_{0.651})\ (BO_3)_3\ [Si_{6.00}O_{18}]\ (OH)_3\ [F_{0.83}O_{0.11}(OH)_{0.06}]$

GRR1719:
$(Na_{0.477}Ca_{0.200}\square_{0.323})\ (Mg_{2.356}Al_{0.305}V^{3+}_{0.059}Ti^{4+}_{0.034}Cr^{3+}_{0.026}Mn_{0.001}Zn_{0.001}\square_{0.218})\ Al_6\ (BO_3)_3\ [Si_{6.00}O_{18}]\ (OH)_3\ [O_{0.58}(OH)_{0.29}F_{0.13}]$

GRR768:
$(Ca_{0.574}Na_{0.398}\square_{0.028})\ (Mg_{2.530}Ti^{4+}_{0.126}V^{3+}_{0.032}Cr^{3+}_{0.018}Zn_{0.002}Mn_{0.001}Fe_{0.001}\square_{0.289})\ (Al_{5.166}Mg_{0.834})\ (BO_3)_3\ [Si_{6.00}O_{18}]\ (OH)_3\ [F_{0.86}O_{0.09}(OH)_{0.05}]$

GRR2467:
$(Ca_{0.563}Na_{0.365}\square_{0.071})\ (Mg_{2.772}Ti^{4+}_{0.108}Cr^{3+}_{0.018}V^{3+}_{0.006}Fe_{0.005}Zn_{0.002}\square_{0.089})\ (Al_{5.966}Mg_{0.034})\ (BO_3)_3\ [Si_{6.00}O_{18}]\ (OH)_3\ [O_{0.62}(OH)_{0.31}F_{0.07}]$

Synthetic:
$(Na_{0.662}\square_{0.338})\ (Al_{2.598}Cr^{3+}_{0.052}Fe_{0.020}Mg_{0.007}\square_{0.321}]\ Al_6\ (BO_3)_3\ [Si_{4.991}Al_{1.009}O_{18}]\ (OH)_3\ [O_{0.67}(OH)_{0.33}]$

Lucchesi (2004), we can estimate that the ^{Z}Mg contents for the Amstall tourmaline are in the range ~0.90–1.25 *apfu*. All these methods for approximating the Mg content at the *Z* site give results that are close. We assume that the strong Mg-Al disorder between the *Y* and the *Z* sites in the Amstall tourmaline derived from the relatively high temperature (~750 °C) during crystallization.

Ertl et al. (2002) showed that the bond-angle distortion (σ_{oct}^2) of the ZO_6 octahedron in a tourmaline is largely a function of the <*Y*-O> distance of that tourmaline, although the occupant of the O3 site (*V* site) also affects that distortion. The covariance, *r*, of <*Y*-O> and the σ_{oct}^2 of the ZO_6 octahedron is –0.991 for all investigated tourmalines that are occupied by 3 (OH) groups, including the samples from Hughes et al. (2004). The tourmaline samples from Amstall both fall on the *V* site = 3 (OH) line in figure 3 from Ertl et al. (2002), defining covariance of the relationship between the bond-angle distortion (σ_{oct}^2) of the ZO_6 octahedron and the <*Y*-O> distance. It is only possible to do a semi-quantitative estimation of the OH content of the O3 site by using this relationship. Hence, we assume that the *V* site in VDR1 and VDR2 is filled by ~3.0 (OH). The optimized formula for the core sample (VDR2) gives the *W*-site occupation with $[(OH)_{0.87}O_{0.13}]$, whereas the *W* site for the rim sample (VDR1) is occupied by $[O_{0.65}(OH)_{0.35}]$. F was below the detection limit. The refinement of VDR2 in fact shows a difference peak of +0.42 $e^-/Å^3$ in a distance of 0.57 Å from O1, which can be assigned to H1. No such peak that can be associated with H1 was found in the refinement of VDR1. Hence, we believe that the optimized values of OH for the *W* sites, which do not result from a direct water determination, are approximately correct, which is supported by the water determination of sample VDR0 by using the total integrated absorbance of the near-infrared OH overtones. Sample VDR2 needs more OH for a charge balanced formula than

VDR1, because of the higher deficiency in Si^{4+}, the higher total amount of Mg^{2+} (which is exchanged by Al^{3+}), and the lower amount of Ca^{2+}. Marschall et al. (2004) described a strongly disordered dravite (with a small amount of $^{[4]}B$) where the *W* site is almost completely occupied by OH groups.

The core sample of this V-bearing tourmaline shows that Mg-rich, Fe- and Mn-poor tourmaline with a relatively high Al content at the *Y* site (reflected by a low <*Y*-O> distance; VDR2: 2.013 Å) can have a relatively high lattice parameter *a* (~16.0 Å) when the *Z* site is occupied by a relatively high content of Mg (~1.2 *apfu*), when the <*X*-O> distance (VDR2: 2.687 Å) is relatively large, and when the <*T*-O> distance (VDR2: 1.626 Å) is significantly enlarged.

Acknowledgements

We thank Erwin Löffler, Emmersdorf an der Donau, Lower Austria, for helping with the collection of the tourmaline samples. Julius Petsch (Idar Oberstein, Germany), Herb Obodda (Short Hills, New Jersey, U.S.A.), and William F. Larson (Fallbrook, California, U.S.A.) provided samples used in this study, and Michail Taran (Kiev, Ukraine) provided additional data about his study of synthetic tourmaline. We sincerely thank Pavel Uher (Bratislava, Slovakia) and Yves Fuchs (Marne La Vallee, France) for their careful reviews of the manuscript. This work was supported in part by NSF grants EAR-0125767 and EAR-0337816 to GRR, and EAR-0003201 and EAR-9804768 to JMH.

References

Armstrong, J. T. (1995): CITZAF: a package of correction programs for the quantitative electron microbeam X-ray analysis of thick polished materials, thin films, and particles. – Microbeam Analysis **4**: 177–200.

Bassett, H. (1953): A vanadiferous variety of tourmaline from Tanganyika. – Rec. Geol. Surv. Tanganyika **3**: 93–96.

Bloodaxe, E. S., Hughes, J. M., Dyar, M. D., Grew, E. S. & Guidotti, C. V. (1999): Linking structure and chemistry in the schorl-dravite series. – Amer. Mineral. **84**: 922–928.

Bosi, F. & Lucchesi, S. (2004): Crystal chemistry of the schorl-dravite series. – Eur. J. Mineral. **16**: 335–344.

Bosi, F., Lucchesi, S. & Reznitskii, L. (2004): Crystal chemistry of the dravite–chromdravite series. – Eur. J. Mineral. **16**: 345–352.

Ertl, A. (1995): Elbait, Olenit, Dravit-Buergerit-Mischkristalle, Dravit, Uvit und ein neuer Al-Turmalin (?) von österreichischen Fundstellen. – Mitt. Österr. Miner. Ges. **140**: 55–72.

Ertl, A., Hughes, J. M. & Marler, B. (2001): Empirical formulae for the calculation of <*T*-O> and *X*-O2 bond lengths in tourmaline and relations to tetrahedrally-coordinated boron. – N. Jb. Miner. Mh. **12**: 548–557.

Ertl, A., Hughes, J. M., Pertlik, F., Foit, F. F. Jr., Wright, S. E., Brandstätter, F. & Marler, B. (2002): Polyhedron distortions in tourmaline. – Can. Mineral. **40**: 153–162.

Ertl, A., Hughes, J. M., Brandstätter, F., Dyar, M. D. & Prasad, P. S. R. (2003a): Disordered Mg-bearing olenite from a granitic pegmatite from Goslarn, Austria: A chemical, structural, and infrared spectroscopic study. – Can. Mineral. **41**: 1363–1370.

Ertl, A., Hughes, J. M., Prowatke, S., Rossman, G. R., London, D. & Fritz, E. A. (2003b): Mn-rich tourmaline from Austria: structure, chemistry, optical spectra, and relations to synthetic solid solutions. – Amer. Mineral. **88**: 1369–1376.

Ertl, A., Rossman, G. R., Hughes, J. M., Wang, Y., O'Leary, J., Dyar, M. D., Prowatke, S. & Ludwig, T. (2006): Elbaite from the Himalaya Mine, Mesa Grande, California. – Gems & Gemol. **42**: 96.

Foit, F. F. & Rosenberg, P. E. (1979): The structure of vanadium-bearing tourmaline and its implications regarding tourmaline solid solutions. – Amer. Mineral. **64**: 788–798.

Grice, J. D. & Ercit, T. S. (1993): Ordering of Fe and Mg in the tourmaline crystal structure: The correct formula. – N. Jb. Mineral. Abh. **165**: 245–266.

Hawthorne, F. C., MacDonald, D. J. & Burns, P. C. (1993): Reassignment of cation site-occupancies in tourmaline: Al-Mg disorder in the crystal structure of dravite. – Amer. Mineral. **78**: 265–270.

Hawthorne, F. C. & Henry, D. J. (1999): Classification of the minerals of the tourmaline group. – Eur. J. Mineral. **11**: 201–215.

Henry, D. & Dutrow, B. (1996): Metamorphic tourmaline and its petrologic applications. – Rev. Mineral. **33**: 503–557.

Holzer, H. (1963): Über einige weitere niederösterreichische Graphitlagerstätten. – Verh. Geol. B.-A. **1963**: 79–91.

– (1964): Die Flinzgraphitvorkommen im außeralpinen Grundgebirge Ober- und Niederösterreichs. – Verh. Geol. B.-A. **1964**: 360–371.

Holzer, H. & Zirkl, E. J. (1962): Weitere Mitteilungen über niederösterreichische Graphitlagerstätten. – Verh. Geol. B.-A. **1962**: 316–330.

Hughes, J. M., Ertl, A., Dyar, M. D., Grew, E. S., Shearer, C. K., Yates, M. G. & Guidotti, C. V. (2000): Tetrahedrally coordinated boron in a tourmaline: boron-rich olenite from Stoffhütte, Koralpe, Austria. – Can. Mineral. **38**: 861–868.

Hughes, J. M., Ertl, A., Dyar, M. D., Grew, E. S., Wiedenbeck, M. & Brandstätter, F. (2004): Structural and chemical response to varying $^{[4]}B$ content in zoned Fe-bearing olenite from Koralpe, Austria. – Amer. Mineral. **89**: 447–454.

Hughes, J. M., Ertl, A., Bernhardt, H.-J., Rakovan, J. & Rossman, G. R. (subm.): Vanadium-rich muscovite from Austria: crystal structure, chemical analysis, and spectroscopic investigations. – Can. Mineral.

Klötzli, U. S., Frank, W., Scharbert, S. & Thöni, M. (1999): The evolution of the SE Bohemian Massif based on geochronological data: a review. – Jb. Geol. B.-A. **141/4**: 377–394.

Marschall, H. R., Ertl, A., Hughes, J. M. & McCammon, C. (2004): Metamorphic Na- and OH-rich disordered dravite with tetrahedral boron, associated with omphacite, from Syros, Greece: chemistry and structure. – Eur. J. Mineral. **16**: 817–823.

MacDonald, D. J. & Hawthorne, F. C. (1995): The crystal chemistry of Si ⇔ Al substitution in tourmaline. – Can. Mineral. **33**: 849–858.

Novák, M., Povondra, P. & Selway, J. B. (2004): Schorl-*oxy-schorl* to dravite-*oxy-dravite* tourmaline from granitic pegmatites; examples from the Moldanubicum, Czech Republic. – Eur. J. Mineral. **16**: 323–333.

Petrakakis, K. (1997): Evolution of Moldanubian rocks in Austris: review and synthesis. – J. Metam. Geol. **15**: 203–222.

Petrakakis, K. & Jawecki, C. (1995): High-grade metamorphism and retrogression of Moldanubian granulites, Austria. – Eur. J. Mineral. **7**: 1183–1203.

Petrakakis, K., Klötzli, U. & Richter, W. (1999): Excursion to the Austrian part of Moldanubia. – Beih. z. Eur. J. Mineral. **11**: 61–90.

Platonov, A. N. & Tarashchan, A. N. (1973): Spectroscopy of vanadium in natural minerals. III. Absorption spectra of V^{4+} and V^{3+} complexes. – Konst. Svoistva Miner. **7**: 75–81 (in Russian).

Prowatke, S., Ertl, A. & Hughes, J. M. (2003): Tetrahedrally-coordinated Al in Mn-rich, Li- and Fe-bearing olenite from Eibenstein an der Thaya, Lower Austria: A chemical and structural investigation. – N. Jb. Miner. Mh. **9**: 385–395.

Scharbert, H. G. & Fuchs, G. (1981) Metamorphe Serien im Moldanubikum Niederösterreichs. – Fortschr. Mineral. **59**: 129–152.

Schmetzer, K. (1978): V(III) als Farbträger bei natürlichen Silikaten und Oxiden. Ein Beitrag zur Kristallchemie des Vanadiums. – Diss., Univ. of Heidelberg, Germany.

– (1982): Absorption spectroscopy and color of vanadium(3+)-bearing natural oxides and silicates – a contribution to the crystal chemistry of vanadium. – N. Jb. Mineral. Abh. **144**: 73–106.

Schmetzer, K. & Bank, H. (1979): East African tourmalines and their nomenclature. – J. Gemmology **16**: 310–320.

Taran, M. N., Lebedev, A. S. & Platonov, A. N. (1993): Optical absorption spectroscopy of synthetic tourmalines. – Phys. Chem. Minerals **20**: 209–220.

Taylor, M. C., Cooper, M. A. & Hawthorne, F. C. (1995): Local charge-compensation in hydroxyl-deficient uvite. – Can. Mineral. **33**: 1215–1221.

Wright, S. E., Foley, J. A. & Hughes, J. M. (2000): Optimization of site-occupancies in minerals using quadratic programming. – Amer. Mineral. **85**: 524–531.

Zirkl, E. J. (1961): Vorläufiger Bericht über die mineralogischen Untersuchungen einiger Graphitvorkommen aus dem niederösterreichischen Waldviertel. – Verh. Geol. B.-A. **1961**: 99–101.

Zwaan, P. C. (1974): Garnet, corundum and other gem minerals from Umba, Tanzania. – Scripta Geol. **20**: 1–41.

Received: June 20, 2007; accepted: September 14, 2007.
Responsible editor: A. Beran

Authors' addresses:

Andreas Ertl, Institut für Mineralogie und Kristallographie, Geozentrum, Universität Wien, Althanstrasse 14, 1090 Vienna, Austria. E-mail: andreas.ertl@a1.net

George R. Rossman, Division of Geological and Planetary Sciences, California Institute of Technology, Pasadena, California 91125-2500, U.S.A.

John M. Hughes, Office of the Provost, University of Vermont, 348B Waterman Building, Burlington, Vermont 05405, U.S.A.

Chi Ma, Division of Geological and Planetary Sciences, California Institute of Technology, Pasadena, California 91125-2500, U.S.A.

Franz Brandstätter, Mineralogisch-Petrographische Abteilung, Naturhistorisches Museum, Burgring 7, 1010 Vienna, Austria.

Eur. J. Mineral.
2008, **20**, 881–888
Published online September 2008

This paper is dedicated to the memory of Werner Schreyer

Tetrahedrally coordinated boron in Al-rich tourmaline and its relationship to the pressure–temperature conditions of formation

ANDREAS ERTL[1,*], EKKEHART TILLMANNS[1], THEODOROS NTAFLOS[2], CARL FRANCIS[3], GERALD GIESTER[1], WILFRIED KÖRNER[4], JOHN M. HUGHES[5], CHRISTIAN LENGAUER[1] and MARKUS PREM[1]

[1]Institut für Mineralogie und Kristallographie, Universität Wien, Geozentrum, Althanstrasse 14, 1090 Wien, Austria
*Corresponding author, e-mail: andreas.ertl@a1.net
[2]Department für Lithosphärenforschung, Universität Wien, Geozentrum, Althanstrasse 14, 1090 Wien, Austria
[3]Harvard Mineralogical Museum, 24 Oxford Street, Cambridge, MA 02138, USA
[4]Department für Umweltgeowissenschaften, Universität Wien, Geozentrum, Althanstrasse 14, 1090 Wien, Austria
[5]Office of the Provost, The University of Vermont, Burlington, VT 05405, USA

Abstract: An Al-rich tourmaline from the Sahatany Pegmatite Field at Manjaka, Sahatany Valley, Madagascar, was structurally and chemically characterized. The combination of chemical and structural data yields an optimized formula of $^{X}(Na_{0.53}Ca_{0.09}\square_{0.38})$ $^{Y}(Al_{2.00}Li_{0.90}Mn^{2+}_{0.09}Fe^{2+}_{0.01})$ $^{Z}Al_6$ $(BO_3)_3$ $^{T}[Si_{5.61}B_{0.39}]O_{18}$ $^{V}(OH)_3$ $^{W}[(OH)_{0.6}O_{0.4}]$, with a = 15.777(1), c = 7.086(1) Å (R_1 = 0.017 for 3241 reflections). The $\langle T$–O$\rangle$ distance of ~ 1.611 Å is one of the smallest distances observed in natural tourmalines. The very short $\langle Y$–O$\rangle$ distance of ~ 1.976 Å reflects the relatively high amount of Al at the Y site. Together with other natural and synthetic Al-rich tourmalines, a very good inverse correlation (r^2 = 0.996) between $^{[4]}$B and the unit-cell volume was found. $^{[4]}$B increases with the Al content at the Y site approximately as a power function with a linear term up until $^{[4]}$B ≈ Si ≈ 3 apfu and ^{Y}Al ≈ 3 apfu, respectively, in natural and synthetic Al-rich tourmalines. Short-range order considerations would not allow for $^{[4]}$B in solid solution between schorl and elbaite, but would in solid solutions between schorl, ''oxy-schorl'', elbaite, liddicoatite, or rossmanite and hypothetical $^{[4]}$B-rich tourmaline end-members with only Al^{3+} at the Y site. By plotting the $^{[4]}$B content of synthetic and natural Al-rich tourmalines, which crystallized at elevated PT conditions, it is obvious that there are pronounced correlations between PT conditions and the $^{[4]}$B content. Towards lower temperatures higher $^{[4]}$B contents are found in tourmaline, which is consistent with previous investigations on the coordination of B in melts. Above a pressure of ~ 1000–1500 MPa (depending on the temperature) the highest observed $^{[4]}$B content does not change significantly at a given temperature. The PT conditions of the formation of $^{[4]}$B-rich olenite from Koralpe, Eastern Alps, Austria, can be estimated as 500–700 MPa/630 °C.

Key-words: Al-rich tourmaline, Manjaka, tetrahedrally coordinated boron, crystal structure, chemical analyses, PT conditions.

Introduction

The general structural formula of tourmaline is given by Hawthorne & Henry (1999) as $X\,Y_3Z_6\,(BO_3)_3\,(T_6O_{18})\,V_3W$, where the V and W are anion sites. The T site is usually occupied by Si and sometimes contains significant amounts of Al (*e.g.*, Foit & Rosenberg, 1979; Foit, 1989; MacDonald & Hawthorne, 1995; Prowatke *et al.*, 2003; Cempírek *et al.*, 2006). B is also found at the T site in Al-rich tourmalines, but in amounts rarely exceeding 0.2 apfu (*e.g.*, Ertl *et al.*, 1997, 2005, 2006, 2007; Hughes *et al.*, 2000, 2004; Marler & Ertl, 2002; Schreyer *et al.*, 2002a and b). Werner Schreyer's group at the Ruhr-Universität, Bochum, Germany, synthesized and characterized Al- and $^{[4]}$B-rich samples at high pressures, 1000–5000 MPa, 400–900 °C (Wodara, 1996; Schreyer, 1997; Schreyer *et al.*, 2000; Wodara & Schreyer, 1997, 1998, 2001; Marler *et al.*, 2002; Schlager, 2003).

In this investigation, we report a natural Al-rich tourmaline with a significant amount of $^{[4]}$B from the Sahatany Pegmatite Field, Madagascar. The pegmatite at Manjaka (west of the village Ihasy), Sahatany Valley, Betafo-Antsirabé region, Antananarivo Province, Madagascar, is located in the Sahatany Pegmatite Field. Gem tourmaline (elbaite) has been mined in this marble-hosted, complex lithium–cesium–tantalum-type pegmatite since about 1900. Associated minerals are albite, microcline, quartz, spodumene, manandonite, bityite, pollucite, fluorapatite, spessartine, manganocolumbite, ixiolite, behierite (type locality), rhodizite and zircon (Lacroix, 1912, 1922; Behier, 1953; Frondel & Ito, 1965). A microthermometric study of fluid inclusions in quartz, topaz and spodumene by Ranorosoa (1986), indicates hydrothermal conditions with temperatures around 350–500 °C for a pressure of 200–300 MPa. These pressures are consistent with the stability field for spodumene (London & Burt, 1982).

The crystal pieces, which were used for structural and chemical investigations, were taken from a hand specimen in the collection of the Harvard Mineralogical Museum,

0935-1221/08/0020-1869 $ 3.60
DOI: 10.1127/0935-1221/2008/0020-1869

Cambridge, MA, USA (sample no. 112628), which Clifford Frondel collected in 1963. This "rubellite" sample consists of several subparallel idiomorphic tourmaline crystals ~ 1–2 mm in diameter and ~ 4–5 cm in lengths, which are enclosed in quartz.

Analytic techniques

Single-crystal structure analysis

A fragment (RUMA1; an equant single crystal ~ 150 μm in diameter) of the core of an idiomorphic purplish-red tourmaline crystal from Manjaka was mounted on a Kappa APEX II CCD X-ray single-crystal diffractometer from Bruker AXS equipped with graphite-monochromated Mo$K\alpha$ radiation (Universität Wien). Data collected at room temperature with sixfold redundancy (upto 80° 2θ) were integrated and corrected for Lorentz and polarization factors and absorption correction by evaluation of multiscans. The structure was refined with SHELXL-97 (Sheldrick, 1997) using scattering factors for neutral atoms and an elbaite starting model from Ertl *et al.* (2006). The H atom bonded to the O3 atom was easily located from a difference-Fourier map and subsequently refined. Refinement was performed with anisotropic thermal parameters for all non-hydrogen atoms. Site occupancies were refined according to well-known characteristics of the tourmaline structure (Na was refined at the *X* site, Al and Li were refined at the *Y* site, and Si and B were refined at the *T* site; for other details see Table 2; the correlation coefficients do not show significant correlations in the refinement, *e.g.*, between site occupancy and overall scale factor). The refinement converged at an $R_1(F)$ value of 1.7 %. Table 1 provides crystal data and details of the structure refinement. In Table 2, we list the atomic parameters (anisotropic displacement parameters are available on request or from the journal's crystal structure database), and in Table 3 we present selected interatomic distances.

Table 1. Crystal data and results of structure refinement for Al-rich tourmaline (sample RUMA1) from Manjaka, Madagascar.

Determination of unit-cell parameters
X-ray radiation: Mo$K\alpha$ (λ = 0.71073 Å)
Reflections used: 9895
Range (°): 5.2–95.5 2θ
Temperature: 298(2) K
Diffraction intensity collection, crystal data and refinement information
X-ray radiation: Mo$K\alpha$ (λ = 0.71073 Å)
Temperature: 298(2) K
Space group, *Z*: *R*3*m* (no. 160), 3
Unit-cell parameters (Å): a = 15.777(1), c = 7.086(1)
Unit-cell volume (Å^3): 1527.4(1)
Frame width, scan time, number of frames, detector distance: 2°, 50 s, 1785, 37.5 mm
Scan mode: ω, φ
2θ range (°): 4–96.4
h, k, l ranges: −31 → 32, −33 → 27, −14 → 14
Measured reflections, full sphere: 45,024
Unique reflections; refined parameters: 3358; 94
Reflections, $F_o > 4\sigma_{(Fo)}$: 3241
Refinement on: F^2
R_1*, $F_o > 4\sigma_{(Fo)}$ = 0.0170; wR_2† = 0.0395; R_{int}‡ = 0.0213
Flack parameter = −0.008(44)
Difference peaks (± eÅ^3): 0.58, 0.55
Goodness-of-Fit§: 0.977

*$R_1 = \Sigma||F_0| - |F_c||/\Sigma|F_o|$.

†$wR_2 = \{\Sigma\left[w\left(F_0^2 - F_c^2\right)^2\right]/\Sigma[w\left(F_o^2\right)^2]\}^{1/2}$;
$w = 1/[\sigma^2\left(F_0^2\right) + (aP)^2 + bP]$, $P = [2F_c^2 + \max\left(F_0^2, 0\right)]/3$.

‡$R_{int} = \Sigma\left|F_0^2 - F_0^2(\text{mean})\right| / \Sigma\left[F_0^2\right]$.

§$\text{GooF} = S = \left\{\Sigma\left[w\left(F_0^2 - F_0^2\right)^2\right]/(n-p)\right\}^{1/2}$.

Chemical analysis

Two crystal fragments (the core sample that was used for the crystal structure determination and another sample from the rim) were subsequently analyzed with a Cameca SX-100 electron microprobe (EMP) at the Department of Lithospheric Research, Geozentrum, Universität Wien, Austria, equipped with four wavelength-dispersive spectrometers (Table 4). We used the following (natural and synthetic) standards and X-ray lines for calibration: albite (Na$K\alpha$), olivine (Mg$K\alpha$), corundum (Al$K\alpha$), quartz (Si$K\alpha$), dravite (B$K\alpha$; with a near-endmember composition and a stoichiometric B content of 3.0 apfu), titanite (Ti$K\alpha$), orthoclase (K$K\alpha$), wollastonite (Ca$K\alpha$), hematite (Fe$K\alpha$), spessartine (Mn$K\alpha$), gahnite (Zn$K\alpha$) and topaz (F$K\alpha$). Matrix corrections were performed using the PAP correction procedure provided by the latest Cameca PeakSight vers. 4.0 software. As the PeakSight software allows switching the analytic conditions within a single measurement, two different sets of analytic conditions were used. In set #1 an accelerating voltage of 15 keV and a beam current of 100 nA were used for the B analyses. To avoid problems dealing with peak shift and peak shape, the full peak width was scanned and integrated to the intensity. The total time of each B measurement was 480 s and the detection limit was 0.6 wt.%. The set of analytic condition #2 was used for all other analyzed elements. The accelerating voltage was the same like that in condition #1 but the beam current was 20 nA. The method of peak to background ratio with counting time 20 s on peak position and 10 s on each background position was used. For both conditions, a 5 μm in diameter defocused beam was used. Under the described conditions, analytic errors are ±2 % relative for major elements (except ±10 % for B_2O_3) and ±5 % relative for minor elements.

The sample preparation for ICP–AES analysis was performed in a clean laboratory using ultrapure acids. To remove surface contamination, the tourmaline grains were leached in 2.5 n HCl for 15 min at about 80 °C. Chemical sample digestion was performed in Zr-cups by using NaOH (heating by a Bunsen burner). ICP–AES analyses were performed on a Perkin Elmer OPTIMA 5300DV (Universität Wien).

To determine the OH content of the tourmaline sample, ~ 20 mg of the core material of the elbaite crystal was used for thermogravimetric analysis (TGA), which was performed on the Mettler-Toledo TGA/SDTA 851 (Universität Wien). The powder was heated from 25 °C to 1100 °C (5 °C/min) under a stream of N_2 gas (gas flow: 25 ml/min).

Table 2. Atom parameters for Al-rich tourmaline (sample RUMA1) from Manjaka, Madagascar.

Atom	*x*	*y*	*z*	U_{eq}	Occ.*
X	0	0	0.2446(2)	0.0225(3)	$Na_{0.709(5)}$
T	0.19141(1)	0.18948(1)	0.01964(2)	0.00539(4)	$Si_{0.935(2)}B_{0.065}$
B	0.10901(3)	0.21802(6)	0.4727(2)	0.0063(1)	$B_{1.00}$
Y	0.12079(3)	0.06040(1)	−0.34151(5)	0.00799(8)	$Al_{0.761(2)}Li_{0.239}$
Z	0.29673(1)	0.26008(1)	−0.37240(3)	0.00647(3)	$Al_{1.00}$
O1(*W*)	0	0	−0.2045(2)	0.0186(2)	$O_{1.00}$
O2	0.06021(2)	0.12042(5)	0.5106(1)	0.0130(1)	$O_{1.00}$
O3(*V*)	0.26139(6)	0.13069(3)	−0.47306(9)	0.01174(9)	$O_{1.00}$
H3	0.256(2)	0.1282(9)	0.411(4)	0.045(7)	$H_{1.00}$
O4	0.09413(2)	0.18826(5)	0.09350(9)	0.00982(8)	$O_{1.00}$
O5	0.18697(5)	0.09348(3)	0.1202(2)	0.01015(9)	$O_{1.00}$
O6	0.19427(3)	0.18381(3)	−0.2005(2)	0.00768(6)	$O_{1.00}$
O7	0.28625(3)	0.28584(3)	0.09589(5)	0.00718(5)	$O_{1.00}$
O8	0.20953(3)	0.27006(3)	0.45705(6)	0.00766(6)	$O_{1.00}$

Note: Definition for U_{eq} see Fischer & Tillmanns (1988). *Only main elements were taken into consideration.

Table 3. Selected interatomic distances (Å) in Al-rich tourmaline (sample RUMA1) from Manjaka, Madagascar.

X site		*T* site	
O2 (×3)	2.502(1)	O6	1.6023(4)
O5 (×3)	2.7151(8)	O7	1.6023(4)
O4 (×3)	2.7862(9)	O4	1.6125(3)
Mean	2.668	O5	1.6270(3)
		Mean	1.6110
Y site		B site	
O1	1.9147(8)	O2	1.3603(10)
O6 (×2)	1.9498(5)	O8 (×2)	1.3781(6)
O2 (×2)	1.9528(5)	Mean	1.3722
O3	2.1351(8)		
Mean	1.9758		
Z site			
O6	1.8729(4)		
O8	1.8809(4)		
O7	1.8828(4)		
O8′	1.8959(4)		
O7′	1.9392(4)		
O3	1.9618(3)		
Mean	1.9056		

Results and discussion

Crystal structure and crystal chemistry

The optimized structural formula of sample RUMA1 (core), which was derived by using chemical and structural data (for details see Table 4) is: $^{X}(Na_{0.53}Ca_{0.09}\square_{0.38})$ $^{Y}(Al_{2.00}Li_{0.90}Mn^{2+}_{0.09}Fe^{2+}_{0.01})$ $^{Z}Al_6$ $(BO_3)_3$ $^{T}[Si_{5.61}B_{0.39}]O_{18}$ $^{V}(OH)_3$ $^{W}[(OH)_{0.6}O_{0.4}]$. The structural formula of sample RUMA2 (rim), which was derived by using chemical data (for details see Table 4) is: $^{X}(Na_{0.49}Ca_{0.06}\square_{0.45})$ $^{Y}(Al_{1.82}Li_{1.02}Mn^{2+}_{0.12}Fe^{2+}_{0.01}\square_{0.03})$ $^{Z}Al_6$ $(BO_3)_3$ $^{T}[Si_{5.81}B_{0.30}]O_{18}$ $^{V}(OH)_3$ $^{W}[(OH)_{0.5}O_{0.5}]$.

The *T* site of the core (RUMA1) is occupied by ~ 0.4 apfu $^{[4]}B$, which is consistent with the relatively low ⟨*T*–O⟩ distance of 1.611 Å, one of the lowest ⟨*T*–O⟩ distances observed to date in natural tourmaline. For a *T* site fully occupied by Si, a ⟨*T*–O⟩ distance of ~ 1.620 Å was proposed by MacDonald & Hawthorne (1995). At the rim (RUMA2) the amount of $^{[4]}B$ and Al_2O_3 decreases (Table 4).

The *Y* site of this Al-rich tourmaline is mainly occupied by Al and Li, and shows only small amounts of Mn and a trace of Fe. The core contains ~ 38 mol. % rossmanite, ~ 35 mol. % elbaite, ~ 14 mol. % olenite and ~ 9 mol. % liddicoatite, whereas the rim contains ~ 45 mol. % rossmanite, ~ 45 mol. % elbaite and ~ 6 mol. % liddicoatite (for the definition of tourmaline end-members, see Hawthorne & Henry, 1999). The MnO content increases slightly from core (~ 0.7 wt.%) to rim (~ 0.9 wt.%), whereas the FeO is < 0.1 wt.% in both (Table 4). The very short ⟨*Y*–O⟩ distance of ~ 1.976 Å, which is one of the lowest observed in tourmaline to date, reflects the relatively high amount of Al (~ 2.0 apfu) at the *Y* site. The *Z* site is occupied only by Al, which results in a ⟨*Z*–O⟩ distance of ~ 1.906 Å (Table 3).

The *X* site is partially occupied by Na and small amounts of Ca. From core to rim, the Na and Ca content decrease slightly as does total occupancy, but in the rim Na is still the dominant component (Table 4).

A H atom (= H3) at the site associated with O3 was easily located in this refinement. Ertl *et al.* (2002) showed that the bond–angle distortion $\left(\sigma^2_{oct}\right)$ of the ZO_6 octahedron in a tourmaline is largely a function of the ⟨*Y*–O⟩ distance of that tourmaline, although the occupant of the O3 site (*V* site) also affects that distortion. The covariance, *r*, of ⟨*Y*–O⟩ and the $\left(\sigma^2_{oct}\right)$ of the ZO_6 octahedron is −0.991 for all investigated tourmalines that are occupied by 3 (OH) groups, including the samples from Hughes *et al.* (2004). The tourmaline RUMA1 lies exactly on the *V* site = 3 (OH) line, which is consistent with O3 being fully occupied by OH. The H atom associated with O1 could not be refined because this position seems to be approximately half-occupied by H as indicated by the chemical analysis. Because the F content is below the detection limit, and for the need of a charge balanced formula, the *W* site in the optimized formulae was assumed to be occupied by ~ $(OH_{0.6}O_{0.4})$. The recalculated

Table 4. Chemical composition (wt.%) of core and rim of the Al-rich tourmaline from Manjaka, Madagascar.

	RUMA1 (core)	RUMA1[c] (core)	RUMA2 (rim)
SiO_2	35.35(40)	35.97	36.74(42)
TiO_2	0.02(1)	–	0.02(1)
B_2O_3	12.99(52)	12.59	12.10(64)
Al_2O_3	42.87(65)	43.52	41.97(62)
FeO	0.08(4)	0.08	0.07(2)
MnO	0.68(18)	0.68	0.93(33)
CaO	0.52(6)	0.53	0.36(3)
Li_2O	1.60[a]	1.44	1.60[a]
Na_2O	1.74(9)	1.75	1.60(15)
K_2O	0.02(1)	–	0.02(1)
H_2O	3.31[b]	3.44[d]	3.31[b]
Sum	99.18	100.00	98.72
N anions	31	31	31
Si	5.55	5.61	5.81
$^{[4]}B$	0.52	0.39	0.30
Sum *T* site	6.07	6.00	6.11
$^{[3]}B$	3.00	3.00	3.00
Al	7.94	8.00	7.82
Mn^{2+}	0.09	0.09	0.12
Fe^{2+}	0.01	0.01	0.01
Li	1.01	0.90	1.02
Sum *Y, Z* sites	9.05	9.00	8.97
Na	0.53	0.53	0.49
Ca	0.09	0.09	0.06
Sum *X* site	0.62	0.62	0.55
Sum cations	18.74	18.61	18.63
OH	3.47	3.58	3.49

Note: RUMA1 (core): average of 10 EMP analyses. RUMA2 (rim): average of 10 EMP analyses. Mg and F are below detection limit. Total Mn and Fe calculated as MnO and FeO. [a]Li_2O was determined by ICP–AES on a bulk analysis of the whole crystal; [b]H_2O was estimated by TGA; [c]Optimized formula calculated for Si + $^{[4]}B$ = 6.00 apfu, the refinement data were used for the $^{[4]}B$ content, and for *Y* site = 3.00 apfu, where Li and ^{Y}Al content were calculated by taking the refinement data into consideration; [d]H_2O was calculated for a charge balanced formula. In addition, 301 ppm Zn and 54 ppm Pb were determined by ICP–AES.

H_2O content is consistent with the content determined by TGA within an error of ~ 4 % (Table 4). In most Al-rich tourmalines ($\geq$ 40 wt.% Al_2O_3) with significant amounts of Li ($\geq$ 0.7 wt.% Li_2O) OH = 4.0 – F (*e.g.*, Schreyer *et al*., 2002b; Ertl *et al.*, 2006), even when the F content is relatively low, *e.g.*, in the Li-bearing olenite from the type locality (0.08 apfu F; Schreyer *et al*., 2002a and b).

$^{[4]}B$ increases with the Al content at the *Y* site approximately as a power function with a linear term, $y = 0.1291\ x + 0.0027\ x^{6.0480}$, up until $^{[4]}B \approx Si \approx 3$ apfu and $^{Y}Al \approx 3$ apfu, respectively, in natural and synthetic Al-rich tourmalines (Fig. 1). This relation reflects different short-range order configurations with ^{Y}Al and $^{[4]}B$, and also including variable *X*-, *Y*- and *W*-site occupancies (Hughes *et al.*, 2000; Ertl *et al.*, 2006). Oxygen atoms bridging *T* sites, one of which is occupied by B, would be undersaturated unless the *X* site is occupied. Short-range order considerations would not allow for $^{[4]}B$ in solid solution between schorl and elbaite, but would in solid solutions between schorl, "oxy-schorl", elbaite, liddicoatite, or rossmanite and hypothetical $^{[4]}B$-rich tourmaline end-members with only Al^{3+} at the *Y* site. Figure 1 shows that the most tourmaline samples plot near the solid solutions of "oxy-schorl"-"olenite 2", rossmanite-"Al-tourmaline" and elbaite-"olenite 1" (compositions of the hypothetical end-members are given in the caption of Fig. 1). The distribution of data points in Fig. 1 reflects the large number of substitutions found in intermediate tourmaline solutions. The substitution of B in the tetrahedral site of tourmaline is a heterovalent substitution, losing one positive charge. In tourmaline, heterovalent substitutions are noted in several sites, but as a rule the *Z* site and the B site do not incorporate substituents in Al-rich tourmalines, being occupied by Al and B, respectively. Thus, the −1 charge that results from the $^{T}(Si_{-1}B_1)$ substitution, as well as any other substitution that results in a residual negative charge, must be balanced by a concomitant substitution that yields a positive charge. Table 5 lists the common substitutions noted in ideal olenite, $NaAl_3Al_6(BO_3)_3[Si_6O_{18}]O_3(OH)$, as defined by Hawthorne & Henry (1999) on the basis of the data in Sokolov *et al*. (1986). The only common substitutions yielding positive charge are $^{X}(Na_{-1}Ca_1)^{+1}$ and $^{V}(O_{-1}OH_1)^{+1}$. Schreyer *et al*. (2002b) reported in a reinvestigation of olenite from the type locality that this tourmaline contains significant

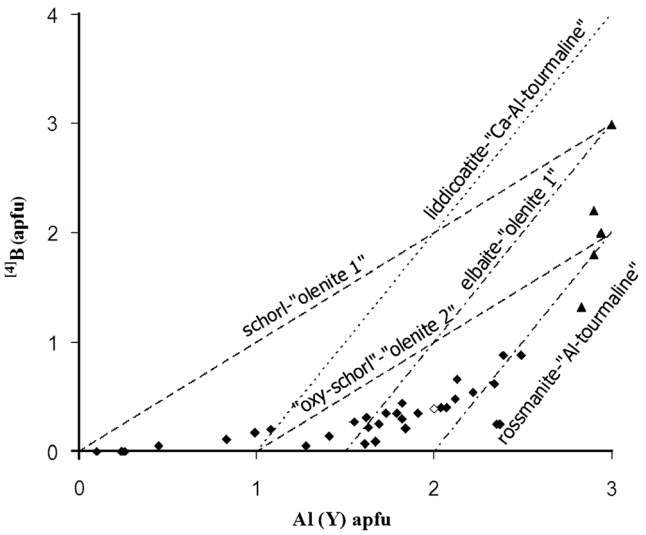

Fig. 1. Relationship between the Al content at the *Y* site and $^{[4]}B$ in natural (diamonds) and synthetic (triangles) Al-rich tourmalines (this work; Bosi *et al*., 2005a; Ertl & Hughes, 2002; Ertl *et al.*, 1997, 2005, 2006, 2007; Hughes *et al.*, 2004; Kalt *et al.*, 2001; Wodara & Schreyer, 2001; Marler *et al.*, 2002; Schlager, 2003; in all samples FeO + MnO < 0.80 wt.%). The tourmaline from Manjaka is marked as an open diamond. Possible solid solutions between different tourmaline end-members are shown as broken, dotted and chain dotted lines. For the definition of the end-members see Hawthorne & Henry (1999), except for the hypothetical B-rich end-members "olenite 1", defined as $NaAl_3Al_6(BO_3)_3[Si_3B_3O_{18}](OH)_4$, "olenite 2", defined as $NaAl_3Al_6(BO_3)_3[Si_4B_2O_{18}](OH)_3O$, "Al-tourmaline", defined as $\square Al_3Al_6(BO_3)_3[Si_4B_2O_{18}](OH)_4$ and "Ca–Al–tourmaline", defined as $CaAl_3Al_6(BO_3)_3[Si_2B_4O_{18}](OH)_4$. All these B-rich end-members contain the maximum possible Si substitution by B to produce charge-balanced formulae.

Table 5. Possible heterovalent substitutions in ideal olenite.

(−)	(+)
$^{X}(Na_{-1}\square_{1})^{-1}$	$^{X}(Na_{-1}Ca_{1})^{+1}$
$^{Y}(Al_{-1}Li_{1})^{-2}$	$^{V}(O_{-1}OH_{1})^{+1}$
$^{Y}(Al_{-1}\square_{1})^{-3}$	$^{W}(O_{-1}F_{1})^{+1}$
$^{W}(OH_{-1}O_{1})^{-1}$	
$^{T}(Si_{-1}B_{1})^{-1}$	
$^{T}(Si_{-1}Al_{1})^{-1}$	

amounts of $^{[4]}$B and that the OH sites are almost completely filled by OH (and only traces by F and O). However, this was not surprising because almost all of the tourmalines found in nature contain between 3 and 4(OH) groups (the *V* site completely and the *W* site partially occupied by OH and F). In the most Al-rich samples of Fig. 1, the *Y* site is essentially completely occupied by Al. To allow substitution for different amounts of Si by B in these synthetic samples, there are only two possibilities for a charge-balanced mechanism. When the amount of $^{[4]}$B increases, the *X* site needs to be occupied and can only have a small portion of vacancies, and the *V* and *W* sites must be occupied by higher total amounts of OH (up to 4(OH) groups, replacing oxygen atoms).

Correlation of cell parameters with tetrahedral boron

Wodara & Schreyer (2001) and Marler *et al.* (2002) found an inverse correlation between the $^{[4]}$B content and the unit-cell volume. A new plot that includes natural Al-rich samples as well as synthetic tourmalines (Fig. 2) shows a tightly constrained inverse linear correlation ($r^2 = 0.996$) for Al-rich tourmalines. Thus, cell volume, which is easily obtained with powder X-ray diffraction, can be used to estimate the amount of $^{[4]}$B, which is difficult to measure accurately.

Variation of tetrahedrally coordinated boron content with pressure and temperature

A plot of the $^{[4]}$B content of synthetic and natural Al-rich tourmalines that crystallized at elevated PT conditions shows a pronounced correlation between PT conditions and $^{[4]}$B content (Fig. 3). The plotted data include Al- and Na-rich tourmalines in the system Na_2O–Al_2O_3–B_2O_3–SiO_2–H_2O (NABSH) synthesized by Schreyer (1997), Schreyer *et al.* (2000) and Wodara & Schreyer (1997, 1998) at high pressures using as a starting material gel with the anhydrous composition $0.625Na_2O{\cdot}4.5Al_2O_3{\cdot}6SiO_2$ to which 100 % excess B_2O_3 (over that of the formula $NaAl_3Al_6(BO_3)_3[Si_6O_{18}]O_3(OH)$) and a surplus of water had been added (for more details, see Schreyer *et al.*, 2000). Also plotted were two Al-rich tourmalines synthesized at 600 °C/2500 MPa (sample 1) and 650 °C/2000 MPa (sample 2) by Marler *et al.* (2002), who refined the crystal structure by the Rietveld method to give $Na_{0.8}Al_{2.9}Al_6(BO_3)_3[Si_{3.8}B_{2.2}O_{18}](OH)_3(OH,O)$ and $Na_{0.7}Al_{2.9}Al_6(BO_3)_3[Si_{4.2}B_{1.8}O_{18}](OH)_3(OH,O)$, respectively. Additional data were obtained from Schlager (2003), who calculated unit-cell parameters by powder diffraction of Al-rich tourmalines

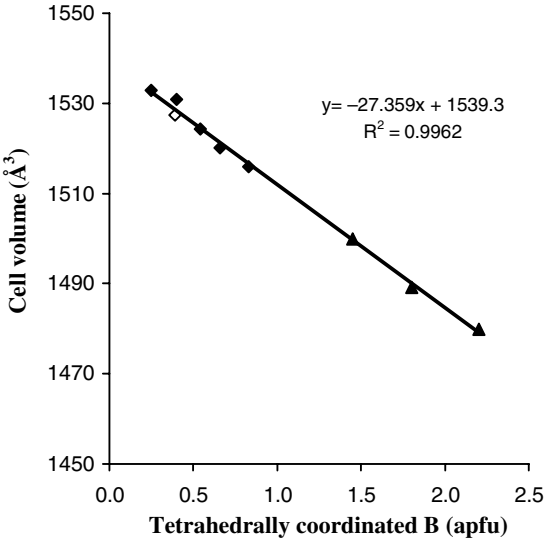

Fig. 2. Relationship between tetrahedrally coordinated boron in Al- and B-rich tourmalines and the unit-cell volume. Natural (squares) and synthetic (triangles) Na-, $^{X}\square$-, Al- and $^{[4]}$B-rich tourmalines ($^{[4]}$B > 0.2 apfu; FeO + MnO < 2.4 wt.%) were plotted (this study; Ertl *et al.*, 1997, 2005, 2007; Hughes *et al.*, 2004; Marler *et al.*, 2002; Schreyer *et al.*, 2000, 2002b; Wodara & Schreyer, 2001). The tourmaline from Manjaka is marked as an open square. Only samples were used where the B content was analyzed.

synthesized at PT conditions in the range 300 MPa/450 °C to 4000 MPa/700 °C. We applied the equation: $^{[4]}B = (V - 1539.3)/(-27.359)$, where $^{[4]}$B – tetrahedrally coordinated B in apfu and *V* – cell volume in Å^3 from Fig. 2, to calculate the $^{[4]}$B content in tourmalines synthesized by Schlager (2003) and one tourmaline synthesized by Wodara (1996).

The trends indicated in Fig. 3 confirm the results of the experiments by Wodara (1996) and Schreyer *et al.* (2000), which had suggested that $^{[4]}$B in Al-rich tourmaline is favored by low temperatures and high pressures (Schreyer, 2000; Marler *et al.*, 2002). Even with 100 % excess B_2O_3 in the starting material, the estimated $^{[4]}$B content in the synthetic tourmalines does not exceed certain values at given PT conditions. $^{[4]}$B content increases with decreasing temperature. Above 1000–1500 MPa (depending on the temperature) the $^{[4]}$B content does not change significantly with pressure at a given temperature. Different investigations of alkali borate and borosilicate melts and glasses have shown that the ratio of $^{[4]}$B to $^{[3]}$B tends to decrease with increasing temperature (Araujo, 1980; Gupta *et al.*, 1985; Majérus *et al.*, 2003).

A $^{[4]}$B-rich tourmaline, with the formula $^{X}(Na_{0.55}Ca_{0.08}Pb_{0.01}\square_{0.36})\ ^{Y}(Al_{2.13}Li_{0.75}Mn^{2+}_{0.01}\square_{0.11})\ ^{Z}Al_6\ (BO_3)_3\ ^{T}[Si_{5.34}B_{0.66}]O_{18}\ ^{V}(OH)_3\ ^{W}[(OH)_{0.50}O_{0.26}F_{0.24}]$, with $a = 15.7561(6)$, $c = 7.0703(5)$ Å (cell volume: 1520.1(2) Å^3), was described from a pegmatite that intruded a peridotite body at Momeik in the Mogok Mineral Tract, Myanmar (Ertl *et al.*, 2007). This peridotite could be interpreted as part of the ophiolites that belong to the Indo-Burma range. This range is interpreted as an accretionary wedge that derived from the subduction of the Bengal oceanic crust during the India–Asia collision

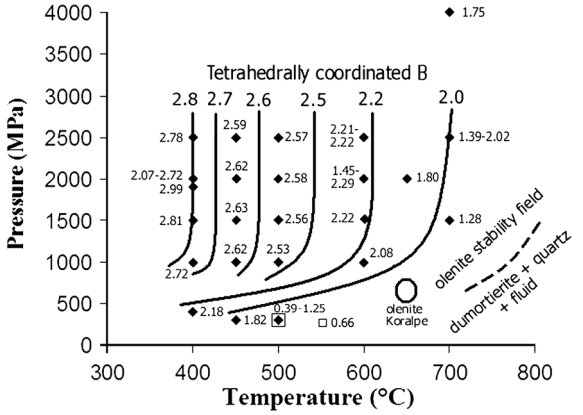

Fig. 3. Relationship between PT conditions and the amount of tetrahedrally coordinated boron in Al-rich tourmaline. Tourmalines synthesized at 300–4000 MPa/400–700 °C (filled diamonds, Marler *et al.*, 2002; Schlager, 2003; Schreyer *et al.*, 2000; Wodara, 1996; Wodara & Schreyer, 2001) and natural tourmalines from Manjaka, Madagascar (larger unfilled square, this study), Momeik, Myanmar (smaller unfilled square, Ertl *et al.*, 2007; this study), and B-rich olenite from Koralpe, Austria (unfilled circle; ~ 0.83 apfu $^{[4]}$B; Ertl *et al.*, 1997; Hughes *et al.*, 2000; updated formula in Ertl *et al.*, 2007). PT stability field of excess-boron olenite is bounded by a dashed line (Schreyer, 2000). The solid lines are interpolated and mark approximately the tourmalines with the maximum observed $^{[4]}$B content. The sample with ~ 2.99 apfu $^{[4]}$B is an outlier and it is not clear, if there is a higher error on this value.

(Socquet *et al.*, 2002). The pegmatitic body, which contains the B-rich tourmaline, possibly intruded a peridotite during that exhumation. Because this tourmaline is associated with petalite (Ertl *et al.*, 2007), the lithium aluminosilicate phase diagram of London (1981, 1984) can be used to estimate PT conditions roughly as ~ 250 MPa/550 °C (Fig. 3).

The most $^{[4]}$B-rich natural tourmaline known to date, an olenite, was described from a pegmatite that intruded discordantly into mylonitic garnet–biotite schists from Koralpe, Eastern Alps, Styria, Austria (Ertl *et al.*, 1997; Hughes *et al.*, 2000; Kalt *et al.*, 2001). No other Li-bearing minerals like spodumene, petalite or lepidolite were verified from this pegmatite (Ertl & Brandstätter, 1998). Ertl *et al.* (1997) reported the unit-cell parameters as a = 15.7395(2), c = 7.0656(2) Å, and the cell volume as 1515.86(5) Å^3. Ertl *et al.* (2007) gave an updated formula for this tourmaline with $^{X}(Na_{0.40}Ca_{0.29}\square_{0.31})\ ^{Y}(Al_{2.40}Li_{0.35}\square_{0.25})\ ^{Z}Al_6\ (BO_3)_3\ ^{T}[Si_{4.89}B_{0.83}Al_{0.27}Be_{0.01}]O_{18}\ ^{V}(OH)_3\ ^{W}[O_{0.58}(OH)_{0.36}F_{0.06}]$. The mylonitization of the gneisses and eclogites in the shear zone of the Koralpe Complex (Eastern Alps) occurred during the eo-Alpine metamorphism. The PT path of the shear zone as reported by Stüwe & Powell (1995) can be characterized by three stages. The first stage involved decompression from > 1800 MPa to 1400–1600 MPa at temperatures above 620 °C reaching the metamorphic peak temperature around 1400–1600 MPa and 700 °C. The second stage involved near-isobaric cooling at this pressure to 600 ± 20 °C. The third stage of the PT path follows a typical Barrovian evolution with a second phase of isothermal decompression to 700–800 MPa/~ 600 °C followed by cooling during final exhumation. Stüwe & Powell (1995) reported that no minerals in their mylonitic gneiss sample have compositions corresponding to growth below ~ 1000 MPa and ~ 600 °C. Because the pegmatite that contained the Al-rich tourmaline intruded the mylonitic schists discordantly, we would expect PT conditions to be < 1000 MPa/≤ 600 °C. However, the temperature was estimated as ~ 630 °C by using the morphology of zircon crystals (thermometer proposed by Pupin, 1980) associated with this tourmaline (Ertl & Brandstätter, 1998). Because of the correlation reported by Henry and Dutrow (1996) between X site vacancies in tourmaline and the temperature conditions, the temperature estimation by using data from Ertl *et al.* (1997) and Hughes *et al.* (2000) gives a similar value for $^{X}\square_{0.31–0.32}$. In summary, ~ 0.83 apfu $^{[4]}$B in the Koralpe olenite (circle in Fig. 3) gives a rough pressure estimate of 500–700 MPa for a temperature of ~ 630 °C.

In case of the tourmaline from Manjaka, Madagascar, a significantly higher $^{[4]}$B content might be possible at the PT conditions estimated for the pegmatite, but because of the relatively high Li content in this sample, more tetrahedral B could not be accommodated because Li constrained the maximum ^{Y}Al to 2 apfu.

Typical Al- and Li-rich tourmalines contain amounts of ≤ 0.40 $^{[4]}$B apfu (*e.g.*, Tagg *et al.*, 1999; Bosi *et al.*, 2005a and b; Ertl *et al.*, 2006), which suggests pressures of ≤ 300 MPa for such Li-pegmatites (see Fig. 3). This is in agreement with the pressure estimations by Taylor *et al.* (1979) and London (1984, 1986).

Dedication

This paper is dedicated to the memory of Werner Schreyer, who collaborated with Andreas Ertl for ~ 10 years on Al- and B-rich tourmalines. Werner, his colleagues and students were the first to synthesize and confirm tetrahedrally coordinated boron in synthetic Al-rich tourmaline. He was always interested in new experiments on Al-rich tourmalines and the PT conditions that are necessary for tetrahedrally coordinated boron, and there is no doubt that he still would work on this interesting theme if he could.

Acknowledgements: We are grateful to Andreas Wagner, Vienna, Austria, for sample preparation. Special thanks to Stephen E. Wright and A. John Bailer at Miami University, Oxford, Ohio, for their help by calculating the power function and George R. Rossman, Pasadena, California, USA for a preliminary review. The authors would like to thank the Associate Editor Edward S. Grew, and the reviewers Hans-Joachim Massonne and Ferdinando Bosi for their constructive comments. This work was supported by Österreichischer Fonds zur Förderung der wissenschaftlichen Forschung (FWF) Project No. P20509.

References

Araujo, R.J. (1980): Statistical mechanical model of boron coordination. *J. Non-Cryst. Solids*, **42**, 209-230.

Behier, J. (1953): Les minéraux de la pegmatite de Manjaka, Vallée de la Sahatany. *Arch. Serv. Géol. Mad.,* A581.

Bosi, F., Agrosì, G., Lucchesi, S., Melchiorre, G., Scandale , E. (2005a): Mn-tourmaline from island of Elba (Italy): crystal chemistry. *Am. Mineral.*, **90**, 1661-1668.

Bosi, F., Andreozzi, G.B., Federico, M., Graziani, G., Lucchesi, S. (2005b): Crystal chemistry of the elbaite-schorl series. *Am. Mineral.*, **90**, 1784-1792.

Cempírek, J., Novák, M., Ertl, A., Hughes, J.M., Rossman, G.R., Dyar, M.D. (2006): Fe-bearing olenite with tetrahedrally coordinated Al from an abyssal pegmatite at Kutná Hora, Czech Republic: structure, crystal chemistry, optical and XANES spectra. *Can. Mineral.*, **44**, 23-30.

Ertl, A. & Brandstätter, F. (1998): Olenit mit Borüberschuß aus einem Metapegmatit östlich der Stoffhütte, Koralpe, Steiermark, Österreich. *Mitt. Abt. Miner. Landesmuseum Joanneum*, **62/63**, 3-21.

Ertl, A. & Hughes, J.M. (2002): The crystal structure of an aluminum-rich schorl overgrown by boron-rich olenite from Koralpe, Styria, Austria. *Mineral. Petrol.*, **75**, 69-78.

Ertl, A., Pertlik, F., Bernhardt, H.-J. (1997): Investigations on olenite with excess boron from the Koralpe, Styria, Austria. *Österr. Akad. Wiss., Math.-Naturw. Kl., Anzeiger Abt. I*, **134**, 3-10.

Ertl, A., Hughes, J.M., Pertlik, F., Foit Jr., F.F., Wright, S.E., Brandstätter, F., Marler, B. (2002): Polyhedron distortions in tourmaline. *Can. Mineral.*, **40**, 153-162.

Ertl, A., Rossman, G.R., Hughes, J.M., Prowatke, S., Ludwig, T. (2005): Mn-bearing "oxy-rossmanite" with tetrahedrally-coordinated Al and B from Austria: structure, chemistry, and infrared and optical spectroscopic study. *Am. Mineral.*, **90**, 481-487.

Ertl, A., Hughes, J.M., Prowatke, S., Ludwig, T., Prasad, P.S.R., Brandstätter, F., Körner, W., Schuster, R., Pertlik, F., Marschall, H. (2006): Tetrahedrally-coordinated boron in tourmalines from the liddicoatite-elbaite series from Madagascar: structure, chemistry, and infrared spectroscopic studies. *Am. Mineral.*, **91**, 1847-1856.

Ertl, A., Hughes, J.M., Prowatke, S., Ludwig, T., Brandstätter, F., Körner, W., Dyar, M.D. (2007): Tetrahedrally-coordinated boron in Li-bearing olenite from "mushroom" tourmaline from Momeik, Myanmar: structure and chemistry. *Can. Mineral.*, **45**, 891-899.

Fischer, R.X. & Tillmanns, E. (1988): The equivalent isotropic displacement factor. *Acta Cryst.*, **C44**, 775-776.

Foit Jr., F.F. (1989): Crystal chemistry of alkali-deficient schorl and tourmaline structural relationships. *Am. Mineral.*, **74**, 422-431.

Foit Jr., F.F. & Rosenberg, P.E. (1979): The structure of vanadium-bearing tourmaline and its implications regarding tourmaline solid solutions. *Am. Mineral.*, **64**, 788-798.

Frondel, C. & Ito, J. (1965): Composition of rhodizite. *Tscherm. Mineral. Petrogr. Mitt.*, **10**, 409-412.

Gupta, P.K., Lui, M.L., Bray, P.J. (1985): Boron coordination in rapidly cooled and in annealed aluminum borosilicate glass fibers. *J. Am. Ceram. Soc.*, **68**, C-82.

Hawthorne, F.C. & Henry, D.J. (1999): Classification of the minerals of the tourmaline group. *Eur. J. Mineral.*, **11**, 201-215.

Henry, D.J. & Dutrow, B.L. (1996): Metamorphic tourmaline and its petrologic applications. *in* "Boron: Mineralogy, Petrology and Geochemistry", E.S. Grew & L.M. Anovitz, eds., *Rev. Mineral.*, **33**, 505-557.

Hughes, J.M., Ertl, A., Dyar, M.D., Grew, E., Shearer, C.K., Yates, M.G., Giudotti, C.V. (2000): Tetrahedrally coordinated boron in a tourmaline: boron-rich olenite from Stoffhütte, Koralpe, Austria. *Can. Mineral.*, **38**, 861-868.

Hughes, J.M., Ertl, A., Dyar, M.D., Grew, E.S., Wiedenbeck, M., Brandstätter, F. (2004): Structural and chemical response to varying $^{[4]}$B content in zoned Fe-bearing olenite from Koralpe, Austria. *Am. Mineral.*, **89**, 447-454.

Kalt, A., Schreyer, W., Ludwig, T., Prowatke, S., Bernhardt, H.-J., Ertl, A. (2001): Complete solid solution between magnesian schorl and lithian excess-boron olenite in a pegmatite from the Koralpe (eastern Alps, Austria). *Eur. J. Mineral.*, **13**, 1191-1205.

Lacroix, A. (1912): Sur quelques minéraux des pegmatites du vakinankaratra (Madagascar). *Bull. Soc. Franc. Mineral.*, **35**, 76-78.

— (1922): Minéralogie de Madagascar. Tome i. Société d'éditions Géographiques, Maritimes et Coloniales, Paris, 624 p.

London, D. (1981): Preliminary experimental results in the system $LiAlSiO_4$–SiO_2–H_2O. *Yearbook Carnegie Inst. Wash.*, **80**, 341-345.

— (1984): Experimental phase equilibria in the system $LiAlSiO_4$–SiO_2–H_2O: a petrogenetic grid for lithium-rich pegmatites. *Am. Mineral.*, **69**, 995-1004.

— (1986): Formation of tourmaline-rich gem pockets in miarolitic pegmatites. *Am. Mineral.*, **71**, 396-405.

London, D. & Burt, D.M. (1982): Lithium minerals in pegmatites. *in* "Short Course in Granitic Pegmatites in Sciences and Industry", P. Černý, ed. Short Course Handbook 8, Winnipeg, 99-133.

MacDonald, D.J. & Hawthorne, F.C. (1995): The crystal chemistry of Si $\Longleftrightarrow$ Al substitution in tourmaline. *Can. Mineral.*, **33**, 849-858.

Majérus, O., Cormier, L., Calas, G., Beuneu, B. (2003): Temperature-induced boron coordination change in alkali borate glasses and melts. *Phys. Rev.*, **B67**, 024210.1-024210.7.

Marler, B. & Ertl, A. (2002): Nuclear magnetic resonance and infrared spectroscopic study of excess-boron olenite from Koralpe, Styria, Austria. *Am. Mineral.*, **87**, 364-367.

Marler, B., Borowski, M., Wodara, U., Schreyer, W. (2002): Synthetic tourmaline (olenite) with excess boron replacing silicon in the tetrahedral site: II. Structure analysis. *Eur. J. Mineral.*, **14**, 763-771.

Prowatke, S., Ertl, A., Hughes, J.M. (2003): Tetrahedrally-coordinated Al in Mn-rich, Li- and Fe-bearing olenite from Eibenstein an der Thaya, Lower Austria: a chemical and structural investigation. *N. Jb. Mineral. Mh.*, **2003**, 385-395.

Pupin, J.P. (1980): Zircon and granite petrology. *Contrib. Mineral. Petrol.*, **73**, 207-220.

Ranorosoa, N. (1986): Etude minéralogique des pegmatites du champ de la Sahatany (Madagascar). Thèse de doctorat de l'Universite Paul Sabatier, Toulouse 3, no. 86 TOU3 0210, Toulouse, 240 p.

Schlager, O. (2003): Hochdruck-Niedertemperatursynthesen von extreme borreichen olenitischen Turmalinen. Diploma Thesis, Ruhr-Universität Bochum, 78 p.

Schreyer, W. (1997): Experimental studies on tourmaline end-members. Abstracts Tourmaline 1997, Nove Mesto na Morave, Czech Republic, 89-90.

— (2000): Is the partitioning of boron between tourmaline and muscovite dependent on the crystallization environment? *J. Czech Geol. Soc.*, **45**, 13-20.

Schreyer, W., Wodara, U., Marler, B., van Aken, P.A., Seifert, F., Robert, J.L. (2000): Synthetic tourmaline (olenite) with excess boron replacing silicon in the tetrahedral site: I. Synthesis conditions, chemical and spectroscopic evidence. *Eur. J. Mineral.*, **12**, 529-541.

Schreyer, W., Ertl, A., Hughes, J., Bernhardt, H.-J., Kalt, A., Prowatke, S. (2002a): Tetrahedral boron in olenite from the type locality: a chemical and structural investigation. EMPG IX, Zürich, Switzerland, 24.-27.3. *J. Conf. Abstr.*, **7**, 1, 97.

Schreyer, W., Hughes, J.M., Bernhardt, H.-J., Kalt, A., Prowatke, S., Ertl, A. (2002b): Reexamination of olenite from the type locality: detection of boron in tetrahedral coordination. *Eur. J. Mineral.*, **14**, 935-942.

Sheldrick, G.M. (1997): SHELXL-97, a program for crystal structure refinement, University of Göttingen, Germany.

Socquet, A., Goffé, B., Pubellier, M., Rangin, C. (2002): Le métamorphism Tardi-Crétacé à Éocène des zones internes de la chaîne Indo-Birmane (Myanmar occidental): implications géodynamiques (Late Cretaceous to Eocene metamorphism of the internal zone of the Indo-Burma range (western Myanmar): geodynamic implications). *Compt. Rend. Geosci.*, **334**, 573-580.

Sokolov, P.B., Gorskaya, M.G., Gordienko, V.V., Petrova, M.G., Kretser, Yu.L., Frank-Kamenetskii, V.A. (1986): Olenite, $Na_{1-x}Al_3Al_6B_3Si_6O_{27}$(O, OH)4 – a new high-alumina mineral of the tourmaline group. (in Russian). *Zap. Vses. Mineral Obsh.*, **115**, 119-123.

Stüwe, K. & Powell, R. (1995): PT Paths from modal proportions: application to the Koralm Complex, Eastern Alps. *Contrib. Mineral. Petrol.*, **119**, 83-93.

Tagg, S.L., Cho, H., Dyar, M.D., Grew, E.S. (1999): Tetrahedral boron in naturally occurring tourmaline. *Am. Mineral.*, **84**, 1451-1455.

Taylor, B.E., Foord, E.E., Friedrichsen, H. (1979): Stable isotope and fluid inclusion studies of gem-bearing granitic pegmatite-aplite dikes, San Diego County, California. *Contrib. Mineral. Petrol.*, **68**, 187-205.

Wodara, U. (1996): Synthese und Eigenschaften von Turmalinen im System Na_2O–Al_2O_3–SiO_2–B_2O_3–H_2O. Diploma Thesis, Ruhr-Universität Bochum, 99 p.

Wodara, U. & Schreyer, W. (1997): Turmaline mit Borüberschuß im System Na_2O–Al_2O_3–B_2O_3–SiO_2–H_2O (NABSH). *Ber. Deutsch. Mineral. Ges., Beih. z. Eur. J. Mineral.*, **9**, 394.

—, — (1998): Tetrahedral boron in tourmalines of the system Na_2O–Al_2O_3–B_2O_3–SiO_2–H_2O. *Terra Abstract, Abstract Suppl. 1 to Terra Nova*, **10**, 68-69.

—, — (2001): X-site vacant Al-tourmaline: a new synthetic end-member. *Eur. J. Mineral.*, **13**, 521-532.

Received 13 February 2008
Modified version received 2 June 2008
Accepted 18 June 2008